A Final Report
Grant No. NAG-3-909

June 1, 1988 - April 17, 1992

MAGNETIC ACTUATORS AND SUSPENSION FOR SPACE VIBRATION CONTROL

Submitted to:

National Aeronautics and Space Administration
Lewis Research Center
21000 Brookpark Road
Cleveland, OH 44135

Attention:

Dr. David P. Fleming, M/S 23-3
Structural Dynamics Branch

Submitted by:

Carl R. Knospe
Assistant Professor

Paul E. Allaire
Mac Wade Professor and Chairman

David W. Lewis
Professor

SEAS Report No. UVA/528292/MANE93/101
May 1993

DEPARTMENT OF MECHANICAL, AEROSPACE
AND NUCLEAR ENGINEERING

SCHOOL OF
ENGINEERING
& APPLIED SCIENCE

University of Virginia
Thornton Hall
Charlottesville, VA 22903

The Journal of the Astronautical Sciences, Vol. 40, No. 2, April-June 1992, pp. 241-259

Optimal Microgravity Vibration Isolation: An Algebraic Introduction[1]

R. D. Hampton,[2] C. M. Grodsinsky,[3] P. E. Allaire,[2] D.W. Lewis,[2] and C. R. Knospe[2]

Abstract

Certain experiments contemplated for space platforms must be isolated from the accelerations of the platform. In this paper an optimal active control is developed for microgravity vibration isolation, using constant state feedback gains (identical to those obtained from the Linear Quadratic Regulator [LQR] approach) along with constant feedforward (preview) gains.

The quadratic cost function for this control algorithm effectively weights accelerations of the platform due to external disturbances by a factor proportional to $(1/\omega)^2$. Low frequency accelerations (less than 50 Hz) are attenuated by greater than two orders of magnitude. The control relies on the absolute position and velocity feedback of the experiment and the absolute position and velocity feed-forward of the platform, and generally derives the stability robustness characteristics guaranteed by the LQR approach to optimality.

The method as derived is extendable to the case in which only the relative positions and the absolute accelerations of the experiment and space platform are available.

Introduction

A space platform experiences local, low frequency accelerations (0.01–30 Hz) due to equipment motions and vibrations, and to crew activity [1, 2], as indicated in Fig. 1 [3]. Certain experiments, such as the growth of isotropic crystals, require an environment in which the accelerations amount to only a few micro-g's [4]. (See Fig. 2 [2].) Microgravity requirements to accommodate such experiments have been specified for Space Station Freedom (SSF). (Fig. 1.) [2] Such an environment is not presently available on manned space platforms [2].

[1]Presented at the Workshop on Aerospace Applications of Magnetic Suspension Technology, September 25–27, 1990, under the title "Microgravity Vibration Isolation: An Optimal Control Law for the One-Dimensional Case."

[2]Department of Mechanical and Aerospace Engineering, University of Virginia, Charlottesville, VA 22901.

[3]NASA Lewis Research Center, Cleveland, OH 44135.

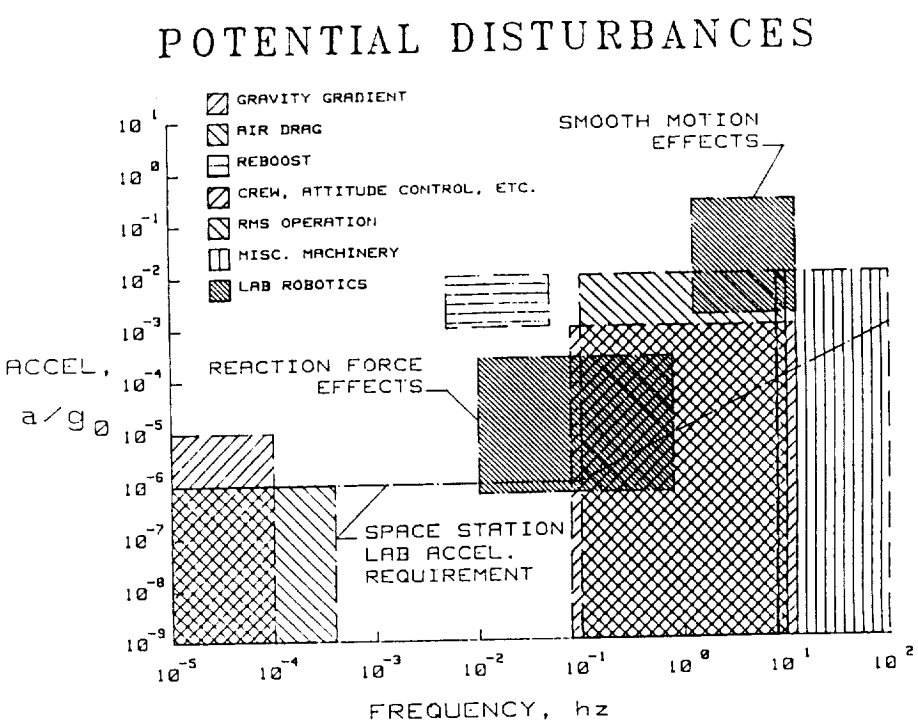

FIG. 1. SSF Microgravity Requirements and Anticipated Acceleration Environment.

Since the experiment and space platform centers of gravity do not coincide, a means is needed to prevent the experiment from drifting into its own orbital motion and into the space platform wall. Additionally, some experiments require umbilicals to provide power, experiment control, coolant flow, communications linkage, or other services. Unfortunately, such measures also mean that unwanted platform accelerations will be transmitted to the experiments. This necessitates experiment isolation. Passive isolators, however, cannot compensate for umbilical stiffness, nor deal adequately with direct disturbances, nor can they achieve low enough corner frequencies even if umbilicals are absent [5]. Active isolation is therefore essential.

The problem, then, is to design an active isolation system to minimize these undesired acceleration transmissions for a tethered payload, while achieving adequate stability margins and system robustness. Spatial and control energy limitations must also be accommodated. Although microgravity isolation systems have been developed and tested [6], no controller offered to date takes into account the effect of umbilicals in isolator control design [7].

Mathematical Model

The general problem has three translational and three rotational degrees of freedom. For simplicity, however, this analysis will consider only the one-dimensional problem. The general problem could be treated in an analogous manner.

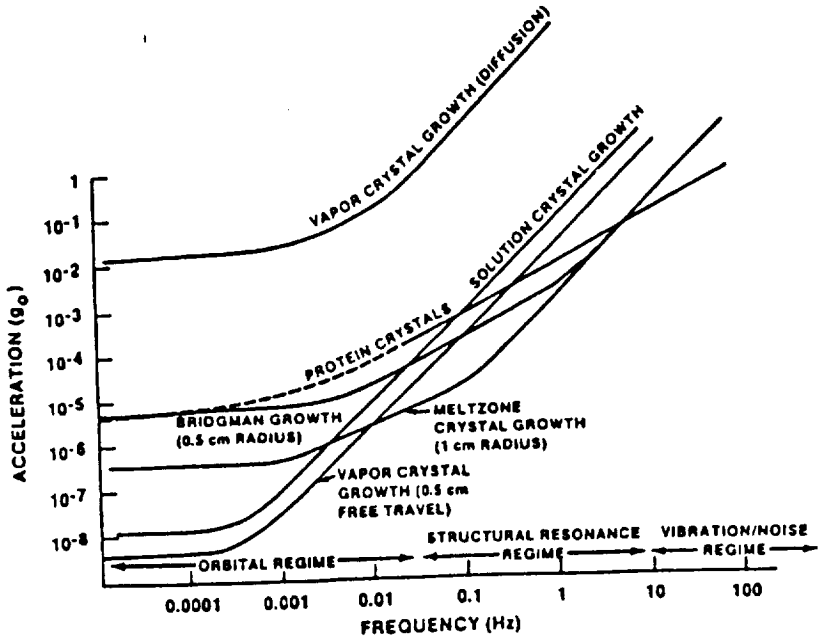

FIG. 2. Experiment Isolation Requirements (Tolerable g-level as a Function of Frequency for a Variety of Materials Science Experiments as Predicted by Order-of-Magnitude Analysis for a Single-Frequency Disturbance [after Demel, 1986, from Nelson, 1991]).

Let the experiment be modeled as a mass m, with position $x(t)$. Assume that the space station has position $d(t)$, and that umbilicals with stiffness k and damping c connect the experiment and space station. Suppose further that a magnetic actuator applies a control force proportional to the applied current $i(t)$, with proportionality constant α. Such a model is shown in Fig. 3.

The system equation of motion is

$$m\ddot{x} + c(\dot{x} - \dot{d}) + k(x - d) + \alpha i = 0 \tag{1}$$

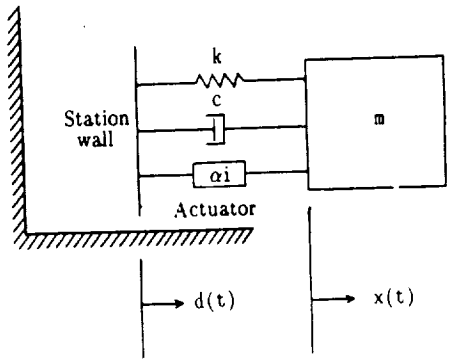

FIG. 3. System Model.

Division by m and rearrangement yields

$$\ddot{x} = -\frac{k}{m}(x - d) - \frac{c}{m}(\dot{x} - \dot{d}) - \frac{\alpha}{m}i \tag{2}$$

In state space notation this becomes

$$\dot{\mathbf{x}} = A\mathbf{x} + \mathbf{b}u + \mathbf{f} \tag{3}$$

where

$$\mathbf{x} = \begin{Bmatrix} x_1 \\ x_2 \end{Bmatrix} = \begin{Bmatrix} x \\ \dot{x} \end{Bmatrix}, \qquad \dot{\mathbf{x}} = \begin{Bmatrix} \dot{x}_1 \\ \dot{x}_2 \end{Bmatrix} = \begin{Bmatrix} \dot{x} \\ \ddot{x} \end{Bmatrix},$$

$$A = \begin{bmatrix} 0 & 1 \\ -\frac{k}{m} & -\frac{c}{m} \end{bmatrix}, \qquad \mathbf{b} = \begin{Bmatrix} 0 \\ -\frac{\alpha}{m} \end{Bmatrix},$$

$$u = i, \qquad \mathbf{f} = \begin{Bmatrix} 0 \\ \frac{k}{m}d + \frac{c}{m}\dot{d} \end{Bmatrix}$$

The objective is to minimize the acceleration $\ddot{x}(t)$.

Optimal Control Problem

The optimal control problem is that of determining the control current $u(t) = i(t)$ which minimizes a suitable performance index

$$J = J(\mathbf{x}, u, t) \tag{4}$$

for the system described by equation (3) subject to the state variable conditions

$$\mathbf{x}(0) = \mathbf{x}_o \tag{5a}$$

$$\lim_{t \to \infty} \mathbf{x}(t) = \mathbf{0} \tag{5b}$$

Another reasonable condition is that $\mathbf{f}(t)$ is bounded, and it will be found mathematically advantageous to assume that $\mathbf{f}(t)$ is also a dwindling function:

$$\lim_{t \to \infty} \mathbf{f}(t) = \mathbf{0} \tag{5c}$$

In actuality, $\mathbf{f}(t)$ is not dwindling, and so neither is $\mathbf{x}(t)$. However, for bounded $\mathbf{f}(t)$ (and a controllable system [8] such as this), the optimal controller developed in this paper has only a vanishing dependence on $\mathbf{f}(t)$ for times in the distant future; and it depends on $\mathbf{x}(t)$ only in a causal fashion. Further, with only minor changes in the performance index [9] (and more complicated mathematics) the dwindling assumptions can be removed without affecting the resulting control, using the basic method of the present paper. [Tomizuka's dynamic programming approach to the command-following problem leads to corresponding results [10].] Hence, the above simplifying assumptions are justified.

A quadratic performance index

$$J = \frac{1}{2}\int_0^\infty [\mathbf{x}^T W_1 \mathbf{x} + w_3 u^2]\, dt \tag{6}$$

has been chosen, as one that lends itself well to the variational approach to optimal controls, since an analytical solution is desired. The upper limit of the definite integral has been selected so as to yield a time-invariant controller. Here W_1 is a square 2×2 constant weighting matrix while w_3 is a weighting constant.

Although W_1 could be a full 2×2 matrix, for this problem a diagonal form has been employed for the sake of simplicity.

$$W_1 = \begin{bmatrix} w_{1a} & 0 \\ 0 & w_{1b} \end{bmatrix} \tag{7}$$

The performance index consequently reduces to

$$J = \frac{1}{2} \int_0^\infty [w_{1a} x_1^2 + w_{1b} x_2^2 + w_3 u^2] dt, \tag{8}$$

so that each state is weighted independently.

If sinusoidal motion of the experiment is considered, so that

$$x(t) = B_1 \sin \omega t$$

and $\ddot{x}(t) = -\omega^2 x(t)$, the cost function can be expressed in terms of the acceleration and control as

$$J = \frac{1}{2} \int_0^\infty \left[\left(\frac{w_{1a}}{\omega^4} + \frac{w_{1b}}{\omega^2} \right) B_1^2 \ddot{x}^2 + w_3 u^2 \right] dt \tag{9}$$

It is apparent that this performance index conveniently weights accelerations at low frequencies much more than at higher frequencies.

Solution

Finding the optimal control to minimize equation (4) is a variational problem of Lagrange, for which the initial steps of the solution are well-known (e.g., Elbert [11]). The variational approach is outlined below, following which the complications added by the nonhomogeneous term $\mathbf{f}(t)$ will be addressed. Current optimal control texts either assume that $\mathbf{f}(t) \equiv \mathbf{0}$ (e.g., [11], p. 262) or require that it have a restricted range space (e.g., [12], p. 238). The solution that follows provides an analytical optimal without imposing such restrictions.

The argument of the cost function J from equation (6) is augmented by the Lagrange multiplier $\boldsymbol{\lambda}$ times the system equation of motion (3) where

$$\lambda = \begin{Bmatrix} \lambda_1 \\ \lambda_2 \end{Bmatrix} \tag{10}$$

The result $\hat{J}$ can be expressed as

$$\hat{J} = \int_0^\infty H dt \tag{11}$$

where the Hamiltonian H is

$$H = \frac{1}{2}(\mathbf{x}^T W_1 \mathbf{x} + w_3 u^2) + \boldsymbol{\lambda}^T(\dot{\mathbf{x}} - A\mathbf{x} - \mathbf{b}u - \mathbf{f}) \tag{12}$$

It is desired to obtain an optimal solution $u = u^*$ which minimizes $\hat{J}$.

The first variation of $\hat{J}(\mathbf{x}, u, \dot{\mathbf{x}})$ is

$$\delta\hat{J} = \int_0^\infty \left[\frac{\partial H}{\partial \mathbf{x}} \delta\mathbf{x} + \frac{\partial H}{\partial u} \delta u + \frac{\partial H}{\partial \dot{\mathbf{x}}} \delta\dot{\mathbf{x}} \right] dt$$

which is set equal to zero to minimize $\hat{J}$. However, integrating by parts,

$$\int_0^\infty \left(\frac{\partial H}{\partial \dot{\mathbf{x}}} \delta\dot{\mathbf{x}} \right) dt = -\int_0^\infty (\dot{\boldsymbol{\lambda}}^T \delta\mathbf{x})\, dt$$

so that the above expression for $\delta\hat{J}$ becomes

$$\delta\hat{J} = \int_0^\infty \left[\left(\frac{\partial H}{\partial \mathbf{x}} - \dot{\boldsymbol{\lambda}}^T \right) \delta\mathbf{x} + \frac{\partial H}{\partial u} \delta u \right] dt = 0 \tag{13}$$

Both $\delta\mathbf{x}$ and δu are arbitrary variations, so $\delta\hat{J} = 0$ only if

$$\frac{\partial H}{\partial \mathbf{x}} = \dot{\boldsymbol{\lambda}}^T \tag{14a}$$

$$\frac{\partial H}{\partial u} = 0 \tag{14b}$$

The conditions given by equation (5) still apply.

Solving equations (14a) and (14b) yields

$$\dot{\boldsymbol{\lambda}} = W_1 \mathbf{x} - A\boldsymbol{\lambda} \tag{15a}$$

$$u^* = \frac{1}{w_3} \boldsymbol{\lambda}^T \mathbf{b} = \frac{1}{w_3} \mathbf{b}^T \boldsymbol{\lambda} \tag{15b}$$

Temporarily eliminating u* produces the result

$$\begin{Bmatrix} \dot{\mathbf{x}} \\ \boldsymbol{\lambda} \end{Bmatrix} = \hat{A} \begin{Bmatrix} \mathbf{x} \\ \boldsymbol{\lambda} \end{Bmatrix} + \begin{Bmatrix} \mathbf{f} \\ \mathbf{0} \end{Bmatrix} \tag{16}$$

where

$$\hat{A} = \left[\begin{array}{c|c} A & \frac{1}{w_3} \mathbf{b}\mathbf{b}^T \\ \hline W_1 & -A^T \end{array} \right]$$

If equation (16) is now solved for $\boldsymbol{\lambda}$ in terms of $\mathbf{x}$ and $\mathbf{f}$, equation (15b) will then furnish an expression for the optimal control u^*.

As noted before, optimal control texts generally treat the homogeneous problem (where $\mathbf{f}(t) \equiv \mathbf{0}$), but they do not provide an analytical solution to the nonhomogeneous system described by equations (5) and (16). Salukvadze has treated the nonhomogeneous problem [13, 14], but his difficult treatment seems largely to have remained either uncomprehended or under-appreciated. This method is especially well-suited to low-frequency disturbance rejection, and has been applied below to the present problem.

The homogeneous solution to equation (15), where $\mathbf{f} = \mathbf{0}$, is

$$\begin{Bmatrix} \mathbf{x} \\ \boldsymbol{\lambda} \end{Bmatrix}_h = e^{\hat{A}t} \begin{Bmatrix} \mathbf{x}_0 \\ \boldsymbol{\lambda}_0 \end{Bmatrix} \tag{17}$$

The four eigenvalues of $\hat{A}$ may be found to be, in ascending order of real parts,

$$\mu_1 = -\left(\frac{-\beta_1 + (\beta_1^2 - 4\beta_2)^{1/2}}{2} \right)^{1/2} \tag{18a}$$

$$\mu_2 = -\left(\frac{-\beta_1 - (\beta_1^2 - 4\beta_2)^{1/2}}{2} \right)^{1/2} \tag{18b}$$

$$\mu_3 = -\mu_1 \tag{18c}$$

$$\mu_4 = -\mu_2 \tag{18d}$$

where β_1 and β_2 are defined as follows:

$$\beta_1 = \frac{2k}{m} - \frac{c^2}{m^2} - \frac{\alpha w_{1b}}{m w_3} \tag{19a}$$

and

$$\beta_2 = \beta_1^2 - 4\left(\frac{\alpha^2 w_{1a}}{m^2 w_3} + \frac{k}{m^2} \right) \tag{19b}$$

The eigenvectors of $\hat{A}$ corresponding to the respective eigenvalues μ_k may be chosen to be

$$\mathbf{P}_k = \begin{Bmatrix} 1 \\ \mu_k \\ \dfrac{\gamma_4}{\mu_k} + \dfrac{\gamma_1^2}{\gamma_3 \mu_k} + \dfrac{\gamma_1(\gamma_2 + \mu_k)}{\gamma_3} \\ \dfrac{\gamma_1 + (\gamma_2 + \mu_k)\mu_k}{\gamma_3} \end{Bmatrix} \tag{20a}$$

where γ_1, γ_2, γ_3, and γ_4 are defined below:

$$\gamma_1 = \frac{k}{m} \tag{20b}$$

$$\gamma_2 = \frac{c}{m} \tag{20c}$$

$$\gamma_3 = \frac{\alpha^2}{m^2 w_3} \tag{20d}$$

$$\gamma_4 = w_{1a} \tag{20e}$$

Using equations (18) through (20) with equation (17) the solution to the homoge-

neous system is

$$\begin{Bmatrix} \mathbf{x} \\ \boldsymbol{\lambda} \end{Bmatrix}_h = \begin{Bmatrix} c_1 e^{\mu_1 t}\mathbf{p}_{1_1} + c_2 e^{\mu_2 t}\mathbf{p}_{2_1} + c_3 e^{-\mu_1 t}\mathbf{p}_{3_1} + c_4 e^{-\mu_2 t}\mathbf{p}_{4_1} \\ c_1 e^{\mu_1 t}\mathbf{p}_{1_2} + c_2 e^{\mu_2 t}\mathbf{p}_{2_2} + c_3 e^{-\mu_1 t}\mathbf{p}_{3_2} + c_4 e^{-\mu_2 t}\mathbf{p}_{4_2} \end{Bmatrix} \tag{21}$$

with $\mathbf{p}_k = \{\mathbf{p}_{k_1}^T \mathbf{p}_{k_2}^T\}^T$, $k = 1, \ldots, 4$ and where $c_1, \ldots, c_4$ are arbitrary constants.

Application of the variation of parameters method with the terminal conditions (5b, c) leads to the general solution of the non-homogeneous system, with two constants of integration yet undetermined.

If the two constants of integration are eliminated by solving for $\boldsymbol{\lambda}$ in terms of $\mathbf{x}$ and $\mathbf{f}$, the general solutions for λ_1 and λ_2 become:

$$\lambda_1 = \xi_1 x_1 + \xi_2 x_2 + \xi_3 e^{-\mu_1 t} + \xi_4 e^{-\mu_2 t} \tag{22a}$$

$$\lambda_2 = \xi_5 x_1 + \xi_6 x_2 + \xi_7 e^{-\mu_1 t} + \xi_8 e^{-\mu_2 t} \tag{22b}$$

in which the ξ_i's are functions of the eigenvalues and eigenvectors of $\hat{A}$, and of the disturbance $\mathbf{f}(t)$.

The Solution Form

Using the fact that

$$u^*(t) = \frac{1}{w_3}\mathbf{b}^T\boldsymbol{\lambda} \quad \text{[cf. (15b)]} \tag{23}$$

the optimal control is found to be

$$u^*(t) = \eta_1 x_1 + \eta_2 x_2 + \eta_3 e^{-\mu_1 t}\int e^{\mu_1 t} f_2(t)\,dt + \eta_4 e^{-\mu_2 t}\int e^{\mu_2 t} f_2(t)\,dt \tag{24a}$$

where

$$\eta_1 = \frac{-m}{\alpha}\left(\frac{k}{m} - \mu_1\mu_2\right) \tag{24b}$$

$$\eta_2 = \frac{-m}{\alpha}\left(\frac{c}{m} + \mu_1 + \mu_2\right) \tag{24c}$$

$$\eta_3 = \frac{m}{\alpha}\left(\frac{1}{\mu_1 - \mu_2}\right)\left(\mu_1^2 + \frac{c}{m}\mu_1 + \frac{k}{m}\right) \tag{24d}$$

$$\eta_4 = -\frac{m}{\alpha}\left(\frac{1}{\mu_1 - \mu_2}\right)\left(\mu_2^2 + \frac{c}{m}\mu_2 + \frac{k}{m}\right) \tag{24e}$$

(It should be noted that the feedback gains η_1 and η_2 are those which would result from applying standard LQR theory to the homogeneous system equation $\dot{\mathbf{x}} = A\mathbf{x} + \mathbf{b}u$.) In equation (24) μ_1 and μ_2 are the eigenvalues of $\hat{A}$ with negative real parts, [see equations (18a, b)] and

$$f_2(t) = \frac{k}{m}d + \frac{c}{m}\dot{d}. \tag{24f}$$

For $\mu_1 = \mu_2 = \mu$ [the critically damped case] equations (24a–e) reduce to

$$u^*(t) = \frac{1}{\alpha}(m\mu^2 - k)x_1 + \frac{1}{\alpha}(2m\mu - c)\left[x_2 - e^{-\mu t}\int e^{\mu t} f_2(t)\,dt\right]$$

By repeated application of the method of integration by parts, the control may be re-expressed in terms of an infinite sum:

$$u^*(t) = \eta_1 x_1 + \eta_2 x_2 + \eta_3\left(\sum_{r=0}^{\infty}\frac{(-1)^r f_2^{(r)}(t)}{\mu_1^{r+1}}\right) + \eta_4\left(\sum_{r=0}^{\infty}\frac{(-1)^r f_2^{(r)}(t)}{\mu_2^{r+1}}\right) \tag{25}$$

Rewriting f_2 in terms of d and $\dot{d}$, the control function becomes

$$\begin{aligned} u^*(t) = {} & \eta_1 x(t) + \eta_2 \dot{x}(t) + \left[\frac{k}{m}\left(\frac{\eta_3}{\mu_1} + \frac{\eta_4}{\mu_2}\right)\right] d(t) \\ & + \sum_{i=1}^{n-1}\left[(-1)^{i-1}\frac{c}{m}\left(\frac{\eta_3}{\mu_1^i} + \frac{\eta_4}{\mu_2^i}\right) + (-1)^i\frac{k}{m}\left(\frac{\eta_3}{\mu_1^{i+1}} + \frac{\eta_4}{\mu_2^{i+1}}\right) d^{(i)}(t)\right. \\ & + \left[(-1)^{n-1}\frac{c}{m}\left(\frac{\eta_3}{\mu_1^n} + \frac{\eta_4}{\mu_2^n}\right)\right] d^{(n)}(t) + \text{higher order terms} \end{aligned} \tag{26}$$

This may be written in a more appealing form as

$$u^*(t) = c_p x(t) + c_v \dot{x}(t) + c_{d0} d(t) + c_{d1}\dot{d}(t) + \text{higher order terms} \tag{27}$$

in which the constant coefficients c_p, c_v, c_{d0}, and c_{d1} may be defined from equations (24) and (26). Clearly, if the infinite sums converge rapidly enough, the optimal control can be approximated by

$$u^*(t) = c_p x(t) + c_v \dot{x}(t) + c_{d0} d(t) + c_{d1}\dot{d}(t) \tag{28}$$

For very low frequency disturbances the higher order terms in equation (26) are negligibly small, and the control (28) closely approximates the optimal. If, in fact, the second- and higher-order derivatives of $d(t)$ are identically zero, the approximation is exact. It can be shown that for the critically damped closed loop system the eigenvalues are real and equal, and that the convergence is more rapid than for the overdamped system. Further, as the closed-loop system eigenvalues become more negative the convergence speed goes up as well.

Control Evaluation

Physical Realizability of the Control

The control (25) is physically realizable, if the states and sufficient derivatives of $d(t)$ are accessible (or estimable by an observer), and if the higher order terms are negligible. It is not necessary that the eigenvalues be real, although the proof of this requires a more general linear-algebra or state-transition-matrix approach.

If values are assigned to the system parameters, associated controller gains can be evaluated. Suppose that m = 100 lbm, k = 0.3 lbf/ft, c = 0 lbf-sec/ft, and α = 10 lbf/Amp. With w_3 arbitrarily set at 1 and w_{1b} varied, associated integer values of w_{1a} can be found below which the eigenvalues μ_1 and μ_2 will always be real. Such values are tabulated in Table 1. Stated otherwise, the tabulated values of the weights w_{1a} and w_{1b} are those integer values (for the sake of simplicity) for

TABLE 1. Optimal F/B and F/F Gains for Selected State Variable and Control Weightings System Parameters: m = 100 lbm, c = 0.000622 lbf-sec/ft (ζ = 0.1%), k = 0.3 lbf/ft, α = 10 lbf/amp

Weights			F/B Gains		F/F Gains					
w_{1a}	w_{1b}	w_3	C_p	C_v	C_{d0}	C_{d1}	C_{d2}	C_{d3}	C_{d4}	C_{d5}
2	1	1	1.3845	1.3637	0.0294	-0.0006	-0.0070	-0.0067	-0.0049	-0.0032
10	2	1	3.1324	1.9863	0.0297	-0.0001	-0.0030	-0.0019	-0.0009	-0.0004
23	3	1	4.7659	2.4413	0.0298	-0.0000	-0.0020	-0.0010	-0.0004	-0.0001
41	4	1	6.3732	2.8210	0.0299	0.0000	-0.0015	-0.0007	-0.0002	-0.0001
64	5	1	7.9701	3.1544	0.0299	0.0000	-0.0012	-0.0005	-0.0001	-0.0000
92	6	1	9.5617	3.4552	0.0299	0.0000	-0.0010	-0.0004	-0.0001	-0.0000
126	7	1	11.1950	3.7354	0.0299	0.0000	-0.0008	-0.0003	-0.0001	-0.0000
165	8	1	12.8153	3.9949	0.0299	0.0000	-0.0007	-0.0002	-0.0001	-0.0000
209	9	1	14.4269	4.2380	0.0299	0.0000	-0.0006	-0.0002	-0.0000	-0.0000
258	10	1	16.0324	4.4674	0.0299	0.0000	-0.0006	-0.0002	-0.0000	-0.0000
581	15	1	24.0740	5.4729	0.0300	0.0001	-0.0004	-0.0001	-0.0000	-0.0000
1034	20	1	32.1259	6.3209	0.0300	0.0001	-0.0003	-0.0001	-0.0000	-0.0000
1617	25	1	40.1819	7.0680	0.0300	0.0001	-0.0002	-0.0000	-0.0000	-0.0000
2329	30	1	48.2297	7.7431	0.0300	0.0001	-0.0002	-0.0000	-0.0000	-0.0000
3171	35	1	56.2816	8.3640	0.0300	0.0001	-0.0002	-0.0000	-0.0000	-0.0000
4143	40	1	64.3361	8.9420	0.0300	0.0001	-0.0001	-0.0000	-0.0000	-0.0000
9325	60	1	96.5360	10.9526	0.0300	0.0001	-0.0001	-0.0000	-0.0000	-0.0000

which the closed loop system is closest to being critically damped without being underdamped. Corresponding controller feedback and feed-forward gains (for the first five derivatives) are also included.

The states $x(t)$ and $\dot{x}(t)$ and the derivatives $d^{(0)}(t)$, $d^{(1)}(t)$, and $d^{(2)}(t)$ are clearly available for an Earth-based system. However, in space, the only absolute measurements which can be directly available are $\ddot{x}(t)$ and $\ddot{d}(t)$, from which $\dot{x}(t)$, $\dot{d}(t)$ and $x(t)$, $d(t)$ are obtainable only by successive integration(s). Rearrangement of equation (28) into

$$u^*(t) = (c_p + c_{d0})x(t) + (c_v + c_{d1})\dot{x}(t) - c_{d0}[x(t) - d(t)] - c_{d1}[\dot{x}(t) - \dot{d}(t)] \quad (29)$$

or

$$u^*(t) = (c_p + c_{d0})d(t) + (c_v + c_{d1})\dot{d}(t) + c_p[x(t) - d(t)] + c_v[\dot{x}(t) - \dot{d}(t)] \quad (30)$$

obviates the need for one accelerometer, but one accelerometer plus two integrations remain necessary for either the platform or the experiment. Since $[x(t) - d(t)]$ (or one of its integrals) has not been weighted in the performance

index J, experiment drift will be a problem that must be corrected either by another control loop or by a change of system states. The latter could be accomplished by incorporating an accelerometer attached to the experiment into the state equation. Alternatively, one could append an integrator to the plant, include the current $i(t)$ as a third state, and optimize the control di/dt. But for the sake of simplicity (i.e., fewer states) the former has been assumed (without development) in this paper.

The higher order terms of the control [equations (25) and (26)] can be neglected, for low frequencies, if the eigenvalues μ_1 and μ_2 are of sufficient modulus. These eigenvalues, in turn, are under the control of the designer, determined by his choice of weights w_{1a}, w_{1b}, and w_3. It is apparent from equation (25) that $u^*(t)$ essentially reduces to two alternating power series. For a sinusoidal disturbance of frequency ω the series form of the control converges for $|\omega/\mu_i| < 1$ $(i = 1, 2)$. It can be shown that each alternating power series converges like $\Sigma_{r=0}^{\infty}(-1)^r(\omega/\mu)^{2r}$. With "low" frequency disturbances (i.e., small relative to system closed loop eigenvalues) a control formed by series truncation very closely approximates the optimal.

For example, suppose that the normalized frequencies $|\omega/\mu_i|$ for a sinusoidal disturbance are less than 1/5, and that only the feedforward control terms $c_{d0}d(t)$ and $c_{d1}\dot{d}(t)$ are included with the feedback terms. Even so, the feedforward portion of the truncated control, at any time t, will be a current that is still within 4% [i.e., $(1/5)^2$] of the feedforward portion of the actual optimal. If the normalized frequencies are below 1/10, this approximation error will be less than 1%. Table 1 shows that the gains c_{di} of higher order derivatives $d^{(i)}(t)$ [see equation (26) for algebraic representations] are, in fact, quite small.

In some circumstances there may be design constraints which prevent the designer from selecting weights that will lead to sufficiently rapid convergence. However, since convergence occurs rapidly even for eigenvalues of relatively small modulus ($|\omega/\mu_i| < 1/3$), in a great many cases the designer will have much latitude in his choice of weights. For "low" frequency disturbances, in these cases, a control which includes only one or two feedforward terms will be "close" to the optimal. These frequencies will be well-attenuated.

Higher frequency disturbances will also be well-attenuated, *provided* the input-to-output transfer function(s) are proper in the Laplace Transform variable s. This will *not* be the case for the present problem if more than three feedforward gains (c_{d0}, c_{d1}, c_{d2}) are included in the control. Practically, this means that only proportional and first-derivative feedforward [equation (25) with $r = 0, 1$ or equation (26) with $n = 2$] should be added to the feedback control terms. As will be seen shortly, however, adding even the proportional feedforward term(s) can dramatically improve the disturbance rejection over that afforded by LQR feedback alone.

Transfer Function and Block Diagram

Neglecting the higher order terms, the transfer function between input and output accelerations or displacements is

$$\frac{s^2X(s)}{s^2D(s)} = \frac{X(s)}{D(s)} = \frac{\left(\frac{c}{\alpha} - c_{d1}\right)s + \left(\frac{k}{\alpha} - c_{d0}\right)}{\left(\frac{m}{\alpha}\right)s^2 + \left(\frac{c}{\alpha} + c_v\right)s + \left(\frac{k}{\alpha} + c_p\right)} \tag{31}$$

and a block diagram of the controlled system can be drawn as in Fig. 4.

Control Stability, Stability Robustness, and General Robustness

Since the control feedback gains are the same as those obtained by solution of the standard Linear Quadratic Regulator (LQR) problem, the closed loop system is stable and enjoys the stability robustness characteristics guaranteed by the (LQR) approach to optimality, viz., a minimum of 60° phase margin, infinite positive gain margin, and 6 dB negative gain margin [12]. Additionally, numerical checks indicate that it enjoys substantial insensitivity, or general robustness to uncertainties in k, c, and m, as indicated by Table 2 and Figs. 5 through 12. By comparing the Bode plots of Figs. 5, 7, 9, and 11 (corresponding to controls using both LQR F/B and proportional F/F) with those of Figs. 6, 8, 10, and 12, respectively (corresponding to controls using LQR F/B only), one can see that adding feed-forward substantially improves disturbance rejection at low frequencies. For example a comparison of Fig. 5 with Fig. 6 indicates that the optimal control method described above can lead to acceleration reductions of greater than four orders of magnitude for all frequencies. This reduction is more than two orders of magnitude below that afforded by LQR feedback alone at the lower frequencies, i.e., those most heavily weighted in the performance index.

The order of the reduction is eventually limited by control cost, of course, probably in terms either of actuator-related limitations (such as heat-removal or force-generation requirements) or of power limitations (especially in a space-

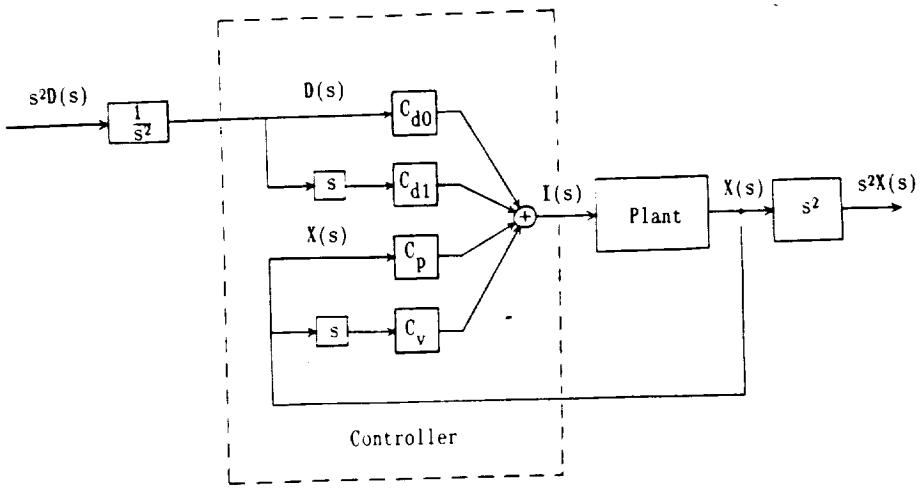

FIG. 4. System Block Diagram.

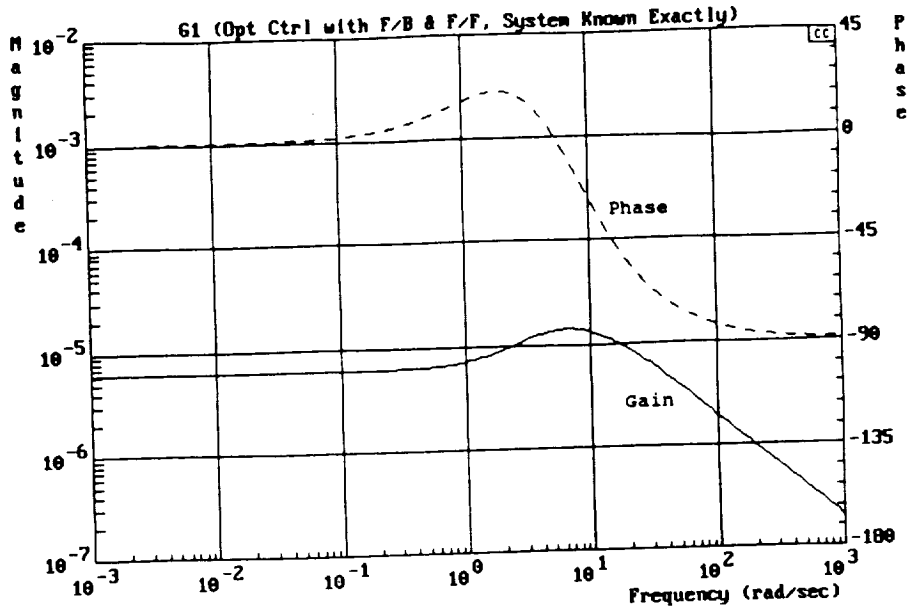

FIG. 5. Bode Plots of Transfer Function G1 (Optimal Control with LQR F/B and Proportional F/F, System Known Exactly).

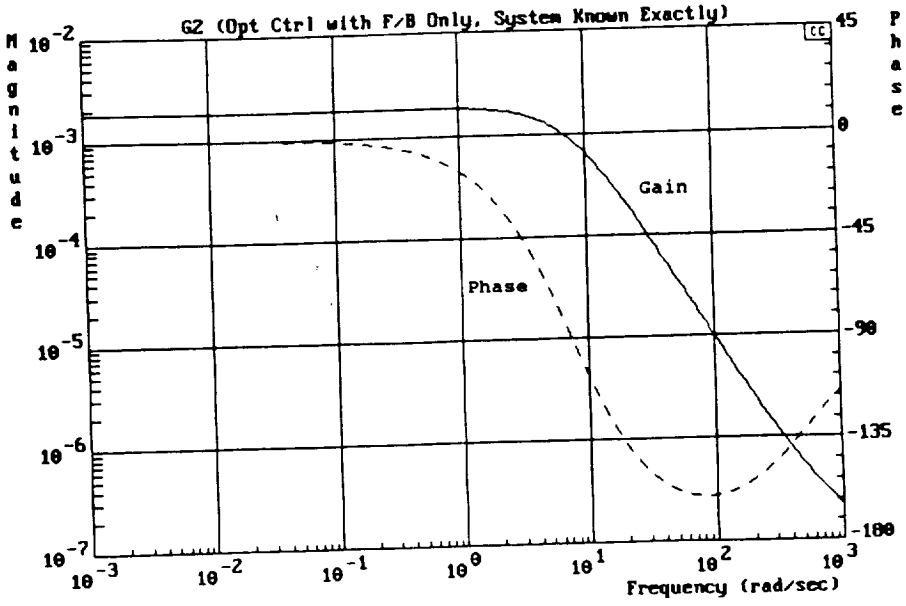

FIG. 6. Bode Plots of Transfer Function G2 (Optimal Control with LQR F/B Only, System Known Exactly).

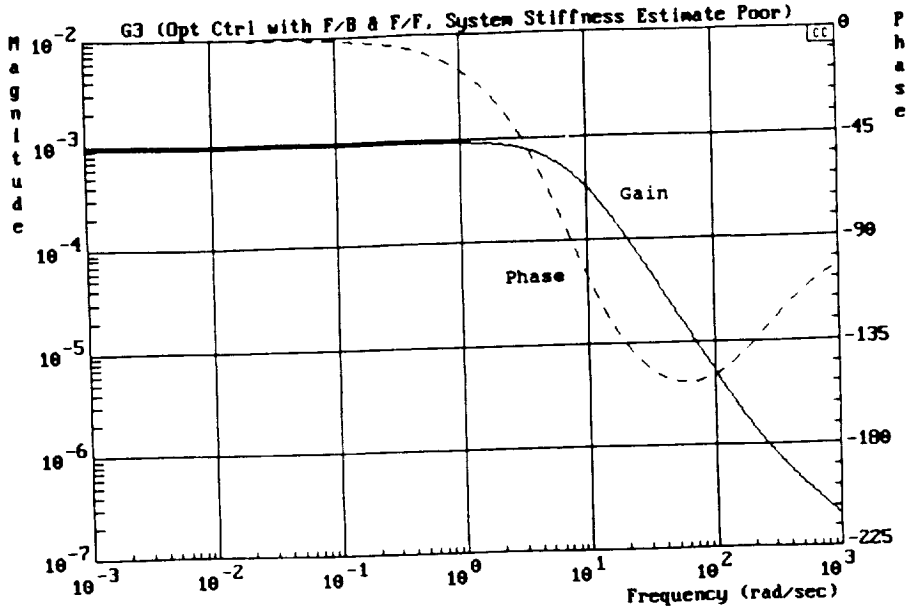

FIG. 7. Bode Plots of Transfer Function G3 (Optimal Control with F/B and F/F, System Stiffness Estimate Poor).

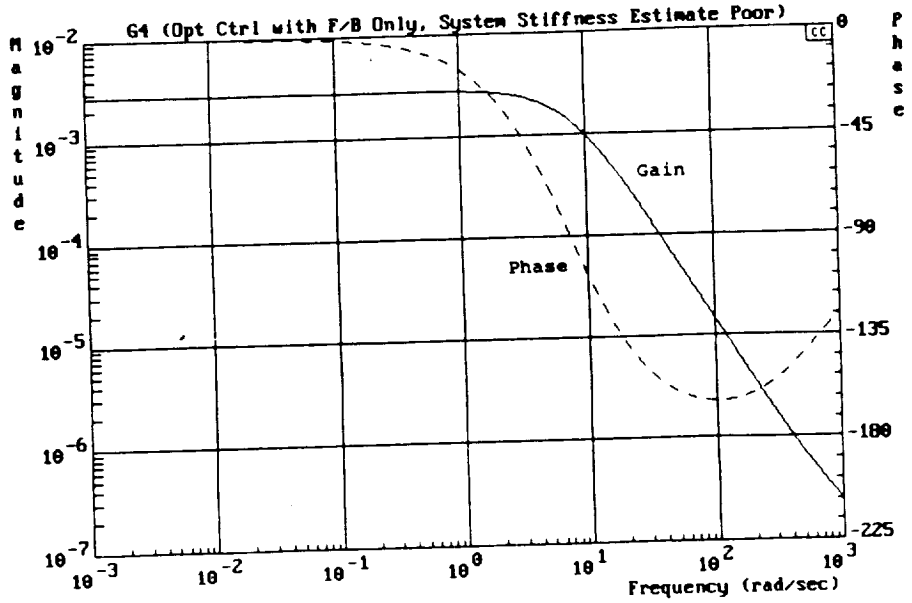

FIG. 8. Bode Plots of Transfer Function G4 (Optimal Control with F/B Only, System Stiffness Estimate Poor).

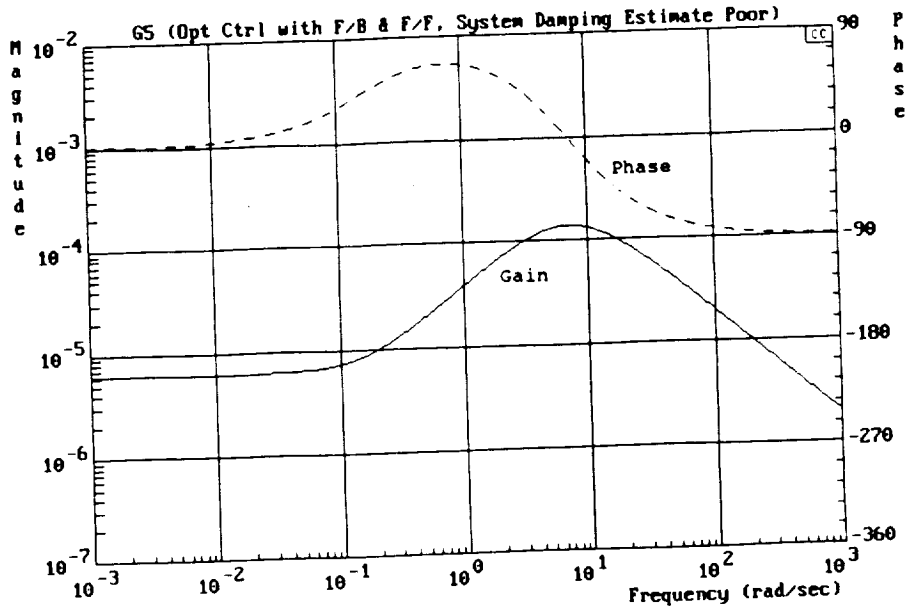

FIG. 9. Bode Plots of Transfer Function G5 (Optimal Control with F/B and F/F, System Damping Estimate Poor).

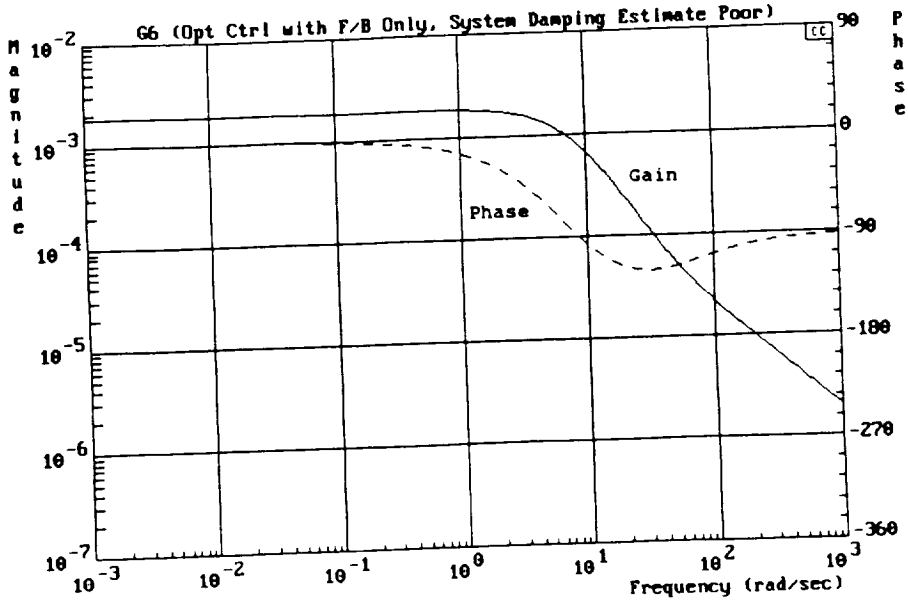

FIG. 10. Bode Plots of Transfer Function G6 (Optimal Control with F/B Only, System Damping Estimate Poor).

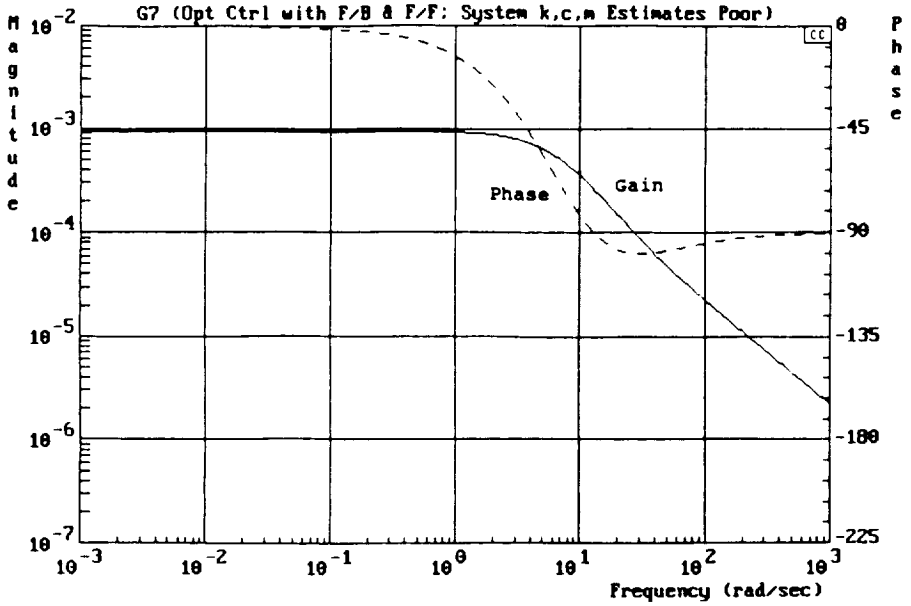

FIG. 11. Bode Plots of Transfer Function G7 (Optimal Control with F/B and F/F, System k, c, m Estimates Poor).

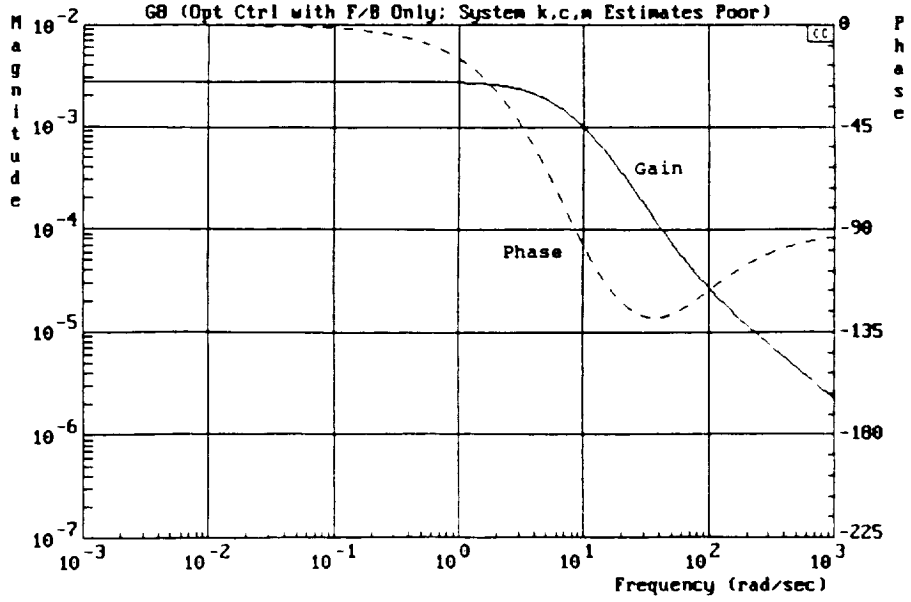

FIG. 12. Bode Plots of Transfer Function G8 (Optimal Control with F/B Only, System k, c, m Estimates Poor).

Concluding Remarks

This paper has applied an existing method for obtaining an optimal control to the microgravity platform isolation problem, for which the disturbances to be rejected are low-frequency accelerations. The system was assumed to be representable in the form $\dot{\mathbf{x}} = A\mathbf{x} + \mathbf{b}u + \mathbf{f}$, with quadratic cost function $J = \frac{1}{2}\int_0^\infty (\mathbf{x}^T W_1 \mathbf{x} + w_3 u^2)\, dt$ and diagonal weighting matrix W_1. The resultant control law was found to be simple, stable, robust, and physically realizable. Further it was shown to have excellent acceleration- and displacement-attenuation characteristics, and to be frequency-weighted toward the low end of the acceleration spectrum.

By making an appropriate choice of states, along with the use of frequency weighting, the method can be extended to the case for which only relative positions and absolute accelerations are available. With this extension one can then weight relative displacements in the performance index. [9] Additionally, since absolute positions and velocities will then not appear as states, accelerometer drift (which affects integrations) will no longer be problematic. Any one of a number of noncontacting relative displacement sensors would be suitable for this application (e.g., eddy current probes, photoelectric sensors, capacitance probes, Hall-effect probes).

The approach as presented is algebraically intensive, but symbolic manipulators can be used to ease the algebraic labors. Further, since the method produces feedback gains identical to those obtained by the LQR approach to optimality, numerical computation to those gains is easily accomplished, even for large systems. The feed-forward gains can be found numerically with comparable ease.

Acknowledgments

The authors would like to recognize NASA for partial funding of this work, Dr. Eric Maslen at the University of Virginia for his many helpful control-related suggestions at problem points and regarding future work, and Dr. Gerald Brown of NASA Lewis for his insights into the microgravity isolation problem in an orbital environment.

References

[1] HAMACHER, H., JILG, R., and MERBOLD, U. "Analysis of Microgravity Measurements Performed During D1," 6th European Symposium on Materials Sciences Under Microgravity Conditions, Bordeaux, December 2–5, 1986.

[2] NELSON, E. S. "An Examination of Anticipated g-Jitter on Space Station and Its Effects on Materials Processes," NASA TM-103775, April 1991.

[3] HOSHI, SEIKO "Summary of NASDA Activities in Vibration Isolation Technology," *Proceedings of the International Workshop on Vibration Isolation Technology for Microgravity Science Applications*, NASA Lewis Research Center, Cleveland, Ohio, April 23–25, 1991.

[4] ALEXANDER, J. IRWAN D. "Experiment Sensitivity: Determination of Requirements for Vibration Isolation," Vibration Isolation Technology Workshop, NASA Lewis Research Center, September 28–29, 1988.

[5] GRODINSKY, CARLOS M. "Development and Approach to Low-Frequency Microgravity Isolation Systems," NASA Technical Paper 2984, August 1990.

[6] ALLAN, A. P., and KNOSPE, C. R. "A Six Degree-of-Freedom Magnetic Bearing for Microgravity Vibration Isolation," *Proceedings of the International Symposium on Magnetic Suspension Technology*, NASA Langley Research Center, Hampton, Virginia, August 19–23, 1991.

[7] KNOSPE, C. R., HAMPTON, R. D., and ALLAIRE, P. E. "Control Issues of Microgravity Vibration Isolation," *Acta Astronautica*, Vol. 25, No. 11, November 1991, pp. 687–697.

[8] SAGE, A. P., and WHITE, C. C., III *Optimum Systems Control*, 2nd edition, Prentice Hall, Inc., Englewood Cliffs, New Jersey, 1977.

[9] HAMPTON, R. DAVID, and KNOSPE, CARL R. "Extended H2 Synthesis for Multiple-Degree-of-Freedom Controllers," *Proceedings of the International Symposium on Magnetic Suspension Technology*, NASA Langley Research Center, Hampton, Virginia, August 19–23, 1991.

[10] TOMIZUKA, M. "Optimal Continuous Finite Preview Problem," *IEEE Transactions on Automatic Control*, Vol. AC-20, No. 3, June 1975, pp. 362–365.

[11] ELBERT, THEODORE F. *Estimation and Control of Systems*, Van Nostrand Reinhold Company Inc., New York, 1984, chapter 6: "Optimal Control of Dynamic Systems."

[12] ANDERSON, B. D. O., and MOORE, J. B. *Linear Optimal Control*, Prentice Hall, Englewood Cliffs, New Jersey, 1971, pp. 70–74.

[13] SALUKVADZE, M. E. "Analytic Design of Regulators (Constant Disturbances)," *Avtomatika i Telemakhanika*, Vol. 22, No. 10, February 1961, pp. 1279–1287; translation in *Automation and Remote Control*, Vol. 22, No. 10, October 1961, pp. 1147–1155.

[14] SALUKVADZE, M. E. "The Analytical Design of an Optimal Control in the Case of Constantly Acting Disturbances," *Avtomatika i Telemakhanika*, Vol. 23, No. 6, July 1962, pp. 721–731; translation in *Automation and Remote Control*, Vol. 23, No. 6, June 1962, pp. 657–667.

[15] POTTER, J. E. "Matrix Quadratic Solutions," *SIAM Journal of Applied Mathematics*, Vol. 14, No. 3, May 1966, pp. 496–501.

[16] LAUB, A. J. "A Schur method for solving algebraic Riccati equations," *IEEE Transactions on Automatic Control*, Vol. AC-24, No. 6, December 1979, pp. 913–921.

EXTENDED H_2 SYNTHESIS FOR MULTIPLE DEGREE–OF–FREEDOM CONTROLLERS

R. David Hampton
Carl R. Knospe

Center for Innovative Technology
University of Virginia

August 16, 1991

SUMMARY

H_2 synthesis techniques are developed for a general multiple–input–multiple–output (MIMO) system subject to both stochastic and deterministic disturbances. The H_2 synthesis is extended by incorporation of anticipated disturbance power–spectral–density information into the controller–design process, as well as by frequency weightings of generalized coordinates and control inputs. The methodology is applied to a simple single–input–multiple–output (SIMO) problem, analogous to the type of vibration isolation problem anticipated in microgravity research experiments.

INTRODUCTION

The vibration environment onboard current and planned manned orbiters requires isolation for microgravity science experiments. The disturbance frequencies are sufficiently low, and the attenuation requirements sufficiently great, so as to preclude a solely passive isolation system (ref. 1).

Since the disturbances to be attenuated are three–dimensional (ref 2, p.2), the isolation actuator must be capable of acting over six degrees of freedom. The requisite multiple–degree–of–freedom (MDOF) controller is much more difficult to design than a single–degree–of–freedom (SDOF) controller, because the isolation system has many inputs (actuator forces) and outputs (measured displacements and accelerations). Multiple–input–multiple–output (MIMO) designs can be very susceptible to unmodeled cross–coupling between channels of input or output (ref. 3), a problem not encountered in SDOF design. The control forces used must therefore be properly coordinated if the controller's performance is to be sufficiently insensitive to unmodeled dynamics (i.e., *robust*). The design of a robust MIMO control system requires the iterative use of synthesis and analysis tools, the former for controller design and the latter for system performance and stability evaluation (ref. 4).

A particular vibration isolation problem may involve different kinds of undesirable outputs, such as excessive absolute accelerations and unacceptable relative displacements. Some of these undesired outputs may be more important than others, and the degree of undesirability may vary with direction or frequency. For example, rattlespace constraints may be highly directional. Or a crystal–growth experiment may be particularly sensitive to accelerations at certain frequencies (ref. 2, p. 7) or in certain directions. One of the

goals, then, must be to design a controller capable of minimizing selected plant outputs as dictated by these considerations.

Plant outputs, however, cannot be minimized apart from consideration of the associated control costs, because any active control both consumes power and releases heat. Since both of these costs are of concern in a space environment, the control effort used should not be excessive. And at higher frequencies control effort should also be minimized in order to limit controller bandwidth for the sake of robustness concerns (ref. 5, p. 218).

This paper describes a design procedure, known as extended H_2 synthesis (ref. 5, p. 267), for developing active isolation system controllers. A single–input–multiple–output design problem is then addressed using the presented procedure.

BASIC PROBLEM AND SOLUTION

Problem Statement

We will use Linear Quadratic Gaussian (LQG) theory to design the MDOF controller. This theory has been extensively studied and ussed. LQG is chosen as a synthesis procedure since the quadratic performance index relates well to root–mean–square statistics and power spectral density.

When linearized, the differential equations of motion of the plant can be representable in state–space form by the first order system of equations

$$\dot{\underline{x}} = A\underline{x} + B\underline{u} + E_d\underline{f}_d + E_s\underline{w}_s \quad (1a)$$
$$\underline{y} = C\underline{x} + D\underline{u} \quad (1b)$$
$$\underline{z} = \underline{y} + M\underline{n} \quad (1c)$$

where $\underline{x}$ is the state vector, $\underline{y}$ is the output vector, $\underline{z}$ is the measurement vector, $\underline{u}$ is the control vector, $\underline{f}_d$ is a known or measurable disturbance vector, and $\underline{w}_s$ and $\underline{n}$ are process– and sensor noise respectively. We begin by making a series of reasonable mathematical assumptions. Assume that not all states are accessible, so that rank $C \leq \dim \underline{x}$. Let the initial conditions on the state vector be $\underline{x}(0) = \underline{x}_0$; let $\underline{x}_0$, $\underline{w}_s$, $\underline{n}$, and $\underline{f}_d$ be independent and bounded; let $\underline{x}_0$ be Gaussian (ref. 6, p. 272); and let $\underline{n}$ and $\underline{w}_s$ be zero–mean white Gaussian, with $\mathrm{cov}[\underline{w}_s(t),\underline{w}_s(\tau)] = V_1\delta(t-\tau)$ and $\mathrm{cov}[\underline{n}(t), \underline{n}(\tau)] = V_3\delta(t-\tau)$ (ref. 6, p. 272). Assume that $\{A,B\}$ and $\{A,E_s\ V_1^{1/2}\}$ are stabilizable, where $V_1 = V_1^{1/2}\ V_1^{1/2*}$ (the asterisk here means "conjugate transpose"); and that $\{C,A\}$ is detectable (ref. 5, p. 226). Let V_1 and V_3 be positive semidefinite (PSD) and positive definite (PD), respectively.

We choose a performance index of the form

$$J = \mathscr{E}\left\{\lim_{T\to\infty} \frac{1}{T}\int_0^T \left\langle [\underline{x}'\ \underline{u}'] \begin{bmatrix} W_1 & W_2 \\ W_1' & W_3 \end{bmatrix} \begin{Bmatrix} \underline{x} \\ \underline{u} \end{Bmatrix} \right\rangle dt\right\} \quad (2)$$

where W_1 is PSD and W_3 is PD (ref. 6; pp. 272, 276). "$\mathscr{E}$" is the expected–value operator, needed since the system is excited stochastically by $\underline{w}_s$. The cost rate functional form

(with "$\lim_{T\to\infty} \frac{1}{T}$") is used to allow both for the white noise disturbance $\underline{w}_s$ and for the non-dwindling disturbance $\underline{f}_d$.

If $\underline{Z}(t)$ is defined by $\underline{Z}(t)= \{\underline{z}(\tau), 0 \le \tau \le t\}$; and if $\underline{u}(t) = \underline{\alpha}[t,\underline{Z}(t),\underline{f}_d]$ defines the set of admissible controls (ref. 6, p. 272), where $\underline{\alpha}$ is a vector operator that is linear in terms of its arguments; the basic problem objective is to find an admissible control function $\underline{u}^*(t)$ which minimizes J with respect to the set of admissible control functions $\underline{u}(t)$. [The asterisk here indicates optimality, in the sense defined by Eqn. (2).]

Problem Decomposition

The basic problem, as stated in Eqns. (1) and (2), can be decomposed into two parallel subproblems, one stochastic and the other deterministic. Suppose that $\underline{x} = \underline{x}_s + \underline{x}_d$, where $\underline{x}_s$ is the portion of the system response due to disturbance $\underline{w}_s$, and where $\underline{x}_d$ is the portion of the response due to $\underline{f}_d$. Let $\underline{y}_s$, $\underline{y}_d$, $\underline{z}_s$, $\underline{z}_d$, $\underline{Z}_s$, $\underline{Z}_d$, $\underline{u}_s$, and $\underline{u}_d$ be correspondingly defined.

$$\text{Then } J = \lim_{T\to\infty} \frac{1}{T} \int_0^T \left\{ \mathcal{E} \left\langle [\underline{x}_s' + \underline{x}_d'] \begin{bmatrix} W_1 & W_2 \\ W_2' & W_3 \end{bmatrix} \{ \begin{matrix} \underline{x}_s + \underline{x}_d \\ \underline{u}_s + \underline{u}_d \end{matrix} \} \right\rangle \right\} dt \tag{3a}$$

can be reduced to $J = J_s + J_d$, where

$$J_s = \lim_{T\to\infty} \frac{1}{T} \int_0^T \left\{ \mathcal{E} \left\langle [\underline{x}_s' + \underline{u}_s'] \begin{bmatrix} W_1 & W_2 \\ W_2' & W_3 \end{bmatrix} \{ \begin{matrix} \underline{x}_s \\ \underline{u}_s \end{matrix} \} \right\rangle \right\} dt \tag{3b}$$

$$\text{and} \quad J_d = \lim_{T\to\infty} \frac{1}{T} \int_0^T \left\langle [\underline{x}_d' + \underline{u}_d'] \begin{bmatrix} W_1 & W_2 \\ W_2' & W_3 \end{bmatrix} \{ \begin{matrix} \underline{x}_d \\ \underline{u}_d \end{matrix} \} \right\rangle dt \tag{3c}$$

The problem is now separable into a stochastic– and a deterministic subproblem, each of which has an analytical solution. The two subproblems are stated, and their solutions presented (without development) below.

Stochastic Subproblem and Solution

Statement:

Given:

$$\dot{\underline{x}}_s = A\,\underline{x}_s + B\,\underline{u}_s + E_s\,\underline{w}_s \tag{4a}$$

$$\underline{y}_s = C\,\underline{x}_s + D\,\underline{u}_s \quad (\text{rank } C \le \dim \underline{x}_s) \tag{4b}$$

$$\underline{z}_s = \underline{y}_s + M\underline{n} \tag{4c}$$

$\{A,B\}$ is stabilizable, $\{C,A\}$ is detectable

$\underline{x}_s(0) = \underline{x}_{s0}$ is Gaussian with zero mean

$\underline{x}_{s0}$, $\underline{w}_s$, and $\underline{n}$ are independent and bounded

such that $\text{cov}[\underline{w}_s(t), \underline{w}_s(\tau)] = V_1\delta(t-\tau)$ (4d)

and $\text{cov}[\underline{n}(t), \underline{n}(\tau)] = V_3\delta(t-\tau)$ (4e)

where V_1 is PSD and V_3 is PD

$$J_s = \lim_{T\to\infty} \frac{1}{T}\left\{ \mathcal{E} \int_0^T \left\langle [\underline{x}_s' \; \underline{u}_s'] \begin{bmatrix} W_1 & W_2 \\ W_2' & W_3 \end{bmatrix} \begin{Bmatrix} \underline{x}_s \\ \underline{u}_s \end{Bmatrix} \right\rangle dt \right\} \quad (4f)$$

where W_1 is PSD and W_3 is PD

$\underline{Z}_s(t) = \{\underline{z}_s(\tau), 0 \le \tau \le t\}$, $\underline{u}_s(t) = \underline{\alpha}_s[t, \underline{Z}_s(t)]$ (4g)

defines the set of admissible controls

Find: An admissible control function $\underline{u}_s^*(t)$ which minimizes J_s with respect to the admissible control functions $\underline{u}_s(t)$

Solution (See ref. 6, pp. 272–277; and ref. 7, ch. 11):

$$\underline{u}_s^*(t) = -K\,\tilde{\underline{x}}_s(t) \quad (5a)$$

where $\tilde{\underline{x}}_s$ is an estimate of $\underline{x}_s$ using a Luenberger observer (ref. 7, pp. 288–289) having observer gain matrix L

$$K = W_3^{-1}(B'P + W_2') \quad (5b)$$

P is the unique PD solution to

$$PA + A'P - (PB + W_2)\,W_3^{-1}(PB + W_2)' + W_1 = 0 \quad (5c)$$

$$L = QC'(M\,V_3\,M')^{-1} \quad (5d)$$

Q is the unique PD solution to

$$AQ + QA' - QC'(M\,V_3M')^{-1}CQ + E_s\,V_1\,E_s' = 0 \quad (5e)$$

P exists if $\{A,B\}$ is stabilizable and $\{C,A\}$ is detectable
or if the system is asymptotically stable

Q exists if $\{A, E_s\,V_1^{1/2}\}$ is stabilizable and $\{C,A\}$ is detectable
or if the system is asymptotically stable

Deterministic Subproblem and Solution

Statement:

Given:

$$\underline{x}_d = A\,\underline{x}_d + B\,\underline{u}_d + E_d\,\underline{f}_d \quad (6a)$$

$$\underline{y}_d = C\,\underline{x}_d + D\,\underline{u}_d \quad (\text{rank } C \le \dim \underline{x}_d) \quad (6b)$$

$$\underline{z}_d = \underline{y}_d \quad (6c)$$

$\{A,B\}$ is stabilizable, $\{C,A\}$ is detectable

$\underline{x}_d(0) = \underline{x}_{d0}$

$\underline{x}_{d0}$ and $\underline{f}_d$ are independent and bounded

$$J_d = \lim_{T\to\infty} \frac{1}{T} \int_0^T \left\langle [\underline{x}_d' \; \underline{u}_d'] \begin{bmatrix} W_1 & W_2 \\ W_2' & W_3 \end{bmatrix} \{\begin{matrix} \underline{x}_d \\ \underline{u}_d \end{matrix}\} \right\rangle dt \tag{6d}$$

where W_1 is PSD and W_3 is PD

$$\underline{Z}_d = \{\underline{z}_d(\tau),\ 0 \le \tau \le t\},\ \underline{u}_d(t) = \underline{\alpha}_d[t,\ \underline{Z}_d(t),\ \underline{f}_d] \tag{6e}$$

defines the set of admissible controls

Find: An admissible control function $\underline{u}_d^*(t)$ which minimizes J_d with respect to the set of admissible control functions $\underline{u}_d(t)$

Solution (refs. 8; 9; and 10, pp. 156–157):

$$\underline{u}_d^*(t) = -K\,\underline{x}_d - W_3^{-1}\,B' \int_t^\infty \exp[-\bar{A}'(t-\tau)]\,PE_d\,\underline{f}_d(\tau)\,d\tau \tag{7a}$$

where $K = W_3^{-1}\,(B'P + W_2')$ (7b)

P is the unique PD solution to

$$PA + A'P - (PB + W_2)\,W_3^{-1}\,(PB + W_2)' + W_1 = 0 \tag{7c}$$

P exists if $\{A,B\}$ is stabilizable and $\{C,A\}$ is detectable
or if the system is asymptotically stable

Combined Solution to Basic Problem

When rank C < dim $\underline{x}_d$, an estimate $\tilde{\underline{x}}_d$ of $\underline{x}_d$ must be used in the feedback. If one uses an asymptotic (i.e., Luenberger) observer, with gains L chosen to give an optimal solution to the stochastic subproblem, he can then combine the stochastic and deterministic subproblem solutions so as to use the same observer and regulator. This allows the optimal solution (feedback portion) to be realized physically. If such a choice is made,

$$\underline{u}^*(t) = u_d^*(t) + \underline{u}_d^*(t) = -K\,\tilde{\underline{x}}(t) - W_3^{-1}\,B' \int_t^\infty \exp[-\bar{A}'(t-\tau)]\,PE_d\,\underline{f}_d(\tau)d\tau \tag{8a}$$

where $\tilde{\underline{x}}$ is an estimate of $\underline{x}$ using a Luenberger observer

having observer gain matrix L

$$K = W_3^{-1}\,(B'P + W_2') \tag{8b}$$

$$L = QC'(M\,V_3\,M')^{-1} \tag{8c}$$

P,Q, and $\bar{A}$ are as defined previously

If $\underline{f}_s$ and $\underline{n}$ are correlated by $\mathcal{E}\,[\underline{f}_s(t),\ \underline{n}(\tau)] = V_2\delta(t-\tau)$, then the above solution has the modification (ref. 7, pp. 414–417) that

$$L = (QC' + E_s\,V_2)(M\,V_3M')^{-1} \tag{8d}$$

where Q is the unique PD solution to

$$\bar{A}Q + Q\bar{A}' - QC'(M\,V_3M')^{-1}CQ + E_s\bar{V}_1E_s' = 0 \tag{8e}$$

$$\text{for } \tilde{A} = A - E_s V_2 V_3^{-1} C \tag{8f}$$

$$\text{and } \tilde{V}_1 = V_1 - V_2 V_3^{-1} V_2' \tag{8g}$$

PROBLEM EXTENSIONS

Frequency Weighting

Suppose now that it is desired to frequency weight the states $\underline{x}$ and the control $\underline{u}$ in the cost rate functional, so that the weightings vary with frequency (ref. 11). Let $\underline{x}$ be considered to be the input to a filter $\mathcal{W}_1(s)$ of which ${}^1\underline{x}$ is the output, and let $\mathcal{W}_1(s)$ have a state–space representation defined by $\{A_1,B_1,C_1,D_1\}$ [i.e., $\mathcal{W}_1(s) = C_1(sI-A_1)^{-1}B_1 + D_1$].

Then

$$\dot{\underline{z}}_1 = A_1 \underline{z}_1 + B_1 \underline{x} \tag{9a}$$

$${}^1\underline{x} = C_1 \underline{z}_1 + D_1 \underline{x} \tag{9b}$$

expresses ${}^1\underline{x}$ in terms of $\underline{x}$, employing pseudostates $\underline{z}_1$. Similarly, if $\underline{u}$ is considered to be the input to a filter $\mathcal{W}_3(s)$ of which ${}^1\underline{u}$ is the output, and if $\mathcal{W}_3(s)$ has a state–space representation defined by $\{A_2,B_2,C_2,D_2\}$, ${}^1\underline{u}$ can be expressed in terms of $\underline{u}$, employing pseudostates $\underline{z}_2$:

$$\dot{\underline{z}}_2 = A_2 \underline{z}_2 + B_2 \underline{u} \tag{10a}$$

$${}^1\underline{u} = C_2 \underline{z}_2 + D_2 \underline{u}_2 \tag{10b}$$

Suppose now that these frequency–weighted states (${}^1\underline{x}$) and controls (${}^1\underline{u}$) are further weighted by constant weighting matrices W_1 and W_2, respectively. The resulting state equations and performance index are as follows:

$$\dot{\bar{\underline{x}}} = {}^1A\,\bar{\underline{x}} + {}^1B\,\underline{u} + {}^1E_d\underline{f}_d + {}^1E_s\,\underline{w}_s \tag{11a}$$

$$\underline{y} = {}^1C\,\bar{\underline{x}} + D\,\underline{u} \tag{11b}$$

$$\underline{z} = \underline{y} + M\,\underline{n} \tag{11c}$$

$${}^1J = \mathcal{E}\left\{\lim_{T\to\infty} \frac{1}{T} \int_0^T \left\langle [\bar{\underline{x}}'\ \underline{u}'] \begin{bmatrix} {}^1W_1 & {}^1W_2 \\ {}^1W_2' & {}^1W_3 \end{bmatrix} \begin{Bmatrix} \bar{\underline{x}} \\ \underline{u} \end{Bmatrix} \right\rangle dt\right\} \tag{11d}$$

where $$\bar{\underline{x}} = \begin{bmatrix} \underline{x} \\ \underline{z}_1 \\ \underline{z}_2 \end{bmatrix} \tag{11e}$$

$${}^1A = \begin{bmatrix} A & O & O \\ B_1 & A_1 & O \\ O & O & A_2 \end{bmatrix} \tag{11f}$$

$$^1B = \begin{bmatrix} B \\ O \\ B_2 \end{bmatrix} \tag{11g}$$

$$^1C = [C\ O\ O] \tag{11h}$$

$$^1E_d = \begin{bmatrix} E_d \\ O \\ O \end{bmatrix} \tag{11i}$$

$$^1E_s = \begin{bmatrix} E_s \\ O \\ O \end{bmatrix} \tag{11j}$$

$$^1W_1 = \begin{bmatrix} D_1'W_1D_1 & D_1'W_1C_1 & O \\ C_1'W_1D_1 & C_1'W_1C_1 & O \\ O & O & C_1'W_3C_2 \end{bmatrix} \tag{11k}$$

$$^1W_2 = \begin{bmatrix} O \\ O \\ C_2'W_3D_2 \end{bmatrix} \tag{11l}$$

$$^1W_3 = [D_2'W_3D_2] \tag{11m}$$

Disturbance Accommodation

Suppose further that the stochastic disturbance is not $\underline{w}_s$ but $\underline{f}_s$, where $\underline{f}_s$ is a stochastically modeled disturbance with power spectral density $S_f(\omega) = S_f^{1/2}(j\omega)S_f^{1/2^*}(j\omega)$. Defining $H_f(j\omega)$ by $S_f^{1/2}(j\omega)\ V_1^{1/2}$, one can consider $\underline{f}_s$ to be the output of a filter $H_f(s)$ excited by zero–mean white Gaussian noise $\underline{w}_s$ (ref. 12) with power V_1 (i.e., $\text{cov}[\underline{w}_s(t), \underline{w}_s(\tau)] = V_1\ \delta(t-\tau)$.

In state–space form,

$$\dot{\underline{\xi}} = A_s\,\underline{\xi} + \underline{w}_s \tag{12a}$$

$$\underline{f}_s = C_s(sI - A_s)^{-1} \tag{12b}$$

such that

$$H_f(s) = C_s(sI - A_s)^{-1} \tag{12c}$$

Incorporating these new pseudostates ($\underline{\xi}$) into the state equations and performance index

yields

$$\dot{\underline{\hat{x}}} = {}^2A\,\underline{\hat{x}} + {}^2B\,\underline{u} + {}^2E_d\,\underline{f}_d + {}^2E_s\,\underline{w}_s \tag{13a}$$

$$\underline{y} = {}^2C\,\underline{\hat{x}} + D\,\underline{u} \tag{13b}$$

$$\underline{z} = \underline{y} + M\,\underline{n} \tag{13c}$$

$${}^2J = \mathcal{E}\left\{\lim_{T\to\infty}\frac{1}{T}\int_0^T\left\langle[\underline{\hat{x}}'\ \underline{u}']\begin{bmatrix}{}^1W_1 & {}^1W_2\\ {}^1W_2' & {}^1W_3\end{bmatrix}\begin{Bmatrix}\underline{\hat{x}}\\ \underline{u}\end{Bmatrix}\right\rangle dt\right\} \tag{13d}$$

where $$\underline{\hat{x}} = \begin{Bmatrix}\underline{\bar{x}}\\ \underline{\xi}\end{Bmatrix} \tag{13e}$$

$${}^2A = \begin{bmatrix}A & O & O & E_s C_s\\ B_1 & A_1 & O & O\\ O & O & A_2 & O\\ O & O & O & A_s\end{bmatrix} \tag{13f}$$

$${}^2B = \begin{bmatrix}B\\ O\\ B_2\\ O\end{bmatrix} \tag{13g}$$

$${}^2C = [C\ O\ O\ O] \tag{13h}$$

$${}^2E_d \begin{bmatrix}E_d\\ O\\ O\\ O\end{bmatrix}$$

$${}^2E_s \begin{bmatrix}O\\ O\\ O\\ I\end{bmatrix} \tag{13j}$$

$${}^2W_1 = \begin{bmatrix}D_1'W_1D_1 & D_1'W_1C_1 & O & O\\ C_1'W_1D_1 & C_1'W_1C_1 & O & O\\ O & O & C_2'W_3C_2 & O\\ O & O & O & O\end{bmatrix} \tag{13k}$$

$$ {}^2W_2 = \begin{bmatrix} 0 \\ 0 \\ C_2'W_3D_2 \\ 0 \end{bmatrix} \tag{13m} $$

$$ {}^2W_3 = [D_2'W_3D_2] \tag{13n} $$

The solution to this problem has been given previously.

SYNTHESIS MODEL

The model given at the close of the previous section is the model from which the controller is synthesized. The synthesis involves the determination of observer gains L and regulator feedback gains K. Preview gains K_{FF} can also be determined, if desired, to approximate the Duhamel integral term of the optimal control. One approach to determining these preview gains has been presented in reference 9. Further study of the determination and use of these gains is needed.

ANALYSIS MODEL

Once the controller has been selected, it must be connected to the actual plant and the resulting "analysis model" used to evaluate closed–loop–system performance and stability. For constant gain matrices K, L, and K_{FF} the open loop transfer function from $\underline{Y}$ to $\underline{U}_{FB}$ [$=-K\,\underline{\hat{X}}$] is

$$ \mathcal{H}^{OL}_{\underline{U}_{FB}\underline{Y}}(s) = \left[\begin{array}{c|c} {}^2A-{}^2BK-L{}^2C & L \\ \hline -K & 0 \end{array}\right], \tag{14a} $$

where the form $\left[\begin{array}{c|c} A & B \\ \hline C & D \end{array}\right]$

indicates $C(sI - A)^{-1} B + D$. The closed loop transfer functions, respectively, from $\underline{F}_d$ and $\underline{F}_s$ to $\underline{X}$, are

$$ \mathcal{H}^{CL}_{\underline{X}\,\underline{F}_d}(s) = \left[\begin{array}{cc|c} A & -BK & E_d+BK_{FF} \\ LC & {}^2A-{}^2BK-L{}^2C & {}^2BK_{FF} \\ \hline I & 0 & 0 \end{array}\right] \tag{14b} $$

$$ \text{and } \mathcal{H}^{CL}_{\underline{X}\,\underline{F}_s}(s) = \left[\begin{array}{cc|c} A & -BK & E_s+BK_{FF} \\ LC & {}^2A-{}^2BK-L{}^2C & {}^2BK_{FF} \\ \hline I & 0 & 0 \end{array}\right] \tag{14c} $$

The return ratio matrices (ref. 4) at the $\underline{Y}(s)$ and $\underline{U}(s)$ nodes, respectively, for $D \equiv O$, are

$$L_2(s) = \left[\begin{array}{cc|c} A^2-BK-L^2C & 0 & L \\ -BK & A & O \\ \hline O & -C & O \end{array}\right] \tag{15a}$$

$$L_1(s) = \left[\begin{array}{cc|c} {}^2A-{}^2BK-L^2C & LC & O \\ O & A & B \\ \hline K & O & O \end{array}\right] \tag{15b}$$

The corresponding return difference matrices and inverse return difference matrices (ref. 4) are as follows:

$$I + L_2(s) = \left[\begin{array}{cc|c} {}^2A-{}^2BK-L^2C & O & L \\ -BK & A & O \\ \hline O & -C & I \end{array}\right] \tag{15c}$$

$$I + L_1(s) = \left[\begin{array}{cc|c} {}^2A-{}^2BK-L^2C & LC & O \\ O & A & B \\ \hline K & O & I \end{array}\right] \tag{15d}$$

$$I + L_2^{-1}(s) = I + [K(sI - {}^2A + {}^2B\,K + L^2C)^{-1}L]^{-1}[C(sI - A)^{-1}B]^{-1} \tag{15e}$$

$$I + L_1^{-1}(s) = I + [C(sI - A)^{-1}B]^{-1}[K(sI - {}^2A + {}^2B\,K + L^2C)^{-1}L]^{-1} \tag{15f}$$

The singular values of these matrices can be used to evaluate system noise and disturbance attenuation, stability margins, and sensitivity (ref. 4). Iterative application of the synthesis– and analysis models can be used to produce the desired controller.

EXAMPLE PROBLEM

Suppose one wishes to develop a controller to isolate a space experiment of mass m and position x(t), from a unidirectional acceleration disturbance $\ddot{d}(t)$. Assume that a wall having position d(t) acts on m through an umbilical with stiffness k and damping c. (See figure 1). Suppose further that rattlespace constraints require the transmissibility to be unity below 10^{-3} Hz, and that it is desired to attenuate the disturbance by at least two orders of magnitude between 0.05 and 10 Hz. Let a linear actuator, applying a force that varies with control current i, be connected between the wall and the experiment in parallel with the umbilical.

For this problem, it is desirable at low frequencies to penalize the relative displacement of the experiment heavily, so that the experiment "tracks" the wall. At intermediate frequencies, however, the absolute acceleration of the experiment should be heavily penalized to accomplish the desired disturbance rejection. The state space model,

then, should have relative position x–d and absolute acceleration $\ddot{x}$ as states, allowing them to be frequency–weighted in the performance index.

The system equation of motion is

$$\ddot{x} = -\hat{k}(x-d)-\hat{c}(\dot{x}-\dot{d}) - \hat{\alpha}i, \text{ where } \hat{k} = \frac{k}{m},\ \hat{c} = \frac{c}{m}, \text{ and } \hat{\alpha} = \frac{\alpha}{m} \tag{16a}$$

In state–space form, the equations can be written as

$$\begin{Bmatrix}\dot{x}_1\\ \dot{x}_2\\ \dot{x}_3\end{Bmatrix} = \begin{bmatrix}0 & 1 & 0\\ -\hat{k} & -\hat{c} & 0\\ -\omega_h\hat{k} & -\omega_h\hat{c} & -\omega_h\end{bmatrix}\begin{Bmatrix}x_1\\ x_2\\ x_3\end{Bmatrix}\begin{Bmatrix}0\\ -\hat{\alpha}\\ -\omega_h\hat{\alpha}\end{Bmatrix}i + \begin{Bmatrix}0\\ -1\\ 0\end{Bmatrix}\ddot{d} \tag{16b}$$

$$\begin{Bmatrix}y_1\\ y_2\end{Bmatrix} = \begin{bmatrix}1 & 0 & 0\\ 0 & 0 & 0\end{bmatrix}\begin{Bmatrix}x_1\\ x_2\\ x_3\end{Bmatrix} \tag{16c}$$

$$\begin{Bmatrix}z_1\\ z_2\end{Bmatrix} = \begin{Bmatrix}y_1\\ y_2\end{Bmatrix} + \begin{Bmatrix}n_1\\ n_2\end{Bmatrix} \tag{16d}$$

where
$$x_1(t) = x(t) - d(t)$$
$$x_2(t) = \dot{x}(t) - \dot{d}(t) \tag{16e}$$
$$X_3(s) = \left(\frac{\omega_h}{s+\omega_h}\right) s^2X(s),\ \omega_h \text{ high,}$$
$$\text{so that } x_3(t) \approx \ddot{x}(t) \text{ for } \omega << \omega_h$$

Frequency–weighting the states so that

$$\begin{Bmatrix}{}^1X_1(s)\\ {}^1X_2(s)\\ {}^1X_3(s)\end{Bmatrix} = \begin{bmatrix}\frac{\omega_3}{s} & 0 & 0\\ 0 & 1 & 0\\ 0 & 1 & \frac{\omega_2 s}{(s+\omega_1)(s+\omega_2)}\end{bmatrix}\begin{Bmatrix}X_1(s)\\ X_2(s)\\ X_3(s)\end{Bmatrix} \tag{17a}$$

(where $\omega_1 < \omega_2$) results in a performance index that penalizes x_1 more highly at low frequencies and x_3 more highly at intermediate frequencies. If the control is frequency–weighted so that

$${}^1U(s) = \left(\frac{\omega_4 s}{s+\omega_4}\right) U(s)\ [\omega_4 < \omega_h]\ , \tag{17b}$$

at higher frequencies the control will be more heavily penalized. This is desirable both for the sake of robustness and since x_3 approximates $\ddot{x}$ only at frequencies sufficiently below ω_h. Finally, let the input acceleration be considered to come from zero–mean Gaussian white noise filtered through $\frac{\omega_f}{s+\omega_f}$.

The resultant state equations are as indicated on page 8, where

$$A_1 = \begin{bmatrix} 0 & 0 & 0 \\ 0 & -(\omega_1+\omega_2) & -\omega_1\omega_2 \\ 0 & 1 & 0 \end{bmatrix} \tag{18a}$$

$$B_1 = \begin{bmatrix} 1 & 0 & 0 \\ 0 & 0 & 1 \\ 0 & 0 & 0 \end{bmatrix} \tag{18b}$$

$$C_1 = \begin{bmatrix} \omega_3 & 0 & 0 \\ 0 & 0 & 0 \\ 0 & \omega_2 & 0 \end{bmatrix} \tag{18c}$$

$$D_1 = \begin{bmatrix} 0 & 0 & 0 \\ 0 & 1 & 0 \\ 0 & 0 & 0 \end{bmatrix} \tag{18d}$$

$$A_2 = -\omega_4$$
$$B_2 = 1$$
$$C_2 = -\omega_4^2$$
$$D_2 = \omega_4$$
$$A_s = -\omega_f$$
$$B_s = 1$$
$$C_s = \omega_f$$
$$D_s = 0$$

Assume that $\text{cov}\,[w_s(t), w_2(\tau)] = 1\ \delta(t-\tau)$
$\text{cov}\,[n_1(t), n_1(\tau)] = 0.001\ \delta(t-\tau)$
and $\text{cov}\,[n_2(t), n_2(\tau)] = 0.001\ \delta(t-\tau)$.

Since A_1 has a zero [1st] column, ^2A will have a corresponding zero [4th] column. To make the frequency–weighted system $\{^2C,^2A\}$ observable, obtain $\int (x-d)\,dt$ as a measured state (i.e., the first pseudostate, Z_{11}) and modify ^2C accordingly. Let the measurement noise associated with Z_{11} be n_3, such that

$$\text{cov}\,[n_3(t), n_3(\tau)] = 0.0001$$

Gain matrix W_1 can be varied to "tune" the optimal control to give the most satisfactory results. The transmissiblity between $\ddot{d}(t)$ and $\ddot{x}(t)$ is given in figure 2. The control uses feedback (and observer) gains obtained from system parameters and weightings as indicated on the figure. Note that the low–frequency transmissibility is unity, as desired, and that for intermediate frequencies the transmissibility rolls off with a slope of –1.

If a different frequency–weighting of x_3 is used, it is to be anticipated that the transmissibility curve will change as well.

For $$ {}^1X_3(s) = \frac{\omega_2^2\, s}{(s+\omega_1)^2(s+\omega_2)^2}\, X_3(s) \qquad (19) $$

the resultant selected transmissibility curve is given in figure 3. The low–frequency transmissibility again, is unity; but now for the intermediate frequencies the transmissibility rolls off with a slope of –2, as expected. Adding another pole at ω_1 and at ω_2 to the $X_3(s)$ frequency weighting would further improve the intermediate–frequency roll–off. The present controller, however, meets the design specifications.

If state frequency–weightings of $$ {}^1X_1(s) = \frac{\omega_3}{s+\omega_3}\, X_1(s) \qquad (20a) $$

and $$ {}^1X_3(s) = \frac{\omega_2^2\, s}{(s+\omega_1)^2(s+\omega_2)^2}\, X_3(s) \qquad (20b) $$

are used, the results (figure 4) are similar to those given previously in figure 3. Note that with this latter choice of frequency weighting however, (i.e., without any"rigid body poles"), the frequency–weighted system $\{^2C,^2A\}$ is observable, without augmenting the actual plant output $\underline{y}$ as was previously necessary. Consequently this is the preferred control.

DISCUSSION

H_2 synthesis, as the example problem indicates, provides a highly versatile loop–shaping tool. It is especially useful in controller development for SIMO and MIMO systems, where classical loop–shaping methods are most lacking. Once the designer has expressed the system equations in terms of states for which he has an intuitive feel, and of measurable outputs, the design process becomes relatively easy. He frequency weights (i.e., filters) the states and control inputs according to his engineering experience and intuition, to indicate the relative importance of each as a function of frequency. Then he weights these frequency–weighted states and controls relati:e to each other. The H_2 synthesis methodology automatically provides him with a set of regulator and observer gains that are optimal with respect to the chosen weightings, given a quadratic performance index. Known aspects of the input disturbances and sensor noise can be incorporated into the design as well. Singular value checks provide the ability to evaluate system robustness. With a few iterations, the skillful engineer can complete his design. Excellent computer software packages already exist to assist in the task.

The frequency weighting tells the H_2 synthesis machinery how much "cost" to place on a state or control input at any frequency, relative to its cost at other frequencies. If, for example, absolute acceleration is undesirable only in a particular frequency range, that is where it should be most heavily weighted. The subsequent weighting of the frequency–weighted states and control inputs tell the synthesis machinery how much cost to place on each frequency–weighted state or control relative to the others.

Subscripts, Superscripts, and Diacritical Marks

postsubscript 0	Value at time t=0
postsubscript 1	With A,B,C,D,$\underline{z}$: related to state–frequency weighting state–space description
	With L: return ratio matrix at control node
	With V: process noise covariance
	With w,W,$\mathscr{W}$: state (or pseudostate) weightings, applied subsequent to any frequency weighting
postsubscript 2	With A,B,C,D,$\underline{z}$: related to state–frequency–weighting state–space description
	With L: return ratio matrix at output node.
	With V,W: cross–weightings
postsubscript 3	With V: measurement noise covariance
	With W,$\mathscr{W}$: control weightings
postsubscript d	Related to deterministic disturbance
postsubscript f	Related to filter for stochastic disturbance
postsubscript s	Related to stochastic disturbance
postsuperscript 1/2	Square root or spectral factorization
postsuperscript '	Transpose
postsuperscript −1	Inverse
postsuperscript *	Optimum or conjugate transpose
underline $\_$	Vector
overbar $-$	With A: closed loop system dynamic matrix
	With $\bar{x}$: augmented with frequency–weighting pseudostates
overhat $\hat{}$	Augmented with frequency–weighting– and disturbance–accommodation pseudostates
overtilde $\sim$	Estimated or associated with cross–correlation
presuperscript 1	With $\underline{x}$,$\underline{X}$,$\underline{u}$, or $\underline{U}$: frequency–weighted
	With other symbols: related to system augmented by frequency weighting
presuperscript 2	Related to system augmented by frequency–weighting and disturbance–accommodation

ACKNOWLEDGEMENTS

This work was supported in part by the NASA Lewis Research Center and by the Center for Innovative Technology of the Commonwealth of Virginia.

REFERENCES

1. Grodsinsky, C.M.; and Brown, G.V.: "Non–intrusive Inertial Vibration Isolation Technology for Microgravity Space Experiments." NASA TM–201386, January 1990.

2. Nelson, E.S.: "An Examination of Anticipated g–Jitter on Space Station and Its Effects on Materials Processes." NASA TM–103775, April 1991.

3. Knospe, C.R.; Hampton, R.D., and Allaire, P.E.: "Control Issues of Microgravity Vibration Isolation." Acta Astronautica, accepted for publication.

4. Safonov, M.G.; Laub, A.J.; and Hartmann, G.L.: "Feedback Properties of Multivariable Systems: The Role and Use of the Return Difference Matrix." IEEE Trans. on Automatic Controls, Vol. AC–26, No. 1, February 1981, pp. 47–65.

5. Maciejowski, J.M.: Multivariable Feedback Design. Addison–Wesley Publishing Company, Inc., Wokingham, England, 1989.

6. Sage, A.P.; and White, C.C., III: Optimum Systems Control, 2nd ed. Prentice Hall, Inc., Englewood Cliffs, New Jersey, 1977.

7. Friedland, B.: Control System Design: An Introduction to State–Space Methods. McGraw–Hill, Inc., New York, 1986.

8. Salukvadze, M.E.: "Analytic Design of Regulators (Constant Disturbances)." Translated in Automation and Remote Control, Vol. 22, No. 10, October 1961, pp. 1147–1155. Originally published in Avtomatika i Telemakhanika, Vol. 22, No. 10, February 1961, pp. 1279–1287.

9. Hampton, R.D.; Knospe, C.R.; Allaire, P.E.; Lewis, D.W.; and Grodsinsky, C.M.: "An Optimal Control Law for Microgravity Vibration Isolation." Workshop on Aerospace Applications of Magnetic Suspension Technology, September 25–27, 1990, NASA Conference Publication 10066, Part 2, March 1991, pp. 447–476.

10. Bryson, A.E., Jr.; and Ho, Yu–Chi: Applied Optimal Control. Hemisphere Publishing Corporation, Washington, D.C., 1975.

11. Gupta, N.K.: "Frequency Shaped Cost Functionals: Extension of Linear – Quadratic–Gaussian Design Methods." AIAA Journal of Guidance and Control, November/December 1980, pp. 529–535.

12. Johnson, C.D.: "Further Study of the Linear Regulator with Disturbances – The Case of Vector Disturbances Satisfying a Linear Differential Equation." IEEE Trans. on Automatic Control (Short Papers), Vol. AC–15, April 1970, pp. 222–228.

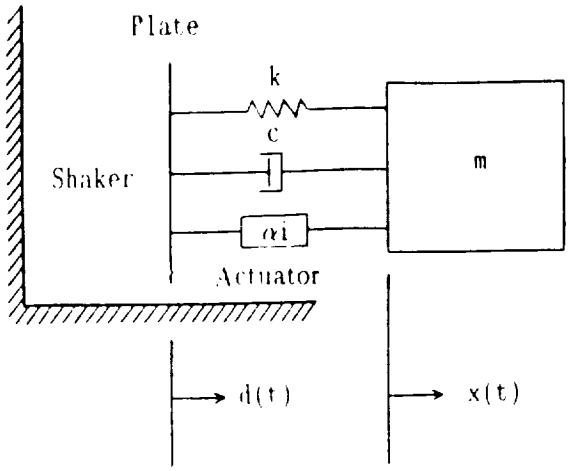

m = 75 lbm
k = 1.544 lbf/ft
c = 0 lbf-sec/ft
α = 2 lbf/amp

FIGURE 1: Example-Problem Model

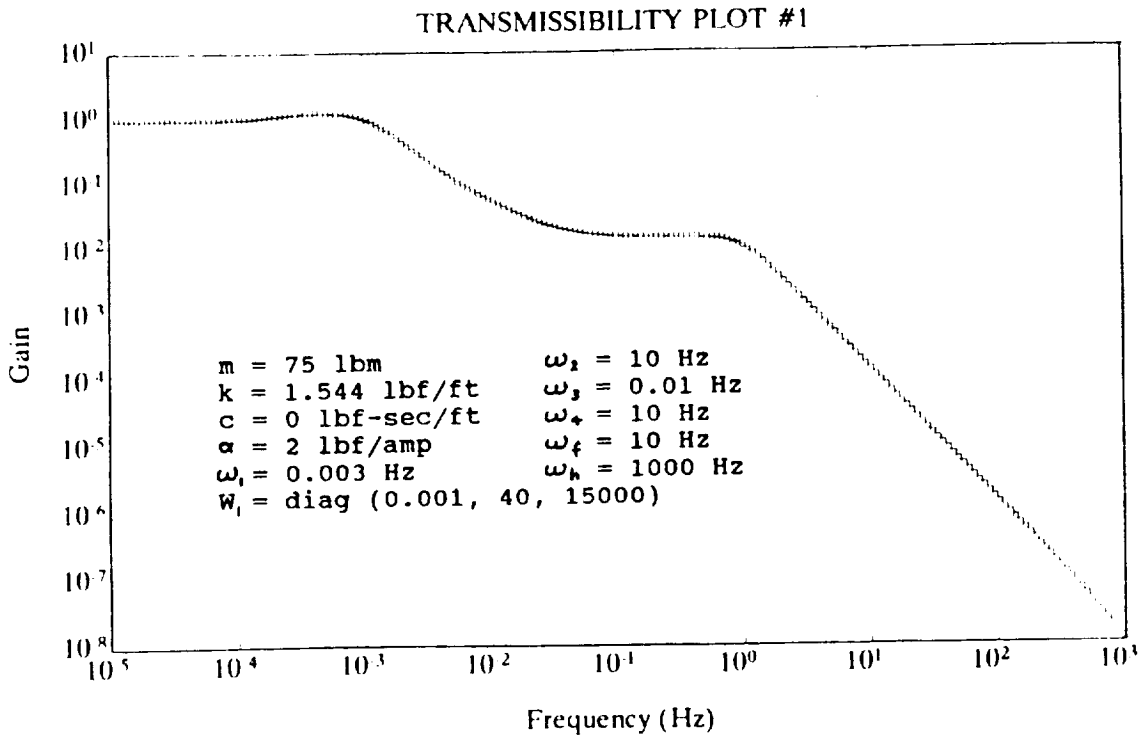

FIGURE 2: Transmissibility Plot for 1st Control Weighting

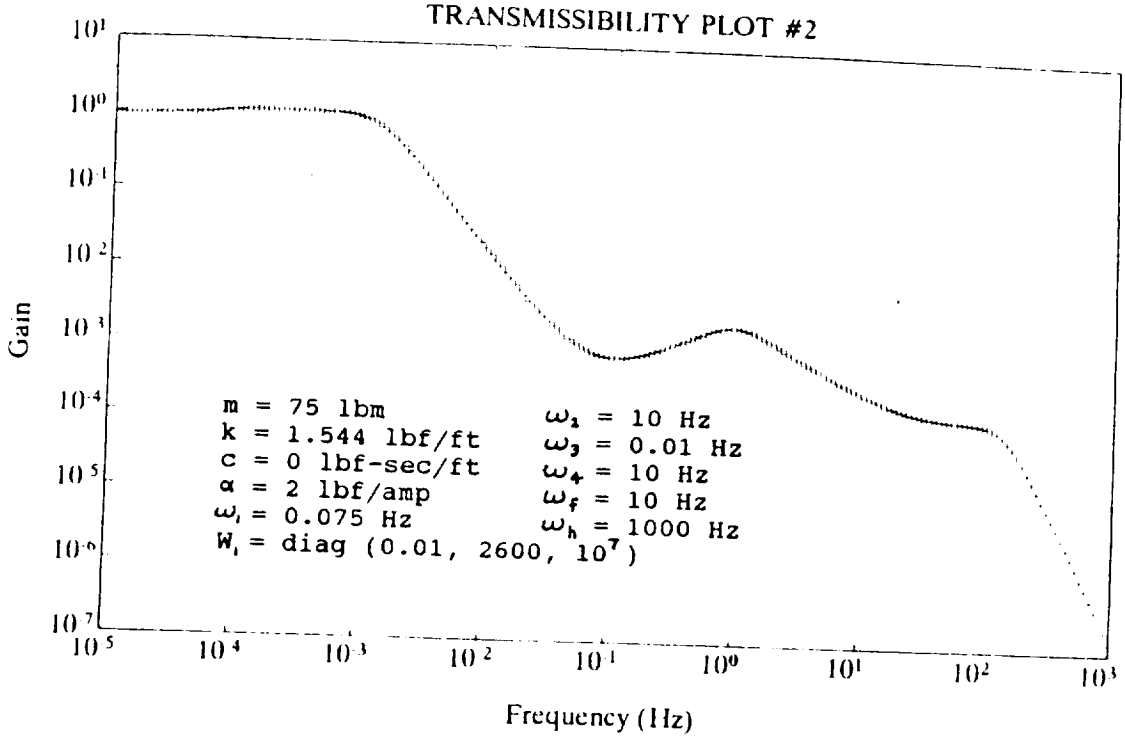

FIGURE 3: Transmissibility Plot for 2nd Control Weighting

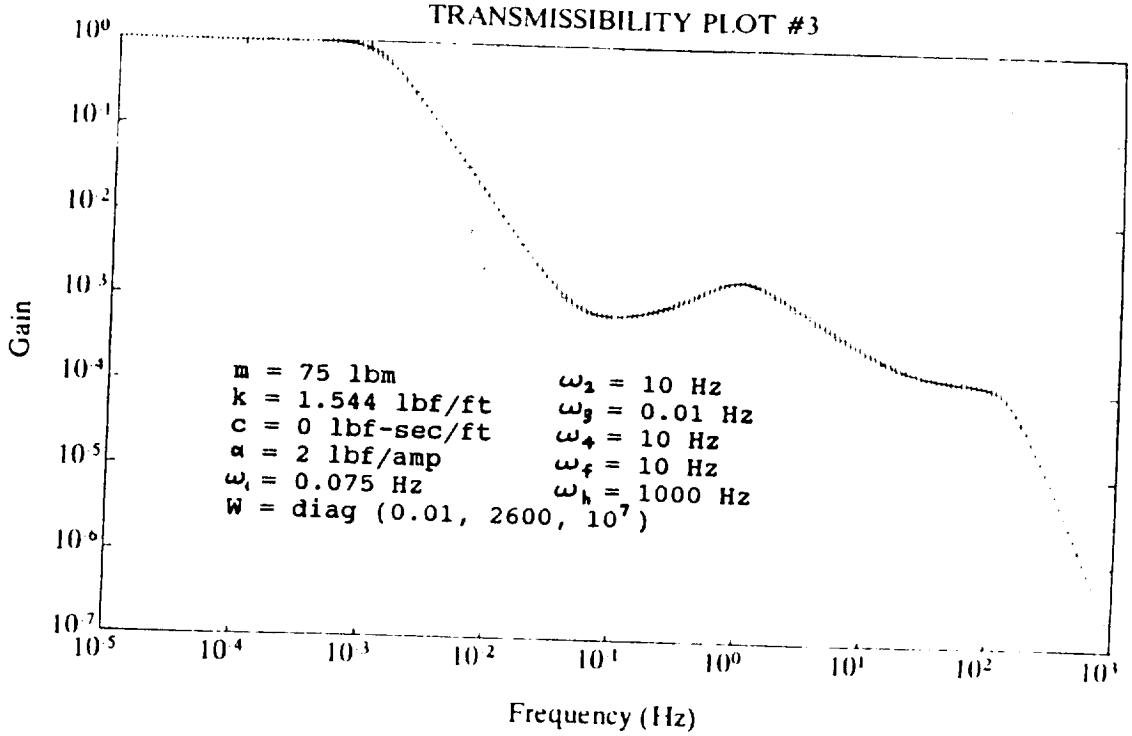

FIGURE 4: Transmissibility Plot for 3rd Control Weighting

N/S

A MICROGRAVITY VIBRATION ISOLATION RIG

Bibhuti B. Banerjee
Carl R. Knospe
Paul E. Allaire

Center for Magnetic Bearings/ROMAC
University of Virginia
Charlottesville, VA 22903 USA

1. ABSTRACT

It is well–known that the spacecraft environment deviates from a state of zero gravity due to various random as well as repetitive sources. Science experiments that require a microgravity environment must therefore be isolated from these disturbances. Active control of noncontact magnetic actuators enables such isolation. A one–degree–of–freedom test rig has been constructed to demonstrate the isolation capability achievable using magnetic actuators. A cylindrical mass on noncontacting electromagnetic supports simulates a microgravity experiment on board an orbiter. Disturbances generated by an electrodynamic shaker are transmitted to the mass via air dashpots representing umbilicals. A compact Lorentz actuator has been designed to provide attenuation of this disturbance.

2. INTRODUCTION

Space exploration was initiated for the investigation of space itself, ranging from the planetary system to the limits of the universe. Resulting benefits of this effort include satellite communications and earth observation and imaging systems. The scope of space exploration widened in the early eighties with the development of the space shuttle – a system capable of transporting a large cargo to a low earth orbit, and recovering the payload or frequently servicing it in space. A parallel development was the gradual change in the role of man in space, starting with the primarily technical function of a pilot and evolving into a more active involvement encompassing interactive work and scientific experimentation in space. Space–based laboratories like the Skylab and the Spacelab were flown to utilize the "vanishingly low" gravitational forces available for extended periods of time. The results, however, were mixed at best, and disappointing in certain cases. This can be explained in part by the fact that the environment aboard the spacecrafts deviates considerably from the ideal of zero gravity due to disturbances produced by machinery and people on board, thruster fire, and other factors.

The incentives for performing science experiments in space include the investigation of phenomena that are influenced by gravity on earth, the development of novel materials and the improvement of processes like crystal

---

This work was supported in part by the NASA Lewis Research Center and the Center for Innovative Technology of the Commonwealth of Virginia.

growth [1]. In theory, a freely orbiting spacecraft offers a state of zero gravity to objects inside it, since the gravitational force is balanced by the centrifugal force [2]. However, in practice, there are various residual forces that disturb the environment.

Attempts to estimate these residual forces have been made in the past few years [3–10]. The orbital microgravity environment can be divided into three classes, as detailed in Table 1. Quasi–steady accelerations are generated by three sources — gravity gradient, aerodynamic drag and rotational acceleration. Any point of an orbiting structure that is at a distance from the structure's center of mass experiences a gravitational field that is different from that at the spacecraft center of mass. Aerodynamic drag due to the earth's atmosphere represents the absolute lower limit of the achievable background microgravity level, if the effect of light pressure is neglected. Finally, in order to keep the same vertical orientation on the space station with respect to the earth, the station must maintain a constant pitch rate about its center of mass. This creates a centripetal force that results in a rotational acceleration.

Orbital thruster fire and the steady–state operation of machinery like fans and pumps on board a spacecraft are among the sources of periodic accelerations, which occur at known frequencies. Impulsive disturbances like crew push–off and the start–up and shut–down of machinery create non–periodic accelerations. The irregular, unpredictable nature of these accelerations complicates attempts at isolation.

Theoretical acceleration requirements for various processes and experimental conditions have been investigated [3,7,11]. The common feature of curves depicting the frequency–dependent requirements is that, for a given process, the acceleration threshold is lowest from steady–state to about (0.01 — 0.1) Hz, depending upon the type of experiment. The acceptable acceleration then increases linearly with increasing frequency, up to (1 — 10) Hz. Subsequently, it increases as the square of the frequency. The acceleration tolerance also typically scales inversely with the volume that characterizes the process. The slopes and breakpoints result from fundamental aspects of a process, and the shape of the curve can be considered to be characteristic of a family of experiments. The acceleration level thresholds range from an extreme level of $(10^{-7} - 10^{-8})$ g_o for some material science and fluid science experiments, to only 10^{-3} g_o for the majority of biology and biotechnology experiments.

A comparison of the microgravity requirements with the actual environment available on the spacecraft indicates the need for vibration isolation. Moreover, the frequency range of interest spans several decades, thus requiring the use of multiple strategies for isolation.

For the high frequency range, passive isolators can serve adequately. Since these are relatively simple and cheap, they can be placed at each interface between a disturbance source and the space station. It should be noted that the sensitivity of various categories of experiments to high frequency disturbances is also comparatively low.

In the quasi–static frequency range, the extremely low stiffness and large motion required make attempts at isolation very difficult. Rattlespace constraints prohibit the occurrence of such large relative motions between the payload and the spacecraft. This imposes a fundamental limitation upon vibration isolation. Consequently, efforts at minimizing the input disturbances, like reducing the surface area presented to the atmosphere so as to reduce atmospheric drag and locating

payloads as close to the spacecraft's center of mass as possible, are necessary. Owens and Jones have also suggested the possibility of canceling such disturbances by continuous thruster control of the whole spacecraft [11].

At intermediate frequencies — approximately between 0.01 Hz and 1 Hz — no passive isolation scheme can be effective due to the displacements and isolation levels required. Only active vibration isolation at the payload–spacecraft interface allows the synthesis of the desired isolator properties and the adjustment of these properties using a control loop.

The actuator used to implement an active control scheme in the intermediate frequency range should ideally be noncontacting. The ideas of acoustic, electrostatic and electromagnetic (Lorentz force) levitation have been considered in the context of containerless processing of materials in a low gravity environment [12–15]. The first two techniques are limited to small objects. Lorentz forces are utilized by placing an electrically conductive sample within a suitably designed coil excited by a radio frequency current. Currents induced in the sample interact with the magnetic field of the coil to produce forces that tend to move the sample away from regions of high magnetic flux density. These currents also tend to heat the sample, which is often utilized to melt it. However, the inability to control this heating effect independently of the coil current required for levitation is a limitation of this technique. Some unwanted stirring of a melt by the induced currents also occurs.

Noncontact magnetic actuators, utilizing electromagnets or permanent magnets, appear to be the best solution for vibration isolation in the intermediate frequency range [16]. These actuators produce relatively large forces and can be applied to the isolation of a variety of science experiments. An active magnetic isolation system can be "tuned" by simply changing control law gains to accommodate changes in the payload or the expected disturbance environment, or to produce improved performance once in orbit. Such experiments need only be enclosed in a container, and can have umbilicals connecting them to the spacecraft.

A Long Action Magnetic Actuator (LAMA) has been proposed for this purpose [17]. This is a magnetic thrust bearing modified to accommodate longer strokes than those found in typical industrial applications. The pole–faces are inclined at an acute angle to the axis of motion, instead of being perpendicular to it. Detailed studies of magnetic thrust bearing design and use have been made [18–20]. The LAMA would be suitable for those intermediate frequencies that require motions not exceeding about a hundred miles. Since the forces called for are of the order of a few pounds at most, such actuators can be quite compact, the size being primarily determined by the stroke required.

A single–axis magnetic actuator similar to a magnetic thrust bearing has been described in [21]. The authors compared various sensing options to close the actuator control loop — gap and current sensing, force sensing and flux sensing. In their experiment, the authors achieved force linearization using flux feedback. Due to shaker and accelerometer limitations, the lowest recorded frequency of their measured data was 5 Hz. A subsequent paper described a similar isolation system extended to six degrees–of–freedom, called the Fluids Experiment Apparatus Magnetic Isolation System (FEAMIS) [22].

An interesting dual–mode approach to vibration isolation of large payloads over long displacements has been discussed in [23]. It was intended to provide the high performance active isolation of noncontact magnetic suspension technology without the limitations on articulation imposed by the small air gaps used in such

systems. In such a tandem system, a "coarse" motion actuator was controlled as a followup actuator, always attempting to keep the gap displacement for the magnetic actuator within its design limits. The magnetic actuator functioned as a "fine" motion actuator, ignoring the presence of the other, coarse actuator. The performance requirements on the coarse actuator were not very stringent, since the imperfections of its motions would be attenuated by the fine actuator.

The operation of microgravity science experiments is likely to require the use of an umbilical. An example is a plastic tube formed into a helical shape and carrying a coolant. Acceleration control to reject disturbances caused by the compliance of the umbilical has been theoretically investigated [24]. The umbilical was assumed to have stiffness, but not damping. The microgravity quality deteriorated with increasing umbilical stiffness, as expected. Acceleration control improved disturbance rejection greatly when compared to position–only control, but there was a price to be paid in the form of a more complicated control system. An active umbilical control strategy, in which the extension of the umbilical is minimized by making one end track the other, was also analyzed. It was found to be effective in principle and comparable in performance to the acceleration control loop technique.

3. EXPERIMENTAL RIG

An experimental rig to demonstrate vibration isolation down to microgravity levels in one degree–of–freedom has been constructed, and is shown in Figures 1 and 2. An innovative long stroke Lorentz actuator, described in detail in the next section, will be used to implement the isolation scheme.

An electrodynamic shaker with a long, peak–to–peak stroke of 6.25 inches represents the space platform. The shaker is mounted, via aluminum plates, on a concrete block resting on the laboratory floor. The shaker can generate sinusoidal, random or impulse waveforms at frequencies down to DC, thus simulating the disturbances typically produced on a space station that require active isolation.

The umbilicals connecting a science experiment to the space platform are expected to be flexible hoses and wires. These will be modeled by air dashpots with adjustable stiffness and damping coefficients. This type of dashpot has been evaluated at NASA Lewis in a single–degree–of–freedom mass–spring–damper system in a fixed–fixed mounting configuration [25]. The test indicated the possibility of a nonlinear stiffness/damping mechanism in these air dashpots. The vibration isolation rig has been designed so that different kinds of umbilicals may be employed, including actual hoses used for fluid transfer. This is important, since very little work has been done to date on vibration isolation to microgravity levels in the presence of an actual physical connection between the experiment and the space platform.

The long stroke Lorentz actuator, in parallel to the umbilical(s), connects the shaker armature to the mass representing a microgravity science experiment in space. This mass is a solid steel cylinder weighing 75 pounds, which is a typical weight for such an experiment. The cylinder is horizontally suspended in space by the magnetic forces generated by a noncontact electromagnetic support system. Similar to radial magnetic bearings, the support system consists of two eight–pole structures, mounted on a concrete base, at the two ends of the cylindrical mass. This concrete base is massive compared to the "experiment" mass, and rests on the same laboratory floor as the separate concrete block on which the shaker is

mounted. Eddy current probes sense the radial position of the cylinder and complete the feedback loop supplying current to the electromagnets. When the electromagnetic support system is turned off, the cylinder rests on a pair of touchdown pedestals made of delrin.

The axial acceleration of the cylinder will be sensed off a sensory plate mounted at its free end, using a very low frequency accelerometer with a maximum resolution of 1 μg. Provision has been made for the use of other types of accelerometers, and the sensing of other states of the system, like position. The accelerometer signal will be fed to a feedback control circuit that determines the current required in the electromagnetic actuator to isolate the cylinder from the disturbances generated by the shaker. A control strategy for such an isolation system with multiple degrees–of–freedom is discussed in [26].

The background vibration levels on the concrete base on which the cylinder is mounted have been measured over twenty–four–hour periods, in both the horizontal and the vertical directions. These vibrations are of the order of milli–g's, the quietest period occurring from late in the night to early in the morning. Operating at this time will yield the highest degree of reproducibility in our results. Figures 3 and 4 show the frequency spectrum of the background acceleration in the horizontal and vertical directions. The vertical vibration shows acceleration components corresponding to natural frequencies of the mounting plate. The horizontal vibration has significant content at 45 Hz. The authors believe this is a floor mode.

4. THE LONG–STROKE LORENTZ ACTUATOR

A compact long–stroke Lorentz Actuator has been designed, built and tested in the laboratory. An intermediate version of the design was presented at the Workshop on Aerospace Applications of Magnetic Suspension Technology at NASA Langley in September, 1990 [27]. The final design described here incorporates many of the same features, but is much more linear with coil position. This was accomplished through modification of the flux distribution.

A schematic of the typical Lorentz Actuator, along with the terminology used, is shown in Figure 5. The current carrying coil moves in and out along the core. A strong permanent magnet in the shell maintains a constant magnetic flux in the cylindrical air gap across the pole faces, irrespective of the current in the coil (within design limits). The Lorentz force generated, therefore, can be linearly varied with coil current [28].

The requirements for the laboratory prototype were fixed at a total stroke of two inches and enough force capability to isolate a mass of 75 lbs. connected by an umbilical (air dashpot) to a source generating very low frequency vibrations. Force linearity with position and with current were also required. Moreover, in view of the ultimate goal of deployment in space, such a device had to be compact and lightweight. Low power consumption and low heat generation during operation were also important.

A computer program was written to implement a simple design algorithm for a Lorentz Actuator. The steps of this algorithm are presented in Figure 6.

Using a permanent magnet material with a very high maximum energy product of 35 MGOe (mega–Gauss–Oersted) [29] resulted in a design that required

a ring magnet of 3.20 in. outer diameter. The magnet manufacturer, however, could make such a magnet in one piece only if its outer diameter were less than 2 in.; making a ring magnet with a 3.20 in. outer diameter would have required the costly assembly of multiple segments, with an escalation of costs.

The possibility of designing a Lorentz Actuator satisfying all the requirements, with the outer diameter of the magnet being additionally constrained to less than 2 in., was therefore explored. The significant parameter in this context is the gap ratio, defined as the ratio of the shell–to–core air gap to the pole–face–to–core air gap. Conventional designs use ratios of 5:1 or higher in order to minimize leakage of magnetic flux from the shell to the core. Figures produced by the design program suggested that the design requirements could be met, along with the additional constraint, if the rule of thumb of using a gap ratio of 5:1 or more were drastically violated. Apparently, flux leakage, which the computer program did not take into account, would result in the failure of such a design. It was then hypothesized that this would not necessarily be the case if the core of the actuator were saturated during normal operation. The permeability of a saturated ferromagnetic material approaches that of air, and so most of the leakage that would have occurred, with such a low gap ratio (less than 2:1) and an unsaturated core, would be prevented.

A good way of verifying this hypothesis, without actually building such an actuator, is the use of finite element analysis. A commercially available magnetic finite element analysis package, MAGGIE, with a nonlinear modeling capability, was chosen. It also allowed us to take leakage and fringing into account, and different materials and geometries could be "tested" with relative ease.

A number of designs incorporating various features, were analyzed using the finite element analysis package. The finite element model was generated so as to achieve as much accuracy as possible, within hardware limitations. The mesh consists predominantly of quad elements. Infinite air elements, used earlier, were found to cause severe restrictions on mesh fineness. A mesh with only about 100 elements could be used. An air thickness of an inch on three sides of the axisymmetric model was specified instead. This was determined to be as accurate as having infinite air elements on all three sides for a model of this size, while a relatively fine mesh with about 400 elements could be used without encountering core memory limitations. Moreover, the finest mesh allowed by the configuration of our 386–based personal computer was used for the analysis.

Position linearity was improved, relative to the intermediate design, by increasing the length of the magnet, imparting a lip to it by reducing the shell outer diameter, and reducing the core diameter. The gap ratio resulting from the last change mentioned above is still only 1.47:1 – much smaller than a typically specified value of 5:1. The use of such an unconventionally low gap ratio enabled the design of a compact and lightweight actuator. Use of a large ratio would also have required a large diameter magnet that could not be made in one piece, thus increasing costs. The decrease in flux, and therefore force, caused by the increase in the length of the magnet was compensated, to some extent, by a reduction in the inner diameter of the magnet and a doubling of the pole piece thickness. Figure 7 shows the design. The overall length of the actuator is 4 in., while the outer diameter is only 1.95 in..

The salient features of the final design of the compact Lorentz Actuator are described below:

• Long Stroke — The requirement of two inches of total stroke is satisfied.

• Position Linearity — Over the whole two inches of stroke, the actuator exhibits a high degree of linearity. For a constant coil current, this means that the actuator force is the same irrespective of the axial position of the coil, within the stroke bounds. Figures 8 and 9 depict this relationship for positive and negative coil currents respectively. Note that flux leakage has been reduced to almost zero over the shell–to–core gap to achieve this. The maximum flux density across the shell–to–core gap is only about 7% of the maximum flux density across the pole–face gap.

• Current Linearity — This requires that the average flux density in the effective air gap remain constant with variations in the coil current between the upper and the lower limits. This is indeed the case, resulting in force vs. current linearity, Figure 10.

• Force — A maximum force of 1.25 lbs is produced by this actuator, which is sufficient for our needs. This peak force requires a coil current of 2.5 A.

• Weight — At 2.28 lb., this actuator is only a tenth of a pound heavier than the previous design.

• Current Density — A value of 1000 A/sq. in. in continuous use ensures cool operation. For peak loads, a fivefold increase in current density is possible.

• Materials — The magnet is made of neodymium iron boron, which has a very high maximum energy density product of 35 MGOe. Selection of such a material helped make the design compact. The high permeability circuit material is a 48% nickel–iron alloy that saturates at 15 kG. The B–H curve for this material, provided by the manufacturer, was input to MAGGIE as a table of a large number of points on the curve. This was necessary because a nonlinear material characteristic was being modeled.

The design specifications of the Lorentz Actuator are detailed in Table 2. This actuator was built and tested in our laboratory. Figure 11 compares the measured magnetic flux density in the radial direction along the shell–to–core and pole–face–to–core gaps with the values predicted by finite element analysis, for no current in the coil. The measured peak value is lower, but is spread over a wider axial distance. There is good agreement, especially over most of the shell–to–core gap, where near–zero values of flux density are crucial to achieve force versus position linearity. The actual actuator force is plotted against position for a number of values of coil current in Figure 12. The measured values of force are greater, in each case, than the predicted values since most of the small amount of leakage flux across the shell–to–core gap was neglected in calculating the predicted forces. Moreover, since the coil does see slightly greater total flux as it moves into the actuator, because of the small amounts of leakage, the forces measured increase somewhat with such motion. However, for low values of current and for coil positions that do not place it very near the closed end of the actuator, the actual forces deviate by less than 10% from the predicted values.

C-2

5. CONCLUSION

The rig designed to demonstrate vibration isolation to microgravity levels in one–dimension has been built and assembled. Measurements of the background acceleration levels have also been made, and the quietest period for operation has been determined. A compact, long stroke Lorentz actuator has also been designed, built, and tested. Its performance has been shown to match that predicted by finite element analysis very well. Microgravity isolation experiments will be conducted in the very near future.

6. REFERENCES

1. Feuerbacher, B., "Introduction," Chapter 1, Materials Sciences in Space, Ed. B. Feuerbacher, et al., Springer–Verlag, Berlin, 1986.

2. Hamacher, H., "Simulation of Weightlessness," Chapter 3, Materials Sciences in Space, Ed. B. Feuerbacher, et al., Springer–Verlag, Berlin, 1986.

3. Teledyne Brown Engineering, "Low Acceleration Characterization of Space Station Environment," Report No. SP858–MSFC–2928, Oct. 1985.

4. Chase, T.L., "Report on Micro–g Measurements for Space Shuttle Experiments," NASA Lewis Research Center, Dec. 1985.

5. Teledyne Brown Engineering, Abstracts, Workshop on Measurement and Characterization of the Acceleration Environment on Board the Space Station. Guntersville, Alabama, Aug. 11–14, 1986.

6. Hamacher, H., R. Jilg and U. Merbold, "Analysis of Microgravity Measurements Performed During D1," 6th European Symposium on "Materials Sciences under Microgravity Conditions." Bordeaux, Dec. 2–5, 1986.

7. Booz, Allen & Hamilton, "Overview of Space Station Microgravity Requirements," report presented to Dr. J.–D. Bartoe, Chief Scientist, Office of Space Station, July 14, 1989.

8. McDonnell Douglas Corporation "Space Station Definition and Preliminary Design," WP–02, DR–02, Book 22, Section 8 (Loads and Structural Dynamics), Dec. 1985.

9. Ramachandran, N., and C.A. Winter, "The Effects of g–Jitter and Surface Tension Induced Convection on Float Zones," 28th Aerospace Sciences Meeting, AIAA, Reno, Nevada, Jan. 8–11, 1990.

10. Armentrout, R.W., "Two–Body Dynamic simulation of Space Station Exercise Treadmill Including Startup Transient Effects," Memo No. A96–J749–STN–M–RWA–900006, Jan. 10, 1990.

11. Owen, R.G., and D.I. Jones, "Columbus Applications Study (WP. 1.1)," Technical Note No. BTN–001, University College of North Wales, School of Electronic Engineering Science, Bangor, Gwynedd, Sep. 1988.

12. Naumann, R.J. and D.D. Elleman, "Containerless Processing Technology," Chapter 12, Materials Sciences in Space, Ed. B. Feuerbacher, et al., Springer–Verlag, Berlin, 1986.

13. Hendricks, C.D., "Levitation, Coating, and Transport of Particulate Materials," Materials Processing in the Reduced Gravity Environment of Space, Ed. G.E. Rindone, et al., vol. 9, pp. 59, Elsevier Science Publishing Co., Amsterdam, 1982.

14. Rhim, W.–K., M. Collender, M.T. Hyson, W.T. Sims and D.D. Elleman, "Development of Electrostatic Positioner for Space Materials, Processing," Rev. Sci. Instrum., vol. 56, no. 2, p. 307, 1985.

27. Banerjee, B.B., P.E. Allaire and C.R. Knospe, "Vibration Isolation of Science Experiments in Space – Design of a Laboratory Test Setup," Workshop on Aerospace Applications of Magnetic Suspension Technology, NASA CP–10066 Part 2, Paper 26, March 1991.

28. Carlson, A.B., D.G. Gisser and F.K. Manasse, "Magnetics and Electromechanics," Chapter 17, Electrical Engineering: Concepts and Applications, Addison–Wesley Publishing Company, Reading Massachusetts, 1989.

29. McCaig, M. and A.G. Clegg, Permanent Magnets in Theory and Practice, John Wiley & Sons, New York, 1987.

15. Frost, R.T. and C.W. Chang, "Theory and Applications of Electromagnetic Levitation," Materials Processing in the Reduced Gravity Environment of Space, Ed. G.E. Rindone, et al., vol. 9, pp. 71, Elsevier Science Publishing Co., Amsterdam, 1983.

16. Grodsinsky, C.M. and G.V. Brown, "Nonintrusive Inertial Vibration Isolation Technology for Microgravity Space Experiments," submitted for publication to Journal of Spacecraft and Rockets, AIAA, Jan. 1990.

17. Allaire, P.E., M.A. Scott and B.B. Banerjee, "Magnetic Actuators for Microgravity Space Isolation," Workshop on Vibration Isolation Technology for Microgravity Science Experiments," NASA Lewis, Cleveland, Ohip, Sep. 28–29, 1988.

18. Banerjee, B.B., "Analysis and Design of Magnetic Thrust Bearings," M.S. Thesis, Univ. of Virginia, Charlottesville, May 1988.

19. Allaire, P.E., A. Mikula, B.B. Banerjee, D.W. Lewis and J. Imlach, "Design and Test of a Magnetic Thrust Bearing," Journal of the Franklin Institute, vol. 326, no. 6, pp. 831–847, 1989.

20. Allaire, P.E., J. Imlach, J.P. McDonald, R.R. Humphris, D.W. Lewis, B.B. Banerjee, B.J. Blair, J. Claydon and R.D. Flack, "Design, Construction and Test of Magnetic Bearings in an Industrial Canned Motor Pump," Proc. of the Sixth International Pump Users Symposium, Texas A&M Univ., College Station, Nov. 1988.

21. Havenhill, D.D. and K.D. Kral, "Payload Isolation Using Magnetic Suspension," AAS 85–014, Annual AAS Guidance and Control Conference, Keystone, Colorado, Feb. 2–6, 1985.

22. Allen, T.S., D.D. Havenhill and K.D. Kral, "FEAMIS: A Magnetically Suspended Isolation System for Space–Based Materials Processing," AAS 86–017, Annual AAS Guidance and Control Conference, Keystone, Colorado, Feb. 1–5, 1986.

23. Hamilton, B.J., J.H. Andrus and D.R. Carter, "Pointing Mount with Active Vibration Isolation for Large Payloads," AAS 87–033, Annual AAS Guidance and Control Conference, Keystone, Colorado, Jan. 31 – Feb. 4, 1987.

24. Jones, D.I., A.R. Owens, R.G. Owen and G. Roberts, "Microgravity Isolation Mount: Design Report," Technical Note No. BTN–009, University College of North Wales, School of Electronic Engineering Science, Bangor, Gwynedd, Sep. 1989.

25. Sutliff, T., "Vibration Isolation: Airpot (Dashpot) Damping Evaluation," PIR No. 89–9, NASA, Lewis, Cleveland, Ohio, 1989.

26. Hampton, R.D. and C.R. Knospe, "Extended H_2 Synthesis for Multiple–Degree–of–Freedom Controllers," International Symposium on Magnetic Suspension Technology, NASA CP–3152, 1992.

Table 1: Typical Disturbance Environment on a Spacecraft

	QUASI-STEADY ACCELERATIONS	
1e-7 g	(0 to 1e-3) Hz	Aerodynamic Drag
1e-8 g	(0 to 1e-3) Hz	Light Pressure
1e-7 g	(0 to 1e-3) Hz	Gravity Gradient
	PERIODIC ACCELERATIONS	
1e-2 g	9 Hz	Thruster Fire (Orbital)
1e-3 g	(5 to 20) Hz	Crew Motion
1e-4 g	17 Hz	Ku Band Antenna
	NON-PERIODIC ACCELERATIONS	
1e-4 g	1 Hz	Thruster Fire (Attitudinal)
1e-4 g	1 Hz	Crew Push-Off

Table 2: Design Specifications for the Lorentz Actuator

LORENTZ ACTUATOR : FINAL DESIGN	
Total length	• 3.87 in
Magnet outer diameter	• 1.95 in
Magnet inner diameter	• 1.25 in
Magnet length	• 2.77 in
Shell outer diameter	• 1.68 in
Pole-piece thickness	• 0.80 in
Core diameter	• 0.75 in
Air gap	• 0.17 in
Shell-to-core gap	• 0.25 in
Gap ratio	• 1.47 : 1
Coil length	• 4.00 in
Coil wire diameter	• 26.67 mils
Number of turns	• 600 turns
Number of layers	• 4 layers
Maximum coil current	• 2.5 A
Air gap flux density	• 0.145 T
Max. force generated	• 1.25 lbf
Actuator wt. (no coil)	• 2.28 lbf

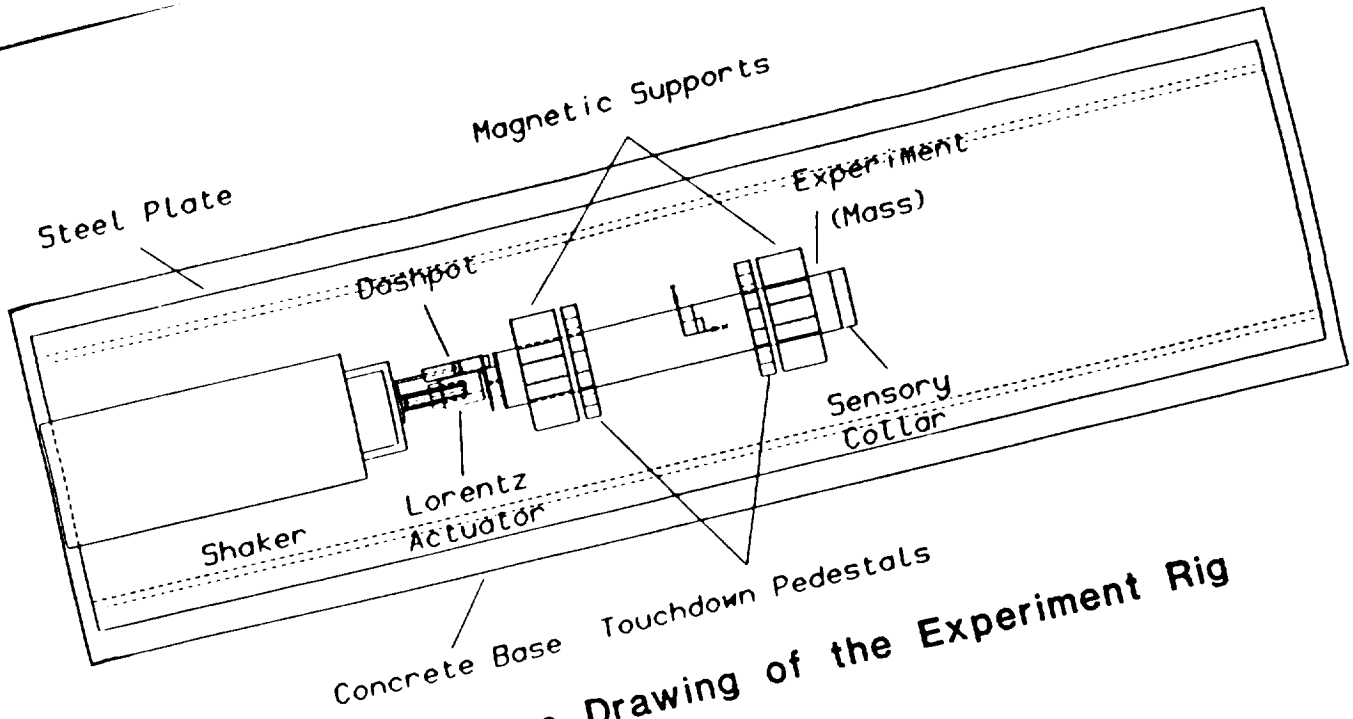

Fig. 1: Design Drawing of the Experiment Rig

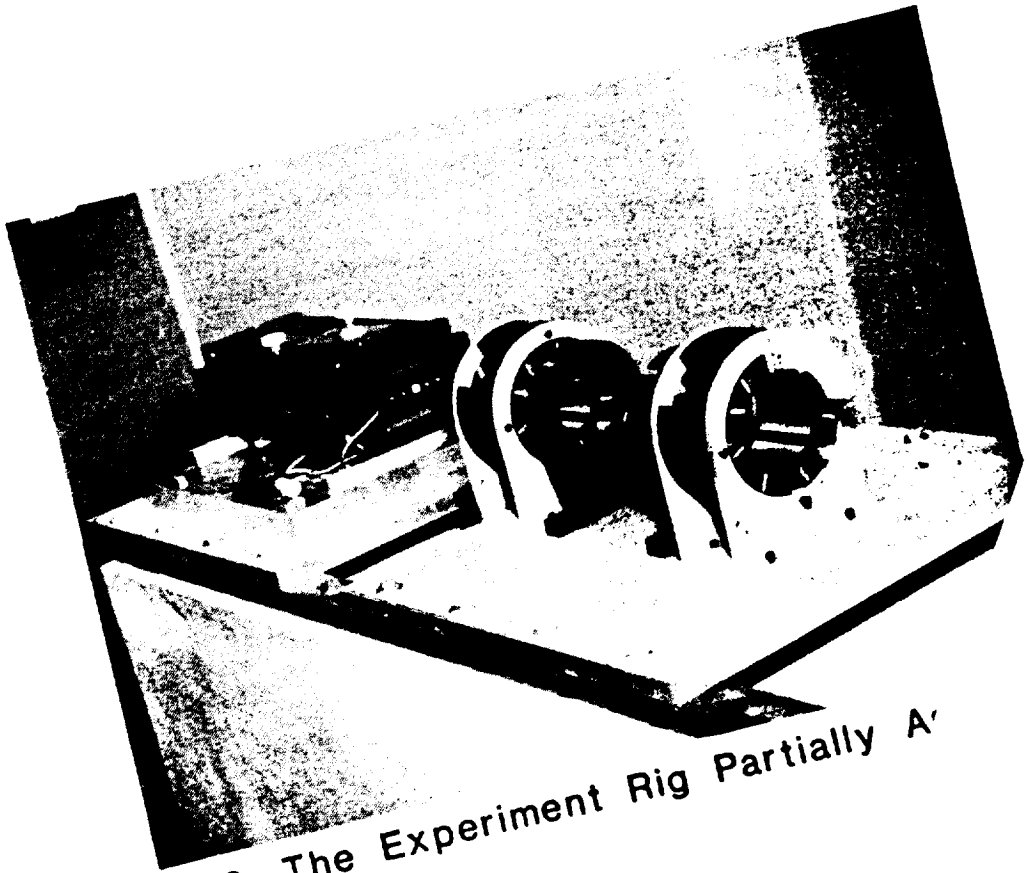

Fig. 2: The Experiment Rig Partially A

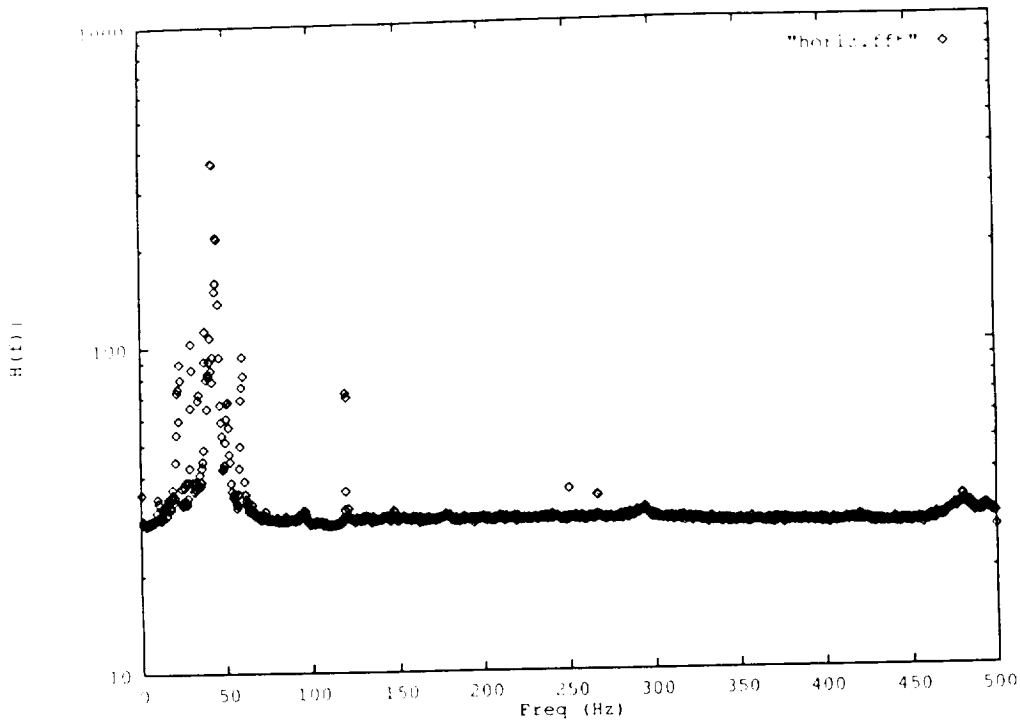

Fig. 3: Background Vibration in the Laboratory -- Horizontal

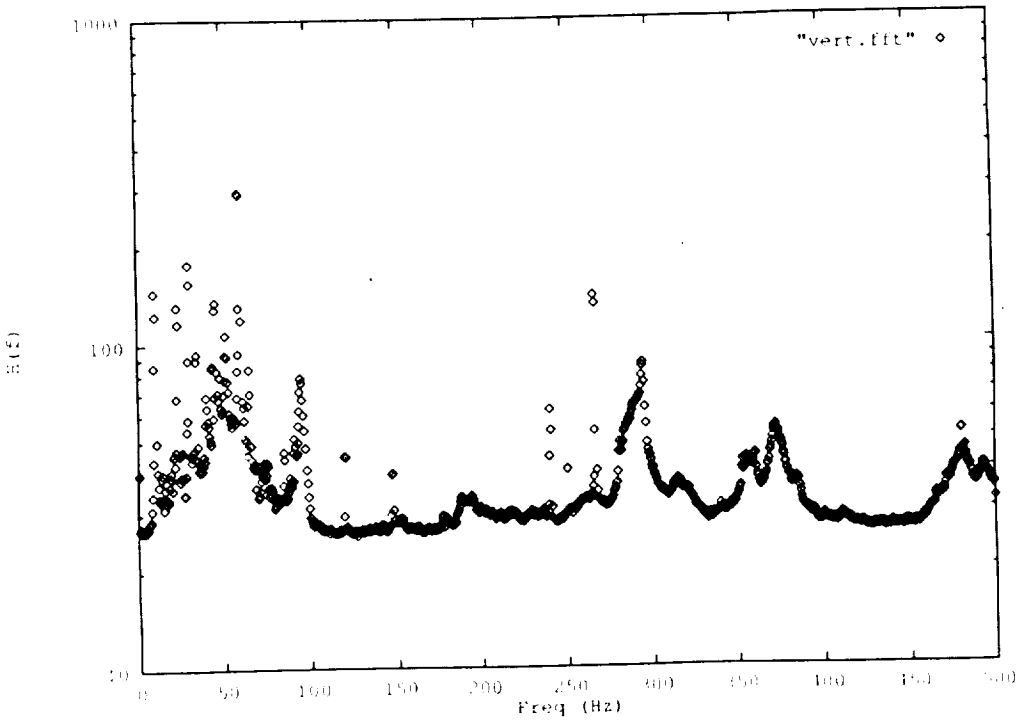

Fig. 4: Background Vibration in the Laboratory -- Vertical

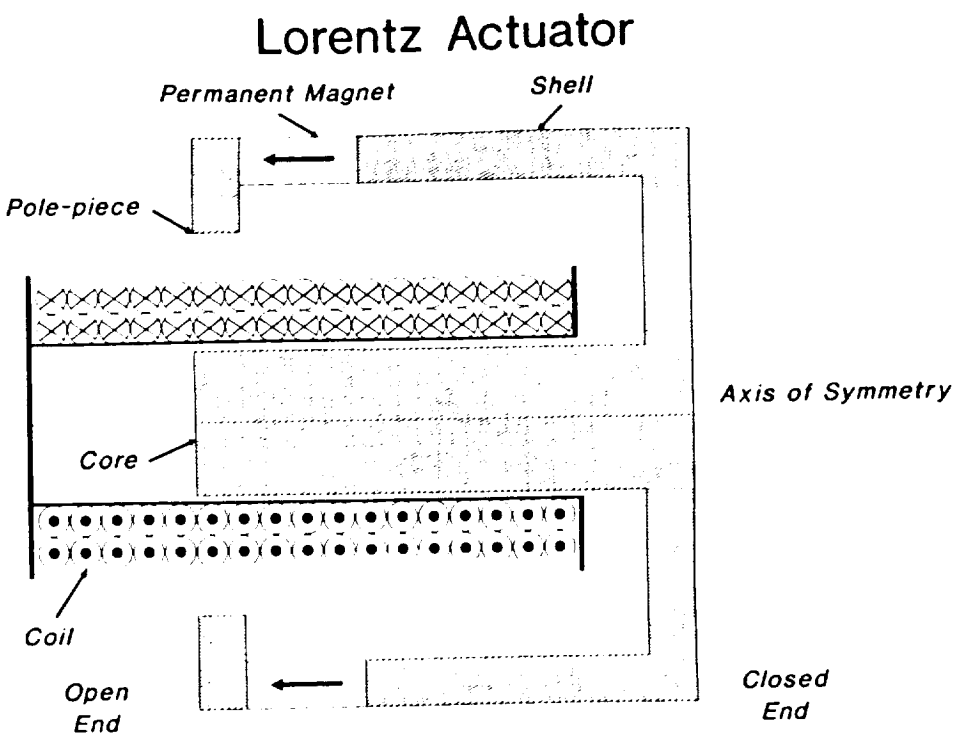

Fig. 5: Schematic of a Lorentz Actuator

LORENTZ ACTUATOR : DESIGN EQUATIONS

1. Assume permanent magnet operating point for maximum energy product : (-H1, B1).
2. Compute magnet flux, fm = B1 • Am.
3. Compute circuit flux, fc = H1 • Lm / R, where R is the circuit reluctance.
4. Compare fm and fc.
5. Adjust operating point until fm = fc = f, the actual operating point. (When saturated, f = saturation flux in saturated segment of circuit.)
6. Calculate air gap flux density, Bg = f / Ag.
7. Compute force capability, F = i • l • Bg, where i is the actuator current and l is the total length of coil wire in the air gap.
8. Change actuator geometry or circuit / magnet material until desired force level is achieved.

Fig. 6: A Simple Algorithm for Designing a Lorentz Actuator

Fig. 7: The Compact, Long-Stroke Lorentz Actuator

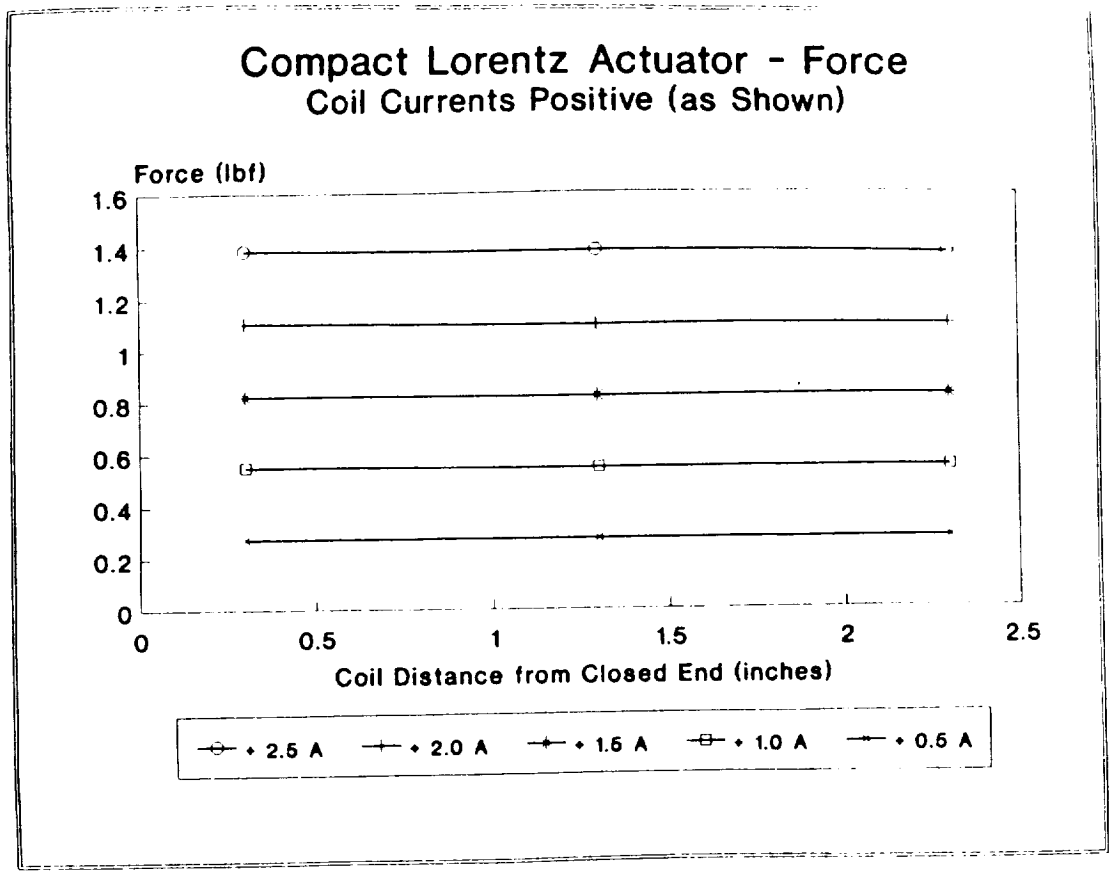

Fig. 8: Force vs. Position (for Positive Coil Currents)

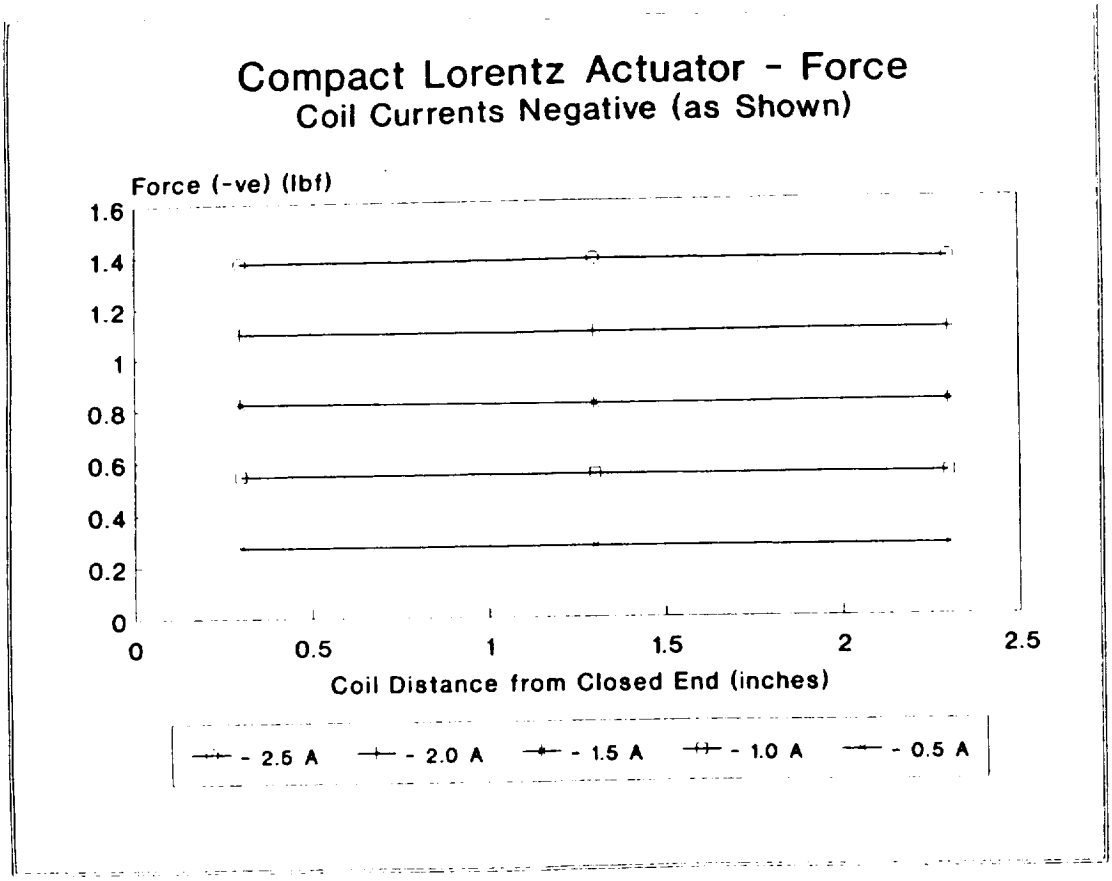

Fig. 9: Force vs. Position (for Negative Coil Currents)

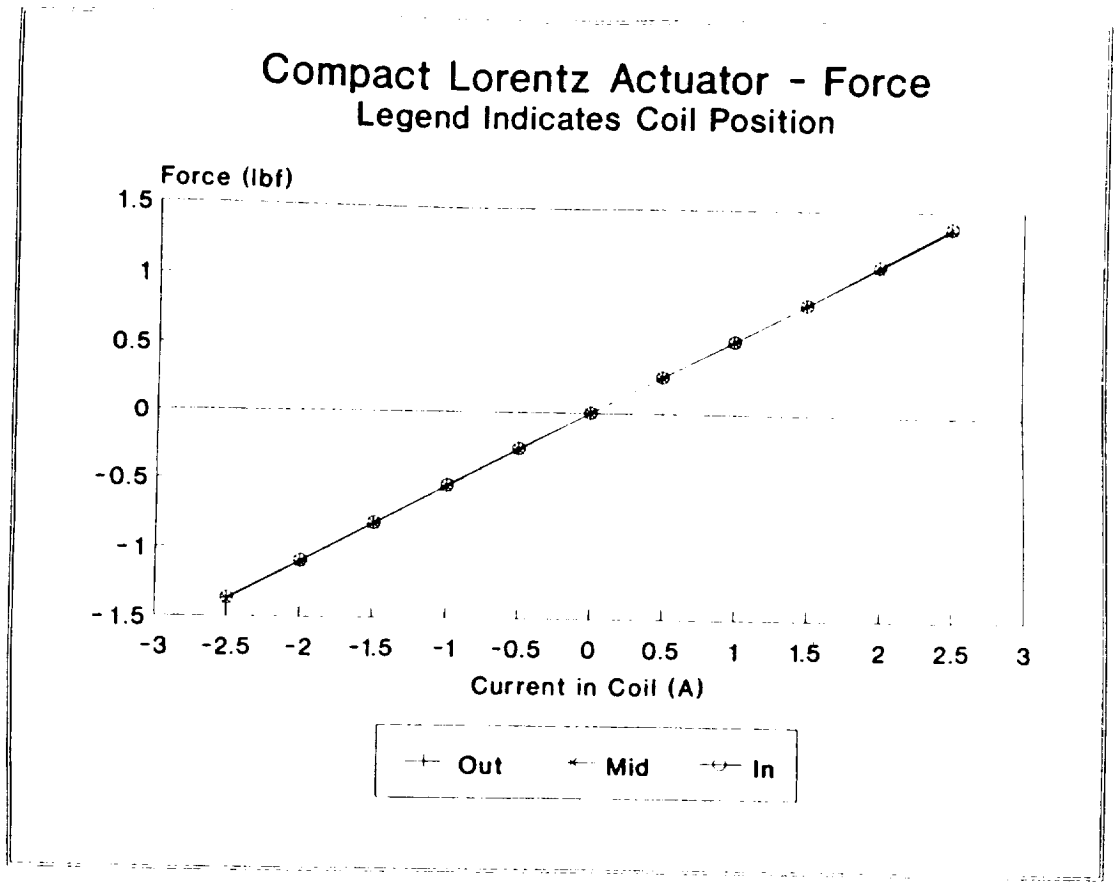

Fig. 10: Force vs. Current (for Three Different Coil Positions)

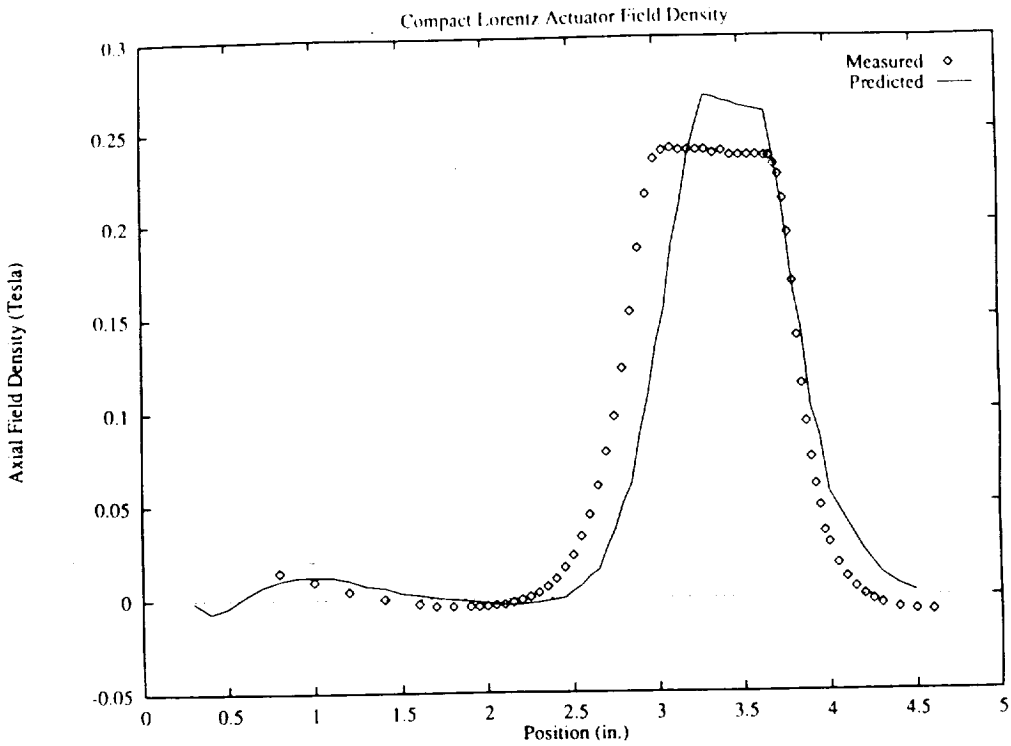

Fig. 11: Comparison of Actual Flux Density with Predicted Values (for No Current in the Coil)

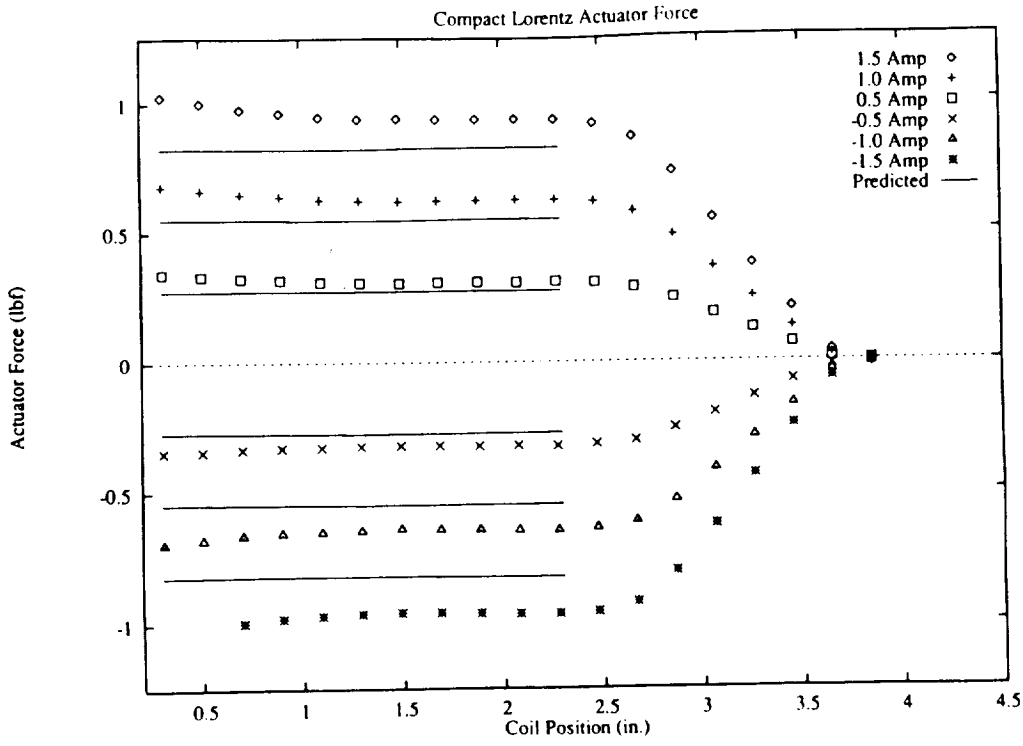

Fig. 12: Comparison of Actual Force vs. Position Characteristics with Analytical Predictions

Acta Astronautica Vol. 25, No. 11, pp. 687–697, 1991
Printed in Great Britain.

0094-5765/91 $3.00 + 0.00

PREV. ANN.

CONTROL ISSUES OF MICROGRAVITY VIBRATION ISOLATION

IAA 11052

C. R. KNOSPE, R. D. HAMPTON and P. E. ALLAIRE
Department of Mechanical and Aerospace Engineering, University of Virginia, Charlottesville, VA 22901, U.S.A.

(Received 25 October 1990; revised version received 27 May 1991)

Abstract—Active vibration isolation systems contemplated for microgravity space experiments may be designed to reach given performance requirements in a variety of ways. An analogy to passive isolation systems proves to be illustrative but lacks the flexibility as a design tool of a control systems approach and may lead to poor designs. For example, it is shown that a focus on equivalent stiffness in isolation system design leads to a controller that sacrifices robustness for performance. Control theory as applied to vibration isolation is reviewed and passive analogies are discussed. The loop shaping trade-off is introduced and used to design a single degree of freedom feedback controller. An algebraic control design methodology is contrasted to loop shaping and critiqued. Multi-axis vibration isolation and the problems of decoupled single loop control are introduced through a two degree of freedom example problem. It is shown that center of mass uncertainty may result in instability when decoupled single loop control is used. This results from the ill conditioned nature of the feedback control design. The use of the Linear Quadratic Regulator synthesis procedure for vibration isolation controller design is discussed.

1. INTRODUCTION

Active vibration isolation for microgravity space experiments has generated much interest lately. A variety of disturbances on-board manned space orbiters contaminates the desired microgravity environment. These accelerations cover a frequency band from d.c. to 100 Hz. Low frequency ($< 10^{-3}$ Hz) sources include drag, solar pressure oscillations, tidal effects, and gravity gradient forces. At the higher frequencies, manned activity, thruster firing, and orbiter systems contribute most significantly. A comprehensive treatment of the orbiter accleration environment is presented in [1] from which Fig. 1, a characterization of the environment, is taken.

The need for the active isolation of materials processing and fluid science experiments in the frequency range 0.01–10 Hz has been demonstrated by Jones *et al.* [1–3]. Above this range passive isolation systems could be used. Below 0.01 Hz the rattlespace available for the experiment is not large enough to accommodate the relative motion. Therefore, these accelerations must be passed by the isolation system to the experiment.

Active isolation systems for microgravity and pointing applications have been designed and constructed by many investigators [3–5]. These systems generally use conventional PID control of a non-contacting actuator, either Lorentz or electromagnetic, to achieve low frequency disturbance attentuation. While an actual microgravity experiment may require umbilicals for cooling and power (at this point, it is not clear whether these functions can be performed otherwise as described in [4]) the isolation systems designed and tested so far preclude an umbilical from consideration. These systems achieve their performance by the very low stiffness made possible by low gain feedback of the relative position of the experiment to the mounting surface. Without an umbilical this stiffness may be set by the designer at will. However, when an umbilical is present, the umbilical stiffness presents a lower bound on achievable stiffness unless the feedback loop is used to introduce a negative stiffness. In this paper, the issues of control system design for the *generic* (i.e. with umbilical) microgravity experiment will be considered.

Previous research in the area of active microgravity vibration isolation has established the importance of the umbilical in control system design. Jones *et al.* [6] present a good preliminary examination of the single-degree-of-freedom control issues for intrusive and non-intrusive isolation systems. Grodsinsky [7] examined the use of acceleration and velocity feedback. Many of the issues these researchers have discussed are revisited here from a control theory perspective. Analysis of the six-degree-of-freedom problem in the literature has been restricted to one-loop-at-a-time design. Generally the effects of cross coupling between the various degrees of freedom have been ignored. Owens and Jones [2] have investigated the effect of cross coupling due to center of mass displacement for a single loop based controller. Their work examines this important problem for the non-intrusive experiment platform case where relative position feedback is sufficient. The authors concluded that satisfactory performance can be achieved if the control loops are designed for the decoupled degrees of freedom and not autonomously for each

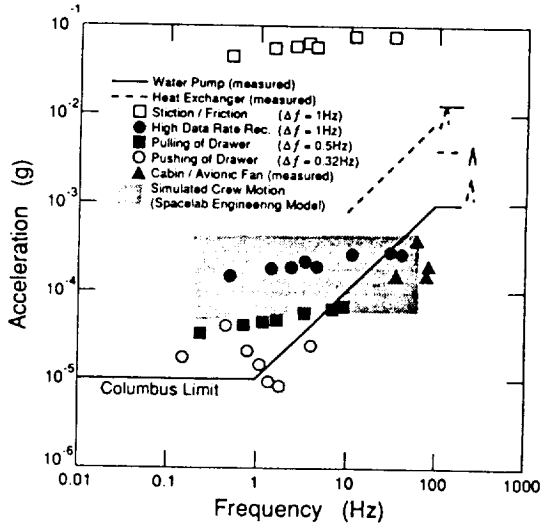

Fig. 1. The microgravity environment (from [1]).

local position. It should be noted that high gains are not required to achieve isolation for the umbilical-free case. An example is presented in this paper which shows that decoupled single loop design may not be sufficient for the generic isolation problem.

Any microgravity isolation system design should meet the following specifications for translational axes:

(1) Unity transmissibility from d.c. to 0.001 Hz so as to prevent the experiment from impacting its enclosure's walls.

(2) At least 40 dB attenuation above 0.1 Hz [3].

(3) Both stability and performance robustness with respect to changes in umbilical/experiment properties, non-collocation or misalignment of sensors and actuators, center of mass uncertainties, and unmodeled cross coupling between the degrees of freedom.

Robustness refers to the ability of the control system to perform satisfactorily when the true plant varies from the nominal plant. Performance requirements of the type (2) for rotational degrees of freedom have not yet been specified to the knowledge of the authors.

In this paper we shall examine the control system issues associated with active microgravity vibration isolation. The purpose here is not to develop new control theory but to apply existing concepts to the problem. We hope that this paper will serve a tutorial function for vibration engineers involved with the microgravity problem. The thesis of this paper is that control system design, not passive isolator design familiar to vibration engineers, is the proper tool for analysis and synthesis. First, the control theory required for the examination is reviewed in Section 2. Section 3 reviews passive isolation and applies it as an analogy to control system design. In Section 4 classical loop shaping is applied to the isolation problem and a controller is designed. A discussion of the result and a passive system analogy follow. An example multi-degree-of-freedom system is explored in Section 5 and system robustness is examined. Section 6 concludes with an examination of the Linear Quadratic Regulator for the isolation problem.

2. CONTROL THEORY PRELIMINARIES†

We examine here the prerequisite control theory for the examination to follow. While the actual isolation problem is multi-dimensional, a single-degree-of-freedom example will be examined first.

The one-degree-of-freedom microgravity vibration isolation problem, depicted in Fig. 2, consists of an experiment of mass m connected by an umbilical and an actuator to a wall of the experiment enclosure. The umbilical is modeled here as a linear element with stiffness k and damping c. The wall's motion (displacement y) is transferred through the umbilical to the experiment resulting in its motion (displacement x). Direct disturbances may also act on the experiment due to the experiment's processes (e.g. motors, valves, shutters). While it may seem that there is no need to distinguish between umbilical and direct disturbances, they are indeed different. The distinction lies in the fact that the actuator influences through the experiment's motion the force transmitted through the umbilical; direct disturbance forces, however, are independent of actuator force. This distinction carries through to both passive isolator performance and control system design.

The equation of motion for the experiment is

$$m\ddot{x} + c\dot{x} + kx = c\dot{y} + ky + d + f \qquad (1)$$

where d is the direct disturbance force and f is the actuator force. We assume here that the spacecraft wall is of sufficient impedance so as to not be affected

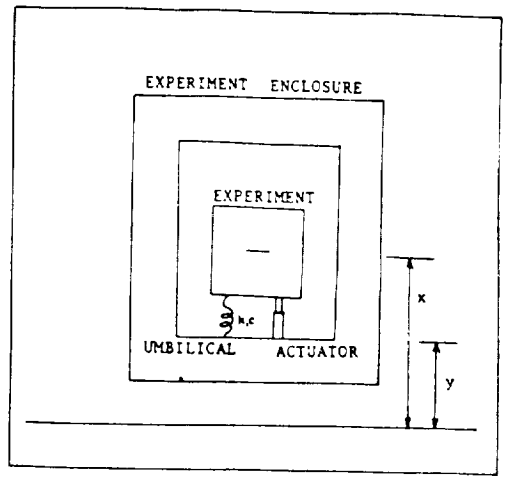

Fig. 2. The one-degree-of-freedom microgravity vibration isolation problem.

† The Nomenclature is given in the Appendix at the end of this paper.

by the actuator force. Under Laplace transformation eqn (1) yields

$$X(s)=\left[\frac{cs+k}{ms^2+cs+k}\right]Y(s)+\left[\frac{1}{ms^2+cs+k}\right][D(s)+F(s)] \quad (2a)$$

or

$$\ddot{X}(s)=\left[\frac{cs+k}{ms^2+cs+k}\right]\ddot{Y}(s)+\left[\frac{s^2}{ms^2+cs+k}\right][D(s)+F(s)]. \quad (2b)$$

This is illustrated in the block diagrams for the isolation system [Fig. 3(a) and (b)]. Here, $H(s)$ is the feedback transfer function, $T(s)$ is the feedforward transfer function, and $v_1(s), v_2(s)$ are measurement noises. The actuator force is therefore a linear function of the wall and the experiment motion. The subscripts p and a throughout this paper refer to whether the model used is in position or acceleration form.

If the umbilical properties are known explicitly and measurement noise is sufficiently small, then transmitted disturbances can be rejected with only feedforward control. Note, however, that direct disturbances can only be attenuated through feedback. As always, the primary purpose of feedback here is to account for uncertainties, either in the disturbance or in the plant model.

The price paid for this property of feedback is the requirement that the feedback be stabilizing over the range of uncertainties in the *nominal plant*, the plant model assumed for design. The nominal stability of the closed loop system may be checked by a variety of methods, the most popular for single-input–single-output (SISO) systems being the Nyquist and Bode plots. Implicit in these methods are measures of system robustness. The Nyquist stability criterion can be generalized to multi-input–multi-output (MIMO) systems, however the robustness measures do not carry over as straightforwardly.

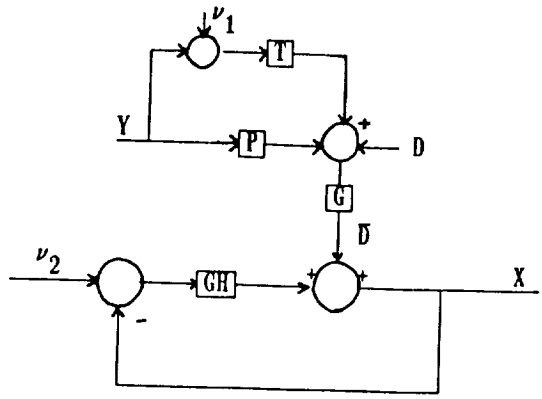

Fig. 4. Unity feedback form of control system.

Both Fig. 3(a) and (b) can be generically expressed in the form of Fig. 4 where $G(s)$ is the plant, $P(s)$ is umbilical's pre-compensation of the wall disturbance and $\bar{D}(s)$ is the equivalent disturbance to the system. Figure 4 has been presented in unity feedback form so as to introduce the concept of loop shaping and the trade-offs inherent in control system design. Denote the transfer functions between $\bar{D}(s)$ and $X(s)$, the *sensitivity function*, as

$$S(s)\equiv\frac{X(s)}{\bar{D}(s)}=\frac{1}{1+GH} \quad (3)$$

and between $v_2(s)$ and $x(s)$, the *complementary sensitivity function*, as

$$C(s)\equiv\frac{X(s)}{v_2(s)}=\frac{GH}{1+GH}. \quad (4)$$

(a)

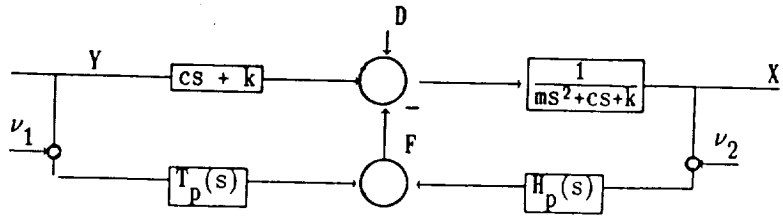

(b)

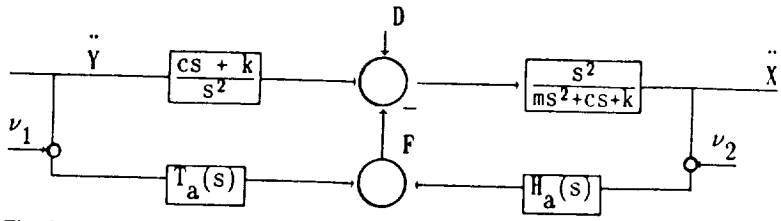

Fig. 3. Displacement (a) and acceleration (b) isolation system block diagrams.

Note that $S(s)+C(s)=1$. Therefore, a feedback controller designed to attenuate external disturbances at a particular frequency

$$|S(j\omega_0)| \ll 1.0 \quad |GH(j\omega_0)| \gg 1.0$$

cannot attenuate the measurement noise signal at that frequency

$$|C(j\omega_0)| \approx 1.0 .$$

Likewise, a controller designed to reject a certain frequency measurement noise, $|C(j\omega_0)| \ll 1.0$, must pass the external disturbance at this frequency, $|S(j\omega_0)| \approx 1.0$. Classical design of control systems usually involves separating (if possible) the frequency spectrum into regions where input disturbances (measurement noise here) and output disturbances (external disturbance here) predominate. The methodology, known as loop shaping, consists of choosing $H(s)$ so that GH is large and therefore $S(s)$ is small at frequencies where output disturbances are dominant, and choosing $H(s)$ so that GH is small and therefore $C(s)$ is small at frequencies where input disturbances are dominant. This would be a relatively simple task if the designer only needed to be concerned with the magnitude of GH. However, stability of the feedback system requires that the argument of GH at crossover, where $|GH(j\omega_0)| \equiv 1.0$, be $> -180°$. That is, the system must have some phase margin. Since the phase of a transfer function is tied to the derivative of its magnitude (in dB) with respect to frequency, as was shown by Bode [8], the loop shaping's results are fundamentally limited by the difference in frequency between the input and output disturbances. The designer may only change through shaping $H(s)$ the magnitude in dB of GH at so fast a rate. Thus, the frequency bands where the magnitude of the sensitivity function and complimentary sensitivity function may be small must be separated in frequency by a crossover region of a certain width. This width is dependent on $G(s)$ as well as on how small $|C(s)|$ and $|S(s)|$ must be.

The trade-off between rejection of input and output disturbances through feedback is also inherent in passive isolation systems. Suppose we are capable of choosing the umbilical stiffness and damping of Fig. 2 so as to design a passive isolator. Note that the transfer function relations

$$\frac{\ddot{X}(s)}{\ddot{Y}(s)} = \frac{G(s)}{1+G(s)} \quad \frac{\ddot{X}(s)}{D(s)/m} = \frac{1}{1+G(s)} \tag{5}$$

apply where

$$G(s) = \left(\frac{cs+k}{ms^2}\right).$$

From this, it is easy to see that direct disturbances act as output disturbances while wall accelerations act as input disturbances. The difference between designing an isolation mount for base disturbances and for direct disturbances is well known and understood by vibration engineers. A soft mount is appropriate for isolating against base disturbances while a stiff mount is appropriate for direct disturbances excitation. The loop shaping capability of springs and dampers is, however, very restricted. Indeed, one cannot shape the loop to yield an unstable system. An active control system may have its loop shaped to an arbitrary specification provided it is possible to meet the specification without sacrificing system stability. Here lies the chief advantage of designing an isolation system from a control paradigm: the interaction of the conflicting specifications, stability and robustness, is clear throughout the loop shaping procedure. It should be noted here that sensitivity and complimentary sensitivity functions are extendable to MIMO systems through the use of singular values.

Robustness in single-input–single-output controller design is measured by *gain* and *phase margins*. The gain margin is the range of gain that can be introduced into the loop while maintaining stability. Similarly, the phase margin is the amount of phase that can be introduced into the loop while maintaining stability. The practical importance of the margins is that the gain and phase of the nominal plant is not the same as that of actual plant. These margins may be easily determined from Nyquist or Bode plots. Loop shaping also implies that a compensator $H(s)$ should not be so large as to extend the crossover frequency of the compensated system into the higher frequency range where nominal models are very inaccurate.

Robustness for MIMO systems can also be specified in terms of the simultaneous gain and phase variations that may be introduced into the loops while preserving stability. However, this description does not account for unmodeled coupling in the dynamics. Uncertainty may be represented in terms of an additive (in parallel) or multiplicative (in series) transfer function matrix appended to the plant. (While these are the most common there are other representations.) Using either uncertainty representation it can be easily shown by the small gain theorem that stability can be guaranteed if uncertainties in the plant are required to be bounded by a norm of the compensated plant. This is best represented in terms of the frequency dependent singular values of the plant and uncertainty transfer function matrices. This measure, however, is conservative since it allows cross coupling dynamics between channels that in actuality could never occur. The structured singular value methodology attempts to alleviate this conservatism through structuring the uncertainty model. Readers interested in a general treatment of MIMO stability and robustness should consult Ref. [9].

3. PASSIVE ISOLATION: AN ANALOGY

We now examine the design of an active vibration isolation system for microgravity space experiments from an analogy to passive isolators. Indeed, the primary reason for pursuing an active rather than a

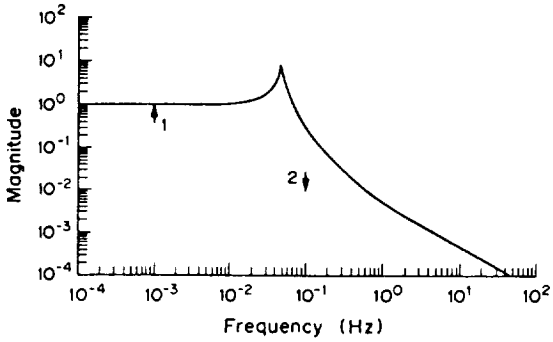

Fig. 5. Specifications (1) and (2) and uncompensated transmissibility $\ddot{X}(s)/\ddot{Y}(s)$.

passive system is not the increased flexibility in loop shaping but the limitations of passive systems in attaining a stiffness low enough to meet the isolation requirements. This is true even when no umbilical is present.

For the generic system model of eqn (1) with the nominal values $m = 220$ kg, $k = 20$ N/m and $c = 6.63$ N · s/m (5% of critical damping). The transmissibility curve between base and experiment acceleration, shown in Fig. 5, is given by

$$\frac{\ddot{X}(s)}{\ddot{Y}(s)} = \frac{2\zeta\omega_n s + \omega_n^2}{s^2 + 2\zeta\omega_n s + \omega_n^2} \tag{6}$$

with

$$\omega_n \equiv \sqrt{k/m} = 0.3 \text{ rad/s} = 0.048 \text{ Hz}$$

$$\zeta = \sqrt{c^2/4mk} \approx 0.05 .$$

Also depicted in Fig. 5 are the transmissibility specifications (1) and (2) discussed in Section 1. While the system satisfies the unity transmissiblity criterion, note that the natural frequency is not low enough to meet the 40 dB attenuation requirement. The system is also deficient in the magnification of disturbances at and near the resonance. Clearly any modification to the umbilical's dynamics through feedback should include increased damping through a positive gain on experiment velocity. Feedback of inertial experiment velocity permits the damping coefficient ζ to be increased in the denominator of eqn (6) without changing it in the numerator. Thus, the resonance can be removed without affecting the roll-off rate [since the zero of eqn (6) is not changed].

If the umbilical were softer, say with $k = 0.20$ N/m, both specifications (1) and (2) could be met by the passive system. Unfortunately, a passive system cannot lower the stiffness with its inherently positive gains on position feedback. An active system, though, permits insertion of a negative stiffness spring in parallel with the umbilical. For example, for the nominal plant with the controller transfer functions of Fig. 3(a) equal to

$$H_p(s) = -(6.0s + 19.8)$$

$$T_p(s) = -(6.0s + 19.8) \tag{7}$$

the natural frequency of the system is moved an order of magnitude lower. (Here, a negative damper has also been introduced so as to maintain the system's 5% critical damping for the purpose of comparison. If less negative damping is introduced in order to remove the resonance, even more negative stiffness must be introduced to meet the 40 dB specification.) Note that this vibration engineering approach, i.e. lowering the stiffness, requires the near cancellation of the umbilical's stiffness with that introduced via feedback. If the negative stiffness exceeds that of the umbilical, the equivalent stiffness of the system will be negative and the system will be unstable. It is not surprising then that the introduction of negative stiffness via the controller has no robustness whatsoever. The design using eqn (7) has $<0.1°$ phase margin. The root locus for the system, shown in Fig. 6, clearly indicates this potential for instability. A focus on equivalent stiffness in isolation system design thus leads to control systems which sacrifice robustness for performance. In addition, a design which achieves isolation through lowering the system stiffness cannot attenuate direct disturbances over the same frequency band, as discussed in Section 2.

From a vibration engineering viewpoint, an alternative means of achieving rejection of disturbances is to fasten the experiment rigidly to an inertial structure. While there is no such structure in space, it is possible to achieve this effect by a high positive gain feedback on inertial experiment position. (The inertial position must be obtained by integrating an accelerometer reading twice. This does pose a problem since this procedure is marginally stable. However, this problem may be ameliorated through replacing the integrators with a second order low pass filter. The authors are aware of this method being employed successfully on a six-degree-of-freedom magnetic suspension isolation rig at NASA Lewis Research Center.) This inertial position feedback acts as a very stiff spring tying the experiment to inertial

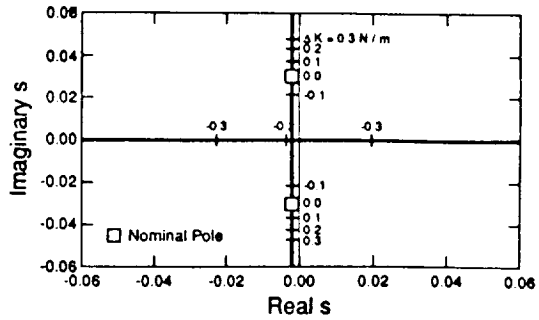

Fig. 6. Root locus for equivalent stiffness design with respect to umbilical stiffness error.

space. A controller and resulting transfer functions in this case are

$$H_p(s) = 2000 \quad T_p(s) = 0$$
$$\frac{\ddot{X}(s)}{\ddot{Y}(s)} = \frac{6.63s + 20}{220s^2 + 6.63s + 2020}$$
$$\frac{\ddot{X}(s)}{D(s)/m} = \frac{220s^2}{220s^2 + 6.63s + 2020}. \quad (8)$$

While this controller meets the 40 dB specification, it does not have unity transmissibility below 0.001 Hz. An experiment controlled in this fashion will collide into the wall. The feedforward transfer function may be adjusted to provide unit gain via

$$T_p(s) = \frac{-2000}{159s + 1}.$$

This feedforward with the feedback term of eqn (8) effectively acts to base disturbances as a high relative stiffness up to 0.001 Hz changing to a large inertial stiffness at higher frequencies. The resulting transmissibility $\ddot{X}(S)/\ddot{Y}(s)$ is presented in Fig. 7. Note that since the feedback loop introduces no damping, the original resonance is still present although less damped and at a higher frequency. This may be corrected by adding inertial damping into the feedback loop. While this design method may be used to meet the specifications with robustness it has three faults: (1) it requires inertial experiment position, inertial wall position, and inertial experiment velocity measurements which are problematic to obtain, (2) it requires very high gains in both feedforward and feedback loops to obtain attenuation, and (3) an extension of the method to multi-degree-of-freedom systems would be difficult. It is also possible that when a flexible wall is considered, rather than the infinite impedance structure assumed, the system will be unstable.

As another method of fastening the experiment to inertial space, one may employ inertial damping via feedback. By feeding back the inertial experiment velocity with a high gain, it is almost possible to achieve both the 40 dB and unity transmissibility specifications without resorting to feedforward. For example, with

$$H_p(s) = 1000s \quad T_p(s) = 0$$

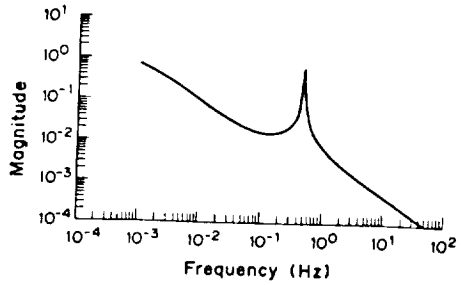

Fig. 7. Transmissibility $\ddot{X}(s)/\ddot{Y}(s)$ for inertial stiffness with feedforward design.

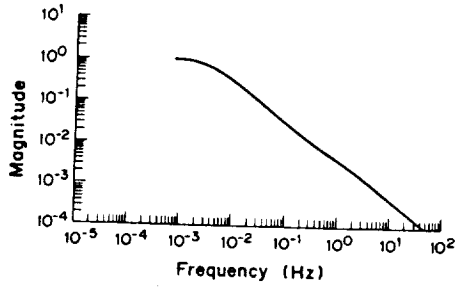

Fig. 8. Transmissibility $\ddot{X}(s)/\ddot{Y}(s)$ for inertial damping design.

the resultant transmissibility is shown in Fig. 8. Unfortunately, the roll-off rate here is approx. 20 dB/decade and therefore it is impossible to achieve both specifications simultaneously. This method has the advantage over the inertial spring of being a great deal simpler and requiring only one inertial measurement (experiment velocity which requires only one integration of accelerometer measurements).

Another passive analogy is the lowering of the natural frequency of the umbilical by increasing the experiment mass. An increased experiment mass would attenuate direct disturbances as well as those transmitted through the umbilical. In addition, at frequencies below the natural frequency of the umbilical, the isolation system would have unity transmissibility. Of course, for space applications any additional mass is very costly. To lower the natural frequency by an order of magnitude would require increasing the experiment mass by a factor of one hundred. Clearly, it is not practical to accomplish increased isolation through the addition of real mass. However, it is possible to increase the effective mass of the system through feedback. This will be examined in the next section, as this idea most properly evolves out of loop shaping.

To summarize, the passive isolation analogy to active control system design yields some insight but falls short as a design tool on three counts: (1) it does not have the flexibility to shape the response with its simple analogical elements, stiffness, damping, and mass, so as to achieve the performance requirements, (2) it cannot be easily or effectively generalized to multi-degree-of-freedom problems, and (3) it completely ignores the robustness problem inherent to active control systems. We advocate, therefore, that vibration engineers consider active isolation a controls problem and address it from an automatic controls perspective.

4. THE CONTROL SYSTEM APPROACH

A simple controller is now designed for the system described by eqn (1) and the nominal values. The authors refer the reader again to Fig. 5 where the transmissibility curve between experiment and wall accelerations (or positions) is presented along with the design specifications (1) and (2). The goal is to

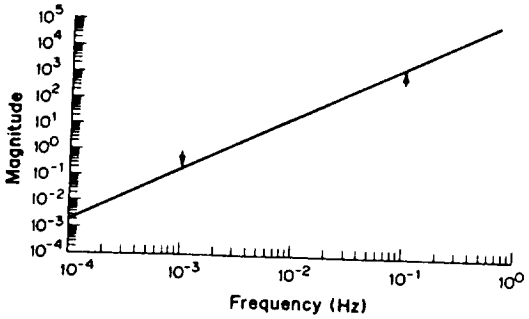

Fig. 9. Designs specifications and $H_p(s)$.

design a feedback control $H_p(s)$ that results in the closed loop transfer function

$$G_{cl}(s) \equiv \frac{X(s)}{Y(s)} = \frac{G_p(s)P(s)}{1 + G_p(s)H_p(s)} \tag{9}$$

satisfying both constraints; i.e.

$$|G_{cl}(j\omega_0)| \approx 1.0 \quad \frac{\omega_0}{2\pi} < 0.001 \text{ Hz}$$

$$|G_{cl}(j\omega_0)| < 0.01 \quad \frac{\omega_0}{2\pi} > 0.1 \text{ Hz}.$$

Here, $G_p(s)$ and $P(s)$ are as indicated in the block diagram of the system [Fig. 3(a)]. Note that the uncontrolled system $G_p(s)P(s)$ already satisfies the first of these constraints; therefore, $H_p(s)$ should be very small in the low frequency band so that the closed loop system will continue to satisfy the unit transmissibility specification. Consequently, this specification yields a condition like

$$\left.\begin{array}{l} |GH_p(j\omega_0)| < 0.01 \\ |H_p(j\omega_0)| < 0.2 \end{array}\right\} \frac{\omega_0}{2\pi} < 0.001 \text{ Hz}.$$

At and above 0.1 Hz, the attenuation of the uncontrolled system is not sufficient. It is desirable to increase the attenuation by approximately two orders of magnitude. This may be accomplished by requiring $H_p(s)$ to be very large in this frequency range, approximately

$$\left.\begin{array}{l} |GH_p(j\omega_0)| > 100 \\ |H_p(j\omega_0)| > 2000 \end{array}\right\} \frac{\omega_0}{2\pi} > 0.1 \text{ Hz}.$$

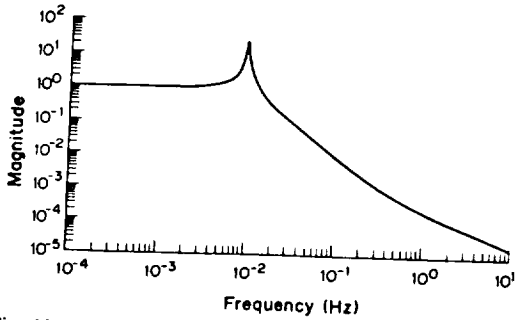

Fig. 10. Resultant transmissibility for loop shaped design.

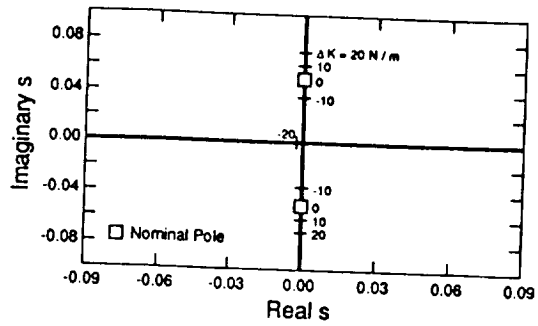

Fig. 11. Root locus of loop shaped design with respect to umbilical stiffness error.

These two design specifications on $H_p(s)$ are shown in Fig. 9 along with a simple function satisfying these conditions,

$$H_p(s) = 5000\, s^2. \tag{10}$$

This controller design results in the closed loop transmissibility between experiment and wall accelerations which is plotted in Fig. 10. Note that both specifications (1) and (2) are met. Inertial damping should be added to this design to eliminate the resonance. It is easily seen from a root locus plot that this design is robust with respect to changes in umbilical/experiment properties (Fig. 11) and actuator finite bandwidth (Fig. 12). In practice, this design would be improved by rolling off the controller gain. This limits the controller bandwidth so as to not affect possible unmodeled lightly-damped high frequency modes of the system (e.g. wall flexure). A controller design would probably also include a weak position integral feedback to provide a slow centering force so that accelerometer bias and noise do not result in wall collision.

The reader might object to the controller of eqn (10) since it is improper (i.e. has more zeros than poles). However, this controller is realizable. Note that $H_p(s)$ multiplies the position measurement to yield the control force. Since the factor s^2 in the time domain is equivalent to two differentations with respect to time, eqn (10) prescribes constant gain acceleration feedback. This, as discussed earlier, increases the effective mass of the system. [Of course, if

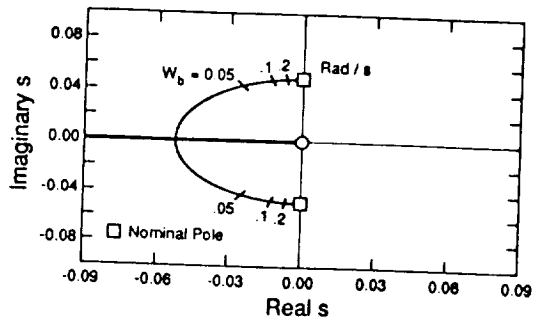

Fig. 12. Root locus of loop shaped design with respect to actuator finite bandwidth, ω_b = actuator pole break frequency.

we modify eqn (10) to limit the controller bandwidth, then the mass analogy only holds within the band.]

While both transmitted and direct disturbances are attenuated, the experiment acceleration level will be approximately the same as the accelerometer measurement noise level. This results from the transmissibility between experiment acceleration and measurement noise being nearly one due to the high gain feedback. This is a fundamental issue as discussed in Section 2; one must trade-off the rejection of disturbances to the system and the rejection of measurement noise. Since the disturbances may be up to 1000 times larger than the measurement noise (accelerometer resolution typically 1 μg) the controller is designed to reject disturbances. The performance of the control system is thus directly a function of the quality of the accelerometer.

Recently, an alternative approach to design of active vibration isolation control systems for microgravity experiments was presented in Ref. [10]. A desired transmissibility ratio $G_{cl}(s)$ is specified along with the plant model $G_p(s)$ and $P(s)$. Equation (9) is then solved via algebraic manipulation for the feedback controller $H_p(s)$ that yields the desired transmissibility (feedback of relative position is also allowed and may be used; if used, a second condition must then be specified for solution). While this approach resembles loop shaping in that it attempts to achieve a certain transmissibility, it is fundamentally different in that it does not properly consider the plant. The algebraic procedure in essence first eliminates the plant and then replaces it with one which will yield the desired transmissibility. As a control design procedure, this methodology has serious flaws: (1) the stability of the resulting system may be entirely dependent on perfect knowledge of the plant, (2) the procedure incorporates none of the known relationships and fundamental trade-offs between stability and attenuation; it implies that any specified transmissibility is achievable, and (3) for systems with right half plane poles/zeros, the methodology may attempt cancellation with right half plane zeros/poles. For a simple controls problem, the algebraic manipulation method may result in a good controller. However, for more difficult problems, the method is questionable. An extension of this methodology to MIMO control would be plagued by many problems.

To summarize, controller design for single-degree-of-freedom vibration isolation problems is best performed through the classical control framework of loop shaping where the natural interplay between performance, stability and robustness are evident. For multiple degree of freedom isolation problems, recent advances in controller design, such as the extension of loop shaping principles via frequency weighting and singular values [11] seems to be most promising. In order to emphasize the question of coordination in control of MIMO systems, we next examine a multiple degree of freedom isolation problem.

5. A MULTIPLE-DEGREE-OF-FREEDOM SYSTEM

A common misunderstanding among many engineers unfamiliar with control system design is the nature of the differences between SISO and MIMO control problems. The relative ease with which the uninitiated comprehend the elimination of one error signal through negative error feedback yields the false impression that the MIMO control problem is little more than the feeding back of multiple error signals. This impression, however, is not totally groundless. Indeed, many MIMO controllers in use today were designed by a single-loop-at-a-time procedure. Design with this method can be quite difficult, time consuming, and non-intuitive. Robustness is difficult to check except by analyzing all the possible permutations to the nominal plant. The fundamental problem in MIMO design is the coordination of the control in coupled channels when the plant is not well known (poorly modeled or time varying).

Easily decoupled active vibration isolation control problems may be deceptively simple. Unmodeled cross-coupling due to inaccuracies in center of mass, sensor, and/or umbilical locations can result in poor performance and even instability. An example isolation problem illustrates. Figure 13 shows a two-degree-of-freedom isolation system composed of an isolated platform (width 0.5 m and height 0.2 m, depth unspecified), two accelerometers, two actuators, an umbilical, and a translating base. The platform may translate vertically or rotate about its center of mass. The actuators and accelerometers are positioned a distance of $q = 0.2$ m symmetrically about the assumed center of mass location. An umbilical of stiffness k (no damping) runs between this location and the base. The platform has mass m and inertia I. The equations of motion for the platform's translation $x(t)$ and rotation $\theta(t)$ are

$$m\ddot{x} + k\Delta\theta + kx = f_1 + f_2 + d_1$$

$$I\ddot{\theta} + k\Delta^2\theta + k\Delta x = (q+\Delta)f_2 - (q-\Delta)f_1 + d_2 \quad (11)$$

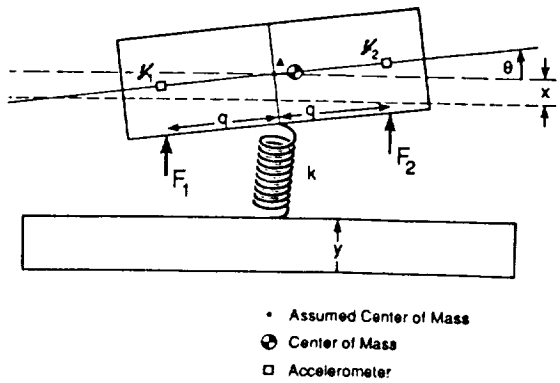

Fig. 13. Two-degree-of-freedom active isolation system.

where d_1 and d_2 are the disturbances, and Δ is the error in the assumed center of mass. The accelerometer readings are

$$y_1 = \ddot{x} - (q - \Delta)\ddot{\theta}$$
$$y_2 = \ddot{x} + (q + \Delta)\ddot{\theta}. \quad (12)$$

The nominal system ($\Delta = 0$) can be decoupled in terms of the degrees of freedom by the change in variables

$$F = f_1 + f_2$$
$$M = q(f_2 - f_1)$$
$$z_1 = (y_1 + y_2)/2$$
$$z_2 = q(y_2 - y_1)/2 \quad (13)$$

which are nominally the translational force, the moment, the translational acceleration, and the angular acceleration for the platform, respectively. The nominal transfer functions for the system are then

$$Z_1(s) = \left[\frac{s^2}{ms^2 + k}\right](F(s) + D_1(s))$$
$$Z_2(s) = \left[\frac{1}{I}\right](M(s) + D_2(s)).$$

For translational motion, the natural frequency of the platform is $\sqrt{k/m}$. The rotational motion of the platform is free since the umbilical is attached to the center of mass. To compensate the nominal system, feedback can be designed for each mode of the system separately, since the system is decoupled. Translational acceleration and velocity feedback are first used to add effective mass and damping.

$$F(s) = -\left(a + \frac{c}{s}\right)Z_1(s). \quad (14)$$

This lowers the natural frequency of translational motion yielding the closed loop transfer function

$$Z_1(s) = \left[\frac{s^2}{(m + a)s^2 + cs + k}\right]D_1(s).$$

Next, angular deflection feedback is used to constrain low frequency rotational motion and some damping is provided.

$$M(s) = -\left(\frac{n}{s} + \frac{b}{s^2}\right)Z_2(s) \quad (15)$$

yielding

$$Z_2(s) = \left[\frac{s^2}{Is^2 + ns + b}\right]D_2(s)$$

The following values are used to illustrate this example

Platform	Control system
$m = 400$ kg	$a = 31600$ kg
$k = 50$ N/m	$c = 1000$ N · s/m
$I = 10$ kg · m^2	$b = 0.015$ N · m
	$n = 0.2$ N · m · s

where the control system values are in effective units. This control design lowers the natural frequency of translational motion from 0.056 to 0.006 Hz with 40% of critical damping. The controlled rotational motion has a natural frequency of 0.006 Hz with 26% of critical damping. This controller design would yield very effective isolation on the nominal system.

The actual close loop transfer functions, however, will be different from the nominal due to the error in the center of mass, Δ. The transmissibility can be derived from eqns (11)–(15) as follows

$$[ms^2 + k]X(s) + [k\Delta]\Theta(s) = F(s) + D_1(s)$$
$$[Is^2 + k\Delta^2]\Theta(s) + [k\Delta]X(s) = M(s) + \Delta F(s) + D_2(s)$$
$$Z_1(s) = [s^2]X(s) + [\Delta s^2]\Theta(s)$$
$$Z_2(s) = [s^2]\Theta(s)$$
$$F(s) = -[a + c/s]Z_1(s)$$
$$M(s) = -[n/s + b/s^2]Z_2(s)$$

yielding

$$\left[\frac{(m + a)s^2 + cs + k}{s^2}\right]Z_1(s) + [m\Delta]Z_2(s) = D_1(s)$$
$$\left[\frac{(as^2 + s + k)\Delta}{s^2}\right]Z_1(s) + \left[\frac{Is^2 + ns + b}{s^2}\right]Z_2(s) = D_2(s).$$

The poles of this system are given by the roots of the characteristic equation

$$[(m + a)s^2 + cs + k][Is^2 + ns + b] - [m\Delta][\Delta(as^2 + cs + k)] = 0 \quad (16)$$

For the nominal plant, $\Delta = 0$, the roots of eqn (16) result in the prescribed natural frequencies and critical dampings. However, as the center of mass error increases, the poles migrate and the system becomes unstable. For an error as small as 6 mm, instability occurs. A plot of the pole movement vs error in center of mass is shown in Fig. 14. This sensitivity results from the ill-conditioned character of the required controller. Ill-conditioned here means that the controller's gain to an output signal varies strongly with the signal's direction. This results in a control system which is not robust to this model's uncertainty (center of mass) [12]. A proper MIMO controller design might remedy this problem. In any case, an analysis of the problem from a MIMO control

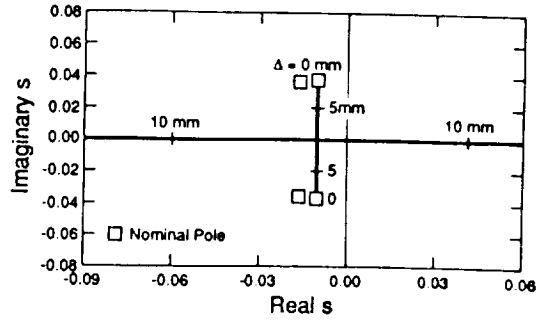

Fig. 14. Root locus of two-degree-of-freedom with respect to center of mass error Δ.

perspective would indicate the potential instability and the nature of the trade-off between performance and robustness. (The authors note that increasing the damping and stiffness for the rotational mode improves the system robustness significantly, while changing the damping or effective mass for the translational mode has little effect.)

6. LINEAR QUADRATIC REGULATOR FOR ISOLATION

MIMO control design, since it requires a high degree of coordination, must proceed by a synthesis procedure. One such method is Linear Quadratic Regulator (LQR) synthesis [13]. This produces a state feedback controller which is optimal with respect to the quadratic (two norm) performance function

$$J = \int_{-\infty}^{\infty} \bar{x}^T(j\omega)Q\bar{x}(j\omega) + u^T(j\omega)Ru(j\omega)\,d\omega \quad (17)$$

where Q and R are respectively the symmetric (usually diagonal) state and control weighting matrices, and $\bar{x}(j\omega)$ and $u(j\omega)$ are the Fourier transforms of the state and control vectors. The state (positions and velocities for vibration isolation) satisfies the differential equation

$$\dot{x} = A\bar{x} + Bu.$$

The quadratic performance function of LQR, eqn (17), is well suited to this problem since vibration isolation quality is usually measured in terms of root-mean-square. However, some modification of the performance function is necessary to apply this synthesis procedure to microgravity isolation controller design. The reader will note that state feedback for the isolation problem is feedback of experiment positions, velocities, angles, and angular velocities. Thus, LQR can only result in inertial stiffness and inertial damping feedback. As was shown in Section 3, these isolation techniques cannot yield acceptable isolation performance. Thus, an LQR performance function of the form of eqn (17) will not yield a satisfactory controller. Note that the differential equation does not include a disturbance term. Consequently, the controller is optimal with respect to white noise. Since the power spectrum of the microgravity environment is not of this shape, the LQR controller will not be optimal with respect to rejection of the disturbance. Through the incorporation of a disturbance model (essentially a shaping filter) the LQR problem may be modified to yield an optimal disturbance accommodating (i.e. rejection) controller. This incorporates the addition of pseudo-states to the state variable model [14].

Closely related to disturbance accommodation is the concept of frequency weighted LQR performance functions [15]. Here, the Q and R matrices are chosen to be even rational functions of frequency. This results in the addition of pseudo-states to the state variable model. Through choice of the weighting functions, the designer can in essence shape the control loops [11]. This also permits the weighting of experiment acceleration. It should be noted that for successful application of LQR theory to the microgravity isolation problem frequency-shaped cost functions must be used. Without this, the control resulting from the synthesis procedure would attenuate the vibration at frequencies below 0.001 Hz (nonunity transmissibility). The reader should note that the well known robustness characteristics of LQR controllers do not apply to most frequency shaped designs or to plants with unmodeled cross coupling.

7. CONCLUSIONS

Successful active isolation for microgravity experiments can be achieved, but only if the problem is analyzed from a controls perspective. A passive isolation analogy, while useful for an understanding of the control problem, is not an effective design tool. Design of active vibration control systems can best be carried out through loop shaping. For intrusive isolation platforms, this results in a high gain acceleration feedback design. A two-degree-of-freedom example was used to illustrate the instability that can result under unmodeled cross coupling when the control system is designed via decoupling/single loop design procedures. The source of this sensitivity was ill-conditioning of the controller. The LQR was examined for the isolation problem. For synthesis of an effective controller, the procedure must be modified to include loop shaping.

Acknowledgements—This work was supported in part by NASA Lewis Research Center and the Commonwealth of Virginia. Some of this research was performed at NASA LRC as part of the Summer Faculty Fellowship Program. The authors would like to thank Dr Gerald Brown and Carlos Grodsinsky of NASA LRC for many helpful discussions.

REFERENCES

1. R. G. Owen and D. I. Jones, *Microgravity Isolation Mount: Columbus Application Study* (WP.1.1). European Space Agency, Technical Note BTN-001 (1988).
2. A. R. Owens and D. I. Jones, Toward a practical microgravity environment. *Proceedings of the Third European Space Mechanisms and Tribology Symposium*, Madrid, Spain, pp. 245–250 (1987).
3. D. I. Jones, A. R. Owens, R. G. Owen and G. Roberts, *Microgravity Isolation Mount: Design Report*. European Space Agency, Technical Note BTN-009 (1989).
4. C. M. Grodsinsky and G. V. Brown, Non-intrusive inertial vibration isolation technology for microgravity space experiments. NASA TM-201386 (1990).
5. B. J. Hamilton, J. H. Andrus and D. R. Carter, Pointing mounts with active vibration isolation for large payloads. *10th Annual Guidance and Control Conference, American Astronautical Society*, Keystone, Colo. (1987).
6. D. I. Jones, A. R. Owens and R. G. Owen, A microgravity isolation mount. *Acta Astronautica* **15**, 441–448 (1987).
7. C. M. Grodsinsky, Development and approach to low-frequency microgravity isolation systems. NASA Technical Paper 2987 (1990).

8. H. W. Bode, *Network Analysis and Feedback Amplifier Design*. Van Nostrand, New York (1945).
9. J. M. Maciejowski, *Multivariable Feedback Design*. Addison-Wesley, New York (1989).
10. A. Sinha, C. K. Kao and C. M. Grodsinsky, A new approach to active vibration isolation for microgravity space experiments. NASA TM 102470 (1990).
11. M. G. Safanov, A. J. Laub and G. L. Hartmann, Feedback properties of multivariable systems: the role and use of the return difference matrix. *IEEE Trans. Automatic Control* **26**, 47–65 (1981).
12. S. Skogestad, M. Morari and J. C. Doyle, Robust control of ill-conditioned plants: high purity distillation. *IEEE Trans. Automatic Control* **33**, 1092–1105 (1988).
13. B. P. O. Anderson, and J. B. Moore, *Linear Optimal Control*. Prentice–Hall, Englewood Cliffs, N.J. (1972).
14. C. D. Johnson, Accommodation of external disturbances in linear regulator and servomechanism problems. *IEEE Trans. Automatic Control* **16**, 635–644 (1971).
15. N. K. Gupta, Frequency-shaped cost functionals: extension of linear-quadratic-gaussian design methods. *J. Guidance Control* **3**, 529–535 (1980).

APPENDIX

Nomenclature

A = system dynamic matrix
a = acceleration feedback coefficient
B = system input matrix
b = rotational stiffness feedback coefficient
$C(s)$ = complimentary sensitivity function
c = damping
$d,D(s)$ = direct disturbance force
$\bar{D}(s)$ = equivalent disturbance
$f,F,F(s)$ = actuator force
$G(s)$ = plant transfer function
$H(s)$ = feedback transfer function
I = moment of inertia
k = stiffness
$M,M(s)$ = control moment
n = rotational damping feedback
$P(s)$ = umbilical precompensation transfer function
Q = state weighting matrix
q = actuator placement
R = control weighting matrix
$S(s)$ = sensitivity function
$T(s)$ = feedforward transfer function
u = control vector
$v(s)$ = measurement noise
$x,X(s)$ = experiment position
$\bar{x}$ = state vector
$y,Y(s)$ = wall position
y = accelerometer measurements
$z,Z(s)$ = decoupled measurements
Δ = center of mass error
$\theta,\Theta(s)$ = angular position
ω_n = natural frequency
ζ = percent critical damping

Subscripts

a = acceleration
cl = closed loop
p = position.

CONTROLLER DESIGN FOR MICROGRAVITY VIBRATION ISOLATION SYSTEMS

R. D. Hampton*, C. R. Knospe**
University of Virginia
Charlottesville, Virginia

C. M. Grodsinsky†
NASA Lewis Research Center
Cleveland, Ohio

Abstract

Manned orbiters will require active vibration isolation for acceleration–sensitive microgravity science experiments. This paper investigates control aspects of the isolation problem and proposes a viable, robust control. Since umbilicals are highly desirable for many experiments, and since their presence greatly affects the vibration isolation problem, they must be considered in control synthesis. Experiment isolation involves reducing undesirable plant outputs, such as excessive accelerations and unacceptable relative displacements. The former are undesirable due to experiment dynamic environmental demands; the latter, due to rattlespace constraints. Ideally, controller design should minimize these outputs, while considering input– and output directionality and frequency content. This paper investigates applying modern control theory to the isolation problem, incorporating frequency–weighting and disturbance accommodation techniques. The resulting controller achieves excellent system performance, for plants within a reasonable range of variations from the nominal. Robust stability and performance guarantees were measured by singular value and structured singular value checks, yielding guarantees on allowable real plant parameter uncertainties, and on acceptable controller and sensor phase and gain variations. The problem of unmodeled high frequency modes was eliminated by using frequency weighting to reduce controller bandwidth. This design method has been developed with the six–degree–of–freedom isolation problem in mind, to which it is fully applicable. In this paper the method is applied successfully to the single–degree–of–freedom isolation problem.

Introduction

The vibration environment onboard current and planned manned orbiters will require isolation for many microgravity science experiments[1]. The disturbance frequencies are sufficiently low, and the attenuation requirements sufficiently great, so as to preclude a solely passive isolation system[2,3].

Since the disturbances to be attenuated are three–dimensional (3–D)[1], the isolation actuator(s) must be capable of acting over six degrees of freedom. Although microgravity isolation systems have been developed and tested[4], most controllers offered to date fail to take into account the effect of umbilicals in a 3–D isolation system design[3]. Since umbilicals are highly desirable for many experiments[5](e.g., for evacuation, power transmission, cooling, material transport), they must be considered in a generally applicable control scheme. Simple application of nonintrusive control methodologies is insufficient[3].

The requisite multiple–degree–of–freedom (MDOF) controller is much more difficult to design than a

* Graduate Research Assistant, Mechanical, Aerospace, and Nuclear Engineering
**Assistant Professor, Mechanical, Aerospace, and Nuclear Engineering
† Mechanical Engineer, Micrograviy Experiments Branch of the Space Experiments Div.

single–degree–of–freedom (SDOF) controller, because the isolation system has many inputs (actuator forces) and outputs (measured displacements and accelerations). Multiple–input–multiple–output (MIMO) designs can be very susceptible to unmodeled cross–coupling between channels of input or output[3], a problem not encountered in SDOF design. The control forces used must therefore be properly coordinated if the controller's performance is to be sufficiently insensitive to unmodeled dynamics (i.e., *robust*). The design of a robust MIMO control system is a nontrivial problem requiring the iterative use of synthesis and analysis tools, the former for controller design and the latter for system stability– and performance evaluation[6].

H_2 synthesis, the controls approach chosen for this work, has been used effectively in MIMO control problems[7]. Additionally, the approach seems appropriate for the present problem, since the quadratic performance index relates well to root–mean–square (rms) statistics and power spectral densities, in which form present orbiter acceleration data is currently made available[4].

The microgravity isolation problem aboard manned orbiters involves reduction of different kinds of undesirable plant outputs, such as excessive accelerations and unacceptable relative displacements. The former outputs are undesirable due to the demands of the experiments themselves[2]; the latter, due to rattlespace constraints[2, 8]. Since some disturbances may be directional, since some undesirable plant outputs may be more important than others, and since the degree of undesirability of these outputs may also vary with direction or frequency, the design of an optimal controller ideally should incorporate these factors.

Plant outputs cannot be minimized apart from consideration of the associated control costs, because active control both consumes power and releases heat. Since both of these costs are of concern in a space environment, the control effort used should not be excessive. And at higher frequencies, the control effort should be reduced in order to limit controller bandwidth for the sake of robustness concerns[9].

H_2 synthesis, more commonly known as LQG (Linear Quadratic Gaussian) or LQR (Linear Quadratic Regulator) synthesis, allows the designer to develop an optimal regulator that consists of full state feedback using constant feedback gains. Inaccessible states are reconstructed by an asymptotic observer that uses constant observer gains. In the LQR synthesis approach the observer gains are chosen to produce a stable observer with poles placed as desired by the designer[10]. In the LQG synthesis approach the observer gains are selected to minimize the rms error of the observed states from the actual states, based on the assumption that the process– and measurement noise vectors are zero–mean white Gaussian[10].

H_2 synthesis can be extended to allow the controller (i.e., the regulator and observer) gains to be optimized for colored process noise[10, 11]. Another extension permits the states and controls independently to be "frequency–weighted", so that certain frequencies of each are more heavily penalized than others, in an rms sense[12, 11]. A third extension allows for the inclusion of deterministic disturbance information into the optimized control expression[13, 14, 15].

The application of basic H_2 synthesis to the tethered microgravity isolation problem was first proposed in 1990[16]; but the most complete treatment to date, of the full extended H_2 synthesis approach, appeared a year later[17]. An algebraic introduction is published in reference (18), and the full deterministic solution is developed in (19). The present paper presents the results of a systematic application of the extended H_2 synthesis method to a realistic 1–D isolation problem. The resulting controlled system is evaluated using singular values and structured singular values ("μ analysis") to determine guarantees of system performance with uncertainties in the umbilical, payload, sensor, and actuator models. An excellent introduction to much of the pertinent analysis methodology is contained in reference (20).

Problem Description

The general 3–D vibration isolation problem for the tethered payload has three translational and three rotational degrees of freedom. In reference (20) Allan and Knospe presented a brief survey of several published 3–D syspension designs. The extended H_2 synthesis – μ analysis approach can be readily applied to a 3–D problem once the system model has been reduced to state–space form (i.e., consisting of a set of 1st order linear ordinary differential equations). However, the simpler 1–D problem offers the benefit of providing a simple model that is highly conducive to developing a physical intuition. Further, the specific mathematical model is much less geometry–dependent. The mathematical theory summarized below is generally applicable to either the 1–D or 3–D problem; but for the reasons noted above, it will be applied only to the 1–D problem in the application section of this paper.

Let the payload (e.g., experiment) be modeled as a lumped mass with inertial position x(t). Assume that the orbiter (i.e., experiment rack) has inertial position d(t), and that massless umbilicals characterized by a stiffness and a damping connect the payload and orbiter. Suppose further that a Lorentz actuator applies a control force proportional to the applied current u(t) with proportionality constant α. Such a model is shown in Figure 1. Typical parameter

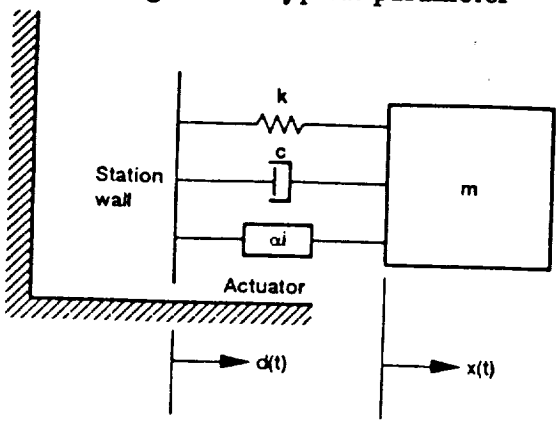

Figure 1.--Physical representation of modeled one-dimensional system

values were chosen: mass = 75 lbm, stiffness = 1.544 lbf/ft, damping = 0.01138 lbf–sec/ft (ζ = 0.3%), and α = 2 lbf/Amp. Clearly this model is inaccurate, since the plant will not be a perfectly rigid mass and since the umbilical is neither massless nor accurately characterizable by a single stiffness–and–damping model. The differences between the actual system and the nominal system will be addressed later. It will be seen that the system (consisting of payload, umbilical, sensor(s), controller, and actuator) is robust to anticipated uncertainties (i.e., remains stable and achieves good performance).

The goal is to find a feedback controller such that the controlled system satisfies the following specifications:

1. Above 0.1 Hz the payload acceleration $\ddot{x}(t)$ should be 40 dB below the orbiter acceleration $\ddot{d}(t)$.
2. Below 0.001 Hz the payload vibration x(t) should track the orbiter vibration d(t) to within 10 percent, in order to prevent collision of the payload with the walls of the experiment rack[8]
3. The payload should track perfectly the DC motion of the orbiter, where no relative motion can be tolerated.
4. The loop gain of the system (plant and controller) should be less than 0.1 above 200 Hz, to avoid controller excitation of orbiter– or payload flexible modes.
5. The system should remain stable and exhibit good performance for anticipated inaccuracies in the system model.

These specifications are derived from the available information concerning existing and required vibration environments,[1] while recognizing that rattlespace constraints will require orbiter tracking at very low frequencies[8].

Figure 2 shows the open loop transmissibility of the plant (i.e., its amplification factor, plotted as a function of harmonic–input frequency), along with specifications (1) and (2).

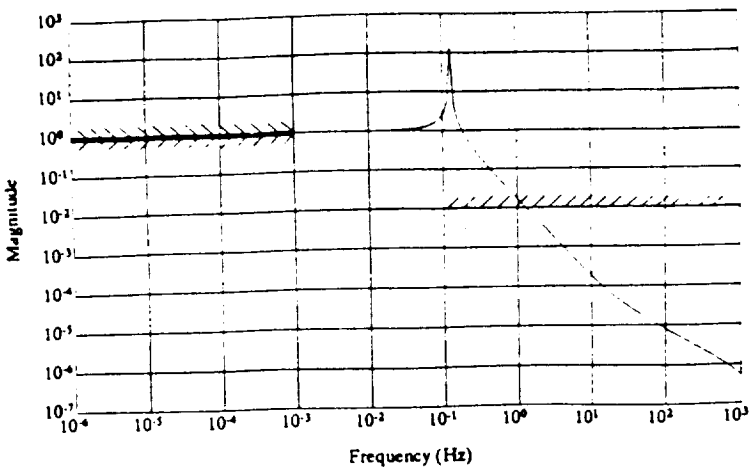

Figure 2.--Open loop transmissibility of the system

Basic Solution

The equation of motion can be expressed in the state–space form

$$\dot{\underline{x}} = A\underline{x} + B\,u + E_s\,\underline{w}_s,$$
$$\underline{y} = C\underline{x} + Du + M\underline{n}_s$$

where $\underline{w}_s$ and $\underline{n}_s$ are white noise vectors reflecting the power spectral densities of d and of the sensor noise, and where the vector $\underline{x}$ includes states derived from the equation of motion (e.g., inertial or relative positions or velocities, or accelerations), along with disturbance–accommodation pseudostates and frequency weighting pseudostates if desired[17]

As outlined in reference (17), once the problem is expressed in the above state space form with a suitably chosen quadratic performance index, an optimal controller can be found readily by the solution of an algebraic Riccati equation. The solution and solution methods are well–known. The resulting controller uses a control current that employs full state feedback, where inaccessible states (or pseudostates) may be reconstructed using an asymptotic observer. If the type of asymptotic observer used is a Kalman–Bucy filter, the observer design also involves the straightforward solution of another algebraic Riccati equation[17] Thus, a controller can be synthesized in a straightforward manner. Considerable insight is necessary, however, in determining how to use the powerful tools of disturbance–accommodation and frequency weighting to one's advantage. Once a controller has been synthesized, it must then be evaluated to see how it fares against the design specifications. This check is straightforward for specifications #1, 2, 3, and 4. However, for specification #5 the check is much more difficult.

μ analysis is a powerful tool that can be used to determine how much uncertainty can be tolerated at various locations in the closed loop system. The measures are conservative, due to aspects of the mathematics involved; but the results provide guaranteed minima of allowable uncertainty magnitudes that can be of immense value to the designer. In brief, the designer places one or more complex uncertainty blocks $\Delta(s)$ at appropriate locations in the system transfer function block diagram. By μ analysis methods he can then determine how large (2–norm) the uncertainty (or uncertainties) can be without driving the system unstable or exceeding specified performance limits. Typically uncertainty blocks fall into the categories of multiplicative input, multiplicative output, additive, and performance uncertainties. These can be used to provide conservative measures of allowable actuator gain and phase variations, sensor gain and phase variations, and unmodeled higher frequency plant dynamics, along with simultaneous performance guarantees. Feedback uncertainty blocks can be used as well to provide measures of allowable plant parameter variations from nominal values.

The rest of this paper is primarily devoted to helping provide insight into how to use extended H_2 synthesis and μ analysis effectively, for microgravity isolation, by reviewing a logical application of the approach to a realistic 1–D problem.

Controller Design

To begin the design process, the one–dimensional problem was first expressed in state–space form, with payload relative position, relative velocity, and acceleration

selected as states. Although many other state choices could have been made, these three were chosen to minimize the number of states necessary and to maximize the physical intuition possible. The selection would result in a state feedback control that respectively modifies the effective umbilical stiffness and damping, and the effective payload mass—all being familiar, accessible, and intuitive system parameters. Relative, rather than inertial, position feedback would help to avoid exceeding rattlespace limits; and relative velocity feedback would provide a means of damping out system resonances. The selection of acceleration as a state was considered desirable due to insight gained from an analogy to passive isolation systems. A controller which increases effective payload mass (by negative acceleration feedback) would potentially be able to accomplish disturbance rejection without unnecessarily sacrificing stability– or performance robustness.

A second important feature of the problem formulation was the decision to incorporate disturbances of two different kinds, the direct (i.e., onboard the experiment) and the indirect (i.e., acting via the umbilical). It had been observed, by examining the pertinent transfer functions, that reducing the effective umbilical stiffness could aid in indirect disturbance rejection only, but that increasing payload effective mass could help reject disturbances of both kinds. Although the primary type of disturbance was considered likely to be the indirect, a means was needed to force the LQR–KBF (also known as LQG) design "machinery" to increase effective mass so as to result in a robust controller. Including a direct disturbance provided this mechanism.

After completing the problem formulation, the next step was to develop a computer code for use in design and analysis. A PC–based design code was written in MATLAB to allow for frequency accom–modation of both direct and indirect disturbances. A large selection of frequency weightings and disturbance accommodation filters was made available to the designer. The code computes both feedback and observer gains. A number of analysis routines were also written to allow the designer to evaluate the resultant designs for purposes of comparison. The number of system states, system performance, stability robustness, parameter sensitivity, and observer quality were items whose comparisons were facilitated by these routines.

With the design and analysis tools in place, the next step was to develop the desired controller. In order to make the controller as simple as possible, it was decided to begin with the basic LQG approach (no frequency weighting, no disturbance accommodation, no direct disturbance) and to add complexity as needed. At each stage of additional complexity an iterative cycle of design and analysis was employed in an attempt to get the "best" achievable controller at that level of complexity.

The basic LQG approach yielded a satisfactory controller in terms of performance; but it had almost no stability robustness to changes in umbilical stiffness from the nominal (as measured by feedback uncertainty). This lack of robustness was due to the fact that LQG found adding negative stiffness to be a "cheaper" means of indirect disturbance rejection than adding effective mass. No frequency weighting was found which could rectify this problem.

A direct white disturbance was added in an attempt to force the LQG design "machinery" to add effective mass. Although there were some gains in stability robustness this was due entirely to changes in observer gain matrix L. The feedback gain matrix K remained unaffected (note that this is fundamental in LQG theory and is not a numerical problem), and the feedback stability robustness was still unsatisfactory.

Disturbance accommodation, with a lowpass filter applied to a large direct (white) disturbance, resulted in a controller with excellent feedback– and multiplicative input stability robustnesses, as measured by singular value checks. The multiplicative output stability robustness was unacceptably

low if cross–coupling was considered possible between states, but structured singular value checks indicated that without cross–coupling the allowable multiplicative output uncertainty was quite satisfactory. Since effective stiffness, effective damping, and effective mass of the controlled system are uncoupled for the true one–dimensional problem, the stability robustness measures of the system were considered acceptable. Further, the performance was excellent, easily exceeding the specifications. However, the controller gains were still large at higher frequencies where unmodeled system modes were of concern (see specification # 4). It was therefore necessary to use state– and control frequency weighting to force the controller to "turn off" by approximately 100 Hz (i.e., to reduce loop gain below a magnitude of one) so as to avoid exciting unmodeled flexible modes.

To reduce the loop gain at the higher frequencies it was necessary in that range (1) to place a high weight on control, (2) to apply low weights to all three states, and (3) to reduce the direct disturbance. At low frequencies the control weighting was left constant (i.e., "flat"), in an attempt to minimize the number of added pseudostates. However, the resulting closed loop system now had very poor low frequency stability robustness to parametric uncertainties, even though it both retained its excellent performance and now provided the desired low controller bandwidth.

A classical design approach to the problem provided a simple solution to the robustness issue. It was noted that for a controller with acceptable nominal performance the low frequency asymptote for controller gain could have slope –1 or 0 or greater (Bode–α, log–log scale). That is, control gain at DC could be zero (slope ≥ 1), finite (slope = 0), or infinite (slope = –1). Zero DC controller gain would, of course, result in a closed loop system that would achieve the unit transmissibility of the open loop system at low frequencies, as desired. But by using a control weighting filter with zero DC gain (slope ≥ 1) the extended H_2 synthesis "machinery" could be freed to consider finite or infinite DC controller–gain options. Consequently the control weighting was made to be zero at DC (at the expense of adding a pseudostate). The result was a controller that satisfied the design specifications and exhibited good stability robustness to parametric and to multiplicative input– and output uncertainties. Considering (for the moment) only single–parameter uncertainties, stability was guaranteed for umbilical stiffness to within ±99.7% of nominal, and umbilical damping could be essentially unknown. Payload mass needed to be known only to within ±65.2% of nominal. Having these initial favorable indicators of system robustness the next step was to reduce the controller size. Further robustness analysis would then be conducted on the reduced–order controller.

The controller described above was a ninth–order controller (i.e., had nine states), with payload acceleration as its only required input. Other states and pseudostates were reconstructed in the observer. To reduce the controller to a smaller order, a routine was written in MATLAB in order to permit removing high frequency modes (modal truncation) and weakly controllable and –observable system dynamics[21]. The result of applying this to the ninth–order controller was a third–order controller that has all the essential features of the ninth–order one. The loop gain, controller, and transmissibility plots for this reduced controller are shown in Figures 3a,b,c. Note from the transmissibility plot

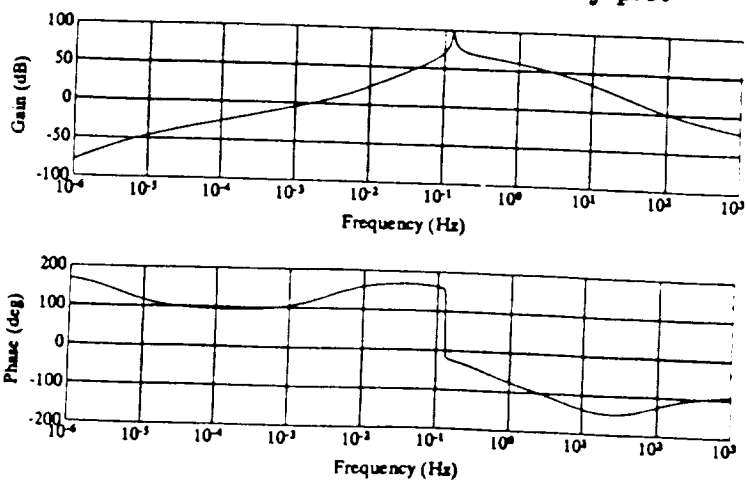

Figure 3a.--Open loop bode plots from control to -control (negative loop gain)

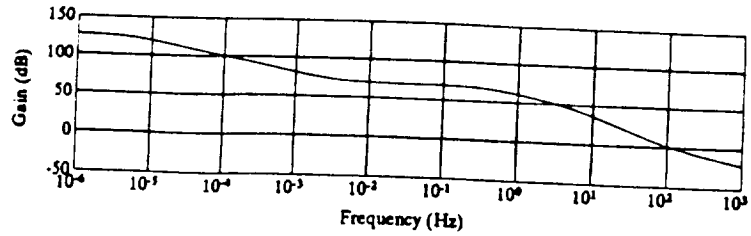

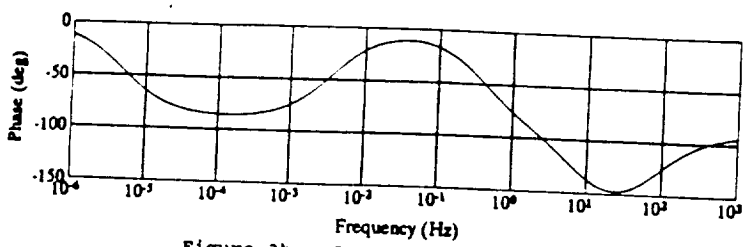

Figure 3b.--Controller bode plots

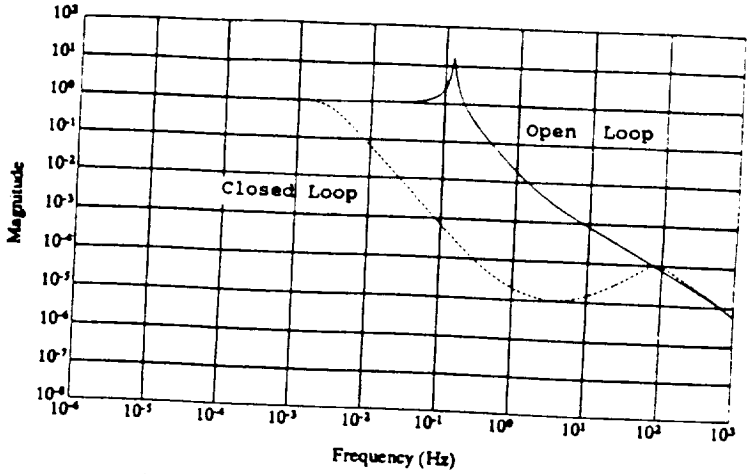

Figure 3c.--Open loop and closed loop system transmissibilities

that the transmissibility is unity up to 10^{-3} Hz and that it is below 10^{-4} at 0.1 Hz. Notice further that the open loop and closed loop Bode plots merge at about 100 Hz. This is due to the fact that the controller has essentially "turned off" by that frequency (see Figure 3b).

There are four basic checks that must be made of any controlled system: nominal stability, nominal performance, robust stability, and robust performance. These four checks are considered below, consecutively.

The extended H_2 synthesis method used for this portion provides an inherent guarantee of stability for a nominal plant with full state feedback. Further, the "separation principle" guarantees that for a perfectly known plant a stable asymptotic observer will not destabilize the system. Thus, nominal stability is assured with the full order observer, provided the observer itself is stable. Reducing the controller order removes this guarantee, but simple eigenvalue checks verify that both the reduced third–order controller as designed and the associated controlled system are stable for the nominal plant. A simple check of the loop gain Bode plot (Figure 3a) confirms the conclusion that the closed loop system is stable, since it is known that the loop gain is minimum phase.

The second necessary check is of nominal performance. As indicated by the closed–loop transmissibility plot (Figure 3c) the nominal performance is quite satisfactory. Note that the "less than 10^{-2}" spec at 0.1 Hz is surpassed by more than an order of magnitude. This overdesign was intentional, and necessary, since plant modeling errors (open loop system, sensors, and actuators) will certainly degrade performance margins.

Robust stability measures are necessary to determine whether the closed–loop system will remain stable given the anticipated sensor, actuator, and plant parameter uncertainties. Three different types of robust stability measures were used, for guaranteeing system stability for multiplicative input, multiplicative output, and feedback uncertainties below certain levels. The multiplicative input uncertainty allowable was found to be equivalent to a guaranteed phase margin (interval) of [–48°, +48°], and to a guaranteed gain margin (interval) of [0.304, 5.434]. The actual margins are even larger (phase margins: [–55°, +55°], gain margins: [0,+∞]). Since only one plant output is sensed (viz., payload acceleration), the multiplicative input and output robust stability guarantees are identical. A feedback uncertainty measure was used to determine guaranteed minimum stability bounds on uncertainties in umbilical stiffness and damping, and on payload mass. It was found, as noted previously (p. 6), that closed–loop system stability was guaranteed for single–parameter uncertainties much larger than anticipated. It was found, by

considering the feedback uncertainty structure, that for simultaneous mass, damping, and stiffness uncertainties of $\pm 20\%$, $\pm 100\%$, and $\pm 69\%$, respectively, system stability could be assured. Higher frequency modes of the system were considered not to be a significant concern since the controller bandwidth was limited during design.

Finally, measures were needed of performance robustness. Structured singular value plots were made to find conservative bounds on multiplicative input (and output) uncertainties that would not lead to plants with unacceptable performance. Below 10^{-3} Hz it was found that for combined sensor and actuator uncertainties of up to $\pm 11^{\circ}$ in phase or of $\pm 19\%$ in gain the performance can be guaranteed to remain acceptable. At higher frequencies the guarantees are much better, so that by 220 Hz uncertainties of up to $\pm 180^{\circ}$ in phase or of $\pm 200\%$ in gain are permissible.

Structured singular value plots were also used in an attempt to find performance robustness guarantees in the face of known parametric uncertainties, but the effort was only partly successful. The checks led to the conclusion that for single–parameter uncertainties in stiffness of $\pm 40\%$ both stability and acceptable performance could be assured. However, single–parameter uncertainty bounds found by this method on damping and mass were too conservative to be useful. Consequently, real parametric studies were conducted on plant–uncertainty effects on closed–loop performance. It was found that closed loop performance appeared acceptable for the various combinations of parametric uncertainties examined, with mass and stiffness varied in the intervals [–50%, +100%] and [–20%, +100%], respectively, and with damping varied by more than ten times its nominal value.

Conclusion

The above extended H_2 synthesis – μ analysis approach was found to produce a controller that easily satisfies the competing demands of the posed 1–D microgravity vibration isolation problem. Further, unlike the classical approach, it is readily extendable for use on a 3–D problem. Frequency weighting and disturbance–accommodation were both found to be necessary if H_2 synthesis is to be used in involving the posed isolation problem. Their inclusion, along with a judicious choice of states, provides the designer with a powerful and intuitive set of weapons for his design arsenal. Disturbance accommodation of a direct disturbance model was found to be effective in forcing the H_2 synthesis machinery to avoid negative–stiffness solutions. The result was an actively controlled system that uses a "smart" form of acceleration feedback to overcome the robustness problems that commonly plague the basic LQG synthesis approach.

REFERENCES

1. Nelson, E.S., "An Examination of Anticipated g–Jitter on Space Station and Its Effect on Materials Processes," NASA TM–103775, April 1991.
2. Grodsinsky, C.M. and Brown, G.V., "Non–intrusive Inertial Vibration Isolation Technology for Microgravity Space Experiments," NASA TM–102386, January 1990.
3. Knospe, C.R., Hampton, R.D. and Allaire, P.E., "Control Issues of Microgravity Vibration Isolation," Acta Astronautica, Vo. 25, No. 11, November 1991, pp. 687–697.
4. Allan, A.P. and Knospe, C.R., "A Six Degree–of–Freedom Magnetic Bearing for Microgravity Vibration Isolation," Proceedings of the International Symposium on Magnetic Suspension Technology, NASA Langley Research Center, Hampton, Virginia, August 19–23, 1991.
5. Owens, R.G., Jones, D.I., Owens, A.R., Roberts, G. and Hadfield, P., "The Microgravity Isolation Mount (MGIM)– A Columbus Facility for Improving the Microgravity Quality of Payloads," Proceedings of the International Workshop on Vibration Isolation Technology for Microgravity Science Applications, NASA Lewis

Research Center, Cleveland, Ohio, April 23–25, 1991.

6. Safonov, M.G., Laub, A.J. and Hartmann, G.L., "Feedback Properties of Multivariable Systems: The Role and Use of the Return Difference Matrix," IEEE Transactions on Automatic Controls, Vol. AC–26, No. 1, February 1981, pp. 47–65.
7. Gangsaas, D., Bruce, K.R., Blight, J.D. and Ly, U.–L., "Application of modern synthesis to aircraft control: three case studies," IEEE Transactions on Automatic Control, Vol. AC–31, No. 11, November 1986, pp. 995–1014.
8. Knospe, C.R. and Allaire, P.E., "Limits on the Isolation of Stochastic Vibration for Microgravity Space Experiments," Journal of Spacecraft and Rockets, Vol. 28, No. 2, March–April 1991, pp. 229–237.
9. Maciejowski, J.M., Multivariable Feedback Design, Wokingham, England: Addison–Wesley Publishing Company, Inc., 1989.
10. Johnson, C.D., "Accommodation of External Disturbances in Linear Regulator and Servomechanism Problems," IEEE Transactions on Automatic Control, Vol. AC–16, December 1971, pp. 635–644.
11. Maslen, E.H., Magnetic Bearing Synthesis, Doctoral Dissertation presented to the Faculty of the School of Engineering and Applied Science, University of Virginia, January 1991.
12. Gupta, N.K., "Frequency–Shaped Cost Functionals: Extension of Linear–Quadratic–Gaussian Design Methods," AIAA Journal of Guidance and Control, November–December 1980, pp. 529–535.
13. Salukvadze, M.E., "Analytic Design of Regulators (Constant Disturbances)," translated in Automation and Remote Control, Vol. 22, No. 10, pp. 1147–1155, March 1992. Originally published in Avtomatika i Telemakhanika, Vol. 22, No. 10, pp. 1279–1287, October 1961.
14. Salukvadze, M.E., "The Analytical Design of an Optimal Control in the Case of Constantly Acting Disturbances," translated in Automation and Remote Control, Vol. 23, No. 6, pp. 657–667, December 1962. Originally published in Avtomatika i Telemakhanika, Vol. 23, No. 6, pp. 721–731, June 1962.
15. Tomizuka, M., "Optimal Continuous Finite Preview Problem," IEEE Transactions on Automatic Control, June 1975, pp. 362–365.
16. Hampton, R. D., Knospe, C. R., Allaire, P. E., Lewis, D. W., and Grodsinsky, C. M., "An Optimal Control Law for Microgravity Vibration Isolation," Workshop on Aerospace Applications of Magnetic Suspension Technology, NASA Langley Research Center, Hampton, Virginia, September 25–27, 1990, NASA Conference Publication 10066, Part 2, March 1991, pp. 447–476.
17. Hampton, R. David, and Knospe, Carl R., "Extended H_2 Synthesis for Multiple–Degree–of–Freedom Controllers," International Symposium on Magnetic Suspension Technology, NASA Langley Research Center, Hampton, Virginia, August 19–23, 1991, NASA Conference Publication 3152, Part 1, pp. 363–381.
18. Hampton, R. D., Grodsinsky, C. M., Allaire, P. E., Lewis, D. W., and Knospe, C. R., "Optimal Microgravity Vibration Isolation: An Algebraic Introduction," Journal of the Astronautical Sciences, Vol. 40, No. 2, April–June 1992, pp. 241–259.
19. Hampton, R. D., Knospe, C. R., Grodsinsky, C. M., Allaire, P. E., and Lewis, D. W., "Microgravity Vibration Isolation: Optimal Preview and Feedback Control," NASA TM–105673, May 19, 1992.
20. Dailey, R.L., Lecture Notes for the Workshop on $H\infty$ and μ Methods for Robust Control, Seattle, Washington: The Boeing Company, presented at the 1990 American Control Conference in San Diego, California, May 21–22, 1990.
21. Allan, A. Peter, and Knospe, Carl R., "A Six Degree–of Freedom Magnetic Bearing for Microgravity Vibration Isolation," International Symposium

on Magnetic Suspension Technology, NASA Langley Research Center, Hampton, Virginia, August 19–23, 1991, NASA Conference Publication 3152, Part 1, pp. 209–218.

22. Moore, B. C., "Principal component analysis in linear systems: controllability, observability, and model reduction," IEEE Transactions on Automatic Control, Vol. AC–26, 1981, pp. 17–32.

International Workshop on Vibration Isolation Technology for Microgravity Science Applications, Cleveland, OH, April 23-25, 1991. NASA Lewis Research Center.

A Six Degree-of-Freedom Actuator Design for Microgravity Vibration Isolation

A. P. Allan and C. R. Knospe
Department of Mechanical and Aerospace Engineering
University of Virginia

April 5, 1991

1 Introduction

It is generally accepted that microgravity space experiments will need to be isolated from the vibrations inherent on spacecraft in earth orbit[3]. The fundamental constraint on any isolation system's capability is the available working envelope[4]. Figure 1 shows the relationship between the envelope (peak-to-peak displacement) and frequency for several sustainable RMS acceleration levels. The graph is for a one degree-of-freedom case and assumes sinusoidal vibrations, but the relationships are acceptable for order of magnitude estimates even if these assumptions are relaxed.

No definitive specification of the required isolation levels or frequency range exists. The proposed US Space Station usable specification[3] is also shown in Figure 1. It is claimed that vibrations below this curve will not adversely affect microgravity experiments. We have pursued the design of an active isolation system with a 'reasonable' envelope of 4 inches of travel, and a sustained 1 μg RMS acceleration. It can be seen from the figure that this will offer isolation down to 0.002 Hz. The amplitude to which vibrations can be attenuated is constrained only by controller design and available instrumentation. Operation at lower frequencies, however requires a larger envelope, which becomes prohibitive in terms of available spacecraft space. We have also required that the system be active in all six degrees-of-freedom, with a rotational range of 40 degrees.

Redundant coarse-fine schemes with magnetic levitation for vibration isolation are discussed in the robotics literature[2]. This approach is particularly attractive in the microgravity application since it allows the use of magnetic levitation while overcoming range of motion limitations. We have chosen the Stewart platform for our coarse stage and a novel magnetic bearing for the fine stage. The approximate regions of activity in the frequency-displacement plane of these two devices are shown in the figure. Both stages act to attenuate spacecraft vibrations, effectively reducing vibration amplitudes below their

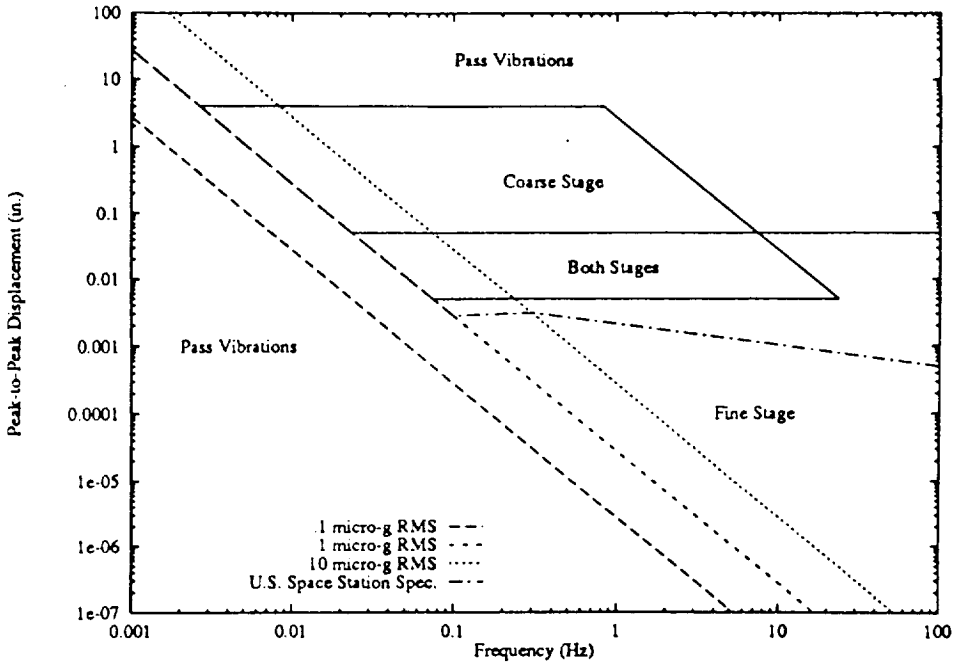

Figure 1: Peak-to-Peak Displacement vs. Frequency for Various RMS Accelerations, U. S. Space Station Usable Specification, and Activity Regions of the Two Actuator Stages

active regions on the plane. As an example, it can be seen in the figure that a vibration of the spacecraft with 10 inches of displacement at a frequency of 1 Hz falls outside the active region and could only be partially attenuated. It should be noted that such a large vibration is unlikely. If the displacement was only 1 inch, however, the coarse stage would absorb all of it except about 0.005 inches, and the remainder would be reduced down to the micro-g level by the fine stage.

The combination of the Stewart platform and a magnetic bearing allows continuous isolation at frequencies above 0.002 Hz, and a compact, reliable package suitable for the application. These choices and some preliminary design concepts will be discussed in detail.

2 Stewart Platform

The Stewart platform is a six degree-of-freedom parallel manipulator first proposed by Stewart[5]. It has been extensively used in aircraft cockpit simulator

applications, and substantial design information is available in the literature[1]. Figure 2 shows the mechanism in our proposed configuration. Six linear actuators (legs) connect a base (bottom) to a platform (top). The base will be mounted in the spacecraft and move with it, while the platform tracks an inertial reference frame. We propose the use of stepper motor driven ball lead-screws as actuators.

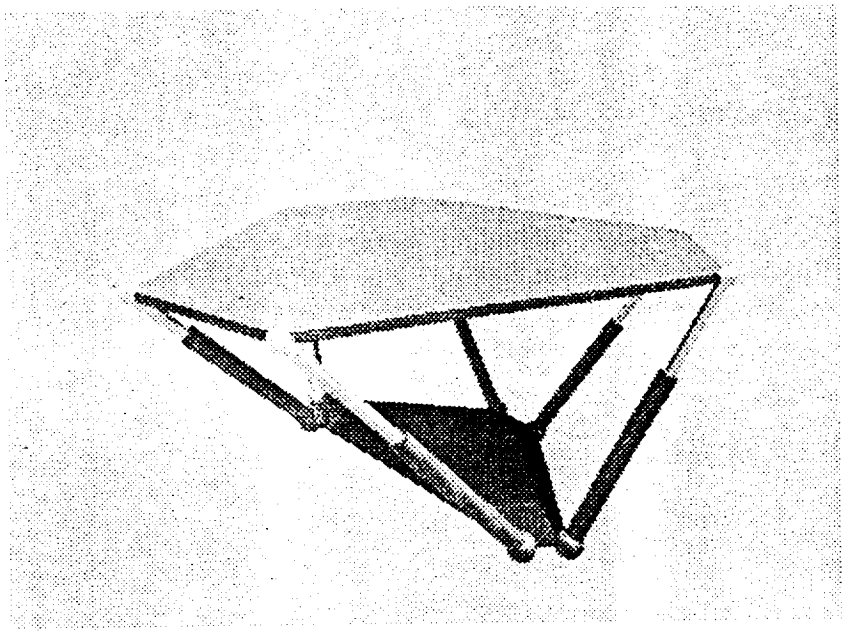

Figure 2: The Stewart Platform

This mechanism was chosen over other candidates such as a carriage/gimbal approach, or a serial linkage mechanism because it has the following features:

- *Inherent rigidity.* The parallel connection of the actuators gives the mechanism rigidity on the order of the extensional rigidity of the actuators. For the proposed actuators, this will allow controller design to ignore the dynamics of the mechanism. The effects of 'umbilical' connection to the platform will also be negligible.
- *Determinate inverse kinematics.* The actuator lengths required to achieve a prescribed orientation are found directly from a coordinate transformation from the base to the platform frame. This is seldom the case for a serial linkage. This will also simplify control.
- *Compactness.* The configuration proposed here places the fine stage on top of the platform for convenience in testing. A fully developed imple-

mentation could locate the fine system and microgravity experiment in the space between the base and platform, resulting in a compact package.

The Stewart platform has some disadvantages that must be considered. It is nonlinear in its response to actuator lengths, its general direct kinematics have not been discovered in closed form, and it has singularities in its operational space. The fist two problems can be overcome with digital controls. The singularities, which are points or loci where the mechanism gains a degree of freedom and the actuators can lose control of it, must be addressed in design.

A simulation code has been written to allow exploration the design alternatives. Figure 2 is an example of its output. Preliminary results indicate that our specification (4 inches translation, 40 degrees rotation) will be achievable with actuators 10.5 inches long in the retracted position, and with 9 inches of stroke. The simulation can confirm that singularities are safely outside the working envelope. Commercial actuators with the required range, load capacity, speed and acceleration have been identified.

3 Magnetic Bearing

Two axes of a six axis magnetic bearing are shown in Figure 3, mounted atop the Stewart platform. A ferromagnetic cube is at the center of the bearing. Two pole pieces protrude from each of its faces (four shown) and each pole piece is surrounded by a coil. This part of the structure is called the core and is mounted to the platform with four posts. Three ferromagnetic bands surround the core (one shown) forming three independent magnetic flux paths. The core is capable of exerting three orthogonal forces, and three orthogonal torques on the bands. For the axes shown, equal currents in each pair of adjacent coils will cause magnetic flux to flow in a local circuit, causing an attractive force to the band. By controlling these currents a prescribed force can be exerted on the band along the axis that crosses the page form left to right. If the currents in adjacent coils are not equal, some flux will flow around the outside of the band and through the center of the cube. This will create a controllable torque on the band around the vertical axis.

Similar pole pieces and coils will protrude from the other faces of the cube, and corresponding bands will surround them. These have been omitted so that all parts can be seen. Also, the size of the bearing and the gaps have been exaggerated for clarity. Flux sensors will be mounted in the pole pieces and this will allow the position of the bands relative to the core to be calculated for control. The microgravity experiment will occupy the space surrounding the bearing, and be attached to the bands.

This configuration was chosen over other levitation approaches such as Lorentz actuators or magnetic actuators located on the periphery of the experiment package because it has the following advantages:

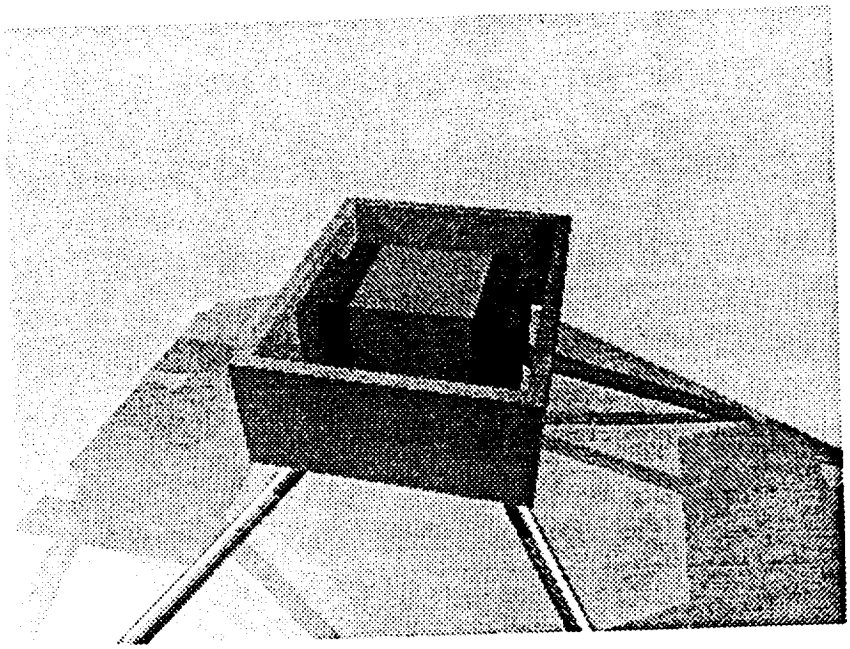

Figure 3: Magnetic Bearing

- *Compactness.* The high force capability of the magnetic bearing relative to a Lorentz actuator of similar size and power consumption suits the application. Testing in earth gravity will be facilitated, and levitation during launch to protect sensitive instrumentation may be feasible. Also, the rigid structure required to mount actuators around the periphery is avoided.

- *Force/torque balance and rotational range.* Actuators capable of the required forces mounted on the periphery of the experiment are capable of torques far greater than is required, and they limit the rotational range of the experiment. The proposed design approach brings the relative force/torque magnitudes closer to the requirement, and allows substantial rotational range.

- *Integral sensor capability.* Compact semiconductor magnetic flux sensors (hall effect or magneto-resistive) can be utilized to both stabilize the system and infer relative position. No elegant integrated approach is known for Lorentz actuators.

Magnetic bearings have typically been avoided in 'large gap' applications because of their nonlinearity (force is proportional to the square of flux). We feel that emerging Digital Signal Processor technology and control work will

allow us to overcome these limitations. Finite element tools will be employed to develop a design that is both capable of high forces and torques, and avoids nonlinearities associated with saturation and flux path variations.

4 Conclusion

A conceptual design is proposed for a coarse-fine actuator pair that synergistically combines two dissimilar six degree-of-freedom actuators. This design is particularly suited to the microgravity isolation application because of the way it spans the useful portion of the frequency-displacement plane. The combination is shown together in Figure 4.

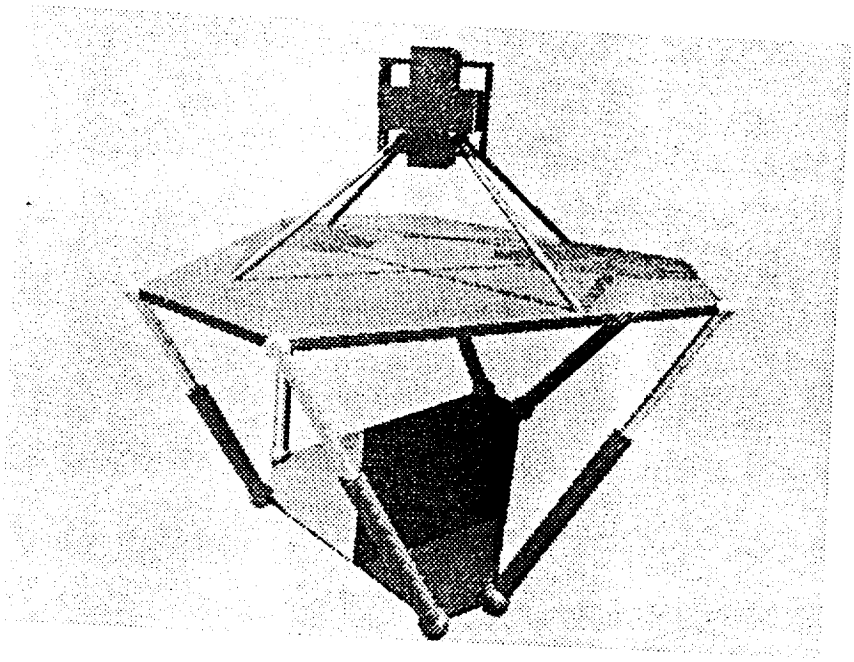

Figure 4: Coarse-Fine Actuator

Ongoing work will more precisely define the exact geometries, materials, and components to be used. Simulation will allow the specification of a Stewart platform that meets the specification, and uses commercially available components. Finite element methods will be used to optimize the magnetic bearing design. A simultaneous effort in controller design will be undertaken. A test rig will then be constructed to verify the design and quantify the performance of the actuators and controller together.

We look forward to and welcome any input that can be worked into our design effort.

5 Acknowledgements

This work was supported in part by the NASA Lewis Research Center and the Commonwealth of Virginia's Center for Innovative Technology.

References

[1] E. F. Fichter. A Stewart platform based manipulator: General theory and practical construction. *International Journal of Robotics Research*, 5(2):157–182, 1986.

[2] R. L. Hollis, A. P. Allan, and S. Salcudean. A six degree-of-freedom magnetically levitated variable compliance fine motion wrist. *Robotics Research*, 4:65–73, 1987.

[3] D. I. Jones, A. R. Owens, and R. G. Owen. A microgravity isolation mount. *Acta Astronautica*, 15(6/7):441–448, 1987.

[4] C. R. Knospe and P. E. Allaire. Limits on the isolation of stochastic vibration for microgravity space experiments. To be published in the *Journal of Spacecraft and Rockets*.

[5] D. Stewart. A platform with six degrees of freedom. *Proceedings of the Institute of Mechanical Engineers*, 180(1):371–386, 1965.

International Symposium on Magnetic Suspension Technology, Hampton, VA, August 19-23, 1991. NASA Langley Research Center.

A Six Degree-of-Freedom Magnetic Bearing for Microgravity Vibration Isolation *

A. Peter Allan and Carl R. Knospe
Department of Mechanical and Aerospace Engineering
University of Virginia

August 20, 1991

1 Introduction

The authors have previously presented a conceptual design for a coarse-fine actuator pair and discussed its efficacy in the microgravity vibration isolation application[1]. The coarse stage comprises a Stewart platform [2] which is mounted in a spacecraft and isolates low frequency, high amplitude vibrations. The fine stage is a novel magnetic bearing mounted on the Stewart platform (between the legs for compactness) and levitates the experiment to isolate all frequencies at low amplitudes. The combination is illustrated in Figure 1.

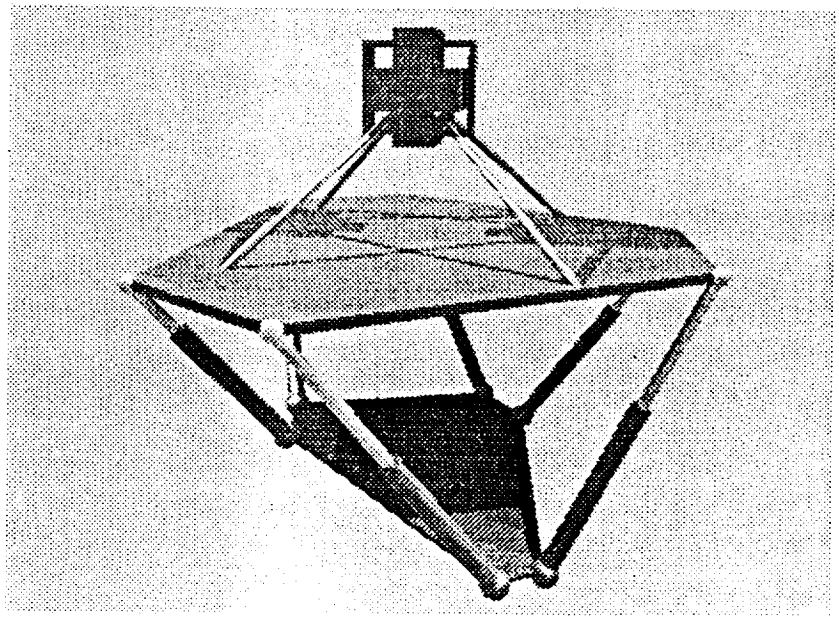

Figure 1: Coarse-Fine Actuator Pair

This paper will present a survey of published 6 DOF levitation designs and discuss a novel magnetic bearing in terms of design, predicted performance, and control issues.

*Supported in part by the NASA Lewis Research Center and the Commonwealth of Virginia's Center for Innovative Technology.

2 Survey of Published Designs

Several designs for 6 DOF levitation are discussed in the literature. A comparison of the specifications for these designs is given in Table 1.

Group	*Trans.*	*Rot.*	*Force*	*Envelope*	*Weight*	*Actuator*	*Sensor*
Honeywell	±5 mm	±1.6°	43 N	27x34x50 cm	36 kg	Mag. Brng.	Eddy & Flux
N. Wales	±5 mm	< ±.2°	.04 N [a]	100x100x100 cm [b]	?	Lorentz	Capacitive
NASA	±4 mm	±3° [c]	445 N	30x30x15 cm [c]	?	Mag. Brng.	Eddy
SatCon	±10 mm	±8° [c]	4 N	40x40x12 cm [c]	4.9 kg	Lorentz	Eddy
IBM	±5 mm	±4°	32 N	25x25x15 cm [c]	?	Lorentz	Optical
Toshiba	±2 mm	±1.5°	20 N [c]	25x25x20 cm	8 kg	Mag. Brng.	Eddy

[a] Requirement, not limitation
[b] Includes experiment package
[c] Estimated by authors

Table 1: Comparison of Published Designs

Four designs specifically for microgravity isolation have been published. Honeywell [3] has a well developed system called FEAMIS with which they have demonstrated impressive isolation performance. The system is designed for the Space Shuttle experiment configuration. The University College of North Wales [4] also has a well developed system designed for the European Space Agency experiment configuration. NASA [5] and SatCon [6] both have laboratory levitation systems.

Two levitation designs were developed for different applications, but they are mentioned here because they are similar and could be easily adapted to the isolation application. IBM [7] has a laboratory levitated robot "wrist" which enhances robot accuracy and performance. Toshiba [8] has a satellite antenna pointing system which is fully developed. Both devices have demonstrated positional accuracies on the order of 1 μm.

Isolation of vibrations with large amplitudes — typically occurring at low frequencies — requires a large translational range. SatCon's system has the largest range, but there is a significant tradeoff with the device's force capability. A coarse-fine approach would allow both a large range, provided by the coarse stage, and a high force capability, since the levitation gaps are small. There is no available data on the rotational range requirements of the application. Isolation with an umbilical disturbance requires a high force capability as is offered by the systems from Honeywell, NASA, IBM, and Toshiba. Space and weight should be minimized in any spacecraft. SatCon, IBM, and Toshiba's systems offer advantages in envelope space and weight.

The choice of the actuator technology between Lorentz force and magnetic bearings has no definitive advantage. Lorentz actuators offer linearity, simplicity, and compactness. Magnetic bearings offer higher force capability and lower power consumption, particularly if gaps are minimized.

Four position sensor technologies offer promising performance. Eddy current position probes are simple and robust, but bulky and heavy for large gaps. Capacitive sensors are simple and light weight, but can be noisy in unconstrained environments. Optical lateral effect photo-diodes are compact and quiet, but they require substantial supporting electronics. Hall effect flux sensors can be used with magnetic bearing designs both to linearize the control problem, and to measure position.

3 Design

The magnetic bearing proposed has two parts: a stator which is attached to the spacecraft, and a surrounding "flotor" to which the experiment is attached.

The stator is illustrated in Figure 2. It has twelve pole pieces and coils arranged around the surface of a cube. The cube and pole pieces are ferromagnetic. Each pair of pole pieces and the region of the cube to which they are attached comprise a typical "horseshoe" electromagnet causing an attractive force toward the nearby flotor. Magnetic flux through the center of the cube will cause an imbalance in the flux levels of a pair of pole pieces, resulting in a net torque on the flotor. Differential Hall effect sensors will be located in the cube side of each pole piece to measure the local flux. All electrical connections will be to the stator.

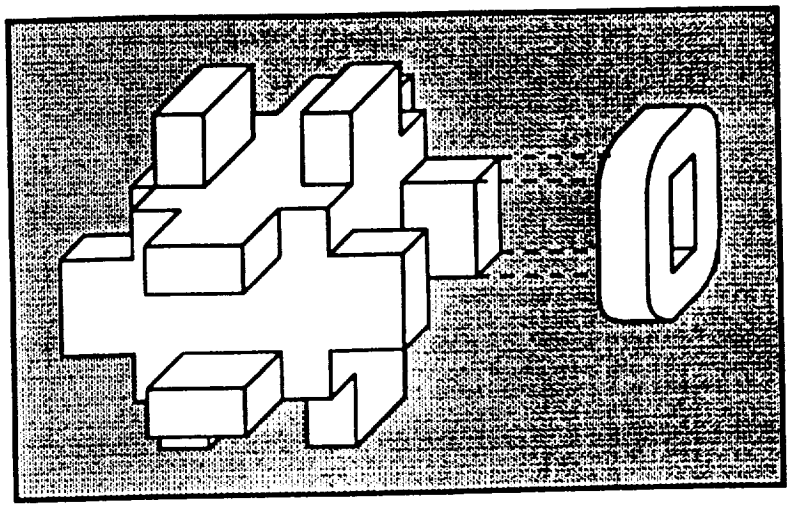

Figure 2: Stator and Typical Coil

The flotor is illustrated in Figure 3. Three ferromagnetic bands are rigidly attached to each other, but form independent flux paths. The bands are thicker in the region near the pole pieces to avoid saturation. Flux which passes through the center of the cube is returned through the remaining portion of the bands.

Four mounting posts will attach to corners of the cube, and pass through clearances in the flotor. These posts could carry cooling fluid to be circulated through the stator if it is required.

Design equations relating force and moments to the coil currents will be derived below referring to Figure 4. The figure shows a schematic slice through the stator and flotor with appropriate nomenclature and sign convention information. It should be noted that a complete model comprises three such systems, but they are identical and orthogonal, so only one will be analyzed.

The relationship between coil currents $(i_1, \ldots, i_4)$ and the force and moment generated in one slice of the stator (F_y, M_z) can be derived from Maxwell's Equations. The first Maxwell equation (1), which relates magnetic field intensity (H) around a closed path to the electric current density (J) through that path, is discretized and applied to closed loops drawn through the slice. N is the number of turns in each coil, and G_i are the air gap lengths which are dependent on the stator's position relative to the flotor. The iron flux paths are ignored because their reluctance is low relative to that of the air gaps. Many such equations can be written (2), but only three are independent.

$$\oint_C \mathbf{H} \cdot d\mathbf{l} = \int_S \mathbf{J} \cdot d\mathbf{a} \tag{1}$$

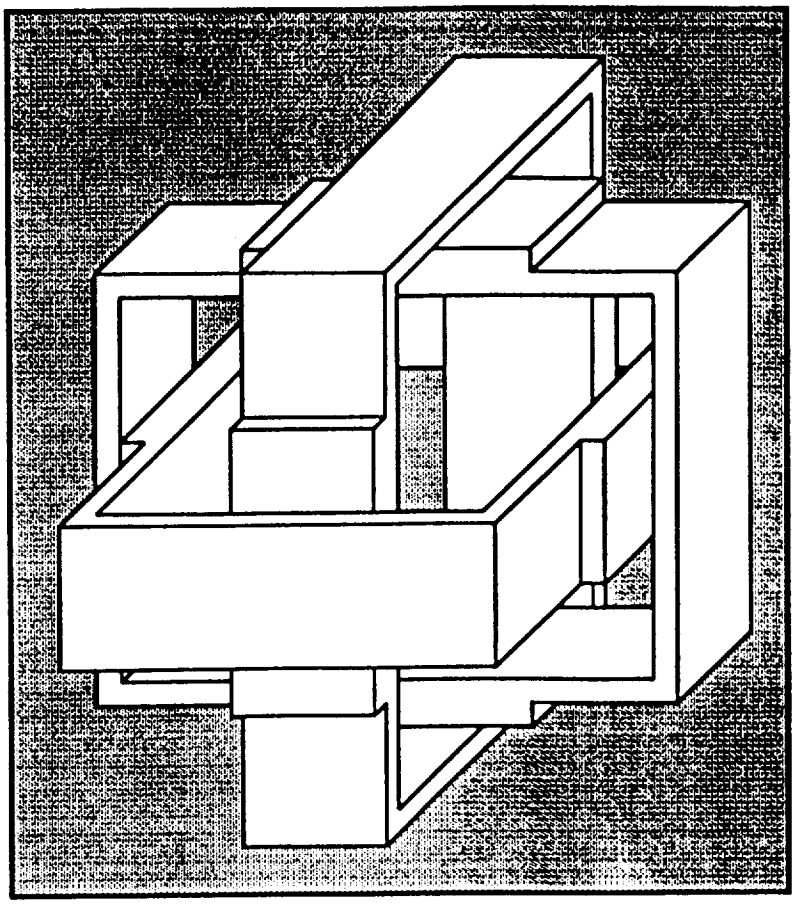

Figure 3: Flotor

$$\begin{aligned} H_1G_1 - H_2G_2 &= N(i_1 - i_2) \\ -H_3G_3 + H_4G_4 &= N(-i_3 + i_4) \\ -H_1G_1 - H_4G_4 &= N(-i_1 - i_4) \\ -H_2G_2 - H_3G_3 &= N(-i_2 - i_3) \\ &\vdots \end{aligned} \tag{2}$$

The second Maxwell equation (3), which ensures conservation of magnetic induction ($\underline{B}$), is used to obtain a fourth independent equation (4).

$$\nabla \cdot \underline{B} = 0 \tag{3}$$

$$B_1 + B_2 - B_3 - B_4 = 0 \tag{4}$$

We can assume linear magnetization in the air gaps (5), where μ_0 is the permeability of free space, to obtain a relation between magnetic induction in the gaps and coil currents (6).

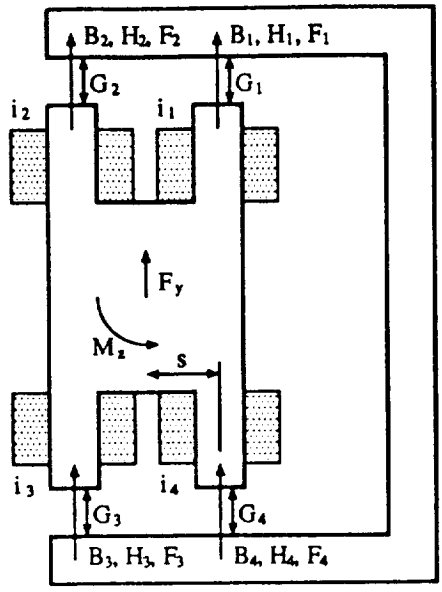

Figure 4: Schematic Cross Section of Magnetic Bearing

$$H_i = \frac{B_i}{\mu_0} \qquad i = 1, \ldots, 4 \tag{5}$$

$$\begin{Bmatrix} B_1 \\ B_2 \\ B_3 \\ B_4 \end{Bmatrix} = \frac{N\mu_0}{G_1G_2G_3 + G_1G_2G_4 + G_1G_3G_4 + G_2G_3G_4} \tag{6}$$

$$\begin{bmatrix} G_2G_3 + G_2G_4 + G_3G_4 & -G_3G_4 & G_2G_4 & G_2G_3 \\ -G_3G_4 & G_1G_3 + G_1G_4 + G_3G_4 & G_1G_4 & G_1G_3 \\ G_2G_4 & G_1G_4 & G_1G_2 + G_1G_4 + G_2G_4 & -G_1G_2 \\ G_2G_3 & G_1G_3 & -G_1G_2 & G_1G_2 + G_1G_3 + G_2G_3 \end{bmatrix} \begin{Bmatrix} i_1 \\ i_2 \\ i_3 \\ i_4 \end{Bmatrix}$$

The four gaps are geometrically related to the offset of the stator with respect to the flotor by the relations (7) which assume small angles.

$$\begin{aligned} G_1 &= G_0 - y - s\theta \\ G_2 &= G_0 - y + s\theta \\ G_3 &= G_0 + y - s\theta \\ G_4 &= G_0 + y + s\theta \end{aligned} \tag{7}$$

G_0 is the air gap length with the stator centered in the flotor.

The magnetic energy stored in the magnetic bearing (ω_m) is found from (8) where A_g is the area of the pole faces.

$$\begin{aligned} \omega_m &= \frac{1}{2}\int_{\infty} \mathrm{B}\cdot\mathrm{H}\, dV \\ &= \frac{A_g}{2\mu_0}\left(B_1^2 G_1 + B_2^2 G_2 + B_3^2 G_3 + B_4^2 G_4\right) \end{aligned} \tag{8}$$

The force and moment on the stator are found from the relations (9) and (10).

$$F_y = \frac{\partial \omega_m}{\partial y} \tag{9}$$

$$M_z = \frac{\partial \omega_m}{\partial \theta} \tag{10}$$

After considerable algebraic manipulation, and introduction (without loss of generality) of the linear current transformations (11) we obtain the force and moment relations sought (12) and (13).

$$\begin{aligned} j_1 &= i_1 + i_2 + i_3 + i_4 \\ j_2 &= i_1 - i_2 + i_3 - i_4 \\ j_3 &= i_1 - i_2 - i_3 + i_4 \end{aligned} \tag{11}$$

$$F_y = \frac{A_g N^2 \mu_0 \left(G_0 j_2 + \theta s j_1 + y j_3\right)\left(G_0^2 j_3 - \theta^2 s^2 j_3 + G_0 y j_2 + \theta s y j_1\right)}{4 G_0 \left(G_0^2 - \theta^2 s^2 - y^2\right)^2} \tag{12}$$

$$M_z = \frac{A_g N^2 s \mu_0 \left(G_0 j_2 + \theta s j_1 + y j_3\right)\left(G_0^2 j_1 + G_0 \theta s j_2 + \theta s y j_3 - y^2 j_1\right)}{4 G_0 \left(G_0^2 - \theta^2 s^2 - y^2\right)^2} \tag{13}$$

The current j_2 is analogous to the bias current in a conventional bidirectional thrust bearing and could be fixed at a constant value — nominally half of the maximum current. The force generated is predominantly driven by j_3 and the moment by j_1. The system is unstable (negative stiffness) in both translation and rotation. The currents $i_1, \ldots, i_4$ can be found by a pseudo-inverse technique from j_1, j_2, j_3. Closed form analytic inverses to (12) and (13) have been found for a known position.

4 Predicted Performance

The equations of the previous section were used to predict the performance of a specific design. The design has a center cube of 2 in. on a side, pole faces of 1 x .5 in., and pole length of 2 in. Maximum current is determined by allowing a coil current density of 5000 amp/in^2 which is known to be conservative from previous designs. The gap in the centered position was chosen to be .125 in. plus an allowance of .030 in. for inclusion of flux sensors and a protective layer on the inside of the bands. The resulting specifications for the design are presented in Table 2. The 53 N force is a continuous worst case, with the stator moved away from the flotor in the direction of the force. The continuous force capability in the centered position is 175 N. Intermittent force capability is limited only by the current capability of the amplifiers, and the saturation limit of the magnetic material used. Using Vanadium Permadur with this design, saturation would occur at about 1000 N. Of the 4.5 kg weight, the flotor comprises only 1.2 kg.

Trans.	*Rot.*	*Force*	*Envelope*	*Weight*
±3.2 mm	±7°	53 N	15x15x15 cm	4.5 kg

Table 2: Specification of UVA Design

When compared with the designs presented in Table 1, the UVA design has several advantages. The envelope is substantially smaller than any of the previous designs, while the performance is similar. In addition to saving space, this compactness allows the flotor to be naturally rigid, and thus avoids control problems with structural dynamics. The design is quite dense in comparison with the others, but it is lighter than the lightest for which data were available.

5 Control

A regulator has been designed to reject the disturbances caused by the umbilical connection to the experiment. A schematic is shown in Figure 5. Nonlinearities in the magnetic bearing are eliminated by using flux feedback in a minor loop [3]. Six accelerometers mounted on the flotor produce a generalized acceleration signal which is fed back through a linear controller. More details on the controller are available in [9]. The desired control force is processed through an inverse magnetic circuit model to obtain a desired flux signal. This model could be either a digital algebraic model, or an appropriately trained neural network.

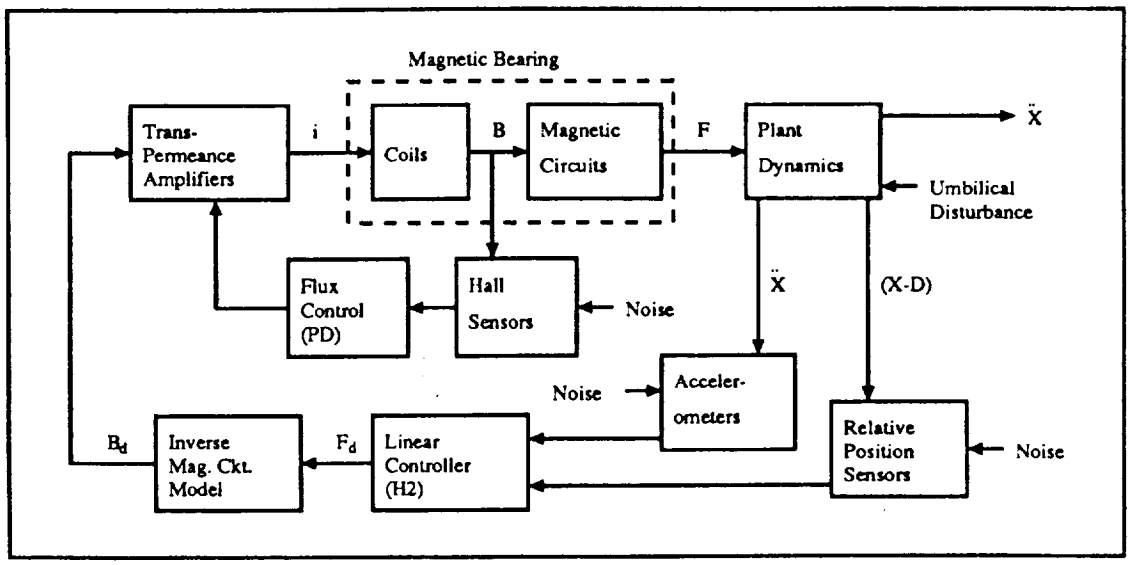

Figure 5: Control Schematic

A relative position sensor has not been chosen but the optical scheme used in IBM's design is a strong candidate. Alternatively, the current and flux signals could be processed to infer position [10]. The purpose of the relative position signal is only to prevent collision with the walls, so accuracy demands are relatively low.

6 Conclusion

A design for a novel magnetic bearing, proposed as the fine stage of a coarse-fine actuator for microgravity vibration isolation, has been presented. The bearing is novel in that it uses a geometry that has just three independent flux path systems. This contrasts the twelve flux path systems (six bidirectional thrust bearings) used in conventional designs. The novel design results in compactness, light weight and high performance, when compared with the published designs. A control system is proposed to reject disturbances caused by an umbilical connection to the experiment.

Future work will focus on building a laboratory version of the bearing and control system.

References

[1] A. Peter Allan and Carl R. Knospe. A six degree-of-freedom actuator design for microgravity vibration isolation. In *International Workshop on Vibration Isolation Technology for Microgravity Science Applications*, Cleveland, Ohio, April 23-25, 1991. NASA Lewis Research Center.

[2] D. Stewart. A platform with six degrees of freedom. *Proceedings of the Institute of Mechanical Engineers*, 180(1):371–386, 1965.

[3] Terry S. Allen, Douglas D. Havenhill, and Kevin D. Kral. FEAMIS: A magnetically suspended isolation system for space-based materials processing. In *Annual AAS Guidance and Control Conference*, Keystone, Colorado, February 1-5, 1986. Rocky Mountain Section, American Astronautical Society.

[4] D. I. Jones, A. R. Owens, and R. G. Owen. A microgravity isolation mount. *Acta Astronautica*, 15(6/7):441–448, 1987.

[5] Carlos M. Grodsinsky. Development and approach to low-frequency microgravity isolation systems. Technical Paper 2984, NASA, August 1990.

[6] Ralph Fenn and Bruce Johnson. A six degree of freedom Lorentz force vibration isolator with nonlinear controller. In *International Workshop on Vibration Isolation Technology for Microgravity Science Applications*, Cleveland, Ohio, April 23-25, 1991. NASA Lewis Research Center.

[7] Ralph L. Hollis, S. E. Salcudean, and A. Peter Allan. A six degree-of-freedom magnetically levitated variable compliance fine-motion wrist: Design, modeling and control. *IEEE Transactions on Robotics and Automation*, 7(3):320–332, 1991.

[8] Kenichi Takahara, Tamane Ozawa, Hiroshi Takahashi, Shitta Shingu, Toshiro Ohashi, and Hitoshi Sugiura. Development of a magnetically suspended, tetrahedron-shaped antenna pointing system. In *22nd Aerospace Mechanisms Symposium*, Hampton, VA, May 4-6, 1988. NASA Langley Research Center.

[9] R. D. Hampton and Carl R. Knospe. Extended H_2 synthesis for multiple-degree-of-freedom controllers. In *International Symposium on Magnetic Suspension Technology*, Hampton, VA, August 19-23, 1991. NASA Langley Research Center.

[10] D. Zlatnik and A. Traxler. Cost-effective implementation of active magnetic bearings. In *2nd International Symposium on Magnetic Bearings*, Tokyo, Japan, July 12-14, 1990. Institute of Industrial Science, University of Tokyo.

Limits on the Isolation of Stochastic Vibration for Microgravity Space Experiments

C. R. Knospe* and P. E. Allaire†
University of Virginia, Charlottesville, Virginia 22901

The limitations on the isolation of stochastic vibrations for microgravity space experiments are explored. These limitations result from the restricted interior space available for vibration isolation. A one-degree-of freedom representation of the experiment-spacecraft system is used, and an ideal vibration actuator is assumed. A kinematic representation results, and the problem becomes one of finding the minimum acceleration trajectory within a pair of stochastic walls. The wall motion is characterized by an ergodic, stationary, zero-mean, Gaussian random process with known power spectral density. The geometry of the wall trajectories is defined in terms of their significant extrema and zero crossings. This geometry is used in defining a composite trajectory that has a mean square acceleration lower than that on the optimal path satisfying the stochastic wall inequality constraints. The optimal control problem is solved on a return path yielding the mean square acceleration in terms of the distributions of significant maxima and first-passage time of the wall process. The methodology is applied to a microgravity isolation problem to find the lower bounds on root-mean-square acceleration given the disturbance power spectral density.

Nomenclature

A	= matrix in state dynamics
B	= vector in state dynamics
c_i	= constants in optimal control
d	= microscopic component of $y(t)$
F	= cumulative distribution function
f	= probability density function
G	= final condition cost
$G(s)$	= transfer function of shaping filter
H	= Hamiltonian
J	= cost function
L	= maximum stroke of experiment
m_{-4}	= fourth moment of a sample of T^{-1}
n	= bandlimited white noise
S	= power spectral density.
s	= complex frequency variable
T	= first-passage time
t	= time
t_1	= time at significant maximum
t_2	= time at zero crossing
u	= experiment acceleration
x	= state vector, $= (x_1\ x_2)^T$
x, x_1	= experiment position
x_2	= experiment velocity
y	= wall process
y_1	= upper wall true position
y_2	= lower wall true position
y_{up}	= upper wall constraint
y_{low}	= lower wall constraint
y_{max}	= maximum of wall process
$\bar{y}, \bar{y}_1$	= macroscopic component at $y(t)$
$\bar{y}_2$	= macroscopic component velocity
z	= significant maximum position
δ	= dirac delta function
λ_i	= Lagrange multiplier for dynamic equations
ϕ	= Lagrange multiplier for final condition
ν	= expected frequency of upcrossings (cycles)
μ	= expected frequency of maxima
ω	= frequency, rad/s
ω_d	= damped natural frequency, rad/s
ξ	= damping coefficient

Subscripts

d	= microscopic component
f	= final time
max	= at maximum
N	= normal
n	= bandlimited white noise
T	= first-passage time
y	= wall process
$\bar{y}$	= macroscopic component
z	= significant maxima position

Received June 29, 1990; revision received Aug. 21, 1990; accepted for publication Sept. 10, 1990.

*Assistant Research Professor, Department of Mechanical and Aerospace Engineering.

†Professor, Department of Mechanical and Aerospace Engineering.

Introduction

THE microgravity environment of space may permit advances in material science experiments. Such experiments could aid in the understanding of basic physical phenomena, quantify the limitations and effects imposed by gravity, and spur application to Earth and space based processes and products. A microgravity environment could potentially eliminate buoyancy-driven convection, sedimentation, and hydrostatic pressure as well as yield other advantages.[1]

At this time, the acceleration environment requirements for various experiments are not well known.[2] An assessment of existing theoretical and experimental data available up to 1985 indicated acceleration levels below $10^{-6}\ g_0$ would be required for frequencies below 0.1 Hz for many of the processes. The requirements at higher frequencies are somewhat lower.[3] Work to determine the levels necessary is in progress by various materials experiment researchers. An example is a twin crystal growth experiment to be carried out on spacecraft.[4]

An essential part of the development of a microgravity experiment program is the characterization of the low acceleration environment aboard spacecraft. NASA has carried out a series of measurements reported at various

Table 1 Microgravity space experiment acceleration environment[7]

g/g_0	F, Hz	Source
	Quasisteady or "dc" acceleration disturbances	
10^{-7}	0 to 10^{-3}	Aerodynamic drag
10^{-8}	0 to 10^{-3}	Light pressure
10^{-7}	0 to 10^{-3}	Gravity gradient
	Period acceleration disturbances	
2×10^{-2}	9	Thruster fire (orbital)
2×10^{-3}	5–20	Crew motion
2×10^{-4}	17	Ku band antenna
	Nonperiodic acceleration disturbances	
10^{-4}	1	Thruster fire (attitude)
10^{-4}	1	Crew push off

conferences.[5,6] A summary of this data was presented in Ref. 7 and is repeated in Table 1. Additional results have been reported in Refs. 8 and 9.

The vibration levels reported in the above literature for spacecraft are significantly greater than allowable for material science experiments. In order to achieve accurate and reproducible results in such experiments, vibration isolation will be required.[3] Acceleration disturbances in the orbiter environment cover a wide frequency bandwidth, from 0 to 100 Hz. Sources include spacecraft drag, light pressure oscillations, manned activity, and thruster fire. The frequency and amplitudes of these accelerations are summarized in Table 1.

The frequency and amplitude of any particular vibration source determines the level of isolation that can be achieved. At relatively high frequencies, above approximately 10 Hz, passive vibration isolation is normally possible. Two examples of such isolation systems are reported in Refs. 10 and 11. For lower frequencies, active vibration isolation is necessary. One of the few such systems is examined in Ref. 12.

A fundamental restriction on active microgravity vibration isolation systems is the limited available volume aboard spacecrafts for experiments. This kinematic constraint cannot be overcome through improvement of the vibration isolation control system, sensors, or actuator. The purpose of this paper is to explore the limitations on vibration isolation systems arising from the stroke restriction. Thus an ideal vibration actuator is assumed, and the problem is solved in part by optimal control theory. This work is an extension of research on isolation limits under sinusoidal excitation.[13] In this paper, the excitation is a wideband, zero-mean stochastic process. A lower bound on the root-mean-square acceleration is determined in terms of the maximum stroke.

Optimal Control Formulation

While the isolation problem for microgravity space experiments is multidimensional, this analysis examines the one-dimensional case. Consider the system illustrated in Fig. 1 with experiment position $x(t)$ and wall positions $y_1(t)$ and $y_2(t)$. The experiment is connected to the spacecraft by umbilicals, such as power or fluid lines, and by a vibration isolation actuator. Although the spacecraft has a finite mass, it may be considered to have infinite impedance for this analysis since the spacecraft-to-experiment weight ratio is very large. The spacecraft acts as an external base motion transmitting forces through the umbilical and the actuator.

An ideal actuator is assumed. Therefore, the acceleration of the experiment is the minimum acceleration possible given that the experiment stay between the two walls. The effects of the power/data/cooling umbilicals represented in Fig. 1 are removed through the ideal actuator. Thus, the problem is reduced to a kinematic representation. The vibration isolation problem becomes an optimal control problem: find the optimal trajectory (minimum acceleration) given the constraint conditions (moving walls). This problem formulation was used previously by the authors to find the limitations on isolation for harmonic disturbances.[13]

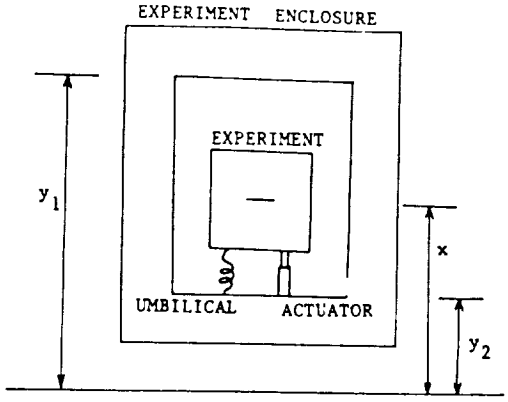

Fig. 1 One-degree-of-freedom isolation problem.

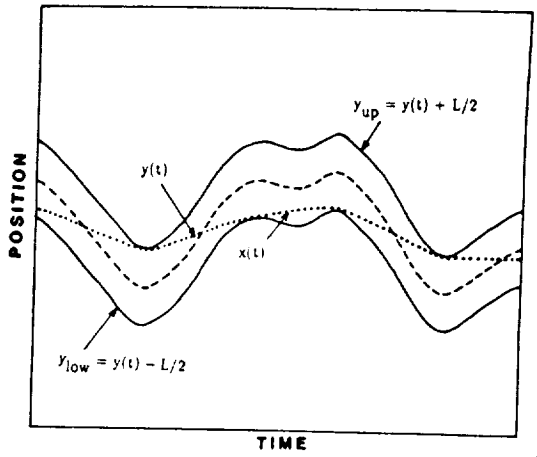

Fig. 2 Optimal path through stochastic walls.

Significant Extrema

The kinematic formulation allows the stochastic problem to be easily conceived. Figure 2 illustrates. An optimal trajectory $x(t)$ is sought between two walls whose motion is described by a single zero-mean stochastic process $y(t)$,

$$y_{up} = y(t) + L/2$$

$$y_{low} = y(t) - L/2$$

where L is the maximum stroke of the experiment between the two walls.

Let the experiment acceleration be denoted as $u(u = \ddot{x})$. Then the cost function J to be minimized is

$$J = \int_0^\infty u^2 \, dt \tag{1}$$

with the constraint

$$y(t) - \frac{L}{2} \le x(t) \le y(t) + \frac{L}{2}, \qquad 0 \le t \tag{2}$$

for a given wall centerline motion $y(t)$. The optimal trajectory will be in general smooth with as few extrema as possible. The trajectory will also cover as little distance as possible. As previously reported in Ref. 13, with a sinusoidal disturbance, the optimal trajectory tangents the maxima of the lower wall and the minima of the upper wall when the amplitude of $y(t)$ is greater than $L/2$. Given these tangencies, it is an easy task to compute the minimum acceleration path connecting them. Although this path may intersect a wall's path, as was reported in Ref. 13, this "cheating" results in less than a 1% reduction in root-mean-square from the true optimal path. By dropping the inequality constraints from the optimal control problem

and replacing them with the tangency conditions at the wall's extrema, a tight lower bound on the minimum root-mean-square acceleration is obtained. This is the approach taken here with the stochastic problem. For this analysis, the wall process $y(t)$ and its derivatives are assumed to be stationary, zero-mean, Gaussian random processes.

Once again, the wall inequality constraints are ignored and are replaced with interior point equality conditions. A tangency condition is assumed at some of the walls' extrema and the trajectory is required to cross zero at the same time as $y(t)$. This last requirement is made to ensure a tight lower bound. Note that a zero crossing of $x(t)$ must occur at or before $y(t)$ leaves the $\pm L/2$ interval. However, for most random processes $y(t)$, the additional requirement of simultaneous zero crossing results in a realistic and tighter lower bound. The upper wall is ignored as a constraint when $y(t) > 0$ as the lower wall is when $y(t) < 0$. Thus, only upper wall minima when $y(t) < 0$ and lower wall maxima when $y(t) > 0$ are eligible tangency condition points. Figure 3 illustrates this geometry and a composite path connecting the prescribed interior points. The optimal composite trajectory satisfying these interior point equality constraints will have a root-mean-square acceleration lower than that of the optimal trajectory satisfying the original inequality constraints under almost all conditions. Note that the composite trajectory is not required to have first derivative continuity at the interior zero crossing points. (It will, of course, have a continuous first derivative at the extrema tangent points.) It should be pointed out that the composite trajectory is not intended to be an implementable optimal control path; the trajectory is a theoretical tool to investigate the limitations on vibration isolation.

Not all eligible lower wall maxima and upper wall minima will be tangented by the optimal composite trajectory. In Fig. 4, note that if $|y(t)| < L/2$, as shown on the left side of the figure, the optimal path is $x(t) = 0$. However, if the eligible extremum crosses zero (i.e., if $|y(t)| > L/2$) as on the right side, the optimal composite path must depart from $x(t) = 0$ to avoid collision with the wall.

Because of the wideband character of the stochastic wall acceleration, many extrema tend to be clustered at every peak of $y(t)$. The composite trajectory will only tangent one of these extrema and that only if $|y(t)| > L/2$. The effort here is to distinguish the extrema which the composite trajectory needs to include (in order to be a useful lower bound) from the bulk of immaterial extrema.

A wall extremum in a time interval that requires an increase in the cost function during the interval is classified here as a significant extremum. (This is, admittedly, not a rigorous definition; however it satisfies the purpose of this investigation.) The optimal composite path, therefore, runs between

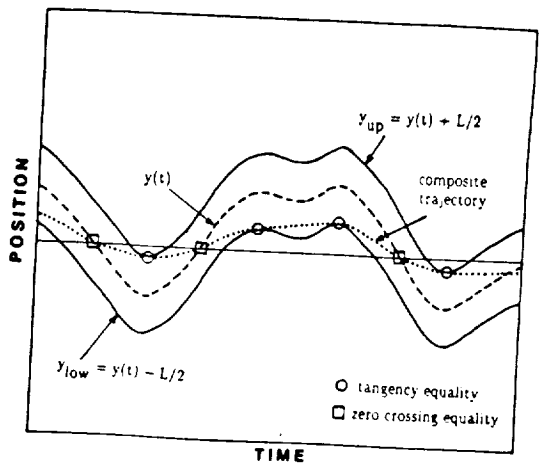

Fig. 3 Stochastic walls, interior point equality conditions, and composite trajectory.

significant extrema and $y = 0$. The composite path is a combination of paths of the experiment at rest, departing to an extremum, and returning from an extremum as indicated in Fig. 4. Each of these cases can be analyzed in terms of a return path. [Departing paths are kinematically the same as returning paths since the random processes $y(t)$ and $\dot{y}(t)$ are independent since they are Gaussian. A rest path is equivalent to a return path when $|y(t)| < L/2$.] By finding the expected value of the mean square acceleration on a return path, the mean square acceleration of the composite path is determined, and a lower bound is set on the optimal trajectory mean square acceleration. Thus, a lower bound is found by characterizing the distribution of the significant extrema in time and position.

Solution in Terms of the Significant Extrema

The return path and its mean square acceleration given a significant extremum is now found. Examine the time history shown in Fig. 5. The optimal path during the interval (t_1, t_2) satisfying the wall inequality constraints over a much larger interval has, in general, a root-mean-square acceleration bounded below by the root-mean-square acceleration on the return path connecting points 1 and 2. [This will be true for all but wideband $y(t)$ processes with large maximum stroke, L. Note that $\ddot{y}(t)$ can be wideband with $y(t)$ not.] The boundary constraints at these two points for the return path are

$$x(t_1) = z \qquad x(t_2) = 0$$
$$\dot{x}(t_1) = 0 \qquad \dot{x}(t_2) = \text{free} \tag{3}$$

where $z = y_{max} - L/2$.

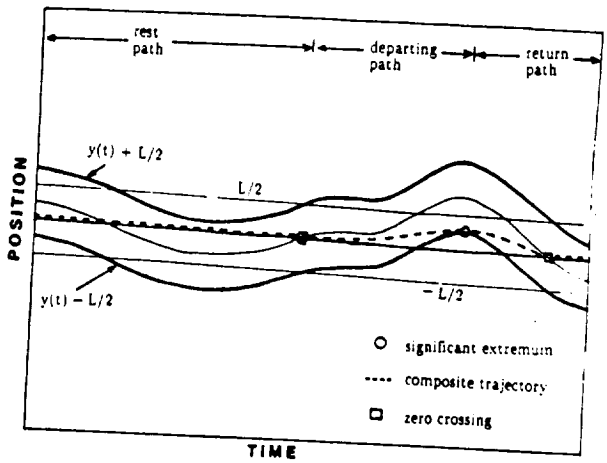

Fig. 4 Significant extrema and composite trajectory.

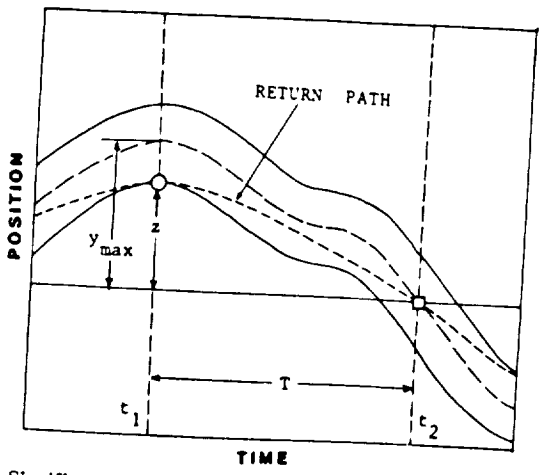

Fig. 5 Significant maximum, return path, and boundary conditions.

The velocity boundary condition at time t_2 is left free since this condition depends on the next significant extremum, the location of which cannot be readily derived even in a probabilistic sense. Therefore, the velocity at time t_2 is unspecified so that the return path root-mean-square acceleration will be a lower bound on the minimum acceleration. The optimal control problem is thus reduced to that over the time t_1 to t_2 with cost function

$$J = \int_{t_1}^{t_2} u^2 \, dt \tag{4}$$

and the boundary conditions of Eq. (3).

This problem is solved by the calculus of variations (Appendix A) yielding the optimal trajectory.[14]

The mean-square acceleration on this trajectory is

$$MS(\ddot{x}) = \left[\frac{1}{(t_2 - t_1)} \int_{t_1}^{t_2} u^2 \, dt\right] = \frac{3z^2}{T^4} \tag{5}$$

where $T = (t_2 - t_1)$, the time from significant extrema to zero crossing, or the first-passage time. This is the lower bound sought. Assuming that the wall process $y(t)$ is ergodic, the minimum mean square experiment acceleration attainable with an ideal isolator must be greater than the mean-square acceleration of the composite trajectory,

$$E\left\{\frac{3z^2}{T^4}\right\}$$

where $E\{\cdot\}$ is the exact value operator[15]

$$E\left\{\frac{3z^2}{T^4}\right\} = \int_0^\infty \int_0^\infty \frac{3z^2}{T^4} f_{zT}(z,t) \, dz \, dT \tag{6}$$

Here, $f_{zT}(\cdot,\cdot)$ is the joint probability density function on the significant maxima z, and the time from significant maxima to zero crossing T. (The significant extrema problem can be solved for in terms of significant maxima because of the symmetry of the problem.) Equation (6) can be rewritten

$$E\left\{\frac{3z^2}{T^4}\right\} = \int_0^\infty 3z^2 f_z(z) \, E\left\{\frac{1}{T^4} | z\right\} dz \tag{7}$$

where $E\{(1/T^4)|z\}$ is the conditional fourth moment of T^{-1}, and $f_z(\cdot)$ is the probability density function of the significant maxima.

Distribution of Significant Maxima

Consider the stationary, zero-mean, Gaussian random process describing the wall's acceleration $\ddot{y}(t)$. This process can be characterized by its power spectral density $S_{\ddot{y}}(\omega)$.[16] The mean square of the wall acceleration is the integral of this over

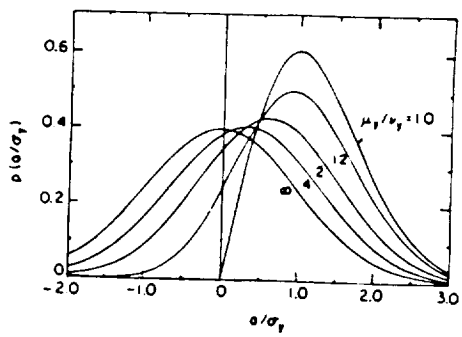

Fig. 6 Probability density function for the distribution of maxima of a stationary Gaussian process.

frequency[17]

$$E(\ddot{y}^2) = \sigma_{\ddot{y}}^2 = \int_{-\infty}^{\infty} S_{\ddot{y}}(\omega) \, d\omega \tag{8}$$

(simply the area underneath the power spectral density curve). The mean square of the velocity and position processes are

$$E(\dot{y}^2) = \sigma_{\dot{y}}^2 = \int_{-\infty}^{\infty} \frac{S_{\ddot{y}}(\omega)}{\omega^2} \, d\omega \tag{9}$$

$$E(y^2) = \sigma_y^2 = \int_{-\infty}^{\infty} \frac{S_{\ddot{y}}(\omega)}{\omega^4} \, d\omega \tag{10}$$

For a Gaussian process, the density of upcrossings of $y = 0$ for the $y(t)$ process[15,18] is

$$\nu_y = \frac{\sigma_{\dot{y}}}{2\pi\sigma_y} \tag{11}$$

and the density of maxima of $y(t)$ is

$$\mu_y = \frac{\sigma_{\dot{y}}}{2\pi\sigma_{\dot{y}}} \tag{12}$$

Rice[19] and Houston and Skopinski[20] have shown that the probability density function for the distribution of the maxima of a stationary Gaussian random process is dependent only on the ratio μ_y/ν_y and the standard deviation of the process σ_y

$$f_{y_{\max}}(y/\sigma_y) = (1 - \nu_y^2/\mu_y^2)^{1/2} f_N\left[\frac{y/\sigma_y}{(1 - \nu_y^2/\mu_y^2)^{1/2}}\right] + (2\pi)^{1/2} \frac{\nu_y}{\mu_y}\left(\frac{y}{\sigma_y}\right) f_N\left[\frac{y}{\sigma_y}\right] F_N\left[\frac{y/\sigma_y}{(\mu_y^2/\nu_y^2 - 1)^{1/2}}\right] \tag{13}$$

where f_N and F_N are the normal probability density function and its integral

$$f_N(x) = (2\pi)^{-1/2} e^{-(x^2/2)}$$

$$F_N(x) = \int_{-\infty}^{x} f(a) \, da \tag{14}$$

(Lin[21] has an interesting discussion on this maxima distribution.)

The ratio μ_y/ν_y can be regarded as the average number of maxima between upcrossings for the $y(t)$ process.[18] Probability density functions for the distribution of maxima of a stationary Gaussian random process are shown for different values of this ratio in Fig. 6.

A random wall process typical of the microgravity vibration environment will have many maxima per zero crossing ($\mu_y/\nu_y \gg 1$). Most of these maxima are clustered near the peaks of the process and can be considered the high frequency component.[18] Figure 7 illustrates. The random process $y(t)$, as was shown by Crandall,[18] can be decomposed into the sums of a macroscopic component $\bar{y}(t)$ and a microscopic component $d(t)$

$$y(t) = \bar{y}(t) + dt \tag{15}$$

The macroscopic component has a much smaller root mean square σ_d and greater frequency of zero crossing ν_d than the macroscopic signal ($\sigma_{\bar{y}}$, $\nu_{\bar{y}}$). The macroscopic component will have nearly the same amplitude as the original signal. The distribution of maxima given in Eq. (13) is the distribution of both the micromaxima and macromaxima. Clearly, the micromaxima do not contribute (substantially) to the cost

function; therefore, they are, by definition, not significant maxima.

The distribution of significant maxima is therefore derived from the distribution of macromaxima, the maxima of the $\bar{y}(t)$ process,

$$f_{y_{max}}(\bar{y}/\sigma_y) = (1-\nu_y^2/\mu_y^2)^{1/2} f\left[\frac{\bar{y}/\sigma_y}{(1-\nu_y^2/\mu_y^2)^{1/2}}\right]$$

$$+ (2\pi)^{1/2}\frac{\nu_y}{\mu_y}\left(\frac{\bar{y}}{\sigma_y}\right) f_N\left[\frac{\bar{y}}{\sigma_y}\right] F\left[\frac{\bar{y}/\sigma_y}{(\mu_y^2/\nu_y^2-1)^{1/2}}\right] \tag{16}$$

To obtain the density function for the distribution of significant maxima from the distribution of macromaxima it is only necessary to recall Eq. (3) with $\bar{y}_{max}$ replacing y_{max}

$$z = \begin{cases} \bar{y}_{max} - L/2 & \bar{y}_{max} > L/2 \\ 0 & \bar{y}_{max} < L/2 \end{cases} \tag{17}$$

find the cumulative distribution on z in terms of the cumulative distribution on $\bar{y}_{max}$

$$F_z(z) = \begin{cases} F_{y_{max}}(z + L/2) & z > 0 \\ 0 & z < 0 \end{cases} \tag{18}$$

and to differentiate with respect to z[15]

$$f_z(z) = \begin{cases} F_{y_{max}}(L/2)\delta(z) + f_{y_{max}}(z + L/2) & z > 0 \\ 0 & z < 0 \end{cases} \tag{19}$$

where $\delta(\cdot)$ is the dirac delta function. Note that the portion of the $\bar{y}_{max}$ distribution between $-\infty$ and $L/2$ maps into a dirac delta at $z = 0$. The integration of this part of $f_z(z)$ in Eq. (7) will be zero

$$\int_0^\infty 3z^2 F_{y_{max}}(L/2)\,\delta(z)\,E\left\{\frac{1}{T^4}|z\right\} dz = 0 \tag{20}$$

The nonsignificant maxima, therefore, do not increase the expected mean square. (Note that $E\{(1/T^4)|z=0\}$ is finite since T is defined as the time for the $\bar{y}(t)$ process to reach $\bar{y}=0$ starting from rest at y_{max}. When $z=0$, $\bar{y}_{max} = L/2$; therefore, T is greater than zero.)

The tightness of the lower bound on experiment mean square acceleration given in Eq. (7) depends on the accuracy of the geometric configuration, Fig. 5, in representing typical wall position histories. The decomposition, or smoothing, of the $y(t)$ process yields a macroscopic random process $\bar{y}(t)$ upon which to base the lower bound. If the random process $\bar{y}(t)$ has close to one maxima per upcrossing on average (it must have at least one since it is continuous), the typical geometric configuration will resemble Fig. 5. Thus, for a narrowband random process $\bar{y}(t)$, the bound will be very tight. (In the limit this approaches a sinusoid with slowly changing random amplitude and phase[22]; the resulting bound would be only a few percent low.) For a wideband macroscopic process the bound will be considerably looser but non-trivial. It is therefore desirable that the decomposition produce a macroscopic process with an average number of maxima per upcrossing (μ_y/ν_y) close to one. The smoothed process $\bar{y}(t)$ should also have nearly the same variance as the original signal $\bar{y}(t)$. A method for the decomposition of $\bar{y}(t)$ and $d(t)$ will be discussed later with the application.

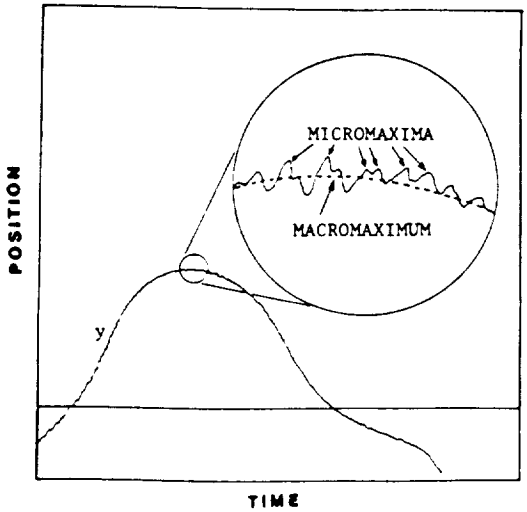

Fig. 7 Macroscopic maxima and microscopic maxima.

First-Passage Problem

An expression for $E\{(1/T^4)|z\}$ can be found explicitly if the conditional probability density function $f_T(T|z)$ is known[15]

$$E\{(1/T^4)|z\} = \int_0^\infty \frac{1}{T^4} f_T(T|z)\, dT \tag{21}$$

The distribution of the first passage time of a stochastic process T is a classical problem probability that has been tackled with limited success by many authors.[23-25] No exact theoretical solution exists. Many approximate methods have been used including series solution,[23] Poison approximation,[24] numerical probability diffusion, and Monte Carlo techniques.[25] The particular variant of the first-passage problem of interest here is nonstationary due to its initial conditions

$$\bar{y}(t_1) = \bar{y}_{max}$$

$$\dot{\bar{y}}(t_1) = 0 \tag{22}$$

and can be expected to have a crossing in the near future since $\bar{y}(t)$ is zero mean (This, in contrast to the first passage of a level $\bar{y} = a \gg \sigma_y$, which will occur extremely infrequently.) The nonstationary, quick-crossing nature of this problem suggests Monte Carlo simulation as the preferred method of solution. It is not necessary to generate the conditional probability density function of T in this manner; only the $E\{(1/T^4)|z\}$ is needed.

To perform the simulation, a forced differential equation with the proper probabilistic characteristics must be found. More specifically, the wall acceleration in the simulation should have a power spectral density that matches that of the acceleration disturbance found aboard the spacecraft in the region where the experiment is to be located. Given a measured power spectral density, the dynamic model, or shaping filter, that transforms Gaussian white noise to the desired random process can be found by spectral factorization.[17,26] This dynamic model can then be used in Monte Carlo simulation (Appendix B).

Application to Microgravity Vibration Isolation

The method described above is now applied to the microgravity problem. As described in Ref. 7, vibration aboard spacecraft is essentially of two frequency regions: 0-10^{-3} Hz and above 1 Hz. Consequently, the power spectral density for analysis here is modeled independently in these two regions. The low frequency portion was not obtained from an experimental power spectral density since such information is unavailable. This part of the spectral density, illustrated in Fig. 8, has therefore been devised for the purpose of this example to fit the known environmental disturbances in this

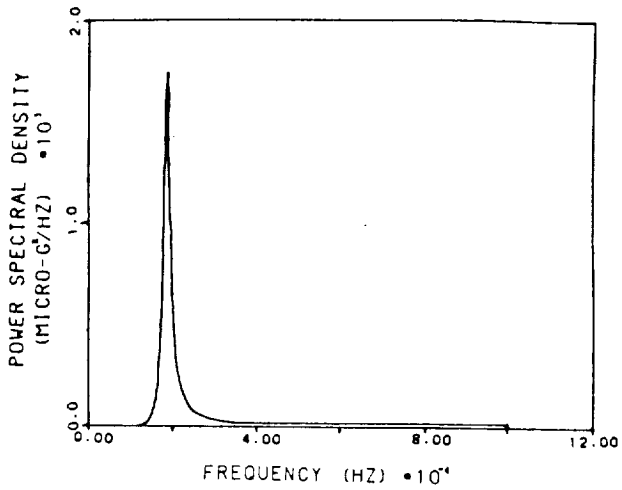

Fig. 8 Acceleration power spectral density in the low frequency range.

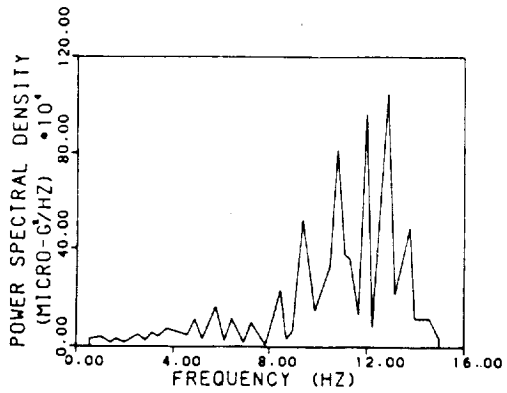

Fig. 9 Acceleration power spectral density in the high frequency range.

frequency range. The spectral density of the analytical model

$$S_{\ddot{y}}(\omega^2) = \begin{cases} \dfrac{75.75\ \omega^4}{(\omega/0.00116)^4 - 1.99\ (\omega/0.00116)^2 + 1} & 0 \le \omega \le 0.006283 \\ 0 & 0.006283 < \omega < 3.14159 \end{cases} \tag{23}$$

has most of its power concentrated near orbital frequency (1.851×10^{-4} Hz, 90 min orbit) with a power corresponding to a root-mean-square acceleration of approximately 0.2 μg. It should be pointed out that the accuracy of the lower bounds generated by this method depends heavily upon the model used in this region.

The high frequency region of the power spectral density, shown in Fig. 9, is from experiments aboard Spacelab.[33] An analytical model could easily be fitted to the curve shown; however, this is not necessary for this application. Note that the method of analysis described previously does not require that disturbance spectral density occupy two separate regions as in this case.

The mean square wall process acceleration, velocity, and position can be found by evaluating Eqs. (8-10) respectively. This may be done through numerical quadrature yielding,

$$\sigma_{\ddot{y}} = 0.016143511 \text{ m/s}^2$$

$$\sigma_{\dot{y}} = 0.0019532654 \text{ m/s}$$

$$\sigma_y = 1.6503623 \text{ m} \tag{24}$$

and by Eqs. (11) and (12)

$$\nu_y = 0.18836582 \times {}^{-3} \text{ upcrossings/s}$$

$$\mu_y = 0.13153971 \times 10^{1} \text{ maxima/s}$$

$$\mu_y/\nu_y = 6983.2 \text{ maxima/upcrossing} \tag{25}$$

Clearly there are many micromaxima per peak of the macroscopic process. The two distinct regions of the power spectral density permit an easy decomposition of the wall processes $y(t)$, $\dot{y}(t)$, and $\ddot{y}(t)$ into macroscopic (low frequency) and microscopic (high frequency) components. For a problem with a continuous power spectral density, a smoothing filter as examined by Crandall[18] may be used for the decomposition.

The decomposition of the Gaussian signal yields two independent random processes[21]

$$E\{\bar{y}(t)\ d(t)\} = 0 \qquad \sigma_y^2 = \sigma_{\bar{y}}^2 + \sigma_d^2$$

$$E\{\dot{\bar{y}}(t)\ \dot{d}(t)\} = 0 \qquad \sigma_{\dot{y}}^2 = \sigma_{\dot{\bar{y}}}^2 + \sigma_{\dot{d}}^2$$

$$E\{\ddot{\bar{y}}(t)\ \ddot{d}(t)\} = 0 \qquad \sigma_{\ddot{y}}^2 = \sigma_{\ddot{\bar{y}}}^2 + \sigma_{\ddot{d}}^2 \tag{26}$$

with

$$\sigma_{\bar{y}} = 0.16503623 \times 10^{1} \text{ m} \qquad \sigma_d = 0.63558716 \times 10^{-4} \text{ m}$$

$$\sigma_{\dot{\bar{y}}} = 0.19030049 \times 10^{-2} \text{ m/s} \qquad \sigma_{\dot{d}} = 0.44024768 \times 10^{-3} \text{ m/s}$$

$$\sigma_{\ddot{\bar{y}}} = 0.25429066 \times 10^{-5} \text{ m/s}^2 \qquad \sigma_{\ddot{d}} = 0.16143511 \times 10^{-1} \text{ m/s}^2 \tag{27}$$

The resulting upcrossing and maxima frequencies are

$$\nu_{\bar{y}} = 0.18351888 \times 10^{-3} \qquad \nu_d = 0.11024073 \times 10^{1}$$

$$\mu_{\bar{y}} = 0.21267216 \times 10^{-3} \qquad \mu_d = 0.58360775 \times 10^{-1}$$

$$\mu_{\bar{y}}/\nu_{\bar{y}} = 0.11588571 \times 10^{1} \qquad \mu_d/\nu_d = 5.2939393 \tag{28}$$

Therefore, the smoothed wall process has an average of 1.158857 maxima per upcrossing (or cycle). Since this is close to one, the wall process geometry closely resembles Fig. 5 and the lower bound will be tight. Further note that

$$\sigma_{\bar{y}}/\sigma_y \cong 1.0 \qquad \nu_{\bar{y}}/\nu_y = 0.97426848 \tag{29}$$

Thus, the smoothed process retains nearly all of the signal's amplitude and has on average fewer cycles per unit time. The apparent drop in "frequency" is due to wall process smoothing removing spurious microcycles. Therefore, the decomposition does not alter the original signal's significant maxima amplitude-time characteristics. Finally, unless the maximum stroke is of the same magnitude as the microscopic component, the smoothed wall acceleration $\ddot{\bar{y}}(t)$ establishes an upper bound $\sigma_{\ddot{\bar{y}}}$ on the minimum root-mean-square experiment acceleration.

With the significant maxima distribution found, attention is now turned to finding the needed first-passage time moment. The low frequency part of the power spectral density, Eq. (23), is converted to an equivalent dynamical system via

spectral factorization yielding the shaping filter

$$G_y(s) = \frac{8.64581}{(s/0.00116)^2 + 0.1(s/0.001160) + 1} \tag{30}$$

with a bandlimited white noise excitation $n(t)$ described by

$$S_n(\omega) = \begin{cases} 1 & 0 \le \omega \le 0.006283 \\ 0 & 0.006283 < \omega \end{cases} \tag{31}$$

Converting Eq. (30) into two first order differential equations produces

$$\dot{\bar{y}}_1 = \bar{y}_2 \tag{32a}$$

$$\dot{\bar{y}}_2 = -1.3456 \times 10^{-6}\bar{y}_1 - 1.16 \times 10^{-4}\bar{y}_2 + 1.16338 \times 10^{-5} n \tag{32b}$$

with initial conditions from Eqs. (15) and (22)

$$\bar{y}_1(0) = \bar{y}_{1_0} = z + L/2$$

$$\bar{y}_2(0) = 0 \tag{33}$$

The bandlimited white noise process $n(t)$ is approximated by the sum of a large number of sinusoids at nearly evenly spaced frequencies between zero and the cutoff frequency via the method advocated by Shinozuka and Jan.[27] The phases are random while the amplitudes are determined by the power spectral density desired. As the number of sinusoids is increased, the approximated signal approaches $n(t)$. It was determined through testing that 40 was a sufficient number of sinusoids for this example.

The differential equations of Eq. (32) are numerically integrated from the initial conditions until the first crossing. If the process rises above the initial position $\bar{y}_{1_0}$, the simulation is stopped and restarted from the initial condition again. This insures that the crossing time obtained is the first-passage time from the maxima. The first-passage time of each simulation is recorded, and the fourth moment of T^{-1} is calculated from the collection of k first-passage times

$$m_{-4}(\bar{y}_{1_0}) = \frac{1}{k}\sum_{i=1}^{k} T_i^{-4} \tag{34}$$

For an ergodic process,[16] as the sample size k grows, this statistic approaches $E\{T^{-4}|\bar{y}_{1_0}\}$. The statistic $m_{-4}(\bar{y}_{1_0})$ is found for a range of $\bar{y}_{1_0}$ values. The results of the simulations for the example are shown in Fig. 10. Note that the data are asymptotic to

$$\left[\omega_d / \tan^{-1}\left(\frac{-\sqrt{1-\xi^2}}{\xi}\right)\right]^4 = 0.26105 \times 10^{-12}\ \mathrm{s}^{-4}$$

as $\bar{y}_{1_0}$ approaches infinity where ω_d is the damped natural frequency of Eq. (32). This is because the noise is essentially negligible when the system's energy is very high. Once the maximum stroke L is specified, the $E\{T^{-4}|\bar{y}_{1_0}\}$ yields the $E\{T^{-4}|z\}$. The data points are cubic spline interpolated to provide an approximation of the function $E(T^{-4}|z)$ suitable for numerical integration.

The experiment acceleration mean square lower bound sought can now be calculated from the significant maximum probability density and the conditional moment on the first-passage time by numerical quadrature of Eq. (7) using Eqs. (16), (19), and (28) along with the interpolation of the inverse moment data. This is done for varying values of

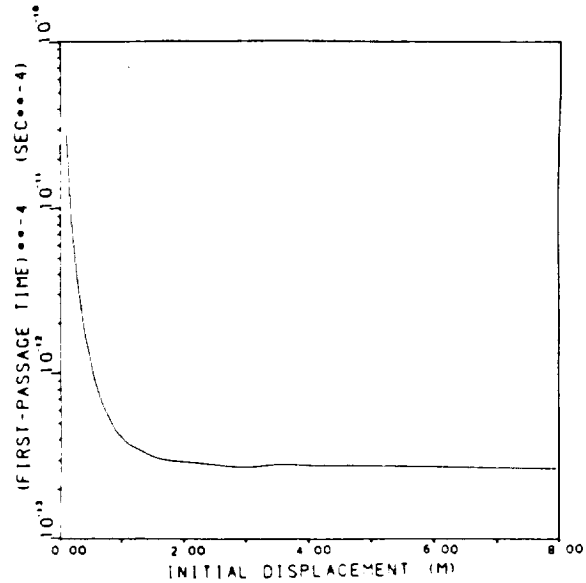

Fig. 10 Numerically computed fourth moments of T^{-1}.

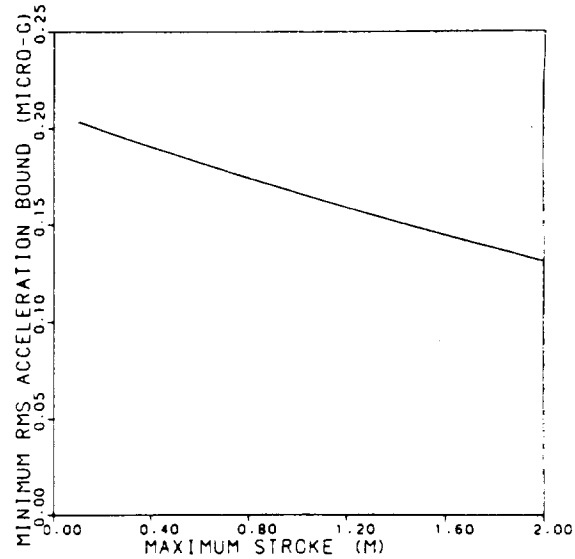

Fig. 11 Lower bound on root-mean-square experiment acceleration under prolonged exposure to specified vibration environment.

maximum stroke. The lower bound on minimum root-mean-square experiment acceleration that can be obtained under prolonged exposure to the example vibration environment given the stroke constraint is thus computed and is plotted in Fig. 11 vs maximum stroke. For example, with a maximum stroke of 1 m, according to the figure the root-mean-square acceleration of an experiment must be greater than 0.17 μg, whereas if a 2-m stroke is permitted, this can be reduced to 0.13 μg. Note that the lower bound is non-zero for finite maximum stroke. This is in contrast to the previously reported results for harmonic disturbances where the maximum acceleration was zero when the maximum stroke was greater than twice the harmonic amplitude.

Conclusions

In this paper, the microgravity vibration isolation problem was formulated as a one-dimensional kinematic problem. The geometry of the stochastic wall trajectories was defined in terms of their significant extrema. An optimal control solution for the minimum acceleration return path determined a lower bound on experiment mean-square acceleration. This bound

was expressed in terms of the probability density function on the significant maxima and the conditional fourth moment of the first passage time inverse. For an example given, the first of these was found analytically while the second was found via Monte Carlo simulation. The experiment root-mean-square acceleration lower bound as a function of available space was then determined through numerical quadrature.

The method of analysis is quite general and intuitive. The authors feel that this could be applied to other problems with stochastic constraints. While such an analysis does not yield a controller, it does aid in the selection of system parameters (for example, the maximum stroke).

Lower bound plots of the type developed here may assist microgravity experiment designers as well as vibration isolation engineers. The lower bound depicted in plots of this type could not be achieved by real systems for several reasons. The levels derived are beneath the theoretical minimums. In addition, a real system is causal and cannot base its current control on unknown future disturbances. Also, any real active control system will have some non-ideal characteristics. The sensors employed to provide feedback will have some error as well. In spite of these comments, the authors of this paper are optimistic about attaining microgravity isolation levels close to the levels depicted here with an active vibration isolation system.

Appendix A: Solution for Optimal Trajectory

The derivation of the optimal trajectory proceeds as follows. Define the system state variables as

$$x_1 = x \qquad \dot{x}_1 = x_2 \qquad \dot{x}_2 = u \tag{A1}$$

and the equations of motion become

$$\dot{\boldsymbol{x}} = \boldsymbol{A}\boldsymbol{x} + \boldsymbol{B}u$$

$$\boldsymbol{x}^T = [x_1\ x_2] \qquad \boldsymbol{A} = \begin{bmatrix} 0 & 1 \\ 0 & 0 \end{bmatrix} \qquad \boldsymbol{B}^T = [\,0\ \ 1\,] \tag{A2}$$

The cost function is adjoined by the equations of motion and the final condition, utilizing three Lagrange multipliers.[14] The result is

$$J = \phi x_{1_f} = \int_{t_1}^{t_2} [u^2 + \lambda_1(x_2 - \dot{x}_1) + \lambda_2(u - \dot{x}_2)]\, dt \tag{A3}$$

which is the general functional for this problem. Define the Hamiltonian and final condition cost[14] as

$$H = u^2 + \lambda_1 x_2 + \lambda_2 u \qquad G = \phi x_{1_f} \tag{A4}$$

Employing the calculus of variations, the minimization equations are

$$\dot{\lambda}_1 \equiv \frac{\partial H}{\partial x_1} = 0 \qquad \dot{\lambda}_2 \equiv -\frac{\partial H}{\partial x_2} = -\lambda_1 \qquad 0 \equiv \frac{\partial H}{\partial u} = 2u + \lambda_2 \tag{A5}$$

with natural boundary conditions

$$\lambda_{1_f} = G_{x_{1_f}} = \phi, \qquad \lambda_{2_f} = G_{x_{2_f}} = 0 \tag{A6}$$

Solving this gives

$$\lambda_1 = C_0, \qquad \lambda_2 = -C_0 t + C_1, \qquad u = \tfrac{1}{2} C_0 t - \tfrac{1}{2} C_1 \tag{A7}$$

Imposing the prescribed and natural boundary conditions yields

$$C_0 = \frac{6z}{T^3}, \qquad C_1 = \frac{6zt_2}{T^3} \tag{A8}$$

and

$$u(t) = \frac{3z}{T^3} t - \frac{3z}{T^3} t_2$$

$$\dot{x}(t) = \frac{(3/2)z}{T^3} t^2 - \frac{3zt_2}{T^3} t - \frac{(3/2)z(t_1^2 - 2t_2t_1)}{T^3}$$

$$x(t) = \frac{(1/2)z}{T^3} t^3 - \frac{(3/2)zt_2}{T^3} t^2 - \frac{(3/2)z(t_1^2 - 2t_2t_1)}{T^3} t + \frac{(1/2)z(2t_2^3 - 6t_1t_2^2 + 3t_1^2t_2)}{T^3} \tag{A9}$$

where $T = (t_2 - t_1)$, the time from significant extrema to zero crossing, or the first-passage time.

Appendix B: Shaping Filter for Simulation

The power spectral density is first approximated by a rational polynomial in ω^2. (This can be done to any required accuracy for a given power spectral density by using higher order polynomials.) This representation of the true power spectral density is then factored into two terms

$$S_y(\omega^2) = G(j\omega)G(-j\omega) \tag{B1}$$

The first term $G(j\omega)$ has all its poles and zeroes in the left half plane, whereas the poles and zeroes of the second term, $G(-j\omega)$, are the mirror images in the right half plane Replacing $j\omega$ in $G(j\omega)$ with the complex frequency variable s yields the transfer function that produces a Gaussian random process with power spectral density $S(\omega)$ from Gaussian white noise input:

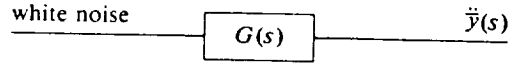

It is a straightforward process to convert the transfer function, or shaping filter, with n poles and m zeroes to $n + m$ first order linear differential equations with white noise input via the inverse Laplace transform and algebraic manipulation.[17,26] (Note that the derivative of white noise is nonexistent.) For most applications only the model of the low frequency component $\bar{y}(t)$ as a set of differential equations is needed to generate the $E\{(1/T^4)|z\}$.

Acknowledgment

This work was supported in part by NASA Lewis Research Center and the Commonwealth of Virginia.

References

[1]Spencer, L., "Overview of NASA Microgravity Programs and Opportunities," Vibration Isolation Technology for Microgravity Science Workshop, NASA Lewis Research Center, Sept. 1988.

[2]Alexander, J. I., "Experiment Sensitivity: Determination of Requirements for Isolation," Vibration Isolation Technology for Microgravity Science Workshop, NASA Lewis Research Center, Sept. 1988.

[3]Sharpe, A. (ed.), "Low Acceleration Characterization of Space Station Environment," Teledyne-Brown, Final Rept., SP85-MISFC-2928, Rev. B, NASA Marshall Space Flight Center, Oct. 1985.

[4]Stuhlinger, E., and Mookherji, T., "Materials Processing Twin Experiment," AIAA Paper 88-0348, Jan. 1988.

[5]Chassay, R. P., and Schwaniger, A. J., "Low-G Measurements by NASA," *Measurement and Characterization of the Acceleration Environment on Board the Space Station*, NASA Marshall Space Flight Center, Aug. 1986.

[6]Henderson, F., "MSL-2 Accelerometer Data Results," *Measurement and Characterization of the Acceleration Environment on Board the Space Station*, Teledyne-Brown, Aug. 1986.

[7]Grodsinsky, C. M., and Brown, J. V., "Low Frequency Vibration Isolation Technology for Microgravity Space Experiments," NASA

TM 101448, Sept. 1989.

[8]Fox, J. C., and McNally, P. J., "Current Orbiter Instrumentation and Acceleration Environment Data," Vibration Isolation Technology for Microgravity Science Workshop, NASA Lewis Research Center, Sept. 1988.

[9]Hamacher, H., Jilig, R., and Merbold, U., "The Microgravity Environment of the D-1 Mission," *Proceedings of the 37th IAF Conference*, Innsbruck, Austria, Paper IAF-86-268, 1986.

[10]Davis, L. P., Wilson, J. F., Jewell, R. E., and Roden, J. J., "Hubble Space Telescope Reaction Wheel Assembly Vibration Isolation System," Sperry Corp., Phoenix, AZ, March 1986.

[11]Wilson, J. F., and Davis, L. P., "Viscous Damped Space Structure for Reduced Jitter," 58th Shock and Vibration Symposium, Huntsville, AL, Aug. 1987.

[12]Hamilton, B. J., Andrus, J. H., and Carter, D. R., "Pointing Mount with Active Vibration Isolation for Large Payloads," AAS 87-033, Jan. 1987.

[13]Knospe, C. R., and Allaire, P. E., "Limitations on Vibration Isolation for Microgravity Space Experiments," *Journal of Spacecraft and Rockets*, Vol. 27, No. 6, pp. 642-646.

[14]Bryson, A. E., and Ho, Y.-C., *Applied Optimal Control: Optimization Estimation and Control*, Hemisphere, New York, 1975, Chaps. 2 and 3.

[15]Papoulis, A., *Probability, Random Variables, and Stochastic Processes*, McGraw-Hill, New York, 1984, Chaps. 5, 10, and 11.

[16]Newland, D. E., *An Introduction to Random Vibration and Spectral Analysis*, 2nd ed., Longman, New York, 1984, Chaps. 4 and 5.

[17]Brown, R. G., *Introduction to Random Signal Analysis and Kalman Filtering*, Wiley, New York, 1983, Chaps. 2 and 3.

[18]Crandall, S. H., "Distribution of Maxima in the Response of an Oscillator to Random Excitation," *Journal of the Acoustical Society of America*, Vol. 47, No. 3, March 1970, pp. 838-845.

[19]Rice, S. O., "Mathematical Analysis of Random Noise," *Bell System Technical Journal*, Vol. 23, 1944, pp. 282-332, Vol. 24, 1945, pp. 46-156.

[20]Huston, W. B., and Skopinski, T. H., "Probability and Frequency Characteristics of Some Flight Buffet Loads," NACA TN 3733, Aug. 1956.

[21]Lin, Y. K., *Probabilistic Theory of Structural Dynamics*, McGraw Hill, New York, 1967, Chap. 9.

[22]Crandall, S. H., and Mark, W. D., *Random Vibration in Mechanical Systems*, Academic Press, New York, 1963, Chap. 1.

[23]Roberts, J. B., "An Approach to the First-Passage Problem in Random Vibration," *Journal of Sound and Vibration*, Vol. 8, Jan. 1968, pp. 301-328.

[24]Vanmarcke, E. H., "On the Distribution of the First-Passage Time for Normal Stationary Random Processes," *Journal of Applied Mechanics*, Vol. 42, March 1975, pp. 215-220.

[25]Crandall, S. H., Chandiramani, K. L., and Cook, R. G., "Some First-Passage Problems in Random Vibration," *Journal of Applied Mechanics*, Vol. 33, pp. 532-538, Sept. 1966.

[26]Maybeck, P. S., *Stochastic Models Estimation, and Control*, Vol. 1, Academic Press, Orlando, FL, 1979, pp. 180-194.

[27]Shinozuka, M., and Jan, C.-M., "Digital Simulation of Random Processes and Its Applications," *Journal of Sound and Vibration*, Vol. 25, Jan. 1972, pp. 111-128.

Earl A. Thornton
Associate Editor

Limitations on Vibration Isolation for Microgravity Space Experiments

C. Knospe* and P. Allaire†
University of Virginia, Charlottesville, Virginia 22901

The limitations on vibration isolation for microgravity space experiments are explored. These limitations result from the restricted interior space available for vibration isolation and the strokes required to achieve isolation. A one-degree-of-freedom representation of the experiment spacecraft system is used, and an ideal vibration actuator is assumed. The wall motion is characterized as sinusoidal at a single frequency. A kinematic representation results, and the problem becomes one of finding the minimum acceleration trajectory within a pair of moving walls. This optimal control problem can be solved via the calculus of variations; however, transcendental equations result. To obtain an analytic solution, the inequality constraints are dropped and initial and final conditions on the trajectory are added. The resulting control is optimal if the inequality constraints are still satisfied. Analysis yields a simple condition under which a closed-form solution is available. A suboptimal solution that always satisfies the inequality constraints is also presented. This solution is shown to have performance very close to optimal. The minimum experiment rms acceleration given the spacecraft vibration frequency and amplitude is obtained from the optimal and suboptimal solutions. Plots are presented, and the limitations on vibration isolation are discussed. These results demonstrate that isolation from low-frequency vibration requires more interior space than is available for vibration isolation on manned space orbiters.

Nomenclature

A	= matrix in state dynamics
B	= vector in state dynamics
A	= amplitude of base motion
c_i	= coefficients of optimal control u_{opt}
F_u	= force on experiment platform
H	= Hamiltonian
J	= cost function
m	= experiment mass
L	= stroke (maximum translation of experiment)
T	= half-period
t	= time
t^*	= boundary constraint exit time
u	= control acceleration
x	= state vector, $=(x_1, x_2)^T$
x, x_1	= position of experiment platform
x_2	= velocity of experiment platform
y	= position of base
f	= frequency of base motion, Hz
α	= coefficient of optimal control u_{opt_2}
λ	= Lagrange multiplier
ω	= frequency of base motion

I. Introduction

THE use of a microgravity environment in space has the potential for advanced materials science experiments. Spencer[1] outlined the goals as 1) an understanding of basic physical phenomena, 2) quantification of limitations and effects imposed by gravity, and 3) application of knowledge to Earth- and space-based processes or products. A microgravity environment can potentially eliminate buoyancy-driven convection, sedimentation, and hydrostatic pressure, and it can have several other advantages.[1]

At this point in time, the actual acceleration requirements for various experiments are not well known.[2] An assessment of existing theoretical and experimental data available up to 1985 was carried out in Ref. 3. Results indicate that acceleration levels below $10^{-6}\,g_0$ at frequencies below 0.1 Hz are required by many processes, but the requirements are somewhat relaxed at higher frequencies. Work to better determine the levels needed is in progress. An example is a twin-crystal growth experiment to be carried out on spacecraft.[4]

An essential part of the development of a microgravity experiment program is the characterization of the low-acceleration environment aboard manned space orbiters. NASA has carried out a series of measurements reported at various conferences.[5,6] A summary of these data was presented by Grodsinsky and Brown[7] and is repeated in Table 1. Additional data on the Space Transportation System was presented in Ref. 8. Similar results have been reported by the European Space Agency.[9]

Vibration levels reported in the aforementioned literature for spacecraft are significantly higher than allowable for materials science experiments. In order to achieve accurate and reproducible results in such experiments, vibration isolation will be required.[3] Acceleration disturbances in the orbiter environment cover a wide frequency bandwidth, from dc to 100 Hz. Sources below 10^{-3} Hz include drag, light pressure oscillations, tidal effects, and gravity gradients. Above this frequency, sources include manned activity, thruster firing, and orbiter flight systems. The frequencies and amplitudes of these accelerations are summarized in Table 1. Low-frequency (10^{-3} to 10^{-2} Hz) structural excitations likely to be present on the space station are not represented in this data. Such flexible structure modes will contribute significantly to the vibration environment.

The capability of isolating the experiment from any particular vibration source is dependent on both frequency and amplitude. At relatively high frequencies, above about 5 Hz, passive vibration isolation is normally possible. Examples include the Hubble space telescope reaction wheel isolation system[10] and viscous dampers for reduced jitter.[11] One of the few active vibration isolation systems is reported in Ref. 12. The volume available in spacecraft for experiments is limited. Therefore, this introduces an additional constraint on active iso ation systems.

Received Dec. 21, 1989; revision received March 21, 1990.

*Research Assistant Professor, Department of Mechanical and Aerospace Engineering.
†Professor, Department of Mechanical and Aerospace Engineering.

Table 1 Microgravity space experiment acceleration environment (from Ref. 7)

g/g_0	F, Hz	Source
	Quasisteady or dc acceleration disturbances	
10^{-7}	$0-10^{-3}$	Aerodynamic drag
10^{-8}	$0-10^{-3}$	Light pressure
10^{-7}	$0-10^{-3}$	Gravity gradient
	Periodic acceleration disturbances	
2×10^{-2}	9	Thruster fire (orbital)
2×10^{-3}	5–20	Crew motion
2×10^{-4}	17	Ku-band antenna
	Nonperiodic acceleration disturbances	
10^{-4}	1	Thruster fire (attitude)
10^{-4}	1	Crew pushoff

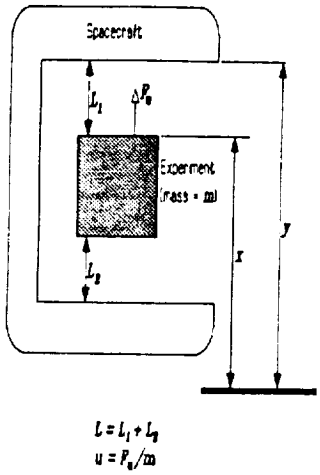

Fig. 1 Kinematic representation of the experiment spacecraft system.

The purpose of this paper is to explore the limitations on vibration isolation for space experiments, rather than to develop the actual control algorithm. Thus, the ideal vibration actuator is assumed, and an optimal control is formulated. The optimal control problem is solved for a sinusoidal excitation to obtain the minimum acceleration trajectory. A suboptimal solution that gives results close to optimal is also explored.

II. Kinematic Formulation

For this analysis, a one-dimensional theory is developed. Clearly, the actual system required will be multidimensional so this work is preliminary in nature. Consider a one-degree-of-freedom system, the experiment, as illustrated in Fig. 1 with position $x(t)$. It is connected to the spacecraft by umbilicals, such as power or fluid lines, and by a vibration isolation actuator. A similar geometry is discussed by Genkin et al.,[13] with stiffness and damping as well as an active vibration isolation actuator. However, that system has one side fixed to the ground and the forced mass in motion. Although the spacecraft actually has a finite mass, it may be considered to have infinite impedance for this analysis since the spacecraft-to-experiment weight ratio is very large. Thus, the spacecraft acts as an external base motion $y(t)$ transmitting forces through the umbilicals and the actuator.

This representation reduces the problem to a kinematic one. Onboard the spacecraft, available interior space for the experiment is limited. The walls around the experiment, which should not be contacted, constrain the maximum translation of the experiment, or stroke, to a fixed distance L. The base motion $y(t)$ imposed on the walls, spaced to permit a stroke of L, forms the problem constraints. The problem of vibration isolation/attenuation becomes one of finding the optimal trajectory (minimum acceleration) given the constraint conditions (moving walls).

III. Optimal Control Formulation

The objective is to formulate and solve the optimal control problem for minimum experiment acceleration trajectory in time. Let the experiment acceleration be denoted as u ($u = F_u/m$). Then the cost function J to be minimized is

$$J = \int_0^\infty u^2\,dt \tag{1}$$

with the constraint

$$y(t) - L \le x(t) \le y(t), \qquad 0 \le t \tag{2}$$

for a given base motion $y(t)$.

This problem is examined for harmonic base motion at a single frequency. Let $y(t)$ have the form

$$y(t) = A[1 - \cos(\omega t)] \tag{3}$$

with the half-period $T = \pi/\omega$. The cost function J now simplifies to

$$J = \int_0^T u^2\,dt \tag{4}$$

due to the periodicity of the problem. Also, the constraint becomes

$$A[1-\cos(\pi t/T)] - L \le x(t) \le A[1-\cos(\pi t/T)] \qquad 0 \le t \le T \tag{5}$$

over the half-period.

This problem may be viewed as finding the optimal path through sinusoidally oscillating walls, as illustrated in Fig. 2. If the base travel $2A$ is smaller than the space L, the minimum acceleration is zero and the problem trivial. However, if the base travel $2A$ is larger than the space available for vibration isolation L, then the optimization problem has active inequality constraints on the state variables. The solution to this problem may be attempted using the calculus-of-variations approach by adjoining the Hamiltonian with a second-order state-variable inequality constraint. This method requires the satisfaction of two interior boundary conditions (position and velocity continuity) at the junction points of constrained and unconstrained path arcs.[14] Because the wall motion is sinusoidal, these tangency constraints require the solution of several transcendental equations. Therefore, no closed-form solution to the general problem is available. As will be shown, under a certain condition the problem can be solved to yield an analytic solution. When this condition does not hold, a suboptimal solution may be employed. Thus, easy-to-use equations and plots for determining vibration isolation limits are made available to microgravity experiment designers.

IV. Analytic Solution

To obtain an analytic solution to the problem, the constraints are simplified to the boundary conditions

$$x(0) = 0, \qquad x(T) = 2A - L \ge 0$$
$$\dot{x}(0) = 0, \qquad \dot{x}(T) = 0 \tag{6}$$

which an optimal solution clearly must satisfy.

Define the system state variables[15] as

$$x_1 = x, \qquad \dot{x}_1 = x_2, \qquad \dot{x}_2 = u \tag{7}$$

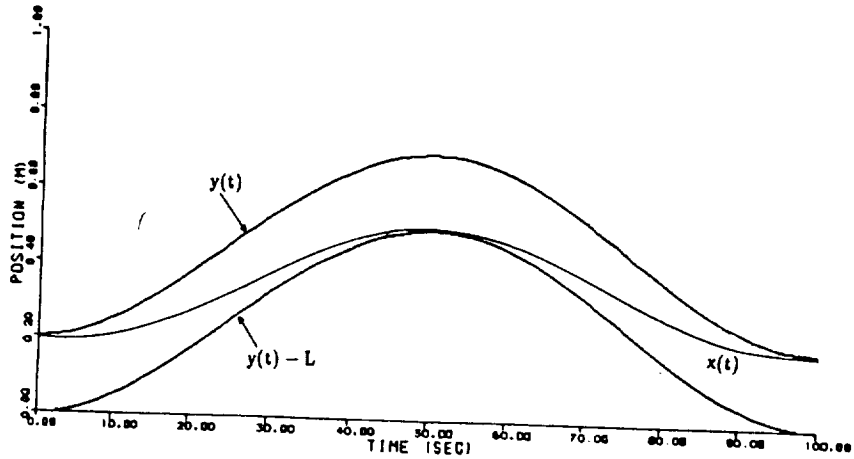

Fig. 2 Optimal path through harmonic walls.

and the equations of motion become

$$\dot{x} = Ax + Bu$$

$$x^T = [x_1 \quad x_2], \qquad A = \begin{bmatrix} 0 & 1 \\ 0 & 0 \end{bmatrix}, \qquad B^T = [0 \quad 1] \tag{8}$$

The cost function is adjoined by the constraint, Eq. (7), using two Lagrange multipliers.[16] The result is

$$J = \int_0^T [u^2 + \lambda_1(x_2 - \dot{x}_1) + \lambda_2(u - \dot{x}_2)]\, dt \tag{9}$$

which is the general functional for this problem.

Define the Hamiltonian as

$$H = u^2 + \lambda_1 x_2 + \lambda_2 u \tag{10}$$

If we employ the calculus of variations, the minimization equations are

$$\dot{\lambda}_1 \equiv -\frac{\partial H}{\partial x_1} = 0$$

$$\dot{\lambda}_2 \equiv -\frac{\partial H}{\partial x_2} = -\lambda_1$$

$$0 \equiv \frac{\partial H}{\partial u} = 2u + \lambda_2 \tag{11}$$

Solving these gives

$$\lambda_1 = c_0$$

$$\lambda_2 = -c_0 t + c_1$$

$$u = \tfrac{1}{2}c_0 t - \tfrac{1}{2}c_1 \tag{12}$$

Imposing the boundary conditions of Eq. (6) yields

$$c_0 = -24(2A - L)/T^3$$

$$c_1 = -12(2A - L)/T^2 \tag{13}$$

and

$$u(t)_{\text{opt}} = \frac{-12(2A - L)}{T^3} t + \frac{6(2A - L)}{T^2}$$

$$\dot{x}(t) = \frac{-6(2A - L)}{T^3} t^2 + \frac{6(2A - L)}{T^2} t$$

$$x(t) = \frac{-2(2A - L)}{T^3} t^3 + \frac{3(2A - L)}{T^2} t^2 \tag{14}$$

$$2A - L \geq 0$$

(Of course, if $2A - L < 0$, the optimal trajectory is clearly $u = 0$, $\dot{x} = 0$, $x = 0$.) The root-mean-square (rms) acceleration of this trajectory is

$$\text{rms}(\ddot{x}_{\text{opt}}) = \left(\frac{1}{T}\int_0^T u^2\, dt\right)^{1/2} = \frac{\sqrt{12}(2A - L)}{T^2} \tag{15}$$

The trajectory of Eq. (10) is the solution to the original problem if the inequality constraints on the platform position, Eq. (5), are satisfied. Note that Eq. (14) is a linear open-loop control law.

V. Conditions on the Analytic Solution

The condition under which Eq. (14) satisfies the inequality constraints can be obtained by expanding Eq. (5) as a Taylor series

$$y(t) = A\left[1 - \cos\left(\frac{\pi t}{T}\right)\right]$$

$$= \frac{A}{2}\left(\frac{\pi t}{T}\right)^2 - \frac{A}{24}\left(\frac{\pi t}{T}\right)^4 + \cdots \tag{16}$$

If we combine Eqs. (5), (14), and (16), $x(t) \leq y(t)$ becomes

$$3(2A - L)\left(\frac{t}{T}\right)^2 - 2(2A - L)\left(\frac{t}{T}\right)^3 \leq \frac{A\pi^2}{2}\left(\frac{t}{T}\right)^2 - \frac{A\pi^4}{24}\left(\frac{t}{T}\right)^4 + \cdots \tag{17}$$

For small t/T,

$$3(2A - L) \leq A\pi^2/2$$

which yields the condition

$$L \geq [2 - (\pi^2/6)]A \tag{18}$$

The symmetry of the optimal trajectory and inequality constraints guarantees that this is also the sufficient condition for Eq. (14) to satisfy the inequality constraint near the final time.

VI. Suboptimal Solution

A suboptimal solution to Eq. (4) that automatically satisfies the inequality constraints of Eq. (5) is

$$x_{\text{sub}}(t) = (A - L/2)[1 - \cos(\pi t/T)], \qquad 2A - L > 0 \tag{19}$$

which has control history

$$u_{\text{sub}} = (A - L/2)(\pi^2/T^2)\cos(\pi t/T) \tag{20}$$

and rms acceleration

$$\text{rms}(\ddot{x}_{sub}) = (\sqrt{2}/4)\pi^2[(2A - L)/T^2] \tag{21}$$

When Eqs. (15) and (21) are compared, it is clear that the suboptimal solution is only slightly inferior to the optimal

$$[\text{rms}(\ddot{x}_{opt})/\text{rms}(\ddot{x}_{sub})] = (4\sqrt{6}/\pi^2) \approx 0.9927 \tag{22}$$

A comparison of the optimal and suboptimal accelerations and trajectories when condition (18) holds is shown in Fig. 3. The optimal solution when condition (18) is invalid is a combination of a linear control law and wall following trajectories,

$$u_{opt_2}(t) = \begin{cases} (A\pi^2/T^2)\cos(\pi t/T), & 0 \le t \le t^* \\ \alpha - 2\alpha t/T, & t^* < t < T - t^* \\ (A\pi^2/T^2)\cos(\pi t/T), & T - t^* < t < T \end{cases} \tag{23}$$

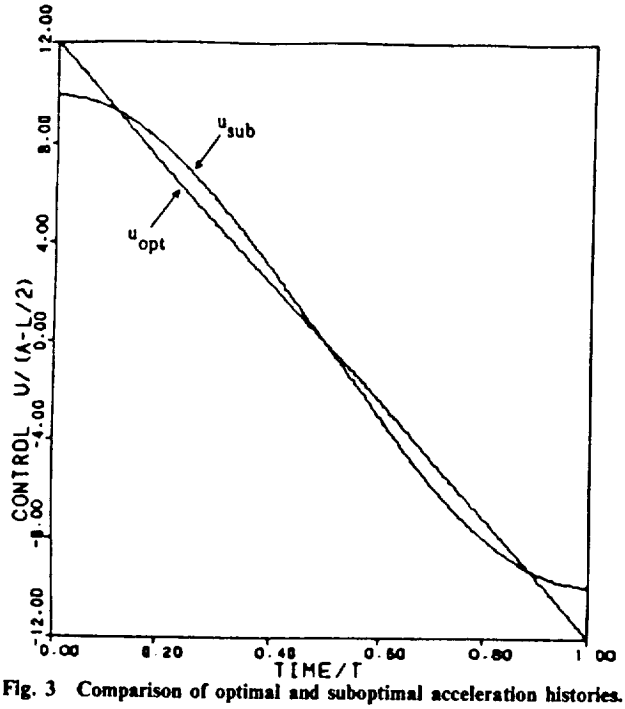

Fig. 3 Comparison of optimal and suboptimal acceleration histories.

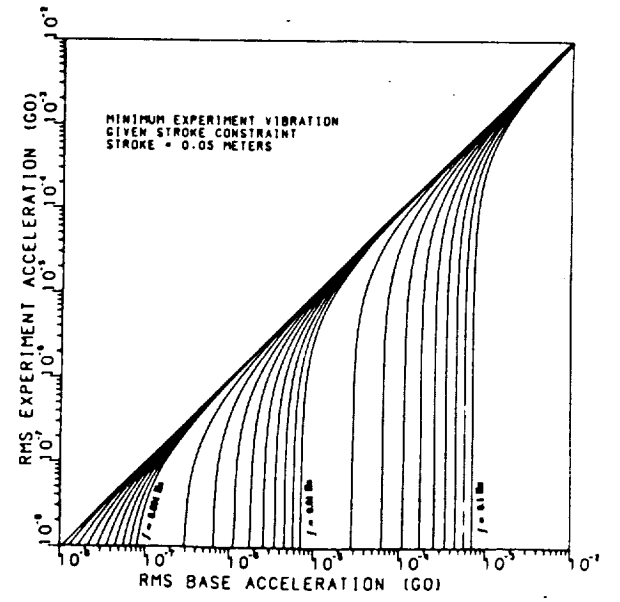

Fig. 4 Minimum experiment acceleration given disturbance frequency, stroke = 5 cm.

where t^* and α are determined by the solution of several transcendental equations expressing position and velocity continuity at t^*. It is clear that the rms of this optimal solution must be bounded between that of the suboptimal and the optimal with the inequality constraints of (5) dropped

$$(\sqrt{12})\frac{(2A - L)}{T^2} \le \text{rms}(u_{opt_2}) < \left(\frac{\sqrt{2}}{4}\pi^2\right)\frac{(2A - L)}{T^2}$$

$$3.4641\frac{(2A - L)}{T^2} < \text{rms}(u_{opt_2}) < 3.4895\frac{(2A - L)}{T^2} \tag{24}$$

The suboptimal solution can obviously be employed as an excellent approximation to the optimal, Eq. (23), when condition (18) is not satisfied.

VII. Limitations on Isolation

The primary purpose of this paper is to determine theoretical limits to vibration isolation. Although a dimensionless plot could have been produced, it was felt that a few typical dimensional plots would be of more use to designers of microgravity materials science experiments. Figures 4–6 present the curves of the minimum experiment acceleration vs base acceleration at constant frequencies for stroke limits of 5, 10, and 20 cm, respectively.

The horizontal axis gives the rms base acceleration calculated from

$$\text{rms}(\ddot{y}) = (\sqrt{2}/2)\omega^2 A \tag{25}$$

The vertical axis is the minimum experiment acceleration from Eq. (15) when Eq. (18) holds and Eq. (21) when it does not.

In Figs. 4–6, the minimum experiment rms acceleration at any given frequency is zero (isolation) until the base displacement amplitude equals one-half the maximum stroke possible. The minimum experiment rms then quickly rises with increases in base acceleration and asymptotically approaches the zero-vibration-reduction line, at 45 deg. Along this line, the base and experiment act as if they were rigidly coupled together and have the same acceleration.

The primary limitation is the length of stroke allowed between the experiment and the base. As an example calculation, consider an rms base acceleration of $1 \times 10^{-3} g_0$ at a frequency of 0.06 Hz. The base travel is given by

$$2A = 2\sqrt{2}[\text{rms}(\ddot{y})/\omega^2] \tag{26}$$

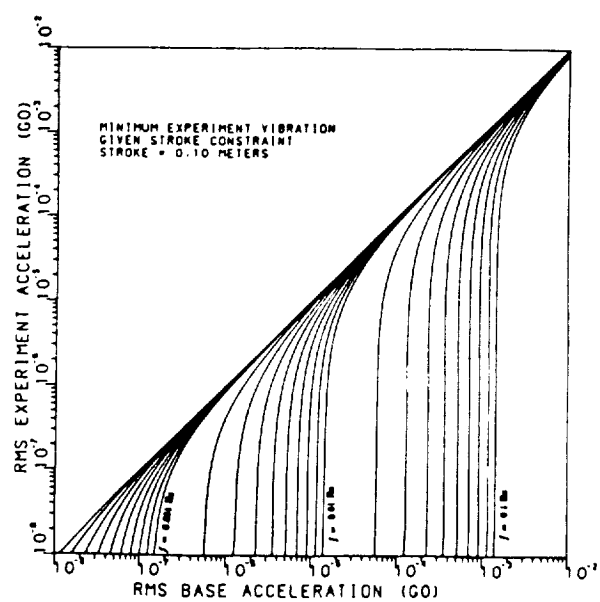

Fig. 5 Minimum experiment acceleration given disturbance frequency, stroke = 10 cm.

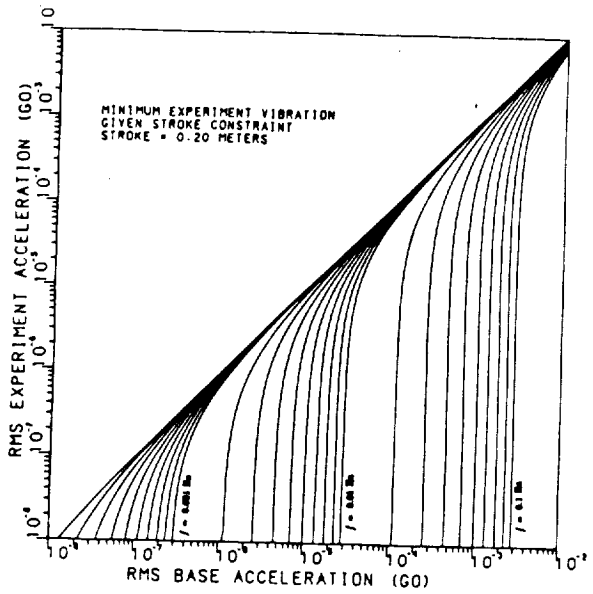

Fig. 6 Minimum experiment acceleration given disturbance frequency, stroke = 20 cm.

which has the numerical value of 19.5 cm for this example. For a stroke $L = 5$ cm, Fig. 4 shows that the experiment acceleration will be at least $7 \times 10^{-4}\, g_0$. When the stroke is increased to $L = 10$ cm, Fig. 5 gives a value of $4.5 \times 10^{-4}\, g_0$.

The last case is a stroke of $L = 20$ cm. Figure 6 indicates that the minimum acceleration is zero. In this case, $L > 2A$ so the stroke is large enough to accommodate the full sinusoidal motion without wall contact.

As an alternative to the plots, Eqs. (15), (18), (21), and (25) may be used directly. These can be simplified for this purpose to

$$\frac{\text{rms}(\ddot{x})}{\text{rms}(\ddot{y})} = \begin{cases} \left(1 - \dfrac{L}{2A}\right), & 0 \le \dfrac{L}{2A} < \left(1 - \dfrac{\pi^2}{12}\right) \\ \dfrac{4\sqrt{6}}{\pi^2}\left(1 - \dfrac{L}{2A}\right), & \left(1 - \dfrac{\pi^2}{12}\right) < \dfrac{L}{2A} < 1 \\ 0, & 1 < \dfrac{L}{2A} \end{cases} \quad (27)$$

with

$$2A = [2\sqrt{2}\,\text{rms}(\ddot{y})/\omega^2]$$

VIII. Conclusions

This paper has developed a kinematic formulation for the microgravity space experiment problem in one dimension. Further, two solutions, one optimal and the other suboptimal but very close to optimal, have been obtained. These permit plots of vibration attenuation for given levels of available space. For the sinusoidal oscillation assumed here, the experiment could be completely isolated if sufficient space were available. Unfortunately, the low-frequency motions (0–0.01 Hz) would require motions with a length much larger than possible aboard spacecraft.

Plots of the type developed here are intended to assist microgravity experiment designers as well as vibration isolation engineers. These plots represent the ideal vibration isolator. Real systems will not be able to attain the ideal for several reasons. The actual motion will have several frequency components as well as a random component. The random component alone will ensure that the full space L cannot be employed. Some safety space will have to be allocated to prevent occasional wall contact. Any real active control system will have some nonideal characteristics. The sensors employed in the active control feedback loop will have some errors as well. The authors of this paper are aware that the development of a very low-frequency accelerometer is difficult. In spite of this, we are optimistic about the levels of vibration isolation discussed here. It seems reasonable to believe that approximately 75% of ideal isolation is possible with an actual control system and actuator.

Acknowledgments

This work was supported, in part, by NASA Lewis Research Center and the Commonwealth of Virginia.

References

[1]Spencer, L., "Overview of NASA Microgravity Programs and Opportunities," Vibration Isolation Technology for Microgravity Science Workshop, NASA Lewis Research Center, Sept. 28–29, 1988.

[2]Alexander, J. I., "Experiment Sensitivity: Determination of Requirements for Isolation," Vibration Isolation Technology for Microgravity Science Workshop, NASA Lewis Research Center, Sept. 28–29, 1988.

[3]Sharpe, A. (ed.), "Low Acceleration Characterization of Space Station Environment," NASA Marshall Space Flight Center, Final Rept. SP85-MSFC-2928, Revision B, Oct. 1985.

[4]Stuhlinger, E., and Mookherji, T., "Materials Processing Twin Experiment," AIAA Paper 88-0348, Jan. 1988.

[5]Chassay, R. P., "Measurements by NASA," *Measurement and Characterization of the Acceleration Environment Onboard the Space Station*, Aug. 1986.

[6]Henderson, F., "MSL-2 Accelerometer Data Results," *Measurement and Characterization of the Acceleration Environment Onboard the Space Station*, Aug. 1986.

[7]Grodsinsky, C. M., and Brown, J. V., "Low Frequency Vibration Isolation Technology for Microgravity Space Experiments," 12th Biennial Conference on Mechanical Vibration and Noise, American Society of Mechanical Engineers, New York, NASA TM 101448, Sept. 1989.

[8]Fox, J. C., and McNally, P. J., "Current Orbiter Instrumentation and Acceleration Environment Data," Vibration Isolation Technology for Microgravity Science Workshop, NASA Lewis Research Center, Sept. 28–29, 1988.

[9]Hamacher, H., Jilig, R., and Merbold, U., "Analysis of Microgravity Experiments Performed During D1," Materials Science Under Microgravity Conditions, 6th European Symposium, Bordeaux, Dec. 2–5, 1986.

[10]Davis, L. P., Wilson, J. F., Jewell, R. E., and Roden, J. J., "Hubble Space Telescope Reaction Wheel Assembly Vibration Isolation System," March 1986.

[11]Wilson, J. F., and Davis, L. P., "Viscous Damped Space Structure for Reduced Jitter," 58th Shock and Vibration Symposium, Huntsville, AL, Aug. 1987.

[12]Hamilton, B. J., Andrus, J. H., and Carter, D. R., "Pointing Mount with Active Vibration Isolation for Large Payloads," 10th Annual Guidance and Control Conference, American Astronautical Society, Washington, DC, Jan.-Feb. 1987.

[13]Genkin, M. D., Yelezov, V. G., and Yablonsky, V. V., "Vibration Isolation System with Enhanced Effectiveness," *Vibration Engineering*, Vol. 2, 1988, pp. 183–186.

[14]Bryson, A. E., and Ho, Y.-C., *Applied Optimal Control: Optimization, Estimation, and Control*, Hemisphere, New York, 1975, pp. 108–127.

[15]Sage, A. P., and White, C. C., *Optimum Systems Control*, 2nd ed., Prentice-Hall, Englewood Cliffs, NJ, 1977, pp. 27–52.

[16]Elbert, T. F., *Estimation and Control of Systems*, Van Nostrand Reinhold, New York, 1989, pp. 262–346.

David H. Allen
Associate Editor

DISTRIBUTION LIST

1 - 3	National Aeronautics and Space Administration Lewis Research Center 21000 Brookpark Road Cleveland, OH 44135 Attention: Dr. David P. Fleming, M/S 23-3 Structural Dynamics Branch
4	National Aeronautics and Space Administration Lewis Research Center 21000 Brookpark Road Cleveland, OH 44135 Attention: Kenneth A. DeLaat, Grants Officer
5	National Aeronautics and Space Administration Lewis Research Center 21000 Brookpark Road Cleveland, OH 44135 Attention: Carlos Grodsinsky, M/S 500-205
*6 - 7	NASA Scientific and Technical Information Facility P. O. Box 8757 Baltimore/Washington International Airport Baltimore, MD 21240
8 - 9	E. H. Pancake, Clark Hall
10 - 11	C. R. Knospe
12	P. E. Allaire
13	D. W. Lewis
**	SEAS Postaward Administration
14	SEAS Preaward Administration Files

*Reproducible copy
**Cover letter

JO#5110:ph

2. ACTUATOR DEVELOPMENT

2.1 Introduction

The University examined the design of actuators for both SDOF and MDOF active microgravity isolation systems. For SDOF systems, two actuators were considered: a special large gap magnetic actuator and a large stroke Lorentz actuator. The magnetic actuator was viewed to be of greater difficulty than the Lorentz actuator with little compelling technical advantage and was dropped from consideration. A Lorentz actuator was designed and built for the SDOF test rig using magnetic circuit and finite element analyses. This design and some experimental results are discussed below.

The University also examined the design of actuators for MDOF isolation systems. This includes the design of an integrated 1 cm gap 6–DOF noncontacting magnetic suspension system and of a "coarse" follower which permits the practical extension of magnetic suspension to large strokes. The proposed "coarse" actuator was a closed kinematic chain manipulator known as a Stewart Platform. The integration of the two isolation systems together, the isolation tasks assigned to each, and possible control architectures were also explored. The results of this research are examined in Section 3.

2.2 Large–Stroke Lorentz Actuator and Test Results

A compact large–stroke Lorentz actuator was designed, built, and tested at University of Virginia The requirements for the laboratory prototype were a total stroke two inches and enough force capability to isolate a mass of 75 lbs. connected by an umbi (air dashpot) to a source generating very low frequency vibrations. Force linearity with cu and independent of position were also desirable. Moreover, in view of the ultimate g deployment in space, such a device had to be compact and lightweight. Low consumption and low heat generation during operation were also important. A desi carried out using a simple computer program based on magnetic circuit analysis. The design required a 3.2 inch diameter ring magnet of very high maximum energy pr

mega–Gauss–Oersted). This design was not only large and heavy, but could not be built from a single piece since magnet manufacturers do not make sizes larger than 2 inches. The cost and difficulty of assembly ruled out an actuator using multiple magnet segments. It therefore became necessary to design the Lorentz actuator using a smaller core gap than is conventionally used. Usually this gap is large to reduce magnetic flux leakage across it so as to yield an actuator that will produce a force independent of coil position. It was hypothesized that this leakage could be substantially reduced by saturating the actuator's core. This could only be verified, short of building a prototype, via finite element analysis. A commercially available finite element analysis package, MAGGIE,

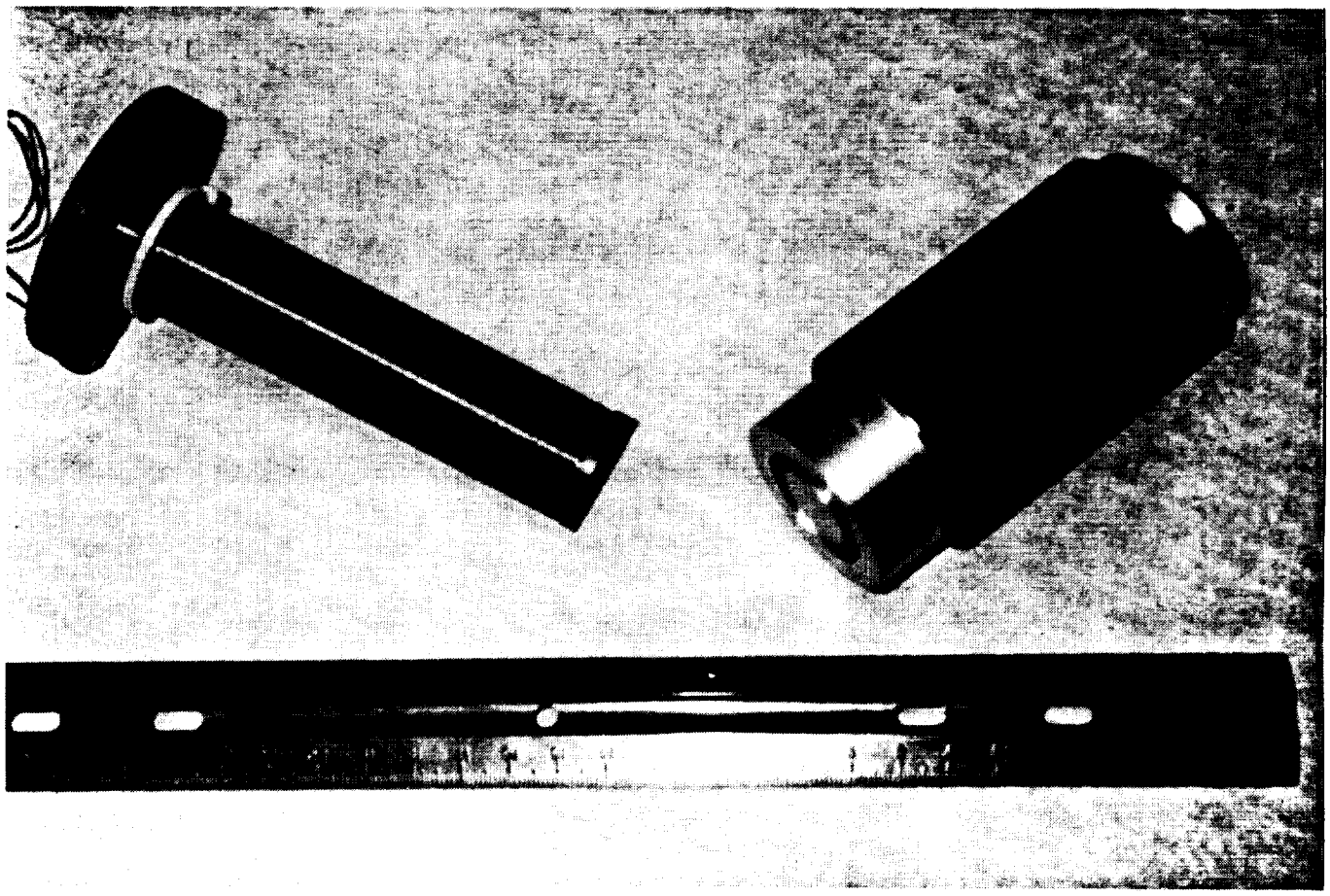

Figure 1: Large–stroke Lorentz actuator

was used to "test" a large number of designs. The final actuator, shown in Figure 1, has an outer diameter of 1.95 inches and a 4 inch length. This actuator has the following features [1]:

* **Long Stroke:** The actuator has two inches of stroke.
* **Position Independence:** Over the entire stroke, the actuator's gain is almost independent of position. For a constant coil current, this means that the actuator force is the same irrespective of the axial position of the coil. This is achieved by the design since the maximum flux density across the core gap is only 7% of the maximum flux density across the pole face gap.
* **Current Linearity:** The average flux density in the effective air gap remains constant with variations in the coil current between the upper and lower limits. This is achieved through the large reluctance of the permanent magnet in the electromagnetic flux circuit and the saturation of the core.
* **Force:** A maximum force of 1.50 lbs is produced by this actuator with a coil current of 2.5 A.
* **Materials:** The permanent magnet is neodymium iron boron, which has a very high maximum energy density product of 35 MGOe. The circuit material is a high permeability nickel–iron alloy that saturates at 1.50 Tesla. These materials permit a compact design.

The experimental results have confirmed the soundness of the design approach [1]. Figure 2a shows the actuator force plotted versus position for a number of values of coil current. Note that the actuator's force is fairly independent of the coil position over the actuator's operating range (0.5 to 2.5 inches). Note also that the actual forces are larger than the predicted forces, but still within 20%. Figure 2b shows the same data in terms of actuator force plotted versus coil current for different positions. As shown in the figure, the actuator has a high degree of linearity with respect to current. Note that the actuator gain (slope of the line in Figure 2b) is fairly independent of coil position and is approximately 0.6 lbf/amp.

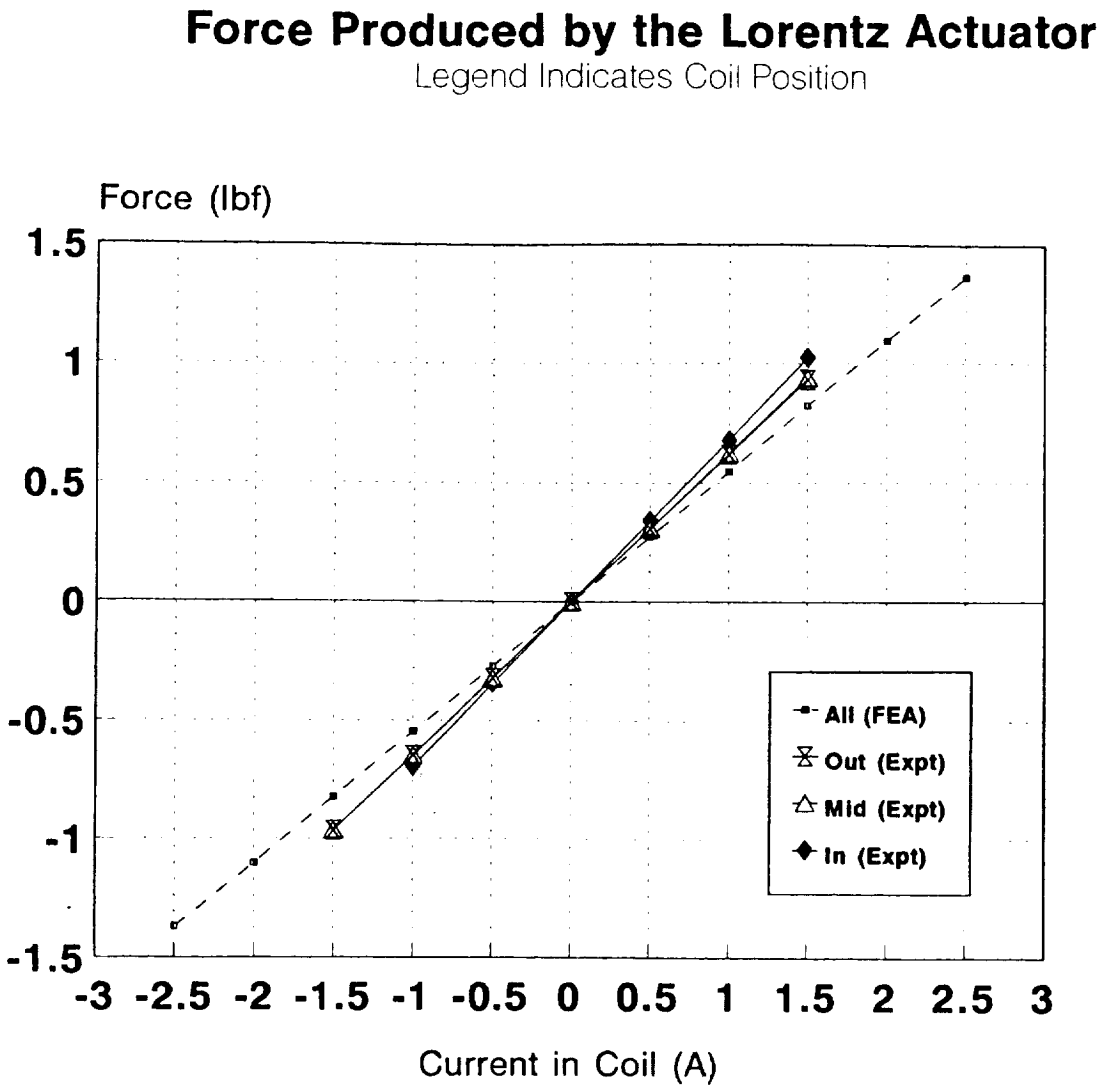

Figure 2: Actuator force vs. current.

3. MULTIPLE DEGREE OF FREEDOM ACTUATOR DESIGN

3.1 Introduction

The University of Virginia also examined the design of multiple–degree–of–freedom actuators for microgravity vibration isolation. The fundamental constraint on isolation performance to be considered during actuator design is the available working envelope [2,3]. The implications of this constraint on active isolation were examined by the University in two journal publications [2,3].

Figure 3 shows the relationship between the envelope (peak–to–peak displacement and frequency for several sustainable RMS acceleration levels [4]. The graph is for a

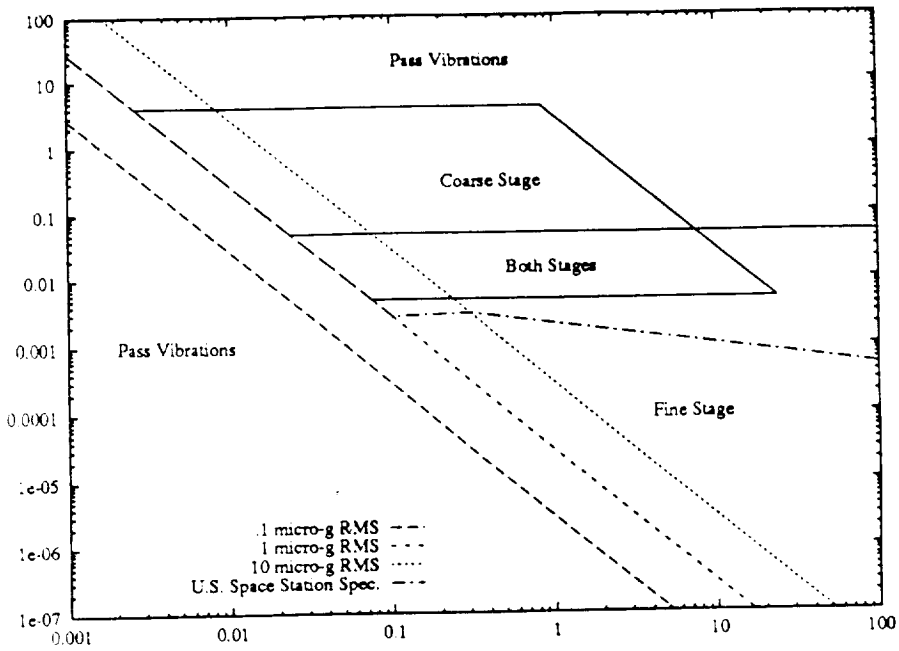

Figure 3: Peak–to–peak displacement vs. frequency

one–degree–of–freedom case and assumes sinusoidal vibrations, but the relationships are acceptable for order of magnitude estimates even if these assumptions are relaxed. No definitive specification of the required isolation levels or frequency range exists. The proposed US Space Station usable specification is also shown in Figure 3. It is claimed that vibrations below this curve will not adversely affect microgravity experiments. The design examined in

this section is an active isolation system with a "reasonable" envelope of 4 inches of travel and a sustained 1 ug RMS residual acceleration. It can be seen from the figure that this will offer isolation down to 0.002 Hz. The amplitude to which vibrations can be attenuated is constrained only by controller design and available instrumentation. Operation at lower frequencies, however, requires a larger envelope, which becomes prohibitive in terms of available spacecraft space. Another specification for the six–degree–of–freedom system considered is a rotational range of 40 degrees.

A redundant coarse–fine scheme with magnetic suspension was chosen. This design is particularly attractive for microgravity applications since it allows the use of magnetic suspension while overcoming range–of–motion limitations. The design uses a Stewart platform for the coarse stage and a novel magnetic bearing for the fine stage [4,5]. The approximate regions of activity in the frequency–displacement plane of these two devices are also shown in Figure 3. Both stages act to attenuate spacecraft vibrations, effectively reducing vibration amplitudes below their active regions on the displacement vs. frequency plane. As an example, it can be seen in the figure that a vibration of the spacecraft with 10 inches of displacement at a frequency of 1 Hz falls outside the active region and could only be partially attenuated. It should be noted that such a large vibration is unlikely. If the displacement was only 1 inch, however, the coarse stage would absorb all of it except about 0.005 inches, and the remainder would be reduced down to the micro–g level by the fine stage.

The combination of the Stewart platform and a magnetic bearing allows continuous isolation at frequencies above 0.002 Hz, and a compact, reliable package suitable for the application. These choices and some preliminary design concepts are discussed below in detail after a survey of other candidate designs.

3.2 Survey of Published Designs

Several designs for 6 DOF levitation are discussed in the literature. While these designs do not have the envelope of the proposed coarse–fine design, they might be suitable if a

coarse stage is not required. They also deserve examination as alternative designs for the fine stage. A comparison of the specifications for these designs is given in Table 1.

Group	Trans.	Rot.	Force	Envelope	Mass	Actuator	Sensor
Honeywell	5 mm	$\pm 1.6^{\circ}$	43 N	27x34x50cm	36kg	Mag. Brng.	Eddy & Flux
N. Wales	± 5 mm	$< \pm .2^{\circ}$	.04 N[a]	100x100x100cm[b]	?	Lorentz	Capacitive
NASA	± 4 mm	$\pm 3^{\circ}$ [c]	445 N	30x30x15cm[c]	?	Mag. Brng.	Eddy
SatCon	± 10 mm	$\pm 8^{\circ}$ [c]	4 N	40x40x12cm[c]	4.9kg	Lorentz	Eddy
IBM	± 5 mm	$\pm 4^{\circ}$	32 N	25x25x15cm[c]	?	Lorentz	Optical
Toshiba	± 2 mm	$\pm 1.5^{\circ}$	20 N[c]	25x25x20cm	8kg	Mag. Brng.	Eddy

[a] Requirement, not limitation
[b] Includes experiment package
[c] Estimated by authors

Table 1: Comparison of Published Designs

Four designs specifically for microgravity isolation have been published. Honeywell has a well–developed system called FEAMIS [6] with which they have demonstrated impressive isolation performance. The system is designed for the Space Shuttle experiment configuration. The University College of North Wales also has a well–developed system [7] designed for the European Space Agency experiment configuration. NASA [8] has a well–tested laboratory system and has done testing in a weightless environment aboard an aircraft in a parabolic trajectory. They also have demonstrated impressive isolation performance for a feedforward control system. SatCon [9] also has a laboratory magnetic suspension system.

Two actuator designs were developed for different applications, but they are mentioned here because they are similar and could be easily adapted to the isolation application. IBM [10] has a laboratory levitated robot "wrist" which enhances robot accuracy and performance.

Toshiba [11] has a satellite antenna pointing system which is fully developed. Both devices have demonstrated positional accuracies on the order of 1 μm.

Isolation of vibrations with large amplitudes – typically occurring at low frequencies – requires a large translational range. SatCon's system has the largest range, but there is a significant tradeoff with the device's force capability. A coarse–fine approach would allow both a large range, provided by the coarse stage, and a high force capability, since the levitation gaps are small. There is no available data on the rotational range requirements of the application. Isolation with an umbilical disturbance may require a high force capability, as is offered by the systems from Honeywell, NASA, IBM, and Toshiba. Volume and weight should be minimized in any spacecraft. SatCon's, IBM's, and Toshiba's systems offer advantages in envelope volume and weight.

The choice of the actuator technology between Lorentz force and magnetic bearings for MDOF isolation systems is not a clear one. Lorentz actuators offer linearity, simplicity, open loop neutral stability, and compactness. Magnetic bearings offer higher force capability and lower power consumption, particularly if gaps are minimized.

Four position sensor technologies offer promising performance. Eddy current position probes are simple and robust, but bulky and heavy for large gaps. Capacitive sensors are simple and lightweight, but can be noisy in unconstrained environments. Optical lateral effect photo–diodes are compact and quiet, but they require substantial supporting electronics. Hall effect flux sensors can be used with magnetic bearing designs both to linearize the control problem and to measure position.

3.3 Coarse Stage

The Stewart platform is a six degree–of–freedom parallel manipulator which has been used extensively in aircraft cockpit simulator applications. Figure 4 shows the mechanism in the proposed configuration [4]. Six linear actuators (legs) connect a base (bottom) to a platform (top). The base would be mounted in the spacecraft and move with it, while the

platform would track an inertial reference frame. Stepper motor driven ball lead–screws are proposed as actuators.

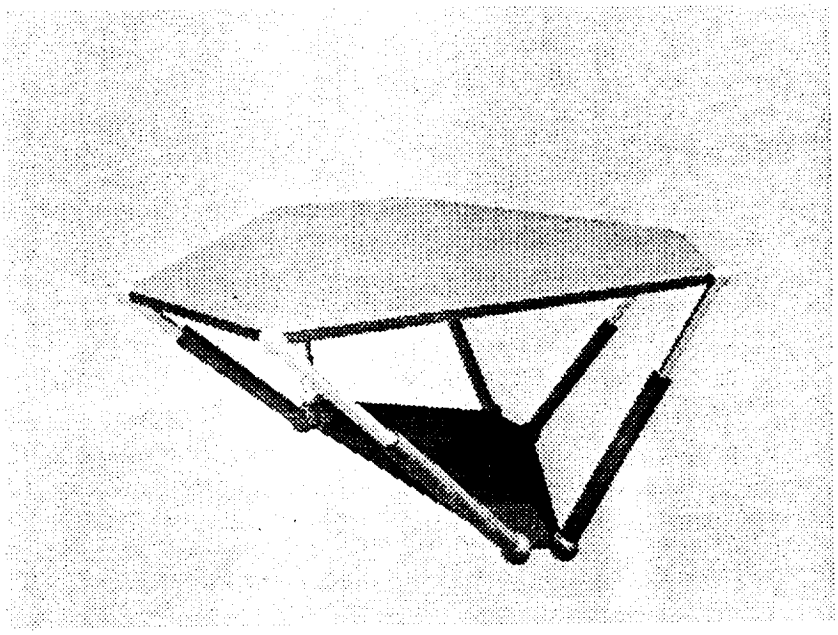

Figure 4: Coarse stage isolation actuator

This mechanism was chosen over other candidates such as a carriage/gimbal assembly, or a serial linkage mechanism, because it has the following features:

* **Inherent rigidity:** The parallel connection of the actuators gives the mechanism rigidity on the order of the extensional rigidity of the actuators. For the proposed actuators, this will allow controller design to ignore the dynamics of the mechanism. The effects of "umbilical" connection to the platform will also be negligible.
* **Determinate inverse kinematics:** The actuator lengths required to achieve a prescribed orientation are found directly from a coordinate transformation from the base to the platform frame. This is seldom the case for a serial linkage. This will also simplify control.

* **Compactness:** The configuration proposed here places the fine stage on top of the platform for convenience in testing. A fully developed implementation could locate the fine system and microgravity experiment in the space between the base and platform, resulting in a compact package.

The Stewart platform has some disadvantages that must be considered. It is nonlinear in its response to actuator lengths, its general direct kinematics have not been discovered in closed form, and it has singularities in its operational space. The first two problems can be overcome with digital controls. The singularities, which are points or loci where the mechanism gains a degree of freedom and the actuators can lose control of the platform, must be addressed by the design.

A simulation code has been written to allow exploration of the design alternatives. Results indicate that our specification (4 inches translation, 40 degrees rotation) will be achievable with actuators 10.5 inches long in the retracted position, and with 9 inches of stroke. The simulations have confirmed that singularities are safely outside the working envelope. Commercial actuators with the required range, load capacity, speed and acceleration have been identified.

3.4 Fine Stage

The magnetic bearing proposed has two parts: a stator which is attached to the Stewart platform, and a surrounding "flotor" to which the experiment is attached. The proposed stator [5] is illustrated in Figure 5. It has twelve pole pieces and coils arranged around the surface of a cube. The cube and pole pieces are ferromagnetic. Each pair of pole pieces and the region of the cube to which they are attached comprise a typical "horseshoe" electromagnet causing an attractive force toward the nearby flotor. Magnetic flux through the center of the cube causes an imbalance in the flux levels of a pair of pole pieces, resulting in a net torque on the flotor.

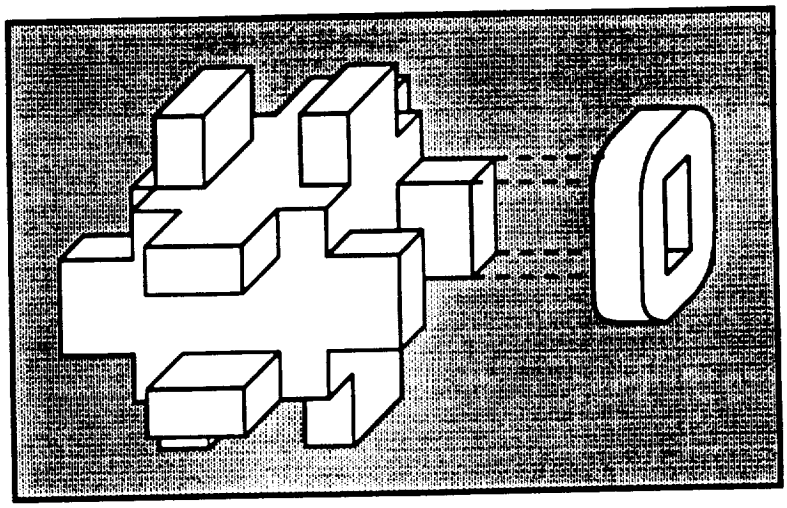

Figure 5: Fine stage isolation stator

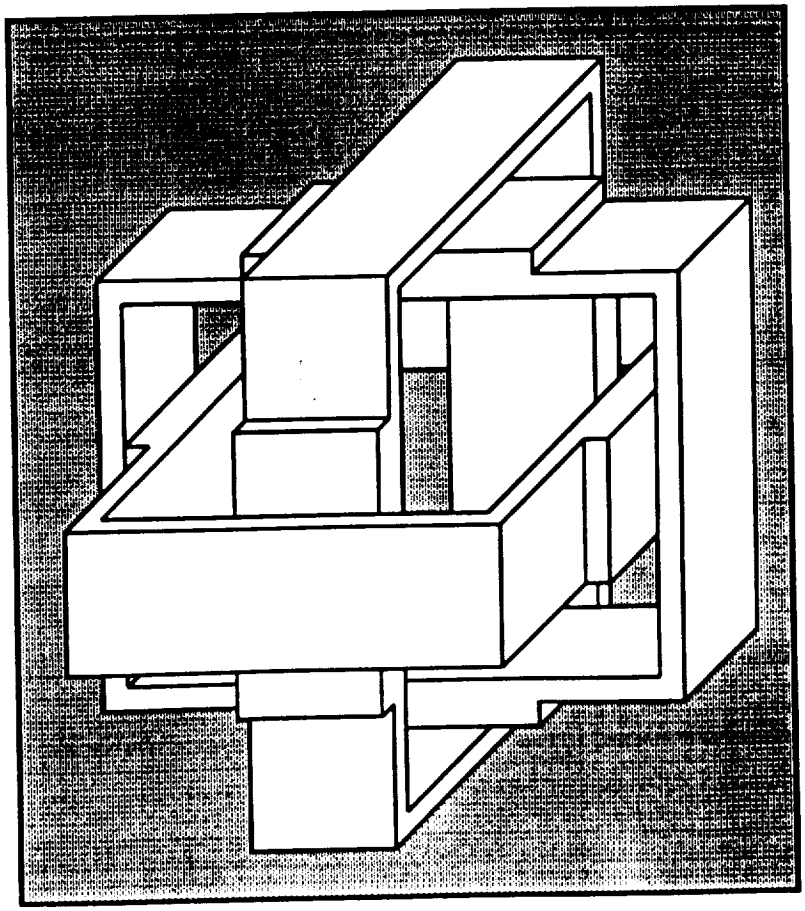

Figure 6: Fine stage isolation flotor

In the proposed design differential Hall effect sensors are located in the base of each pole piece to measure the local flux. All electrical connections will be to the stator.

The flotor concept is illustrated in Figure 6. Three ferromagnetic bands are rigidly attached to each other, but form independent flux paths. The bands are thicker in the region near the pole pieces to avoid saturation. Flux which passes through the center of the cube is returned through the remaining portions of the bands.

Four mounting posts are attached to corners of the cube, and pass through clearances in the flotor. These posts could carry cooling fluid to be circulated through the stator if it is required.

This configuration was chosen over other suspension approaches such as Lorentz actuators or magnetic actuators located on the periphery of the experiment package because it has the following advantages:

* **Compactness:** The high force capability of the magnetic bearing relative to a Lorentz actuator of similar size and power consumption suits the application. Testing in earth gravity will be facilitated, and suspension during launch to protect sensitive instrumentation may be feasible. Also, the rigid structure required to mount actuators around the periphery is avoided.
* **Force/torque balance and rotational range:** Actuators capable of the required forces mounted on the periphery of the experiment are capable of torques far greater than is required, and they limit the rotational range of the experiment. The proposed design approach brings the relative force/torque magnitudes closer to the requirement, and allows substantial rotational range.
* **Integral sensor capability:** Compact semiconductor magnetic flux sensors (Hall effect or magneto–resistive) can be utilized both to stabilize the system and to infer relative position. No elegant integrated approach is known for Lorentz actuators.

3.5 Predicted Performance

The specific design examined at the University has a center cube of 2 in. on a side, pole faces of 1 x .5 in., and pole length of 2 in. Maximum current is determined by allowing a coil current density of 5000 amp/in^2 which is known to be conservative from previous designs. The gap in the centered position was chosen to be .125 in. plus an allowance of .030 in. for inclusion of flux sensors and a protective layer on the inside of the bands. The resulting performance of the design is presented in Table 2. The 53 N force is a continuous worst case, with the stator moved away from the flotor in the direction of the force. The continuous force capability in the centered position is 175 N. Intermittent force capability is limited only by the current capability of the amplifiers, and the saturation limit of the magnetic material used. Using Vanadium Permandur with this design would enable 1000 N force before saturation. Of the 4.5 kg mass, the flotor comprises only 1.2 kg.

Trans.	Rot.	Force	Envelope	Mass
+3.2 mm	+7°	53 N	15x15x15 cm	4.5 kg

Table 2: Specification of UVA Design

When compared with the designs presented in Table 1, the UVA design has several advantages. The envelope is substantially smaller than any of the previous designs, while the performance is similar. In addition to saving space, this compactness allows the flotor to be naturally rigid, and thus avoids control problems with structural dynamics. The design is lighter than other designs for which data were available [5,6].

4. CONTROL SYSTEM DESIGN ISSUES

4.1 Introduction

The control issues of active microgravity vibration isolation were another area of investigation at the University. The thrust of this research has been the design of feedback/feedforward controllers using modern control synthesis. As part of this investigation we also examined passive vibration isolation analogies. In addition, a control architecture for the six–degree–of–freedom actuator discussed in the last section was proposed.

Active isolation systems for microgravity and pointing applications have been designed and constructed by many investigators. These systems generally use conventional PD control of a noncontacting actuator, either Lorentz or electromagnetic, to achieve low frequency disturbance attenuation. While an actual microgravity experiment may require umbilicals, the isolation systems designed and tested so far cannot provide isolation for such an experiment. These systems achieve their performance by the very low stiffness made possible by low gain feedback of the relative position of the experiment to the experiment rack. Without an umbilical, this stiffness may be set by the designer at will. However, when an umbilical is present, the umbilical stiffness presents a lower bound on achievable stiffness unless the feedback loop is used to introduce a negative stiffness. The University has concentrated its work on the design of control systems for the generic (i.e. with umbilical) microgravity isolation problem. The University has set the following specifications for an active microgravity isolation system [12]:

(1) Unity transmissibility from D.C. to 0.001 Hz so as to prevent the experiment from impacting its enclosure's walls.

(2) At least 40 dB attenuation above 0.1 Hz.

(3) Both stability and performance robustness with respect to changes in umbilical experiment properties, non–collocation or misalignment of sensors and actuators, center–of–mass uncertainties, and unmodeled cross coupling between the degrees of freedom.

Robustness refers to the ability of the control system to perform satisfactorily when the true plant varies from the nominal plant. Performance requirements of the type (2) for rotational degrees of freedom have not yet been specified by NASA or microgravity users, to our knowledge.

4.2 Passive Isolation: An Analogy

The design of an active vibration isolation system for microgravity space experiments was examined from an analogy to passive isolators [12]. It should be noted that the primary reason for pursuing an active rather than a passive system is not the increased flexibility in loop shaping accompanying active control, but the limitations of passive isolation systems. The stiffness of the umbilical precludes achieving a soft enough support so as to meet the isolation requirements for indirect (transmitted through the umbilical) disturbances. Also, a passive isolation system cannot isolate the payload from both indirect and direct (onboard the experiment) disturbances. An active system allows these limitations to be overcome. For example, an active system permits the insertion of a negative stiffness spring in parallel with the umbilical. Note, however, that this approach, i.e. lowering the stiffness, requires the near cancellation of the umbilical's stiffness with that introduced via feedback. If the negative stiffness exceeds that of the umbilical, the equivalent stiffness of the system will be negative and the system will be unstable. It is not surprising then that the introduction of negative stiffness via the controller has no robustness whatsoever. A focus on equivalent stiffness in isolation system design thus leads to control systems which sacrifice robustness for performance. In addition, a design which achieves isolation through lowering the system stiffness cannot attenuate direct disturbances over the same frequency band.

From a vibration engineering viewpoint, an alternative means of achieving rejection of disturbances is to fasten the experiment rigidly to an inertial structure. While there is no such structure in space, it is possible to achieve this effect by high gain feedback on inertial experiment position. This inertial position feedback acts like a very stiff spring tying the

experiment to inertial space. While such a controller may meet the 0.1 Hz 40 dB specification, it will not satisfy the specification on unit transmissibility [12]. If an inertial position feedforward loop is added, this problem can be eliminated. However, this method would be difficult to use effectively for multiple–degree–of–freedom isolation.

Another method of fastening the experiment to inertial space examined by the University is the use of inertial damping via feedback. By feeding back the inertial experiment velocity with a high gain it was shown for an example problem that it is almost possible to achieve both the 40 dB and the unity transmissibility specifications without resorting to feedforward. Unfortunately, the roll–off rate is approximately 20 dB/decade, so that both specifications can not be simultaneously achieved [12].

Another passive analogy examined was the lowering of the natural frequency of the umbilical by increasing the experiment mass. An increased experiment mass would attenuate direct disturbances as well as those transmitted through the umbilical. In addition, at frequencies below the natural frequency of the umbilical–mass system, the isolation system would have unity transmissibility. Of course, for space applications any additional mass is very costly. To lower the natural frequency by an order of magnitude would require increasing the experiment mass by a factor of one hundred. Clearly, it is not practical to accomplish increased isolation through the addition of real mass. However, it is possible to increase the effective mass of the system through feedback [12].

To summarize, the passive isolation analogies examined yield some insight but they fall short as design approaches on three counts: (1) they do not have flexibility to shape the response so as to achieve the performance requirements, (2) they cannot be easily generalized to multi–degree–of–freedom problems, and (3) they completely ignore the robustness problems inherent with active control systems.

4.3 Classical Control Design

A one–dimensional isolation problem, shown in Figure 7, was examined using a classical controls loop–shaping approach, to gain insight into controller design and limitations. System

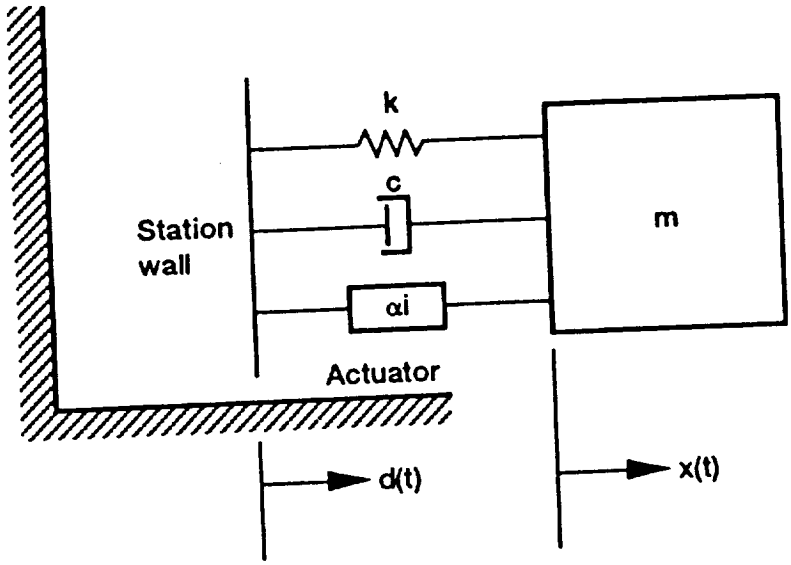

Figure 7: One–dimensional isolation problem

parameters were chosen to be representative values which yielded a low natural frequency ($k/m = 0.1$, $\omega_n \approx 0.05$ Hz [0.316 rad/sec]), and damping was assumed light ($\zeta = 0.1$). In the following discussion the variables d, x, and u represent experiment rack position, payload position, and control force, respectively; and it is assumed that the only available measurement is payload acceleration. The problem is to design a feedback controller, satisfying the following specifications:

1. Above 0.1 Hz the payload acceleration $\ddot{x}(t)$ should be 40 dB below the spacecraft acceleration $\ddot{d}(t)$.
2. Below 0.001 Hz the payload vibration x(t) should track the spacecraft vibration d(t) to within 10 percent, in order to prevent collision of the payload with the walls of the experiment rack surrounding it.
3. The payload should track perfectly the DC motion of the spacecraft, where no relative motion can be tolerated.

4. The loop gain of the system (plant and controller) should be less than 0.1 above 200 Hz, to avoid controller excitation of spacecraft– or payload flexible modes.
5. The payload acceleration should be less than or equal to 1.1 times the spacecraft acceleration at all frequencies.
6. Large phase margins should be attempted at all crossover frequencies.

The system equation of motion is

$$m\ddot{x} + c\dot{x} + kx = c\dot{d} + kd - u$$

and the system transfer functions are

$$s^2X(s) = \left[\frac{cs+k}{ms^2+cs+k}\right] s^2D(s) + \left[\frac{-s^2}{ms^2+cs+k}\right] U(s)$$

with a system block diagram as shown in Figure 8. R(s) represents the input disturbance (rack acceleration, Laplace domain), C(s) represents the payload acceleration, $H_1(s)$ represents the controller, and U(s) represents the control force. G(s) and $\frac{-s^2}{cs+k}G(s)$ are the two plant transfer functions, and H(s) is defined as indicated in Figure 8 for convenience.

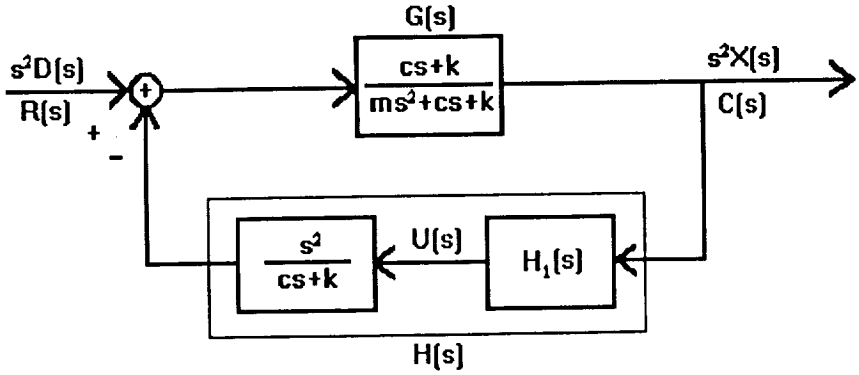

Figure 8: One–dimensional isolation system block diagram

The first five specifications can now be re–expressed, respectively, in the following form:

1. $\left|\frac{C(s)}{R(s)}\right| < 0.01$ above 0.1 Hz (0.628 rad/sec).

2. $0.9 < \left|\frac{C(s)}{R(s)}\right| < 1.1$ below 0.001 Hz ($6.28 \cdot 10^{-3}$ rad/sec).

3. $\lim_{s \to 0} \left|\frac{C(s)}{R(s)}\right| = 1.$

4. $|H(s)\, G(s)| < 0.1$ above 200 Hz (1256 rad/sec).

5. $\left|\frac{C(s)}{R(s)}\right| \leq 1.1$ for all frequencies.

In order to use the classical approach efficiently, the above specifications must be reduced to loop–gain form. This reduction yields, respectively, the following:

1. $\left|\frac{G}{1+HG}\right| < 0.01$ above 0.628 rad/sec, which in turn requires roughly that $|H| > 22$ (i.e., greater than 100/G1) at that point.

2. The second specification, $0.9 < \left|\frac{G}{1+HG}\right| < 1.1$ below $6.28 \cdot 10^{-3}$ rad/sec, is roughly equivalent (since $|G| \approx 1$ below ω_n) to the requirement that $|HG| < 0.1$ below $6.28 \cdot 10^{-3}$ rad/sec.

3. $\lim_{s \to 0} |HG| = 0.$

4. $|HG| < 0.1$ above 1256 rad/sec (same form as before).

5. $|HG| > 7$ in the vicinity of ω_n (where $|G| \approx 6.5$) to reduce the transmissibility to about unity in that region.

Standard loopshaping methods can now be used in a straightforward manner. See Figure 9 for asymptotic Bode–α plots of the specifications and of G(s); and for "first–pass" plots of the loop gain "L(s)" [i.e., H(s)G(s)] and of the controller $H_1(s)$.

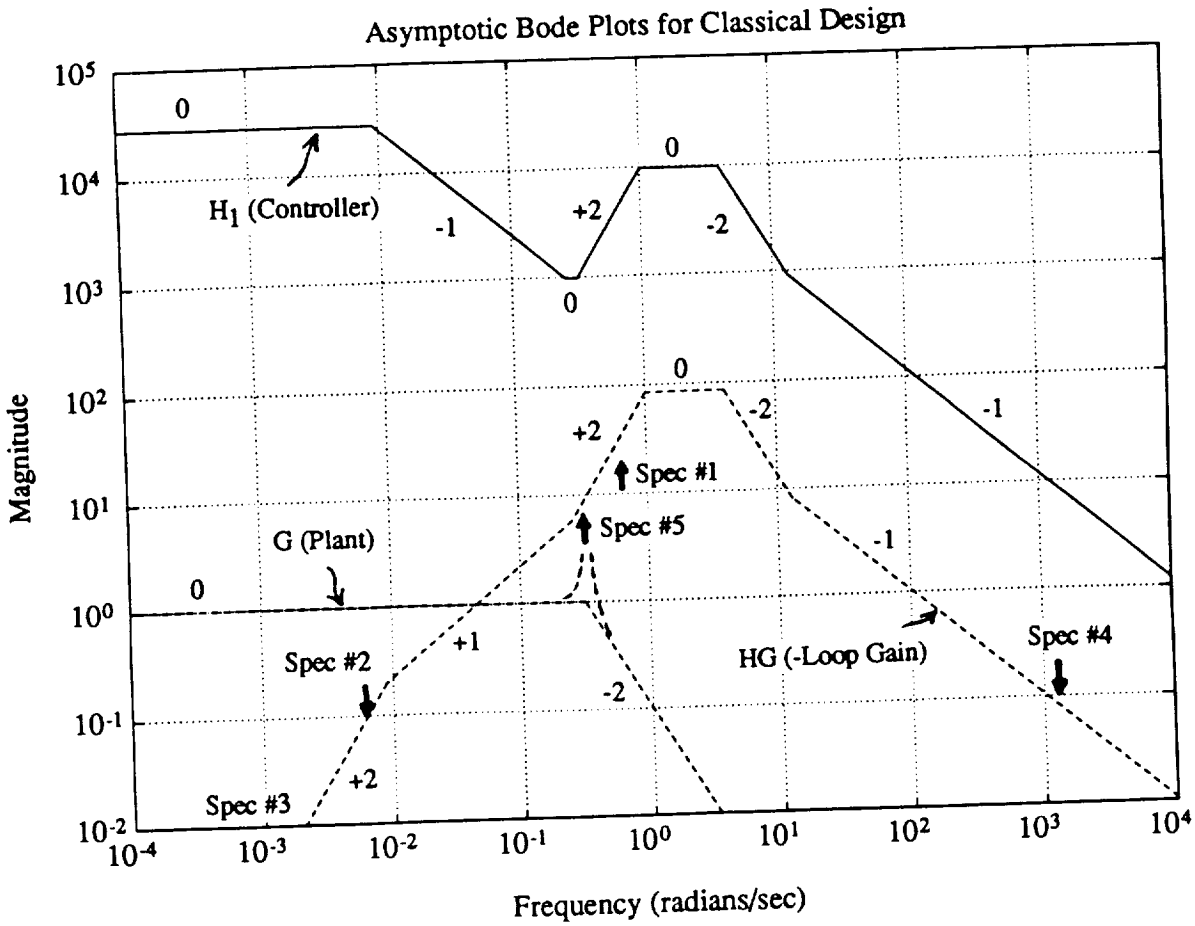

Figure 9: Asymptotic Bode–α plot of plant G(s) and "first–pass" loop gain L(s)

The controller developed first led to a transmissibility resonance at ω_n (not shown) so a filter of form $\frac{(s+0.316)^2}{s^2+0.1}$ was added, resulting in the following controller:

$$H_1(s) = \frac{1.2 \cdot 10^3 \ (s + 0.25)(s + 12)(s + 0.316)^2(s^2 + 0.063\ s + 0.1)}{(s + 0.009) \quad (s + 1)^2 \ (s + 4)^2 \ (s^2 + 0.1)}$$

Figures 10a,b,c represent loop gain, controller, and transmissibility plots, respectively. The control meets all specifications except for the goal of no more than a transmissibility of 1.1 at all frequencies; and this specification is almost met. The two phase margins associated with the above controller are 59^0 and 88^0, respectively.

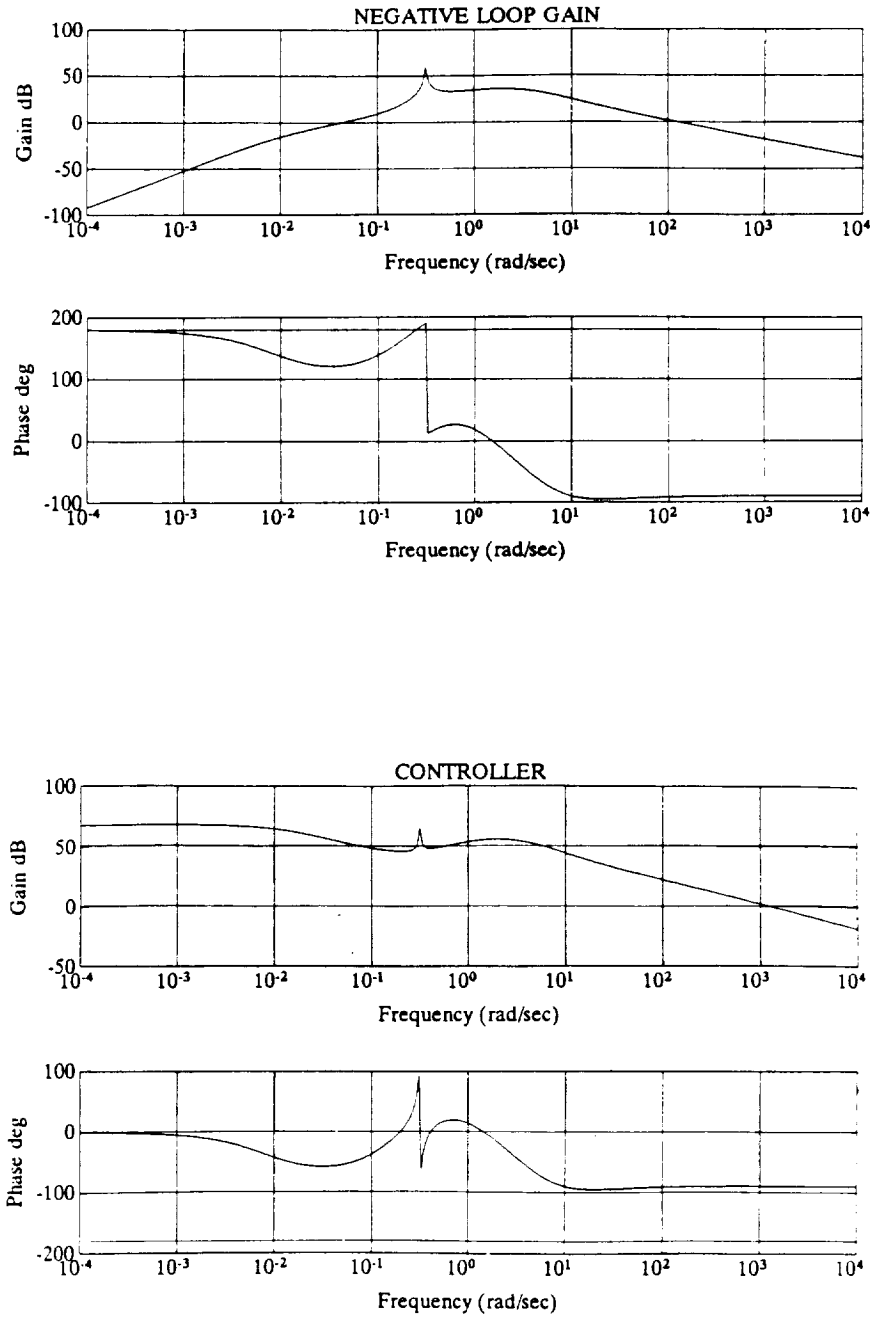

Figure 10: (a) Loop gain Bode plot, (b) controller Bode plot

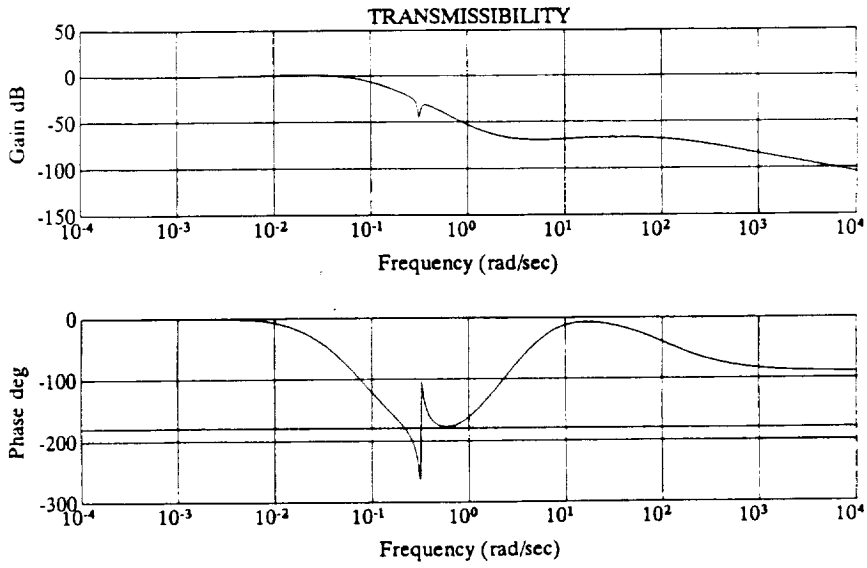

Figure 10: (c) Closed–loop transmissibility plot designed using classical control methods

From the above analysis the following conclusions can be drawn:

1. The requirement that $\left|\frac{C}{R}\right|$ be less than some fraction β_2 above some frequency ω_2 [spec #1] means that the open loop gain L(s) [i.e., H(s)G(s)] must be greater in magnitude than $\frac{1}{\beta_2}\left|G(s)\right|$ above ω_2. This means that there is a tradeoff between β_2 and PM_1. The smaller β_2 is, the smaller PM_1 can be. That is, the better the disturbance rejection above ω_2, the lower the achievable phase margin PM_1:

   $\beta_2 \downarrow \Rightarrow PM_1 \downarrow$. (Lowering β_2 will also tend to reduce PM_2, but not as directly.)

2. Raising ω_2 will improve PM_1 but degrade PM_2:

   $\omega_2 \uparrow \Rightarrow PM_1 \uparrow$, $PM_2 \downarrow$

3. The requirement to keep $|L(s)|$ below β_3 above ω_3 [spec #4] (so as to avoid exciting higher modes) has a cost in terms of PM_2 : $\beta_3 \downarrow \Rightarrow PM_2 \downarrow$.

4. Raising ω_3 raises PM_2: $\omega_3 \uparrow \Rightarrow PM_2 \uparrow$.

5. The requirement to hold $\left|\frac{C}{R}\right|$ within some fraction β_1 of unit transmissibility below some frequency ω_1 [spec # 2] means that $|L(s)|$ must be less than $\frac{1}{\beta_1}|G(s)|$ below ω_1. There is, then, a tradeoff between β_1 and PM_1: $\beta_1 \downarrow \Rightarrow PM_1 \downarrow$. (Changing β_1 does not significantly affect PM_2.)

6. Lowering ω_1 will improve PM_1: $\omega_1 \downarrow \Rightarrow PM_1 \uparrow$.

7. Lowering the natural frequency ω_n eases the difficulty in obtaining adequate PM_1 by lowering the constraint at ω_2 (see Figure 9) at ω_2: $\omega_n \downarrow \Rightarrow PM_1 \uparrow$. This means that reducing the physical umbilical stiffness or increasing the physical payload mass will make for an easier control problem.

8. The problem can be simplified, and both PM_1 and PM_2 can be increased, if the umbilical is damped such that the resonance near ω_n is small. (Refer to spec #5, p. 23.)

9. The controller need not have zero gain at DC to be acceptable, as long as $\lim_{s \to 0} s^2 H_1(s) = 0$. The controller may have a low frequency asymptote with slope –1, 0, or greater.

Although the classical approach is not readily extendable to the MIMO problem, it does provide some useful insights for informing the extended H_2 synthesis approach that we will examine in Section 5. Weighting $\ddot{x}(t)$ more heavily above ω_2 is analogous to lowering β_2 (see conclusion #1 above), so that better disturbance rejection is achieved at the expense of phase margin (esp. PM_1). Weighting the control u(t) more heavily at higher frequencies corresponds to trying to reduce β_3, so that a reduction in controller bandwidth is purchased at the expense of phase margin (PM_2) (see conclusion #3). At the lower end of the frequency spectrum, increased weighting of relative displacement (x–d), reduced weighting of absolute acceleration ($\ddot{x}$), or increased weighting of the control (u) each corresponds to attempting to lower β_1, at the cost of reducing PM_1 (see conclusion #5). Since an acceptable controller can have large, even infinite, DC gain (see conclusion #9) it is not necessary to weight u(t) highly at low frequencies. In fact for phase margin considerations (PM_1) it may be best to have "cheap" control at low frequencies, as previously noted (see conclusion #5). Unity transmissibility, then, could be "requested" at low frequencies by a relatively high low–frequency weighting of relative displacement.

4.4 Extending to the Multiple Degree–of–Freedom Problem

The University has extensively examined the design of multiple–input–multiple–output (MIMO) controllers for the multiple–degree–of–freedom active isolation problem. This work will be examined in detail in the next section. Here, we will introduce some of the problems of extending single–input–single–output (SISO) methods to MIMO problems by examining a simple multiple–degree–of–freedom benchmark problem [12], shown in Figure 11.

This problem illustrates how controller design via decoupling an isolation problem into its open loop modes, designing controllers for each mode, and recoupling back into the actuators, will often result in poor robustness due to unmodeled cross–couplings. This method of design, converting a MIMO control problem to a series of SISO problems, is often practiced. The example system is composed of an isolated platform (width 0.5 m and height 0.2 m, depth

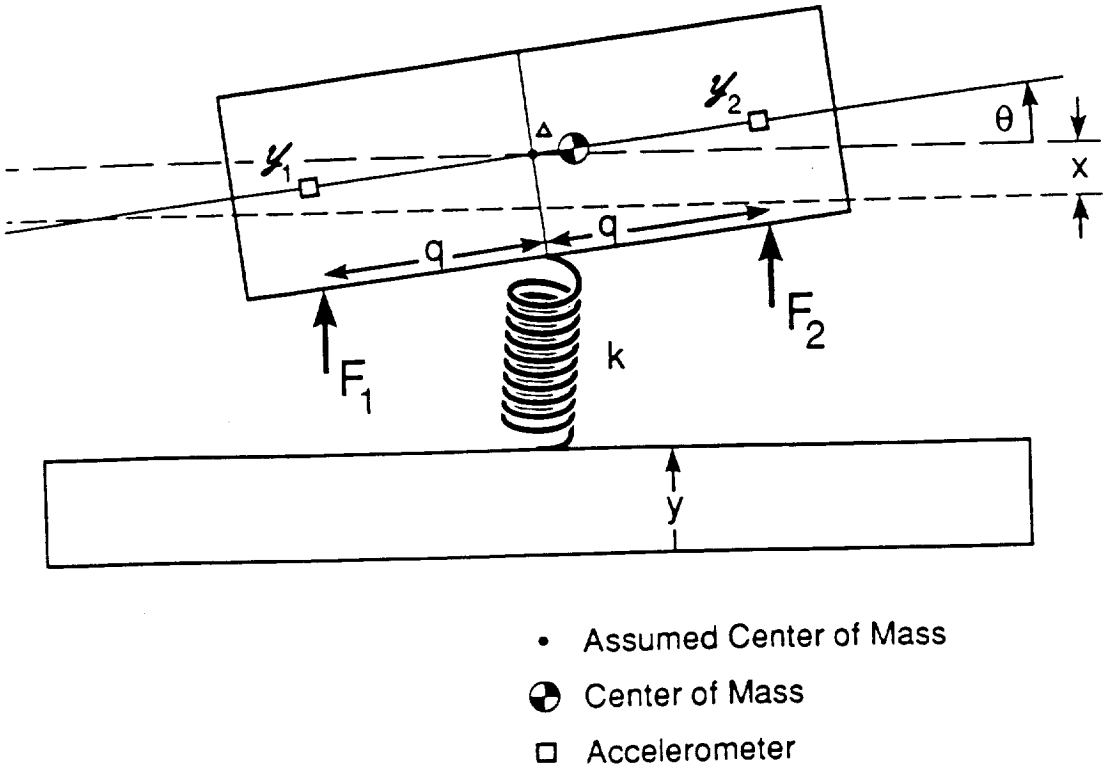

Figure 11: Simple multiple–degree–of–freedom benchmark isolation problem

unspecified), two accelerometers, two actuators, an umbilical, and a translating base. The platform may translate vertically or rotate about its center–of–mass. The actuators and accelerometers are positioned a distance of q = 0.2 m symmetrically about the assumed center–of–mass location. An umbilical of stiffness k (no damping) runs between this location and the base. The platform has mass m and inertia I. The equations of motion for the platform's translation x(t) and rotation $\theta(t)$ are

$$m\ddot{x} + k\Delta\theta + kx = f_1 + f_2 + d_1$$

$$I\ddot{\theta} + k\Delta^2\theta + k\Delta x = (q + \Delta)f_2 - (q - \Delta)f_1 + d_2$$

where d_1 and d_2 are the disturbances, and Δ is the error in the assumed center of mass. The

accelerometer readings are

$$y_1 = \ddot{x} - (q - \Delta)\ddot{\theta}$$

$$y_2 = \ddot{x} - (q - \Delta)\ddot{\theta}$$

The nominal system ($\Delta = 0$) can be decoupled in terms of the degrees of freedom by the change in variables

$$F = f_1 + f_2$$

$$M = q(f_2 - f_1)$$

$$z_1 = (y_1 + y_2)/2$$

$$z_2 = q(y_2 - y_1)/2$$

which are nominally the translational force, the moment, the translational acceleration, and the angular acceleration for the platform, respectively. The nominal transfer functions for the system are then

$$Z_1(s) = \left[\frac{s^2}{ms^2 + k}\right](F(s) + D_1(s))$$

$$Z_2(s) = \left[\frac{1}{I}\right](M(s) + D_2(s))$$

For translational motion, the natural frequency of the platform is $\sqrt{k/m}$. The rotational motion of the platform is free since the umbilical is attached to the center–of–mass. To compensate the nominal system, feedback can be designed for each mode of the system separately, since the system is decoupled. Translational acceleration and velocity feedback are first used to add effective mass and damping.

$$F(s) = -\left[a + \frac{c}{s}\right]Z_1(s).$$

This lowers the natural frequency of translational motion, yielding the closed loop transfer function

$$Z_1(s) = \left[\frac{s^2}{(m + a)s^2 + cs + k}\right] D_1(s).$$

Next, angular deflection feedback is used to constrain low frequency rotational motion and some damping is provided.

$$M(s) = -\left[\frac{n}{s} + \frac{b}{s^2}\right] Z_2(s)$$

yielding

$$Z_2(s) = \left[\frac{s^2}{Is + ns + b}\right] D_2(s)$$

where the control system values are in effective units. A control system was designed to lower the natural frequency of translational motion from 0.056 to 0.006 Hz with 40% of critical damping. The controlled rotational motion has a natural frequency of 0.006 Hz with 26% of critical damping. This controller design would yield very effective isolation on the nominal system.

The actual close loop poles, however, will be different from the nominal due to the error in the center–of–mass Δ. The poles of the actual system are given by the roots of the characteristic equation

$$[(m + a)s^2 + cs + k][Is^2 + ns + b] - [m\Delta][\Delta\{as^2 + cs + k\}] = 0$$

For the nominal plant ($\Delta = 0$), this results in the prescribed natural frequencies and critical dampings. However, as the center–of–mass error increases, the poles migrate and the system becomes unstable. For an error as small as 6 mm for this system, instability occurs [12]. A plot of the pole movement vs. error in center–of-mass is shown in Figure 12. This sensitivity results from the ill–conditioned character of the designed controller. A proper MIMO

controller design might remedy this problem. In any case, an analysis of the problem from a MIMO control perspective would indicate the potential instability and the nature of the trade–off between performance and robustness.

In the next section, the MIMO design methods developed at the University of Virginia are examined in detail. Special attention is given to the issue of robustness.

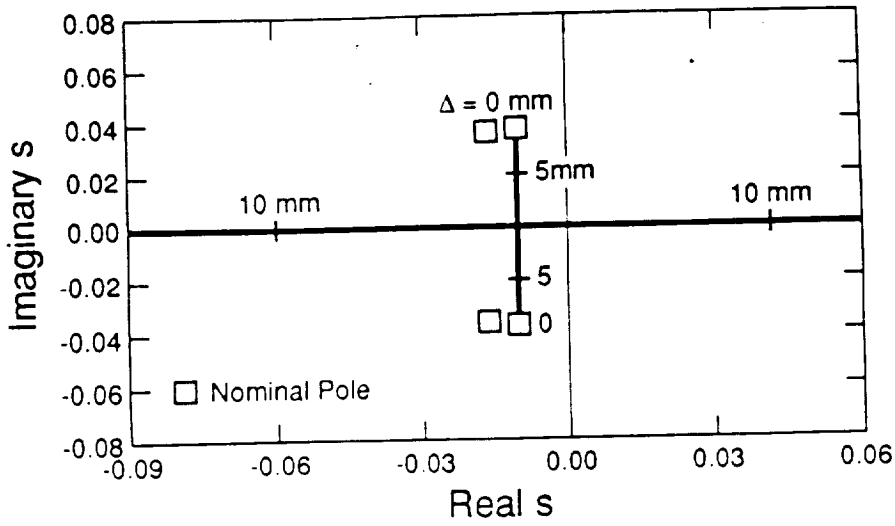

Figure 12: Loci of closed–loop poles as a function of center–of–mass error

5. MODERN CONTROL THEORY DESIGN

5.1 Modern Control Methods: An Overview

Researchers at the University have investigated the use of Linear Quadratic Regulator (LQR) and the Kalman–Bucy Filter (KBF) synthesis methods for the design of controllers for microgravity vibration isolation platforms [13,14,15]. The LQR method produces a state feedback controller which is optimal with respect to the quadratic (two norm) performance index

$$J = \int_{-\infty}^{\infty} \bar{x}^T(j\omega)Q\bar{x}(j\omega) + \bar{u}^T(j\omega)R\bar{u}(j\omega)\, d\omega$$

where Q and R are respectively the symmetric (usually diagonal) state and control weighting matrices, and $\bar{x}(j\omega)$ and $\bar{u}(j\omega)$ are the Fourier transforms of the state and control vectors. The state (positions and velocities for vibration isolation) satisfies the differential equation

$$\dot{x} = Ax + Bu$$

The quadratic performance index of LQR is well suited to this problem since vibration isolation quality is usually measured in terms of root–mean–square. However, it has been shown by researchers at the University that some modification of the performance function is necessary to apply this synthesis procedure to microgravity isolation controller design. State feedback for the isolation problem is feedback of experiment positions, velocities, angles, and angular velocities. Thus, LQR can only result in (inertial or relative) stiffness and damping feedback. As was discussed previously, these isolation techniques cannot yield acceptable isolation performance. Thus, an LQR performance index will not yield a satisfactory controller unless frequency weighted Q and R matrices are used, or the plant model is changed so as to have an acceleration pseudo–state [12]. Either of these methods results in the addition of pseudo–states to the state variable model. Frequency weighted Q and R matrices are also necessary to achieve robustness. Through choice of the weighting functions, the designer can, in essence, shape the control loops.

The differential equation above does not include a disturbance term. Consequently, the resulting controller is optimal with respect to white noise (a weakness of the LQR machinery). Since the power spectrum of the microgravity environment is not of this shape, the LQR controller will not be optimal with respect to rejection of the disturbance. Through the incorporation of a disturbance model (essentially a shaping filter), the LQR problem may be modified to yield an optimal disturbance accommodating (i.e. rejection) controller. This also incorporates the addition of pseudo–states to the state variable model. Disturbance accommodation may also aid in increasing the controller's robustness through loop shaping. Through the incorporation of the pseudo–states for frequency weighting and disturbance accommodation, controllers have been designed by University researchers using the standard Algebraic Ricatti equations of LQR–KBF. These calculations have been done using batch files written in the MATLAB language [15]. These controllers are then tested for robustness with respect to structured and unstructured uncertainties using singular value and structured singular value analysis. These analysis tools are the MIMO equivalent of the familiar gain margin, phase margin, and root locus robustness tests. Results for a one–degree–of–freedom problem are discussed below. MIMO vibration isolation research is ongoing at the University. These modern control methods require a considerable degree of skill and insight to employ properly.

5.2 Modern Control Results

The one–dimensional problem was first expressed in state–space form, with payload relative position, relative velocity, and acceleration selected as states. Although many other state choices could have been made, these three were chosen to minimize the number of states necessary and to maximize the physical intuition possible. The selection would result in a state feedback control that respectively modifies the effective umbilical stiffness and damping, and the effective payload mass—all being familiar, accessible, and intuitive system parameters. Relative, rather than inertial, position feedback would help to avoid exceeding

rattlespace limits; and relative velocity feedback would provide a means of damping out system resonances. The selection of acceleration as a state was considered desirable due to insight gained from the passive control studies. A controller which increases effective payload mass (by negative acceleration feedback) would potentially be able to accomplish disturbance rejection without unnecessarily sacrificing stability– or performance robustness.

A second important feature of the problem formulation was the decision to incorporate disturbances of two different kinds, the direct (i.e., onboard the experiment) and the indirect (i.e., acting via the umbilical). It had been observed that reducing the effective umbilical stiffness could aid in indirect disturbance rejection only, but that increasing payload effective mass could help reject disturbances of both kinds. Although the primary type of disturbance was considered likely to be the indirect, a means was needed to force the LQR–KBF (also known as LQG) "machinery" to increase effective mass so as to result in a robust controller. Including a direct disturbance provided this mechanism.

After completing the problem formulation, the next step was to develop a computer code for use in design and analysis. A PC–based design code was written in MATLAB to allow for accommodation of both direct and indirect disturbances. A large selection of frequency weightings and disturbance accommodation filters was made available to the designer. The code computes both feedback and observer gains, and also determines the constant feedforward (preview) gains for which the theory was developed in [16]. Although the feedforward option remains available, subsequent analysis determined that for the present application the feedforward gains do not make a significant enough contribution to warrant the additional controller complexity required. A number of analysis routines were also written to allow the designer to evaluate the resultant designs for purposes of comparison. The number of system states, system performance, stability robustness, parameter sensitivity, and observer quality are items whose comparisons are facilitated by these routines.

With the design and analysis tools in place, the next step was to develop the desired controller. In order to make the controller as simple as possible, it was decided to begin with

the basic LQG approach and to add complexity as needed. At each stage of additional complexity an iterative cycle of design and analysis was employed in an attempt to get the "best" achievable controller at that level of complexity.

The basic LQG approach (no frequency weighting, no disturbance accommodation, no direct disturbance) yielded a satisfactory controller in terms of performance; but it had almost no stability robustness to changes in umbilical stiffness from the nominal (as measured by feedback uncertainty). This lack of robustness was due to the fact that LQG found adding negative stiffness to be a "cheaper" means of indirect disturbance rejection than adding effective mass. No frequency weighting was found which could rectify this problem.

A direct white disturbance was added in an attempt to force the LQG design "machinery" to add effective mass. Although there were some gains in stability robustness this was due entirely to changes in observer gain matrix L. The feedback gain matrix K remained unaffected (note that this is fundamental in LQG theory and is not a numerical problem), and the feedback stability robustness was still unsatisfactory.

Disturbance accommodation, with a lowpass filter applied to a large direct (white) disturbance, resulted in a controller with excellent feedback– and multiplicative input stability robustnesses, as measured by singular value checks. The multiplicative output stability robustness was unacceptably low if cross–coupling was considered possible between states, but structured singular value checks indicated that without cross–coupling the allowable multiplicative output uncertainty was quite satisfactory. Since effective stiffness, effective damping, and effective mass of the controlled system are uncoupled for the true one–dimensional problem, the stability robustness measures of the system were considered acceptable. Further, the performance was excellent, easily exceeding the specifications. However, the controller gains were still large at higher frequencies where unmodeled system modes were of concern (see specification #4). It was therefore necessary to use state– and control frequency weighting in an attempt to force the controller to turn off by approximately 100 Hz (i.e., to reduce loop gain below a magnitude of one) so as to avoid exciting unmodeled

flexible modes. To reduce the loop gain at the higher frequencies it was necessary in that range (1) to place a high weight on control, (2) to apply low weights to all three states, and (3) to reduce the direct disturbance.

At low frequencies the control weighting was left constant (i.e., "flat"), in an attempt to minimize the number of added pseudostates. However, the resulting closed loop system now had very poor low frequency stability robustness to parametric uncertainties, even though it both retained its excellent performance and now provided the desired low controller bandwidth.

A classical design approach to the problem provided a simple solution to the robustness issue. It was noted that for a controller with acceptable nominal performance the low frequency asymptote for controller gain could have slope –1 or 0 or greater (Bode–α, log–log scale). Therefore, the control weighting at DC could be zero (filter slope ≥ 0) and the extended H_2 synthesis "machinery" could be freed to consider finite or infinite DC controller–gain options. This results, however, in the addition of a pseudostate. This change yielded a controller that satisfied the design specifications and exhibited good stability robustness to parametric and to multiplicative input– and output uncertainties. Considering (for the moment)only single–parameter uncertainties, stability was guaranteed for umbilical stiffness to within $\pm$99.7% of nominal, and umbilical damping could be essentially unknown. Payload mass needed to be known only to within $\pm$65.2% of nominal. Having these initial favorable indicators of system robustness the next step was to reduce the controller size. Further robustness analysis would then be conducted on the reduced–order controller.

The controller described above was a ninth–order controller (i.e., had nine states), with payload acceleration as its only required input. Other states and pseudostates were reconstructed in the observer. To reduce the controller to a smaller order, a routine was written in MATLAB in order to permit removing high frequency modes (modal truncation) and weakly controllable and –observable system dynamics [17]. The result of applying this to the ninth–order controller was a third–order controller that has all the essential features of the ninth–order one. The loop gain, controller, and transmissibility plots for this reduced

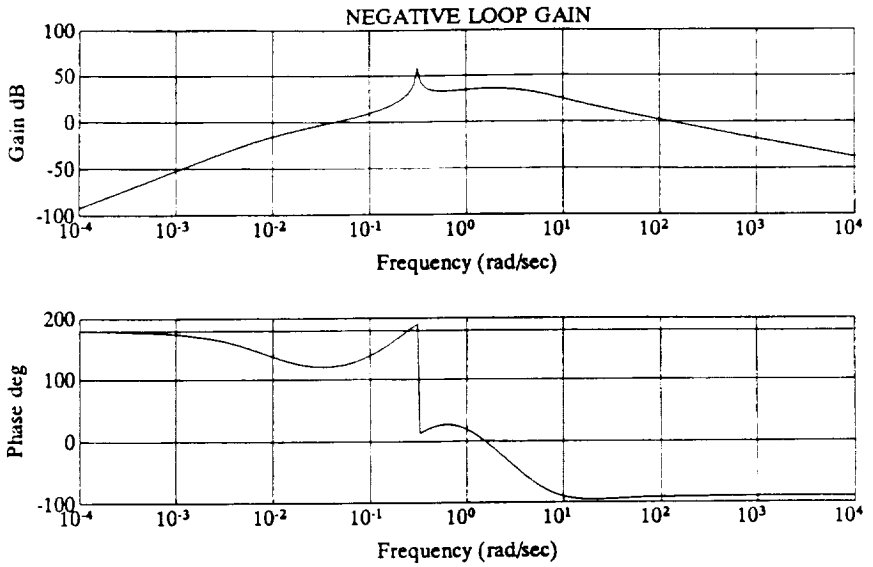

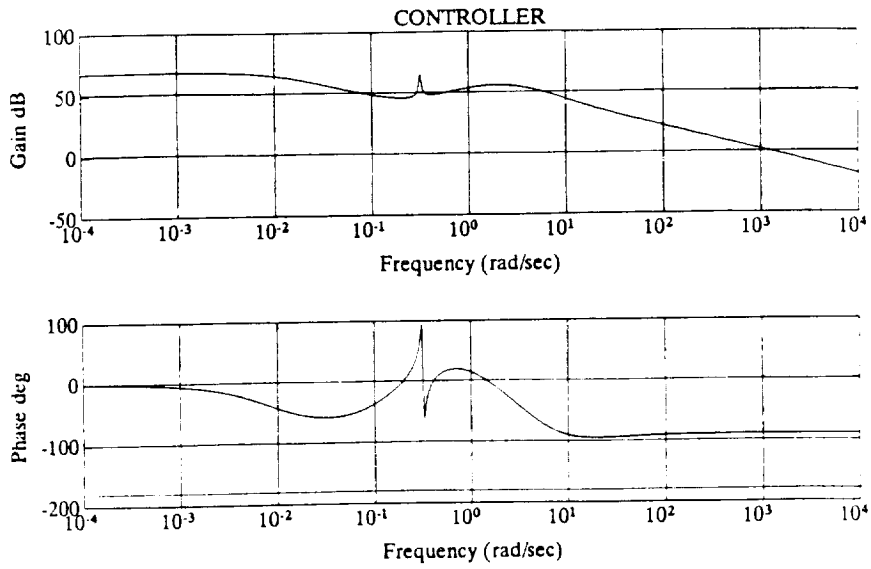

Figure 13: (a) Loop gain Bode plot, (b) controller Bode plot

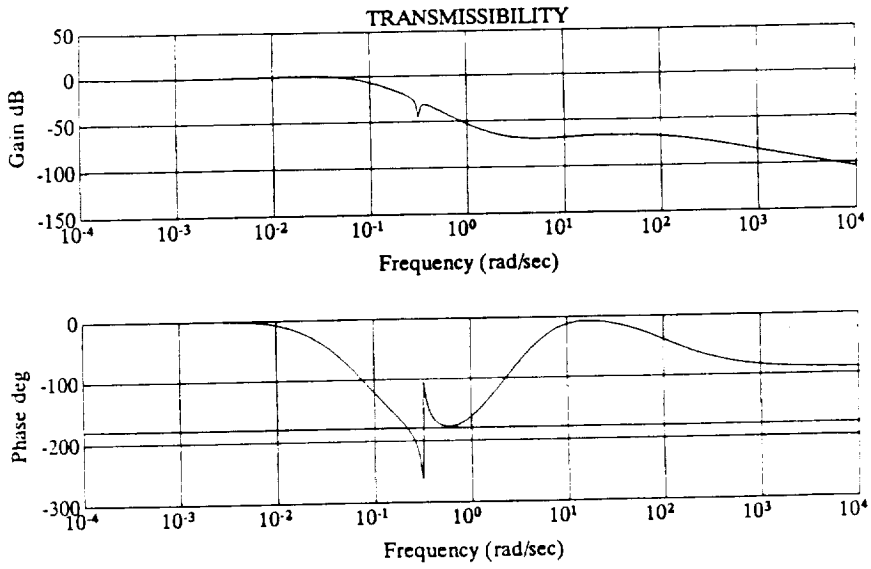

Figure 13: (c) Closed–loop transmissibility plot of system designed using extended H^2 synthesis

controller are shown in Figures 13a,b,c. Note from the transmissibility plot that the transmissibility is unity up to 10^{-3} Hz and that it is below 10^{-4} at 0.1 Hz. Notice further that the open loop and closed loop Bode plots merge at about 100 Hz. This is due to the fact that the controller has essentially "turned off" by that frequency (see Figure 13b).

There are four basic checks that must be made of any controlled system: nominal stability, nominal stability, robust stability, and robust performance. These four checks are considered below, consecutively.

The extended H_2 synthesis method used for this portion provides an inherent guarantee of stability for a nominal plant with full state feedback. Further, the "separation principle" guarantees that for a perfectly known plant a stable asymptotic observer will not destabilize the system. Thus, nominal stability is assured with the full order observer, provided the observer itself is stable. Reducing the controller order removes this guarantee, but simple eigenvalue checks verify that both the reduced third–order controller as designed and the associated controlled system are stable for the nominal plant. A simple check of the loop gain Bode plot (Figure 13a) confirms the conclusion that the closed loop system is stable, since it is known that the loop gain is minimum phase.

The second necessary check is of nominal performance. As indicated by the closed–loop transmissibility plot (Figure 13c) the nominal performance is quite satisfactory. Note that the "less than 10^{-2}" spec at 0.1 Hz is surpassed by more than an order of magnitude. This overdesign was intentional, and necessary, since plant modeling errors (open loop system, sensors, and actuators) will certainly degrade performance margins.

Robust stability measures are necessary to determine whether the closed–loop system will remain stable given the anticipated sensor, actuator, and plant parameter uncertainties. Three different types of robust stability measures were used, for guaranteeing system stability for multiplicative input, multiplicative output, and feedback uncertainties below certain levels. The multiplicative input uncertainty allowable was found to be equivalent to a guaranteed phase margin (interval) of [–48°, +48°], and to a guaranteed gain margin (interval) of [0.304,

5.434]. The actual margins are even larger (phase margins: [–55°, +55°], gain margins: [0,+∞]). Since only one plant output is sensed (viz., payload acceleration), the multiplicative input and output robust stability guarantees are identical. A feedback uncertainty measure was used to determine guaranteed minimum stability bounds on uncertainties in umbilical stiffness and damping, and on payload mass. It was found, as noted previously (p. 34), that closed–loop system stability was guaranteed for single–parameter uncertainties much larger than anticipated. By considering the feedback uncertainty structure, it was shown that for simultaneous mass, damping, and stiffness uncertainties of ±20%, ±100%, and ±69%, respectively, system stability could be assured. Higher frequency modes of the system were considered not to be a significant concern since the controller bandwidth was limited during design.

Finally, measures were needed of performance robustness. Structured singular value plots were made to find conservative bounds on multiplicative input (and output) uncertainties that would not lead to plants with unacceptable performance. Below 10^{-3} Hz it was found that for combined sensor and actuator uncertainties of up to ±11° in phase or of ±19% in gain the performance can be guaranteed to remain acceptable. At higher frequencies the guarantees are much better, so that by 220 Hz uncertainties of up to ±180° in phase or of ±200% in gain are permissible.

Structured singular value plots were also used in an attempt to find performance robustness guarantees in the face of known parametric uncertainties, but the effort was only partly successful. The checks led to the conclusion that for single–parameter uncertainties in stiffness of ±40% both stability and acceptable performance could be assured. However, single–parameter uncertainty bounds found by this method on damping and mass were too conservative to be useful. Consequently, real parametric studies were conducted on plant–uncertainty effects on closed–loop performance. It was determined that closed loop performance appeared acceptable for the various combinations of parametric uncertainties

examined, with mass and stiffness varied in the intervals [–50%, +100%] and [–20%, +100%], respectively, and with damping varied by more than ten times its nominal value.

The above extended H_2 synthesis – μ analysis approach produced a controller that easily satisfies the competing demands of the posed 1–D microgravity vibration isolation problem. Further, unlike the classical approach, it is readily extendable for use on a 3–D problem. Frequency weighting and disturbance– accommodation were both found to be necessary if H_2 synthesis is to be used in involving the posed isolation problem. Their inclusion, along with a judicious choice of states, provides the designer with a powerful and intuitive set of weapons for his design arsenal. Disturbance accommodation of a direct disturbance model is necessary to force the H_2 synthesis machinery to avoid negative–stiffness solutions. The result was an actively controlled system that uses a "smart" form of acceleration feedback to overcome the robustness problems that commonly plague the basic LQG synthesis approach.

6. EXPERIMENTAL RIG

6.1 Introduction

The University began construction of a one–degree–of–freedom experimental rig to demonstrate active microgravity isolation in the fall of 1990. The rig, now completed, was designed so as to illustrate active isolation of a tethered mass down to very low frequencies (0.01 Hz). This required both a large–stroke actuator and acceleration feedback as discussed in Sections 2 and 4. To our knowledge, this is the first microgravity rig to address either tethered or large–stroke active isolation.

6.2 Rig Description

The experimental rig built at the University of Virginia is shown in Figure 14. The rig consists of a 75 lb. steel cylinder representing a microgravity experiment, two air dashpots representing umbilicals, an electrodynamic shaker representing the vibrating experiment rack, and the large–stroke Lorentz actuator. The steel cylinder is suspended with magnetic supports so that it may freely move horizontally along its axis [16]. Similar to radial magnetic bearings, each support consists of four horseshoe electromagnets. Eddy current probes sense the radial position of the cylinder and complete the magnetic suspension feedback loops supplying current to the electromagnets. The supports hold the cylinder firmly in place but produce no friction. When the electromagnetic support system is turned off, the cylinder rests on a pair of touchdown pedestals.

The electrodynamic shaker (representing the experiment rack aboard the orbiter) has a long peak–to–peak stroke of 6.25 inches. This is the vibration source from which the steel cylinder (experiment) must be isolated. The shaker is mounted, via aluminum plates, on a concrete block resting on the laboratory floor. The shaker can generate sinusoidal, random or impulse waveforms at frequencies down to DC, thus simulating the disturbances typically produced on a manned orbiter.

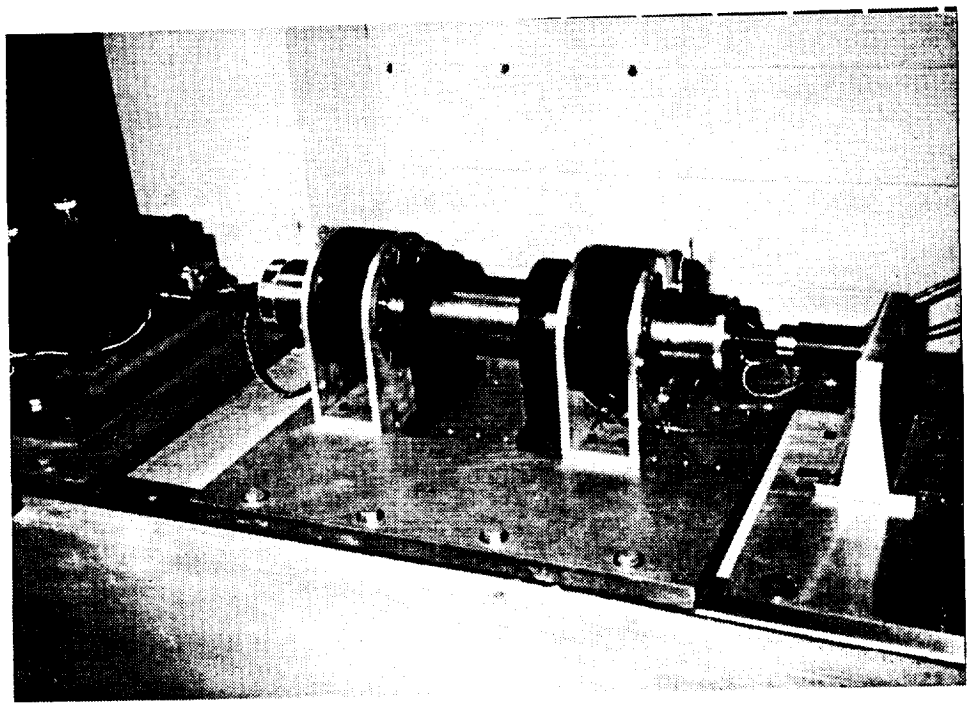

Fig. 14. Microgravity isolation rig at the University of Virginia

The umbilicals connecting a microgravity experiment to the orbiter are expected to be flexible hoses and wires. These are modeled by air dashpots with adjustable stiffness and damping coefficients. The vibration isolation test rig at the University has been designed so that different kinds of umbilicals may be employed, including actual hoses like those used for fluid transfer. The large–stroke Lorentz actuator connects the levitated steel cylinder to a plate connected to the concrete base.

The axial acceleration of the cylinder is sensed off a sensory plate using a very low frequency accelerometer with a resolution of approximately 1 μg. The accelerometer signal is fed through a low pass filter and a transconductance bipolar linear amplifier to produce the required current. This current is applied to the Lorentz actuator to isolate the cylinder from the disturbances generated by the shaker.

The background vibration levels on the concrete base on which the cylinder is mounted have been measured over several twenty–four–hour periods, in both the horizontal and the vertical directions. These vibrations are of the order of milli–g's, the quietest period occurring from late in the night to early in the morning [18]. Operating at this time will yield the highest degree of reproducibility in our results.

6.3 Experimental Results

Preliminary results have been obtained for vibration isolation in the (1–3) Hz range. An air dashpot (umbilical) was the only direct connection between the shaker armature (space platform) and the cylinder (science experiment requiring isolation).

An HP Structural Dynamics Analyzer was used for data acquisition. Figure 15 is a typical example illustrating the isolation obtained using simple lowpass acceleration feedback. The shaker generated a sinusoidal armature motion at a frequency of 2 Hz. For this case, the shaker's acceleration had an amplitude of 14,000 μg. The cylinder had a peak acceleration amplitude of approximately 7,000 μg with the controller "off" and 465 μg with the controller "on". Therefore, a fifteen–fold reduction of vibration has been obtained through acceleration feedback.

The control system is now being modified to improve the isolation capability of the controller.

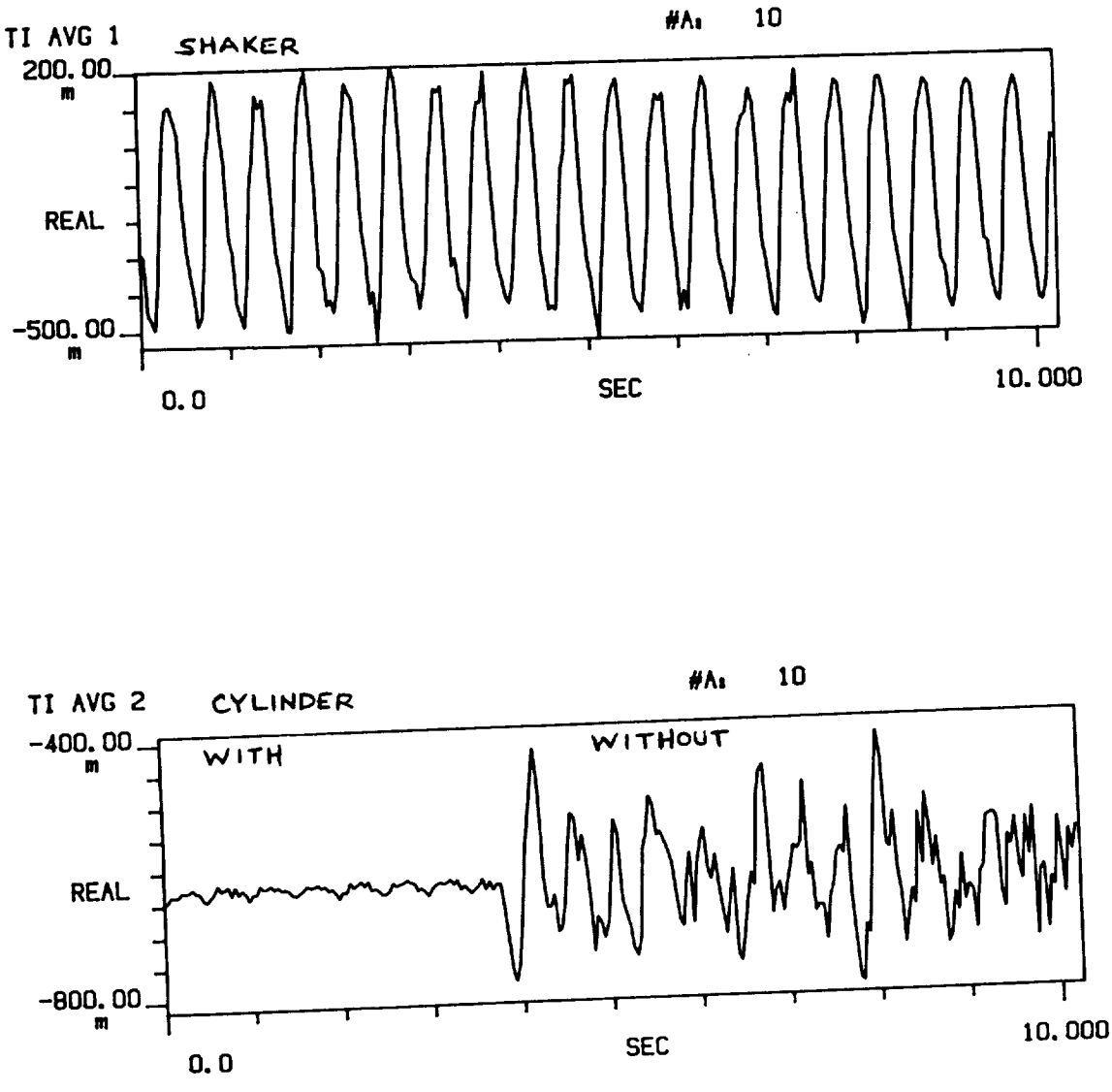

Figure 15: Shaker acceleration and cylinder acceleration with and without feedback control

7. CONCLUSION

The University has made substantial progress in many areas of active microgravity isolation in the last three years. We have primarily addressed the design of actuators and control systems for the active isolation of tethered experiments. In actuator research, our work has examined electrodynamic and electromagnetic actuators for single and multiple–degree–of–freedom isolation, and the use of coarse–fine systems for the practical extension of electromagnetic isolation to large strokes. For control system design, we have addressed performance limitations, robustness issues, and the use of H^2 methods for synthesis. Finally, we have constructed a single–degree–of–freedom test rig and demonstrated active isolation of a tethered mass through acceleration feedback. Our research is ongoing and several important results are still to be achieved. The University looks forward to continuing its work in microgravity vibration isolation and to continued collaboration with NASA Lewis Research Center.

To make a microgravity environment available for space experiments in the near future, we recommend the following:

* **The umbilicals to be used to service the experiments need to be identified and their properties need to be examined.** As the research conducted at the University over the last three years demonstrates, the difficulty of achieving a microgravity environment is very directly related to the umbilical's properties. For multiple–degree–of–freedom isolation, the uncertain coupling of degrees–of–freedom through the umbilical may present a challenge to controller design. For this reason, it is also recommended that controlled umbilicals be examined.
* **The issue of direct disturbances needs to be addressed.** Acceleration feedback, like that developed in our work, will be effective against direct disturbances as long as the frequencies of these disturbances are below that of the first flexible mode of the experiment structure. Perhaps a specification for

experiment designers on the frequencies and amplitudes (or power spectrum) of allowable direct disturbances can be written. Such a specification would require that direct disturbances be acceptable without active vibration control for frequencies near and above the first flexible mode. This may help focus attention on the issue of direct disturbances and experiment design so that any required technology development may begin soon. For example, such a specification may result in the inclusion of passive vibration isolation mounts onboard the experiment package to isolate the sensitive process from high frequency direct disturbances produced by auxiliary equipment (e.g., pumps, fans, shutters, valves).

* **The isolation frequency and amplitude requirements of microgravity experiments and the microgravity vibration environment of the space shuttle and space station need to be better characterized.** This is very important in the low frequency (0–1 hz) range. Only when these quantities are specified can the required stroke of the actuator be determined. If strokes larger than 1 cm are necessary, a coarse–fine actuation system should be used. In this case, a technology development program needs to be started. The authors believe that a significant degree of development may be required for such a coarse–fine actuation scheme.

* **A six–degree–of–freedom microgravity isolation system needs to be flown aboard the space shuttle in the near future.** Only when we start developing actual hardware and software for an orbiting isolation system will we make significant progress toward practical isolation for space experiments. While we have learned a great deal from the experiments conducted so far, many of the difficulties that remain cannot be fully simulated or anticipated using ground based hardware.

[1] B. B. Banerjee, C. R. Knospe, and P. E. Allaire. Compact Lorentz Actuator: Final Design. In *International Workshop on Vibration Isolation Technology for Microgravity Science Applications*, April 1991.

[2] C. R. Knospe and P. E. Allaire. Limitations on Vibration Isolation for Microgravity Space Experiments. *AIAA Journal of Spacecraft and Rockets*, 27(6):642–646, November–December 1990.

[3] C. R. Knospe and P. E. Allaire. Limits on the Isolation of Stochastic Vibration for Microgravity Space Experiments. *AIAA Journal of Spacecraft and Rockets*, 28(2):229–237, March–April 1991.

[4] A. P. Allan and . R. Knospe. A Six Degree–of–Freedom Actuator Design for Microgravity Vibration Isolation. In *Internal Workshop on Vibration Isolation Technology for Microgravity Science Applications*, April 1991.

[5] A. P. Allan and C. R. Knospe. A Six Degree–of–Freedom Magnetic Bearing for Microgravity Vibration Isolation. In *International Symposium on Magnetic Suspension Technology*, August 1991.

[6] Terry S. Allen, Douglas D. Havenhill, and Kevin D. Kral. FEAMIS: A magnetically suspended isolation system for space–based materials processing. In *Annual AAS Guidance and Control Conference*, Keystone, Colorado, February 1–5, 1986. Rocky Mountain Section, American Astronautical Society.

[7] D. I. Jones, A. R. Owens, and R. G. Owen. A microgravity isolation mount. *Acta Astronautica*, 15(6/7):441–448, 1987.

[8] Carlos M. Grodinsky. Development and approach to low–frequency microgravity isolation systems. Technical Paper 2984, NASA, August 1990.

[9] Ralph Fenn and Bruce Johnson. A six degree of freedom Lorentz force vibration isolator with nonlinear controller. In *International Workshop on Vibration Isolation Technology for Microgravity Science Applications*, Cleveland, Ohio, April 23–25, 1991. NASA Lewis Research Center.

[10] Ralph L. Hollis, S. E. Salcudean, and A. Peter Allan. A six degree–of–freedom magnetically levitated variable compliance fine–motion wrist: Design, modeling and control. *IEEE Transactions on Robotics and Automation*, 7(3):320–332, 1991.

[11] Kenichi Takahara, Tamane Ozawa, Hiroshi Takahashi, Shitta Shingu, Toshiro Ohashi, and Hitoshi Sugiura. Development of a magnetically suspended, tetrahedron–shaped antenna pointing system. In *22nd Aerospace Mechanisms Symposium*, Hampton, VA, May 4–6, 1988. NASA Langley Research Center.

[12] C. R. Knospe, R. D. Hampton, and P. E. Allaire. Control Issues of Microgravity Vibration Isolation. *Acta Astronautica*, Vol. 25, No. 11, pp. 687–697, 1991.

[13] R. D. Hampton and C. R. Knospe. Extended H2 Synthesis for Microgravity Vibration Isolation. In *International Workshop on Vibration Isolation Technology for Microgravity Science Applications*, April 1991.

[14] R. D. Hampton, C. M. Grodsinsky, P. E. Allaire, D. W. Lewis, and C. R. Knospe. Optimal Microgravity Vibration Isolation: An Algebraic Introduction. *Journal of the Astronautical Sciences*, 40(2): 241–259, April–June, 1992.

[15] R. D. Hampton and C. R. Knospe. Extended H2 Synthesis for Multiple–Degree–of–Freedom Controllers. In *International Symposium on Magnetic Suspension Technology*, August 1991.

[16] R. D. Hampton, C. R. Knospe, C. M. Grodsinsky, P. E. Allaire, and D. W. Lewis. Microgravity Vibration Isolation: Optimal Preview and Feedback Control, NASA TM–105673, May 19, 1992.

[17] R. D. Hampton, C. R. Knospe, C. M. Grodsinsky. Controller Design for Microgravity Vibration Isolation Systems, 43rd Congress of the International Astronautical Federation IAF–92–0969, August 28–September 5, 1992.

[18] B. B. Banerjee, C. R. Knospe, and P. E. Allaire. A Microgravity Vibration Isolation Rig. In *International Symposium on Magnetic Suspension Technology*, August 1991.

A Final Report
Grant No. NAG-3-909

June 1, 1988 - April 17, 1992

MAGNETIC ACTUATORS AND SUSPENSION FOR SPACE VIBRATION CONTROL

Submitted to:

National Aeronautics and Space Administration
Lewis Research Center
21000 Brookpark Road
Cleveland, OH 44135

Attention:

Dr. David P. Fleming, M/S 23-3
Structural Dynamics Branch

Submitted by:

Carl R. Knospe
Assistant Professor

Paul E. Allaire
Mac Wade Professor and Chairman

David W. Lewis
Professor

Department of Mechanical, Aerospace and Nuclear Engineering
School of Engineering and Applied Science
Thornton Hall
Charlottesville, VA 22903-2442

SEAS Report No. UVA/528292/MANE93/101
May 1993

Copy No._____

ABSTRACT

This report summarizes the research performed at the University of Virginia under Grant No. NAG–3–909 from NASA Lewis Research Center. This research on microgravity vibration isolation was focused in three areas: (1) the development of new actuators for use in microgravity isolation, (2) the design of controllers for multiple–degree–of–freedom active isolation, and (3) the construction of a single–degree–of–freedom test rig with umbilicals. Described herein are the design and testing of a large stroke linear actuator; the conceptual design and analysis of a redundant coarse–fine six–degree–of–freedom actuator; an investigation of the control issues of active microgravity isolation; a methodology for the design of multiple–degree–of–freedom isolation control systems using modern control theory; and the design and testing of a single–degree–of–freedom test rig with umbilicals.

CONTENTS

1. INTRODUCTION

The University of Virginia began research in microgravity vibration isolation in 1988 under a three–year grant from NASA Lewis Research Center. The goals of this project were (1) to develop new actuators for use in microgravity isolation, (2) to investigate the design of controllers for multiple–degree–of–freedom (MDOF) active isolation, and (3) to construct a single–degree–of–freedom (SDOF) test rig with umbilicals. The Principal Investigator for the first two years of this project was Dr. Paul E. Allaire. Dr. Carl R. Knospe became the Principal Investigator for the final year of the grant. Other faculty working with the project included Dr. Robert H. Humphris and Dr. David W. Lewis. Several graduate students have aided in this effort: Mr. Bibhuti Banerjee in actuator and test rig design, Mr. R. David Hampton in the multivariable control theory of active isolation, and Mr. A. Peter Allan in actuator design and instrumentation. Several University personnel have worked at NASA Lewis during the summers, and contact between NASA and the University has been frequent. This final report on the contract reviews the research performed over the three years of the grant. Both experimental and theoretical work in microgravity isolation continues at the University. The University aspires to become a center of excellence in active vibration isolation systems for space applications.

The next six sections discuss the research efforts of the University in meeting the isolation technology needs of the microgravity community. In Section 2, the design and testing of a single–degree–of–freedom, large–stroke actuator are reviewed. Section 3 examines multiple–degree–of–freedom actuator design. A survey of published designs is presented and a new coarse–fine actuator is proposed and analyzed. In Section 4, the design of active isolation control systems is examined. Results and discussion of the University's design methodology, frequency–shaped Linear Quadratic Regulator and Kalman–Bucy Filter synthesis, are given in Section 5. In Section 6, the design and early experimental results of the microgravity vibration isolation test rig are examined. Experimental results demonstrate that active vibration isolation of experiments with umbilicals can be obtained using loop–shaped acceleration

feedback. Section 7 concludes this final report, with a summary of our results and recommendations for future research. An appendix contains all papers presented, published, or submitted during the grant.